New Fuzzy Control Architectures Applied to Industrial Applications

Sergio Enrique Pinto Castillo
Student Registration Number: 200375470

Industrial Control Centre
Department of Electronic and Electrical Engineering
University of Strathclyde
50 George Street
Glasgow G1 1QE
United Kingdom

Submitted for the Degree of Doctor of Philosophy

August 2011

Declaration of Author's Rights

Abstract

The research considered the design, analysis and application of the several fuzzy controllers (i.e. Mamdani's and Takagi-Sugeno-kang Models) on Industrial applications. It starts with the representation of the Discrete-time Nonlinear Difference Equation by a Neuro-Fuzzy Difference Equation, which was a novel development. It also includes Neuro-Fuzzy modeling mixed with a stochastic control and a predictive control structure. It results in a new control algorithm called Neuro-Fuzzy Generalized Minimum Variance Control for nonlinear systems, and is applied to a stirred tank reactor with a cooling jacket.

An Adaptive Fuzzy structure was also combined with the Sliding Mode Controller approach in order to develop the Adaptive Fuzzy Sliding Mode Controller that is applied to the nonlinear model of a Power Electronic Ballast-Igniter-Lamp. After that, several neuro-fuzzy control structures are used with a car engine model. Finally, a novel nonlinear predictive control algorithm based on multiple models and the Takagi-Sugeno-Kang Model is applied to a MIMO Waste Water Treatment problem.

Acknowledgements

I want to express my great acknowledgements saying thanks a lot to my supervisors, Professor Mike J. Grimble and Dr. Reza Katebi, because they always gave me support, guidance and the necessary help to pursue my research by shown them me great patient and understanding. They created for me the appropriated research environment in order to have the last scientific knowledge and industrial experience in my field providing me with the actual information and the best link of technical networking. Moreover, I would like to acknowledge the great atmosphere created by all colleagues and personal working in the Industrial Control Centre, especially to Mrs. Sheila Campbell and Mr. Drew Smith. Also, I want to acknowledge my colleague and friend, Dr. Arkadiusz Stanisław Dutka, for his support and advice about the car engine application.

Also, I want to thank to my friends, B.Sc. Robert and M.B.A. Pilar Dempster, for their great support and impulse as a family in Scotland. Also, I would like to thanks my friends Dr. Michael Freeman and MBA. Julio Oya Steinbruggen because they always gave me the right words, time and impulse to continue with my research supporting me like brothers, most of the time. Nevertheless, I like to thank my friend and colleague Dr. Rene Osorio Sánchez for his great collaboration, support and encouragement to develop as a team the power electronic control applications.

Finally, I would like to say “thanks a lot” to my wife Leticia Hernandez-Reyes and my children Sergio Enrique Pinto-Hernandez and Daniel Alberto Pinto-Hernandez for their encouragement, patient, support and love during all the period of this work. They gave me the necessary strength and inspiration in order to finish my research.

List of Contents

List of Contributions

Theoretical and application contributions were presented as contribution in the development of this thesis.

Theoretical contributions:

The theoretical fundaments and analysis of the *Fuzzy Difference Equations* were developed in:

Pinto Castillo, S. E. and M. J. Grimble and R. Katebi (2011), *Fuzzy Difference Equation founded in Neuro-Fuzzy Systems with Takagi-Sugeno-Kang Models*, IEE Proceedings Fuzzy Set and Systems,(In preparation).

- The main contribution of the article was to develop a novel analysis of the Neuro-Fuzzy Systems such as formal structure of a nonlinear difference equation. This development was founded in the NARX model structure. It represents the link between the formal mathematics and the artificial intelligent approaches. Further analysis and developments could be found in Chapter 2.

The theory, analysis and design of the Neuro-Fuzzy Generalised Minimum Variance control algorithm were introduced in:

Pinto Castillo S.E. and M.J. Grimble and R. Katebi (2004), Neuro-*Fuzzy Generalized Minimum Variance for Nonlinear Systems*, 2nd IFAC Symposium on System, Structure and Control, Mexico.

- In this paper, for the first time, the Neuro-Fuzzy System was used for modelling purposes for the development of the Nonlinear Generalised Minimum Variance Controller. It was developed arranging the Neuro-Fuzzy System structure to a specific structure defined in the initial design of Grimble (2003).

Pinto Castillo S.E. (2004), Neuro-Fuzzy Generalised Minimum Variance Control Algorithm, Internal Report ICC-REP 214, Industrial Control Center, University of Strathclyde.

- This internal report is an extended version of the Neuro-Fuzzy Generalised Minimum Variance control law. It included a deeper analysis of the Fuzzy Model, comparison between the nonlinear surfaces produced by the nonlinear model and Neuro-Fuzzy model. This analysis was the main motivation for the development of the Fuzzy Difference equation on the Chapter 2.

Pinto Castillo S.E. and M.J. Grimble and R. Katebi (2005), *Self-Tuning Neuro-Fuzzy Generalized Minimum Variance Controller*, 16th IFAC World Congress in Prague, Czech Republic, ISBN: 0-08-045108-X.

- The aim of this paper was the inclusion of a fuzzy self-tuning mechanism in the original Neuro-Fuzzy Generalised Minimum Variance controller. The self-tuning algorithm was developed obtaining the expert rules and after that developing a Mamdani's Fuzzy structure where these rules where used as a self-tuning algorithm. Further analysis and developments are included in Chapter 3.

The analysis, design and application of nonlinear control techniques over to the Ballast plus the igniter and Lamp (Power Electronics Applications) were developed in:

Osorio R., and M.A. Oliver and M. Ponce and S.E. Pinto and M. Juarez, and Reza Katebi and Mike J. Grimble (2005), *Analysis and Design of Discrete-Sliding-Mode Control for a Square-Waveform-Ballast*, 44th IEEE Conference on Decision and Control and European Control Conference, 0-7803-9568-9/05/$20.00 ©2005 IEEE.
.

- This paper was developed from the modeling, design, simulation and implementation of the Sliding-Mode Control System. The main contribution of the control system designed was the reduction of the electronic components, making the implementation more sustainable. In this article was applied a

discrete-time sliding mode control in a resonant ballast. The aim of the article was apply a nonlinear controller in order to improve the performance and make easier the implementation in a microcontroller.

R. Osorio, S. E. Pinto, M. Ponce,M. A. Oliver, R. Katebi, M. J. Grimble (2005), Dimming Control Using Adaptive-Fuzzy-Sliding Surface for Square-Waveform Ballast, Congreso Nacional de Control Automático, CNCA'05, Mexico, ISBN 970-32-4025-9.

.

- An Adaptive-Fuzzy-Sliding Surface was used to develop a Dimming Control System applied on an Square-Waveform Ballast. The Adaptive-Fuzzy-Sliding Surface was designed by using an Adaptive PI Fuzzy control algorithm used by Pinto (2001). It improved the performance of the no-resonant ballast and made it more robust against variation of the lamp parameters.

- In the paper was developed a linear model of HID lamp useful for the design of linear controllers applied on non-resonant ballast.

R. Osorio, N. Vázquez, C. Hernández, E. Rodríguez, S. E. Pinto, M. Juárez (2010), *Electric Dynamic Modeling of HID Lamps for Electronic Ballast Design*, IEEE Transactions on Industrial Electronics, Vol. 57 , Issue: 5, pp: 1655-1662, ISSN: 0278-0046.

- The aim of the article was introduce to the development of a simple dynamic nonlinear model of AID lamps with easy estimation of parameters using electric measurements.

The analysis and design of the Nonlinear Model Based Predictive Controller based on Takagi-Sugeno-Kang Models were introduced in:

O'Brien M. and S.E. Pinto Castillo and R. Katebi (2005), *Model Based Predictive Control for Wastewater Application*, 16th IFAC World Congress in Prague, Czech Republic, ISBN: 0-08-045108-X.

- The two previous articles introduce a new algorithm of the *Nonlinear Model Based Predictive Controller*. It was founded in *Takagi-Sugeno-Kang Fuzzy Structure* and multiple models. This approach was based in dividing the nonlinear operating range in several sub-operating range. As we know, we can solve a complex problem by solving several small problems, making sometimes more efficient the solution. *Further developments were included in Chapter 6.*

LIST OF FIGURES

LIST OF ABBREVIATIONS

Abbreviation	Meaning
AC	Alternating Current
A/F	Air-Fuel
AFR	Air-Fuel Ratio
AFSMC	Adaptive Fuzzy Sliding Mode Control
AF_sp	Air-to-Fuel Ratio Set Point
AI	Artificial Intelligence
ANFIS	Adaptive Neuro Fuzzy Inference Systems
ANFIS	Adaptive Network-based Fuzzy Inference Systems
ANN	Artificial Neural Network
AANN	Adaptable Artificial Neural Network
ANNs	Artificial Neural Networks
ASM	Activated Sludge Model
BIO	Biological
BP	Backpropagation
BT	Brake Torque
CAC	Cylinder Air Charge
CCM	Continuous Conduction Mode
CD	Direct Current
CO	Carbon Monoxide
CRI	Common Rail Injection
CSTRCJ	Continuous Stirred Tank Reactor with Cooling Jacket
DC	Direct Current
DCM	Discontinuous Conduction Mode
DISC	Direct Injection Stratified Charge
DO	Dissolved Oxygen
DSMC	Discrete Sliding Mode Control
DSP	Digital Signal Processor
ECS	Engine Control Systems
ECU	Engine Control Units
EGR	Exhaust Gas Recirculation
ETC	Electronic Throttle Control
FDE	Fuzzy Difference Equation
FDEs	Fuzzy Difference Equations
FFC	Feed-Forward Control
FFNN	Feedforward Neural Networks
FL	Fuzzy Logic
FM	Fuzzy Mapping
EKF	Extended Kalman Filter
EMS	Engine Management System
FMBPC	Fuzzy Model Based Predictive Controller
FMPC	Fuzzy Model Predictive Controller

FPW	Fuel Pulse Width
FS	Fuzzy System
FTP	Federal Test Procedure
GA	Genetic Algorithms
GD	Gradient Descent
GDI	Gasoline Direct Injection
GMV	Generalised Minimum Variance
GNN	Gaussian Neural Network
GPC	Generalised Predictive Controller
HC	Hydrocarbons
H_c	Control Horizon
HL	Hybrid Learning
H_p	Prediction Horizon
HID	High Intensity Discharge
JPL	Jet Propulsion Lab
Lambda	Normalized Air to Fuel Ratio
Lambda_sp	Normalized Air to Fuel Ratio Set Point
LLMBPC	Local Linear Model Based Predictive Controller
LMI	Linear Matrix Inequality
LOLIMOT	Local Linear Radial Basis Function Network
LSE	Least Square Estimator
MAF	Mass Airflow
MAP	Intake Manifold Pressure
MBPC	Model Based Predictive Controller
MIMO	Multiple Input Multiple Output
MISO	Multiple Input Single Output
MPN	Multilayer Perceptron Network
MV	Minimum Variance
N	Engine Speed
$N(t)$	Engine Speed
NARX	Nonlinear Autoregressive with Exogenous Input
NARMAX	Nonlinear Autoregressive Moving Average
NF	Neuro-Fuzzy
NFDE	Neuro-Fuzzy Difference Equation
NFS	Neuro-Fuzzy System
NFM	Neuro-Fuzzy Model
NFSs	Neuro-Fuzzy Systems
NFGMV	Neuro-Fuzzy Generalised Minimum Variance
NFMBPC	Neuro-Fuzzy Model Based Predictive Controller
NGMV	Nonlinear Generalised Minimum Variance
NMBPC	Nonlinear Model Based Predictive Controller
NMPC	Nonlinear Model Predictive Controller
NN	Neural Network
NO_x	Oxides of Nitrogen

P_{amb}	Ambient Pressure
Pamb	Ambient Pressure
PCM	Driver or Engine Controller
P_{em}	Exhaust Manifold Gas Pressure
PI	Proportional – Integral
P_{im}	Intake Manifold Pressure
PID	Proportional - Integral - Derivative
PLM	Polytopic Linear Model
RBF	Radial Basis Function
RNN	Recurrent Neural Networks
RPM	Engine Speed
RPM_sp	Engine Speed Set Point
SA	Spark Advance
SD	Steepest Descent
SDM	Steepest Descendent Method
SG	Speed-Gradient
SI	Spark Ignition
SISO	Single Input Single Output
SMC	Sliding Mode Control
SP	Throttle Position Command
STNFGMV	Self-Tuning Neuro-Fuzzy Generalised Minimum Variance
TA	Throttle Angle
T_{amb}	Ambient Temperature
Tamb	Ambient Temperature
Tcool	Coolant Temperature
TDC	Top Dead Centre
T_{em}	Exhaust Manifold Gas Temperature
T_{im}	Intake Manifold Temperature
TITO	Two-Input-Two-Output
T_{man}	Intake Manifold Gas Temperature
TP	Throttle Position
TSK	Takagi – Sugeno – Kang
TWC	Three-Way Catalytic
TWCC	Three Ways Catalysis Converter
UWS	Urban Wastewater System
VGT	Variable Geometry Turbocharger
VTG	Variable Turbine Geometry
VVT	Variable Valve Timing

LIST OF TABLES

Chapter 1 Introduction

This chapter introduces the general background of this research project. The arguments start in section 1.1., with the motivation and historical development of the Soft Computing. It is a promising research area, which has been applied in the design of nonlinear control systems using intelligent modelling and control as presented in section 1.2. In the last decades, the formal mathematical justifications for the artificial intelligence approaches were almost impossible but the exponential increment of the applications shown a partial justification of the area. The real applications of the AI techniques are briefly introduced in the section 1.3. Finally, the last section 1.4 describes the summarized contributions of this thesis.

1.1. Soft Computing Approaches

The Soft Computing is a subset of the Artificial Intelligence algorithms. AI was motivated initially to emulate the human decision and organic behaviour in order to find the real problems solutions. As Soft Computing approaches are commonly recognized the Artificial Neural Networks (McCullock and Pitts, 1943; Hebb, 1949; Farley and Clark, 1954; Rosenblatt, 1958; Rochester, et. al., 1956), the Fuzzy Logic (Zadeh, 1965; Mamdani and Assilian, 1975; Lee, 1990a; 1990b; Driankov, et. al, 1996), the Neuro-Fuzzy Systems (Sugeno and Kang, 1988; Lin and Lee, 1996;; Jang, 1992a; Brown and Harris, 1994; Jang, et. al., 1997; Nauck, et al., 1997; Babuška, 1998; Babuška and Verbruggen, 2003) and the Genetic Algorithms (i.e. intelligent optimizer) (Barricelli, 1954; 1957; Fraser, 1957; Fraser and Burnell; 1970; Holland, 1975). Based on these approaches have been developed a new generation of AI algorithms are called Bio-Inspired and Mimetic algorithms (Passino, 2004; Floreano and Mattiussi, 2008; Negoita and Hintea, 2009). Sometimes, when there is not an expert in the target process then the intelligent control algorithms represent a good alternative.

The real world has many physical phenomena which are not defined totally for its quantitative characteristic (or differential equations). Sometimes, our senses are not enough for the description of these phenomena. Because of that, Soft Computing

techniques are useful in order to develop a linguistic (qualitative) representation of the real phenomena to catch the uncertainties and reduce the level of complexity of the mathematical representations (Pinto, 2004).

Artificial Neural Networks (ANNs) are a data processing system with processing units called neurons connected between them by means of the weightings (synaptic). The learning process performed in the ANNs is quite similar to the learning process in the cerebral neurons of the brain, taking the knowledge from the experience. The knowledge is transmitted between the neurons through the synaptic connectors. The dynamical behaviour of the ANNs is described by the structure of the network, the connection type of the weightings, the value of weightings and the type of node's function. The ANN is a nonlinear mapping from input-output data using its adaptive characteristics.

Fuzzy logic is a nonlinear mapping able to represent many real world uncertainties expressed using expert knowledge the qualitative features. Actually, the great functionality in Fuzzy Logic applications has been demonstrated by an exponential increment of the applications in several fields of knowledge (Pinto, 2001). Fuzzy Logic is the way to use qualitative representations of the nonlinear process by means of fuzzy rules with linguistic variables (see chapter 2). Highly nonlinear processes without an exact mathematical model can be replaced by a small amount of fuzzy rules. The Fuzzy rules have an antecedent part and a consequent part, where the consequent part defines the type of Fuzzy System (i.e. Mamdani's and Takagi-Sugeno-Kang's models). The key to develop the Fuzzy rules is founded in dynamic information that can be obtained from specific variables (or states) of the nonlinear process. The Fuzzy rules of the nonlinear plant define its Fuzzy model. In Chapter 2, it is proved that the Fuzzy model is equivalent a formal mathematical model. Fuzzy models are used to define nonlinear processes with state variables partially defined due to the uncertainties.

Finally, the Genetic Algorithms (GA) is an optimization method that uses genetic information of the data in order to find a solution for an specific cost function (Zbigniew, 1998; Chambers, 2000; Sakawa, 2005; Gen, et. al., 2008). GA are closely related to the self-adaptive biological processes. It analyzes the genetic information of a data population applying the rules of reproduction of the stronger parents (selection),

genetic crossover, heritage, and evolution (mutation) to pseudo-organisms, so those "organisms" can preserve the best genetic qualities and transferring those to the new generations. The performance optimization of a system by the best selection of its parameters, testing and fitting quantitative models are the most common issues of the GA.

Soft Computing techniques have been widely applied in identification, modelling, control, monitoring, fault detection and reconfiguration of nonlinear processes improving the performance simplifying the implementation procedure.

1.2. Nonlinear Control Systems – Intelligent Control Approaches

Nonlinear control systems have always represented a hard problem to solve for the industrial (real) applications, especially when the processes are multivariable with time-delay in the input or output paths. Nevertheless, the nonlinear control approaches have a better performance than the linear (or conventional) controllers when the target processes are nonlinear.

Control Engineering is a multidisciplinary profession that requires strong theoretical and practical skills. The control engineer needs to know in advance the physical laws that govern the real application to be solved by a control system design and implementation. In other words, the control engineer needs to be an expert on the dynamic behaviour of the target nonlinear process. An industrial control application involves the design and implementation using theoretical knowledge, software programming skills, mathematical analysis tools, electronic instrumentation and microcontroller technology, combining all the previous resources with the practical skills for the final step of implementation.

Before any modelling, identification and control design, it is necessary to have the expert knowledge about the nonlinear process from the mathematical (i.e. differential equations) and/or qualitative (i.e. fuzzy rules) model of the nonlinear phenomenon. An accurate nonlinear modelling is always reflected in a good performance index of the nonlinear control technique. Depending on the nature of the nonlinear model, it could be developed from:

1. Physical equations and parameter identification, obtaining a mathematical model of the nonlinear process (called white box).
2. Input-Output data obtained from measurements of the nonlinear process, obtaining a linguistic (qualitative) model, called black box. These models are generally designing using ANNs and Look-Up table.
3. Using both mathematical and linguistic models, called commonly hybrid model or model based on grey box. These models are founded on the combined model of differential equations with ANNs and/or Fuzzy Systems. The Fuzzy and Neuro-Fuzzy models have been also defined as a gray box because the fuzzy rules given us a qualitative model with dynamic information (fuzzy difference equation) about the system, especially when it is used a NARX model (Pinto, 2004; Pinto, et. al., 2009).
4. Multiple Linear Models overlapped with Takagi-Sugeno-Kang Structure as the example designed by Pinto and widely explained in the chapter 6. It was used in a multivariable example of nonlinear predictive controller published by O'brien, Pinto and Katebi (2005).

After development of the nonlinear model, the second step to design the nonlinear controller. Particularly, for this research project were used the Neuro-Fuzzy modelling as nonlinear models. The Neuro-Fuzzy model will be used in the chapters 2, 3 and 4 and the Multiple model will be used in the chapter 6.

The nonlinear controllers are classified by designing them based on:

- The formal mathematical properties and techniques (i.e. Lie Derivative, Passivity) of the nonlinear systems (Isidori, 1986; 1999; Schaft, 2000; Lu, et. al., 2001; Astolfi and Marconi, 2007; Gasparyan, 2008; Osorio, et. al., 2005a).
- AI approaches (Jan, et. al., 1997; Pinto, 2001; Cirstea, et. al., 2002; Pinto, 2005; Kovačić and Bogdan, 2006).
- The combination between the AI approach and another control technique (Pinto, 2004; Espinosa, et. al., 2005; Osorio, et. al., 2006b).

1.3. Industrial and Power Electronic Applications

The industrial processes are real applications with nonlinear dynamic behavior, multiple and/or multivariable loops inside of the subsystems (Luyben 1990; Marlin 2000). Also, the industrial applications have mass and energy transfer between processing units or sub-systems, which are commonly tanks, pipes, valves, pumps, compressors, condensers, boilers, reactors, motors, generators, heaters, heat exchangers, burners, turbines, coolers, separators, distillation columns, mixers and evaporators (Umez-Eronini, 1998).

The processing units are governed by some physical laws of mass and energy conservation and Newton´s momentum law. In addition, there are expressions which describe the material behavior. All the laws before mentioned are used to find a model of the process for parameter identification and simulation purposes, but even with the physical laws there are always various degrees of uncertainty. These uncertainties increase with the complexity of the model, especially for modeling of nonlinear and multivariable processes.

Specifically the nonlinear and industrial applications considered were the Levitation System, Dual Process Simulator KJ 100, Continuous Stirred Tank Reactor with Cooling Jacket, Car Engine, A Ballast and Igniter plus Lamp and the Waste Water Treatment process. All the applications will be explained in details in the corresponding chapter.

1.4. Thesis Roadmap

The main benefits obtained in this thesis include the theoretical and application developments. The thesis was developed in order to carry out research in nonlinear and Neuro-Fuzzy control theory. The amount of academic examples presented demonstrates the benefits of the developed theory.

The contributions of each chapter are described as follow:

- In Chapter 2, the theoretical foundation of the Artificial Neural Networks, the Fuzzy Logic and the Neuro-Fuzzy systems was revisited with original academic examples and

mathematical foundations (Pinto, 2005). The theoretical analysis of the different topics was widely explained using original examples in order to understand the way of data processing. Moreover, the training methods applied to the Artificial Neural Networks and the Neuro-Fuzzy systems were described. Finally, the main contribution was a novel theoretical and mathematical (with definitions and theorems) development of the Fuzzy Difference Equations. This last section includes two academic examples of the Fuzzy Difference Equations.

- In Chapter 3, the nonlinear optimal, self-tuning and Neuro-Fuzzy control algorithms were developed. It starts with the theoretical foundation of the Neuro-Fuzzy Generalised Minimum Variance (GMV). Using mathematical properties of the system, new structures were developed for the Neuro-Fuzzy GMV controller as a contribution in this Chapter. Finally, two academic examples of the Neuro-Fuzzy GMV control and the Self-Tuning Neuro-Fuzzy GMV control were designed and applied to a Continuous Stirred Tank Reactor with Cooling Jacket (Pinto, et. al., 2004a; 2004b; 2005).

- In Chapter 4, the automotive powertrain model developed by Dutka (2005) was explained and simulated. A Neuro-Fuzzy model of the car engine model was then developed in order to apply it to a Neuro-Fuzzy GMV Air-Fuel Ratio controller. In addition, several Neuro-Fuzzy Air-Fuel Ratio control systems applied to the car engine were simulated in MATLAB/Simulink environment.

- In Chapter 5, a nonlinear model of the Ballasts including the igniters plus the lamp model was developed and validated with the real process. Moreover, a nonlinear controller using Adaptive Fuzzy Sliding Mode and Dimming Fuzzy Controllers were developed and applied. The results were compared with the real process of the Ballast with the igniter plus the lamp. Finally, a stability analysis of the nonlinear model of the Ballast including the igniter plus the lamp model was developed.

- In Chapter 6, a novel nonlinear predictive controllers was designed and developed for nonlinear processes. The nonlinear predictive controller was founded on the multiple

model overlapping based on the Takagi-Sugeno-Kang structure. The nonlinear processes used for simulation was the Waste Water Treatment Plant (MIMO).

Chapter 2 Theory of Neuro-Fuzzy Systems

2.1. Introduction

The aim of the chapter is to develop new Fuzzy Difference Equations based on the concepts of the Artificial Neural Networks, Fuzzy Logic and Neuro-Fuzzy Systems (NFS). The mathematical reasoning used in the development of the Neuro-Fuzzy Difference Equations is a new and a formal way to show the signal processing used by the NFS. It drives to the origin of the novel and formal Fuzzy Difference Equations (FDEs), which are the main contribution of this chapter. Also, the reasons behind to the FDEs development are to prove the existence of physical meaning, establish a link between the Artificial Intelligence and the formal mathematics opening a path for the formal analysis of convergence and stability of the NFS. It could help to avoid the rejection of the formal Scientist and Mathematicians.

This chapter is also concerned with the theoretical foundations of the NFS. Frequently, these systems are called ANFIS, which means either *Adaptive Neuro Fuzzy Inference Systems* or *Adaptive Network-based Fuzzy Inference Systems* (Lin and Lee, 1996; Jang et. al., 1997; Nauck, et al., 1997; Pinto, 2001). The NFS uses a hybrid approach which has been used with success in many fields such as modelling, identification, control, signal processing, fault detection and isolation (Pinto, et. al., 2003).

This chapter starts with the description of the bases for the ANN and Fuzzy System (FS). This is followed by the way to process the information in the NFS using the algorithms of back propagation and the hybrid learning rule. The off-line and on-line training methods are also described here. The ANNs cannot be represented neither by explicit mathematical equations nor expert rules and due to those it is frequently referred to as a “black box” method. A complete analysis of several properties of the NFS (“gray box”) is also discussed from a different point of view. The chapter also includes the development of the new vector form for the Gradient Descent

algorithm. Finally, a novel equation for a formal Fuzzy Difference Equation was developed by means of the universal approximator property of the NFS.

2.2. Artificial Neural Networks (ANN)

The ANNs try to emulate the Learning Processes of the Neurons in the Brain in order to learn from experience (Bishop, 1995). They are a mix between the adaptive control and identification techniques. They have directional links connected between several nodes. The nodes represent a unit process. The links define the causal relationship between the connected nodes. The nodes may be either fixed or adaptive. Process units are defined in the nodes as linear or nonlinear functions. Each single node is generated by a static node function with its incoming signals. A static mapping is developed from input(s) to output(s). They can generate a nonlinear mapping from data observations. An ANN is a processing system with neurons interconnected in a network by mean of the weightings (synaptics). The structures of the networks, value of weightings and the node's functions define the behaviour of the Neural Networks (NN). The first and the last layers are known as input layer and output Layer, respectively.

2.3. Applications of the Artificial Neural Networks

As a universal approximator the ANNs can emulate the behaviour of nonlinear and complex systems, including system with time-varying delays (Pinto, et. al., 2004). The NN uses a nonlinear relationship (mapping) between the input and outputs in order to represent a nonlinear model in the discrete-time domain of a target plant. To guarantee an acceptable nonlinear mapping with high accuracy, it is necessary to apply the approximation theorem using lagged inputs and outputs.

ANN would avoid the use of complex mathematical models and develop a nonlinear model with a good accuracy under a wider range of uncertainties (Pinto, 2006). Moreover, ANN is a nonlinear function because it is a composition function of the

linear functions in each layer of the network. After the neuro (nonlinear) model is obtained, the neuro control techniques can be applied to the target process.

There are many applications of the ANNs in the areas of Times Series Prediction (Bishop, 1996; Dorffner, 1996, Frank, et. al., 2001), Nonlinear Modelling and Identification (Psichogios and Ungar, 1992; Bhama and Singh, 1993; Dayan and Abbott, 2001; Hageman, et. al., 2003), Encompass simulation (Kilmer, et. al., 1999; Grassmann and Anlauf 1999), Prediction (Odom M. D. And R. Sharda, 1990; Reese, 2000; 2001), Fault Detection and Reconfiguration (Rauch , 1994; Bernieri, et. al.,1994; Vemuri A.T.and M.M. Polycarpou 1997; Khomfoi and Tolbert 2007; Xu, et. al., 2008), Nonlinear Control System Design (Ferrari and Stengel 2002; Sato, 2003; Ge and Zhang, 2003; Žilková, et. al., 2006), Adaptive Control (Zhang, et. al., 2000; Thapa, 2001), Robust and Optimal Control (Yang and Chundi, 1999; Kim, et. al., 2007; Chatchanayuenyong and Parnichkun 2006), Nonlinear Regression (Veaux, et. al., 1998; Razi M. A. and K. Athappilly, 2005), Pattern Recognition (Bishop, 1996; Ripley, 1996), Signal Processing (Hu and Hwang, 2001; Suah, et. al., 2003; Pande, et. al., 2008), Intelligent Agents (Lee, 2006; Anderson and Anderson, 2008; Balakrishnan and Honavar 2009), Condition Monitoring (Kaewkongka, et. al., 2001; Saxena and Saad, 2005; Mesquita Brandão, et. al, 2010), Economic (Hiemstra, 1996; Haefke, C. and C. Helmenstein, 1996) and Medicine (Malmgren, et. al., 2000; Maiellaro, et. al., 2004; M. Denaï, et. al., 2009, Ross, et. al., 2009).

All of the ANNs structures are not suitable for use in control and modelling. An important factor for the stability of a Neural Network is the optimization algorithm used for a specific learning algorithm. The guarantee of convergence and the stability in the ANNs are the most important factors for a successful application. The most common ANN applied in Modelling and Control is the Multilayer Perceptron Network (MPN) with the Radial Basis Function (RBF) in the hidden layer.

The mathematical model of the MPN with Bias is defined by as follows:

$$\hat{y}_i(t) = g_i\left[\sum_{j=1}^{n_h} W_{i,j}\ \ f_j\left(\sum_{l=1}^{n_x} w_{j,l}\ x_l(t) + w_{j,0}\right) + w_{i,0}\right] \tag{2.1}$$

where $\hat{y}_i(t)$ and $x(t)$ are the output vector and the inputs vector, respectively. The weightings and bias are defined as $\{w_{j,l}, W_{i,j}\}$ and $\{w_{j,0}, w_{i,0}\}$, respectively. The inputs are clamped to 1 by means of the bias. The activation (composition) functions are defined by $f_i(\cdot)$ and $g_i(\cdot)$.

There are two types of ANNs, which are the Feedforward Neural Networks (FFNN) and the Recurrent Neural Networks (RNN). The output of each node is propagated from the input to the output paths (always) in the FFNN**.** An example of the FFNN is shown in Figure 2.1. In the RNN the output of some nodes are propagated to the same node which implies that this network is a dynamic system with memory due to the algebraic relationship between the input and output of the recurrent nodes. The RNN is shown in Figure 2.2. The memory presents in the some nodes of the RNN imply time-delays in the feedbacks in these Networks. For obvious reasons, the difference between the FFNN and RNN is the type of connection between some of their nodes.

There are different types of classification of the ANNs reported in the literature and these are classified in accordance to some criteria such as Learning methods (supervised and unsupervised), Architectures (feedforward and recurrent), Output types (binary and continuous), Node types (uniform and hybrid), Implementations (software and hardware), Connections weights (adjustable and hardwired) and Operations (biologically motivated and psychologically motivated) (Jang, et. al., 1997).

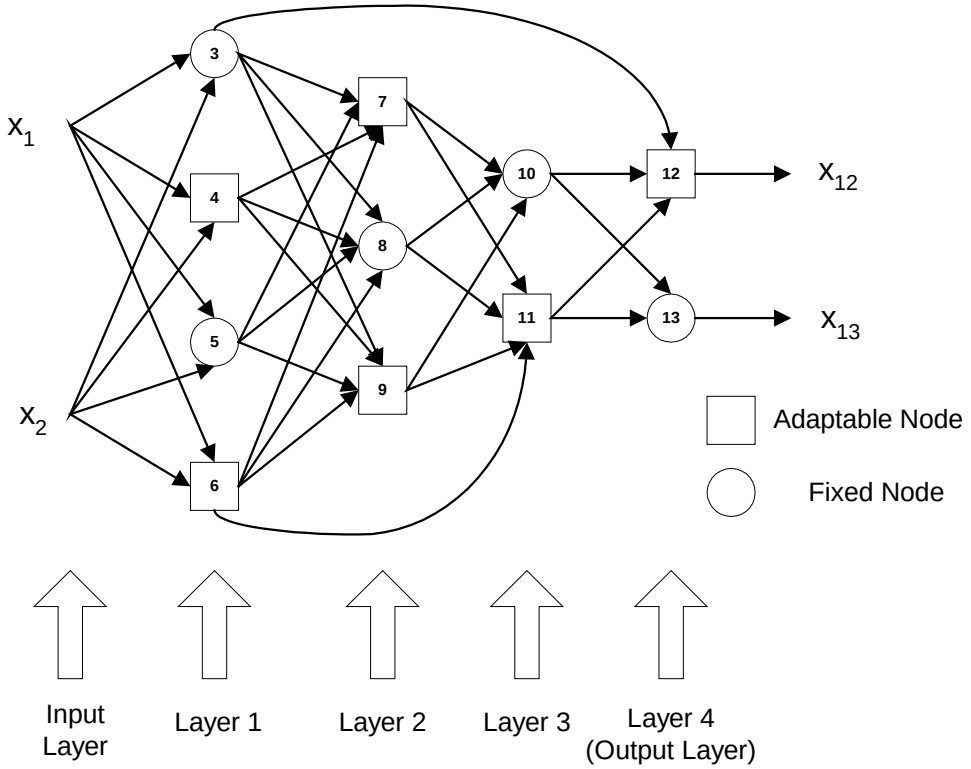

Figure 2.1 Representation of a Feedforward Neural Network

Figure 2.1 shows a connection between nodes in the previous layer and the next layers (i.e. connection from the node 6 to 11) and Figure 2.2. shows a connection between nodes in the next layer and the previous layers (i.e. connection from the node 12 to 7).

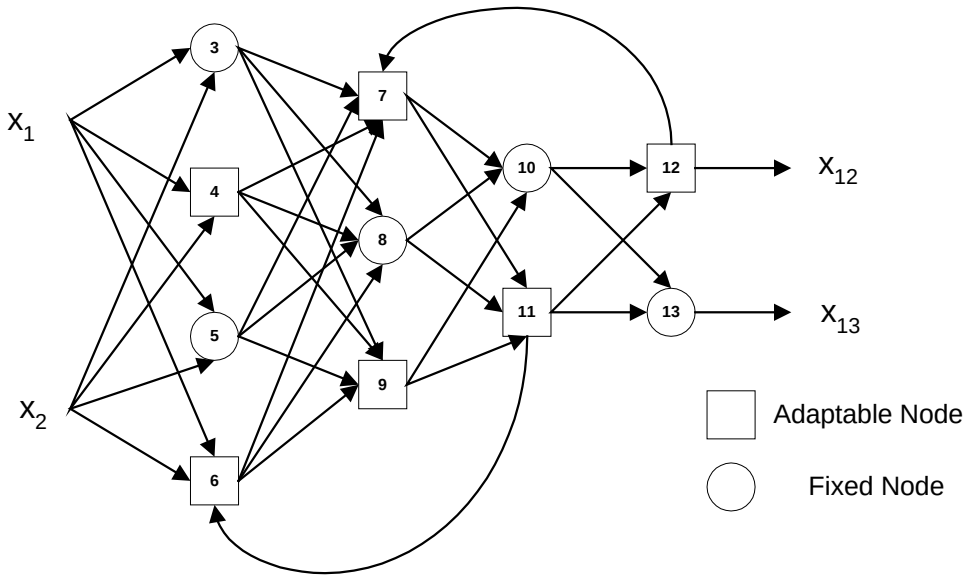

Figure 2.2 Representation of a Recurrent Neural Network

Several basic concepts about the ANNs are shown in Appendix A.1. Examples for decomposition of adaptable nodes are shown in Appendices A.1.1. After that, a briefly explanation of the training process of the ANNs was developed in the Appendix A.1.2.

2.4. Fuzzy Systems

Some physical phenomena in the real world cannot be expressed as a unique qualitative characteristic and it is necessary to define a partial form of two or more qualitative characteristics (Pinto, 2001). Frequently, the target phenomena are described only with the qualitative characteristics (with implicit uncertainties) observed by the human senses. Fuzzy logic provides the possibility of incorporating in a strict manner qualitative knowledge by means of fuzzy control. Fuzzy control applies a mapping between the continuous space and the fuzzy space. This allows us to catch the imprecision and uncertainties that are present in all real physical phenomena.

The theoretical foundation of Fuzzy Logic (FL) was developed by Lofti A. Zadeh, using the concept of fuzzy sets, which are a generalization of conventional set theory (Zadeh, 1965). Fuzzy sets were based on ideas from combined multivalued logic, probability theory, artificial intelligence (AI) and artificial neural networks (Pinto, 2001). FL has been criticised by some researchers because its mathematical treatment is quite different to the conventional mathematics (i.e. differential equations, algebraic formulas, etc). There exist qualitative models which use fuzzy rules in order to develop the fuzzy difference equations developed in this Chapter by Pinto and partners (2010). Fuzzy controllers are represented by means of fuzzy rules, which can reduce the computations required by conventional controllers. A high number of conventional computations are reduced through the use of fuzzy rules, making implementations easier and efficient.

In general, FS have been used in control and identification of industrial process and in many other fields of the science (Pinto and Madrigal, 2001). There are numerous applications of the FS. The most famous application is the Sendai's Underground in Japan. The FS include systems with any fuzzy structure mixed with another type of approach (Proportional Integral Derivative (PID) control, Nonlinear control, Optimal control, Robust control, etc).

The most popular types of fuzzy systems are: Mamdani fuzzy model (Mandani and Assilian, 1974; Mamdani, 1975), Takagi-Sugeno-Kang (TSK) fuzzy model (Takagi and Sugeno, 1985; Sugeno and Kang, 1988), Tsukamoto fuzzy model (Tsukamoto, 1979; Babuška, 1996), Singleton fuzzy model (Friedman, 1991; Jang and Sun, 1993; Brown and Harris, 1994).

Fuzzy Mapping (FM) is a nonlinear mapping technique, which transform the crisp or continuous values in fuzzy values. The aim of the FM is to reproduce the nonlinear surface of the target nonlinear plant. FM is a concept extended over such areas as algorithms, learning theory, automatons, formal languages, pattern classification, probability theory and the decision making processes. In general, nonlinear systems, systems with uncertainties in the model, unknown model process, systems with delays, complex systems have been the most successful areas of the application of the FL. A detailed explanation of the Fuzzy Systems is shown by Pinto (2001).

2.5. Neuro-Fuzzy Systems

Neuro-Fuzzy Systems (NFS) (Jang, 1992a) were based on the Takagi-Sugeno-Kang (TSK) fuzzy models (Takagi and Sugeno, 1985; Sugeno and Kang, 1988). The NFS are a combination of the ANN and the Fuzzy Systems. Also, they use feedforward adaptive networks in order to avoid the use of more complex asynchronously operated model. The objective of the NFS is to take advantage of interpretability by expert rules and the automatic learning capabilities of the FS and the ANNs (Pinto, 2004). They built the qualitative models by means of the generation of fuzzy rules from input-output data.

The NFS system uses an optimization algorithm (i.e. Backpropagation (BP) or Gradient Descent (GD), Least Square Estimator (LSE), Hybrid Learning (HL), and Genetic Algorithms (GA)) in order to compute the antecedent (nonlinear) and consequent (linear) parameters. They also reduce the modelling errors produced by human experts caused by incompleteness of expert knowledge or difficulties generating the rules and catch all the modelling uncertainties (Mourot, et. al., 1999; Gorzalczany and Gluszek, 2000). The input dimension of the NFS defines the size and complexity of the model, which grows exponentially. Higher dimension of the inputs (> 4 inputs) create a high-dimensional problems, where the optimization algorithm (i.e. BP or GD) may lead to local minimum solutions instead of the global minimum. The qualities of the input-output data are an important factor to guarantee the generation of an optimal model. In other words, the input-output data have to cover all operating ranges and they do not have to include noise.

2.5.1. Nonlinear System Modelling

Continuous nonlinear plants are commonly obtained in a discrete-time structure using the NARX (nonlinear autoregressive with exogenous input) input-output model, which is a nonlinear causal model normally used to obtain an approximate representation of a target nonlinear plant (Nørgaard, et. al., 2003; Babuška and Verbruggen, 2003):

$$y(k) = F(\mathbf{x}(k)) \tag{2.2}$$

with

$$\mathbf{x}(k) = \left[y(k-1),\ y(k-2),\cdots, y(k-Ny),\ u(k-d),\ u(k-d-1),\ldots, u(k-d-Nu)\right]^T \tag{2.3}$$

where $y(k)$ and $\mathbf{x}(k)$ are the current output approximated in the time instant k and the regressor vector expressed as a function of lagged inputs and outputs. The

constants Ny and Nu are degree of the output and input signals. The delay from the input signal to the output signal is expressed as "d".

Based on equations (2.2) and (2.3), the predicted output of the system can be expressed as follows:

$$y(k+1) = F(\mathbf{x}(k+1)) \tag{2.4}$$

and

$$\mathbf{x}(k+1) = [y(k),\ y(k-1),\cdots, y(k-Ny+1),\ u(k-d+1),\ u(k-d),\ldots, u(k-d-Nu+1)]^T \tag{2.5}$$

If the nonlinear system to identify is a single-input single-output (SISO) model then the NARX model is a multiple-input single-output (MISO) model. In order to apply this identification technique with success, it is necessary to know in advance the degree of the plant (Ny and Nu) and the delay "d"of the nonlinear system. The degree of the plant defines the amount of delayed inputs and outputs signals to be used. If the nonlinear system to identify is a multiple-input multiple output (MIMO) system then the NARX model has a MIMO (or several MISO models defined by the amount of the outputs) structure. Frequently, the model represented by equations 2.4 and 2.5 is used as predictive model of the nonlinear plant.

2.5.1.1.Neuro-Fuzzy Models

A Neuro-Fuzzy system will use its interpolation capacity of the local linear models in order to approximate the target nonlinear system. TSK Fuzzy models are in essence a Neuro-Fuzzy System (Pinto, 2004). The linguistic or qualitative modelling was the first name adopted by the fuzzy modelling (Sugeno and Yasukawa, 1993). The linguistic model for the TSK fuzzy model was defined as follows:

$$R_i : \text{If } \underbrace{\mathbf{x}(k) \text{ is } A_i}_{\text{Antescedent}} \text{ then } \underbrace{y_i(k) = f_i(\mathbf{x}(k))}_{\text{Consequent}} \quad i = 1, 2, \ldots, N \tag{2.6}$$

with $\mathbf{x}(k) \in R^p \subset X \times U$ and $y(k) \in R$

where R_i, $\mathbf{x}(k)$, A_i are the i-th fuzzy rule, the regressor vector and the i-th antecedent of the i-th fuzzy rule. $\mathbf{x}(k)$ and A_i define the antecedent part of the fuzzy rule. N is the total amount of the fuzzy rules. $y_i(k)$ is the i-th local model or consequent part. The i-th antecedent fuzzy A_i is expressed by a multivariable membership function defined by:

$$\mu_{A_i}(\mathbf{x}(k)) : R^p \rightarrow [0, 1] \tag{2.7}$$

The target nonlinear model is approximated with the contribution of each local model in the fuzzy subset $X \times U$. Equation (2.7) is used to split the input space into p-subfuzzy areas. Expressing equation (2.6) with univariate membership functions splitting the regressor vector with fuzzy relationship of conjunctions is obtained the following equation:

$$\begin{aligned} R_i : \text{If } & y(k-1) \text{ is } A_{i1} \text{ and } y(k-2) \text{ is } A_{i2} \text{ and } \ldots y(k-Ny) \text{ is } A_{i\,Ny} \text{ and} \\ & u(k) \text{ is } A_{i\,Ny+1} \text{ and } y(k-2) \text{ is } A_{i\,Ny+2} \text{ and } \ldots u(k-Nu) \text{ is } A_{i\,Nu} \\ & \text{then } y_i(k) = f_i(\mathbf{x}(k)) \quad , \; y_i(k) = y_i(\mathbf{x}(k)) \end{aligned} \tag{2.8}$$

The mathematical structure of the TSK fuzzy models was defined as follows:

$$y(k) = \sum_{i=1}^{N} \gamma_i(\mathbf{x}(k))\, y_i(\mathbf{x}(k)) \tag{2.9}$$

with

$$\gamma_i(\mathbf{x}(k)) = \frac{\prod_{j=1}^{p} \exp\left[-\frac{1}{2}\left(\frac{x_j - c_{ij}}{\sigma_{ij}}\right)^2\right]}{\sum_{i=1}^{N} \prod_{j=1}^{p} \exp\left[-\frac{1}{2}\left(\frac{x_j - c_{ij}}{\sigma_{ij}}\right)^2\right]}, \quad \sum_{i=1}^{N} \gamma_i(\mathbf{x}(k)) = 1 \quad \text{and} \quad \gamma_i(\mathbf{x}(k)) \geq 0 \tag{2.10}$$

where $y(k)$, $\gamma_i(\mathbf{x}(k))$ and $y_i(\mathbf{x}(k))$ are the output signal, the i-th normalized degree of fulfilment and the i-th local lineal model. $\mathbf{x}(k)$ is the regressor vector. x_j is the j-th input signal. c_{ij} and σ_{ij} are the i-th parameters of the membership function in the j-th subfuzzy area.

The equation (2.9) could be also expressed as follows:

$$y(k) = \frac{\sum_{i=1}^{N} \beta_i(\mathbf{x}(k))\, y_i(\mathbf{x}(k))}{\sum_{i=1}^{N} \beta_i(\mathbf{x}(k))} \tag{2.11}$$

$$\beta_i(\mathbf{x}(k)) = \mu_{A_{i1}}(y(k-1)) \times \mu_{A_{i1}}(y(k-Ny)) \times \ldots \times \mu_{A_{i\ Nu+Nu+1}}(y(k-Nu)) \tag{2.12}$$

where the degree of fulfilment is defined as $\beta_i(\mathbf{x}(k))$. Equation (2.12) uses the product operators in order to compute the minimum value of the degree of fulfilment (Pinto, 2001). Another choice is to compute the degree of fulfilment by computing the minimum of the membership functions of the $\mu_{A_{i1}}(y(k-1))$, $\mu_{A_{i1}}(y(k-Ny))$, ... $\mu_{A_{i\ Nu+Nu+1}}(y(k-Nu))$.

The structures of the local lineal models in the TSK fuzzy model define its classification. The local linear models are defined as follows:

$$y_i(\mathbf{x}(k)) = \mathbf{a}_i^T\, \mathbf{x}(k) \tag{2.13}$$

$$y_i(\mathbf{x}(k)) = b_i \tag{2.14}$$

$$y_i(\mathbf{x}(k)) = \mathbf{a}_i^T\, \mathbf{x}(k) + b_i \tag{2.15}$$

where $\mathbf{a}_i$ and b_i are the i-th parameter vector and the i-th offset constant of the local model. Equations (2.13) and (2.14) define the homogeneous local linear models and local linear singleton (weighting). Equation (2.15) defines the piece-wise local linear models or Polytopic Linear Model (PLM). A complete analysis about PLM's properties was exposed by Angelis (2001). TSK models represent one of the most used models for identification, modelling, control, condition monitoring and fault detection (Pinto, 2004; Pinto, 2006). A more complete classification of the TSK fuzzy systems are shown in the Appendix A.2. It shows the fuzzy rules and the linguistic model belonging to each TSK fuzzy system.

2.5.1.1.1. Takagi-Sugeno-Kang Fuzzy Models

Takagi-Sugeno-Kang (TSK) models were developed using local linear models, which are overlapping trying to produce smooth changes between the linear regions of the nonlinear process (Pinto, 2006).

The last decade has been used to developed different mathematical analysis and development of the TSK models. A complete analysis of the dynamic TSK fuzzy model based in local linearization using Taylor's Series reveal that the local behaviour of the nonlinear system is only valid for an area near to the point selected for the linearization (Johansen, et. al., 2000).

The properties as a universal approximator of the TSK fuzzy models was proved and studied in (Ying, 1995; Wang, 1997; Ying, et. al., 1999; Wang and Wei, 2000; Spooner, et. al., 2002). Tanaka and Sugeno (1992) found a common symmetric positive definite matrix *P* for *N* subsystems, which defined the stability of the TSK fuzzy models. One of the most important results of the previous papers was the

Tanaka's stability theorem for TSK fuzzy systems. A stability analysis of the second order fuzzy systems was developed by (Kawamoto, et. al., 1992). A new methodology used to find the common matrix using the Linear Matrix Inequality (LMI) was developed by Tanaka (1995). Xia and Chai (1995) used the ad hoc membership values in order to establish a stability condition.

A control design and stability analysis were also developed by (Wang, et. al., 1995; Zhao, 1995) using the quasi-linear structure of the homogeneous TSK fuzzy models. Tanaka and partners (1996) studied the new stability conditions for the TSK fuzzy models applying Quadratic stability, H_∞ control theory and Linear Matrix Inequalities (LMI). Stability analysis frequency methods for MIMO TSK fuzzy models were studied in (Cuesta, et. al., 1999) in order to find multiple equilibrium points or limit cycles. Some applications and studies using LMI were developed in (Tanaka and Wang, 2001). A stability analysis founded in multiple Lyapunov's functions was studied in (Tanaka, et. al., 2003). Kim (2004), studied a Bilinear Matrix Inequalities approach applied to the stability analysis of the Zero-Order TSK fuzzy models.

Example of Takagi-Sugeno-Kang Model

The best way to show the concept of the TSK fuzzy (ANFIS) systems is using an example of a TKS fuzzy system with 2 inputs, 4 fuzzy rules and 4 affine local linear models. The input space was partitioned into 4 fuzzy regions, because of the amount of the inputs and fuzzy sets (Pinto, 2006).

The Fuzzy model of the previous ANFIS defined is represented by four fuzzy rules and expressed as follows:

$$R_i: \text{If } x_1 \text{ is } A_i \text{ and } x_2 \text{ is } B_i, \text{ then } y_i = p_i x_1 + q_i x_2 + b_i;\ i = 1,\ldots,N.\ N = 4. \tag{2.16}$$

Expressing the TSK fuzzy model by the final expression was obtained:

$$y = \sum_{i=1}^{N=4} \gamma_i(x_1, x_2)\, y_i = \sum_{i=1}^{N=4} \gamma_i(x_1, x_2) \left\{ \begin{bmatrix} p_i & q_i \end{bmatrix} \begin{bmatrix} x_1 \\ x_2 \end{bmatrix} + b_i \right\} = \sum_{i=1}^{N=4} \gamma_i(x_1, x_2) \left[\mathbf{a}_i^T \begin{bmatrix} x_1 \\ x_2 \end{bmatrix} + b_i \right]$$

$$= \sum_{i=1}^{N=4} \gamma_i(x_1, x_2) \begin{bmatrix} p_i & q_i \end{bmatrix} \begin{bmatrix} x_1 \\ x_2 \end{bmatrix} + \sum_{i=1}^{N=4} \gamma_i(x_1, x_2)\, b_i \qquad (2.17)$$

with

$$\mathbf{a}_i^T = \begin{bmatrix} p_i & q_i \end{bmatrix}, \quad \sum_{i=1}^{N=4} \gamma_i(x_1, x_2) = 1 \;\; and \;\; \gamma_i(x_1, x_2) \geq 0 \quad \gamma_i(x_1, x_2) = \gamma_i(\mathbf{x}),\ \mathbf{x} = \begin{bmatrix} x_1 \\ x_2 \end{bmatrix}$$

Expressing the previous TSK fuzzy model as affine linear model:

$$y = \mathbf{C}\,\mathbf{x} + b \qquad (2.18)$$

where,

$$\mathbf{C} = \sum_{i=1}^{N=4} \gamma_i(x_1, x_2) \begin{bmatrix} p_i & q_i \end{bmatrix} \quad ; \quad b = \sum_{i=1}^{N=4} \gamma_i(x_1, x_2)\, b_i \qquad \mathbf{x} = \begin{bmatrix} x_1 & x_2 \end{bmatrix}^T$$

where $\mathbf{x}$ and $\gamma_i(x_1, x_2)$ are the regressor vector and the normalized degree of fulfilment.

The equivalent architecture of the corresponding Neuro-Fuzzy Model (NFM) is shown in the Figure 2.3, which have two input, one output and five layers.

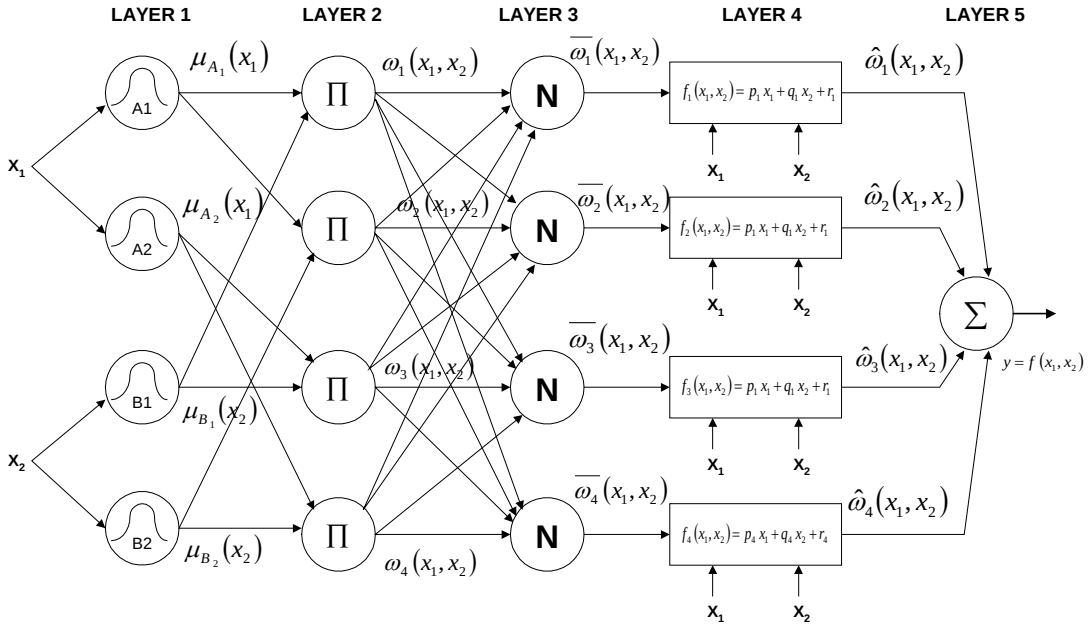

Figure 2.3 Neuro-Fuzzy System with 2 Inputs and 1 Output

The training objective is based on the error comparing the output signal of the NFS with the output signal of the target plan to be identified. Layer 5 produce a nonlinear function developed in detail in the Appendix A 2.2 with the equation (A.20). Before the analysis of the NFS layer by layer was necessary to establish the following equality:

$$\gamma_i(x_1, x_2) = \overline{\omega}_i(x_1, x_2) \tag{2.19}$$

where $\gamma_i(x_1, x_2)$ is the normalized degree of fulfilment. The signal processing and the analysis of the variables in each Layer of the Figure 2.3 are shown in Appendix A.2.2. It shown how the direct and invert fuzzy mapping is developed, proving that the output of the NFS is a nonlinear function.

2.5.2. Training Methods for Fuzzy Systems

The training methods most generally used in NFSs are the same ones used to train the ANNs because the NFSs are in essence a hybrid combination between the ANNs and Fuzzy Systems (Pinto, 2005). The optimization techniques usually used are the Steepest Descent (SD) (also called Gradient Descend (GD) or Backpropagation (BP)) algorithm and the Hybrid Learning (HL) approach. The HL rule is a combination of the BP (or SD) algorithm and the Least-Square Estimator (LSE). Both BP and HL methods are used in identification, modelling and control.

First at all, the input and output variables of the nonlinear process have to be identified in order to select the input and output signals of the NFSs. In the present section the GD method was developing using a matrix approach and it was described by equations (2.20) to (2.23), making easier the application of the GD optimization algorithm. The gradient descend matrix approach was developed for the NFS shown in Figure 2.3 (with 2 inputs signals). Based on the analysis of the GD algorithm the new matrix form for the GD Algorithm was developed (one of the chapter contribution). It was developed as follows:

$$\mathbf{f}_{l,j} = \left[f_{l,1}, \cdots, f_{l,4} \right]^T \tag{2.20}$$

where $f_{l,i} = x_{l-1,\,i} \left(p_i\, x_1 + q_i\, x_2 + b_i \right) \qquad i = 1,\ldots,4. \quad l = 4$

$$\mathbf{E}_{l+1,\,j} = \left[\in_{l+1,1}, \ \cdots, \in_{l+1,4} \right]^T \tag{2.21}$$

$$\mathbf{E}_{l,\,j} = \left[\in_{l,1}, \ \cdots, \in_{l,4} \right]^T \tag{2.22}$$

$$\mathbf{E}_{l,\,j} = \mathbf{E}_{l+1,\,j}\, \mathbf{J}\left(\frac{\partial \mathbf{f}_{l,\,j}}{\partial \mathbf{x}_{l,\,j}} \right) \Bigg\{ \begin{array}{l} l = 1,\ldots,m \\ j = 1,\ldots,N(l) \end{array} \tag{2.23}$$

where $\mathbf{E}_{l,\,j}$ and $\mathbf{E}_{l+1,\,j}$ are the backpropagation error vectors of the $(l+1)\_th$ and $\bar{l}\_th$ layers. $\mathbf{J}\left(\frac{\partial \mathbf{f}_{l,\,j}}{\partial \mathbf{x}_{l,\,j}} \right)$ is the Jacobian matrix of the activation function of the l_th layer. The number of the layer and the node are defined by l and j, respectively.

The training methods are easily explained in Appendix A.3. An example for the application of the Backpropagation (or Gradient Descent) algorithm layer by layer was developed in Appendix A.3.2.

As it is well known, in order to apply the LSE in the NFSs, it is necessary to define the complete system with the following structure:

$$A\theta = y \tag{2.24}$$

where A and θ are the constant parameter matrix and the unknown parameter vector, respectively.

The BP (or SD) is applied to the antecedent (nonlinear) and LSE algorithm is applied to the consequent (linear) parameters in the HL algorithm. The complete application of the HL algorithm is shown in Appendix A.3.3.

The NFS are in essence an ANN and a FS, taking from each approach the advantages in order to compensate the weaknesses of each other. The NFS are a type of Nonlinear Adaptive Structure, able to learn as an ANN, using a different type of learning algorithm (Nauck, 1997). Also, these can be expressed by Fuzzy Rules (IF THEN), making the physical meaning of the model more clear. Jang and co-workers (1997) demonstrated that the speed of convergence of the NFSs is faster than the speed of convergence of the ANNs.

In the next section a novel nonlinear difference equation based on the NFSs will be introduced. This represents another tool for the formal analysis and design of stability and convergence.

2.6. Neuro-Fuzzy Difference Equation

The main contribution of the chapter was the development of the novel Neuro-Fuzzy Difference Equations (NFDE). The NFDE were in essence developed using dynamic TSK fuzzy models with NARX model structure (Pinto, et. al., 2006; Pinto, et. al., 2010).

NFDE are linguistic (or qualitative) models, which originate from expert rules obtained from the knowledge of the physical laws. The NFDE are classified as gray box because the expert rules provide the NFS some physical meaning using a linguistic model.

2.6.1. State of the Art of Fuzzy Differential and Fuzzy Difference Equations

Developing the fuzzy differential equations in order to obtain the model of a nonlinear system always has been the crucial point in the interpreting of the physical meaning, the analysis and the interpretation of the fuzzy models using the fuzzy rules. The majority of the developments for the fuzzy equations have been on continuous time. Tanaka and partners (1992; 1996) presented one of the first fuzzy differential equations using the semiformal treatment (Fuzzy rules). Many

semiformal fuzzy differential equation were solved using some linear technique by Buckley (1990; 1991a; 1991b; 1992a; 1992b; 1995) and Zhang (1998a; 1998b). Buckley and Feuring (1999a; 1999b) studied the frequency/time domain methods for solutions of N-order and fuzzy partial differential equations.

Leland (1995), considered the fuzzy differential equation with fuzzy inputs and fuzzy initial conditions as a fuzzy systems. He obtained a partial differential equations for a membership function using a fuzzy sample path approach and obtained a fuzzy convex solution under sufficient continuous condition. The concept of differentiation as a generality of the H-differentiability of Puri and Ralescu (1983), for the Cauchy problem of the fuzzy differential equations $x^{'} = f(x,t),\ x(t_0) = x_0$, when $f(\cdot)$ is meant to fulfill the Lipschitz condition was developed by (Song and Wu, 2000).

The Hurukawa´s derivative was used for the formulation of the fuzzy differential equations and the results did not reproduce the varied and rich behaviour of the normal differential equations (Phil, 2000). Also, Phil studied the properties of stability (Lyapunov), attraction, and periodicity founded on the interpretation of differential inclusions. The global existence of the solution for the fuzzy differential equation was proved for several results in (Song, et. al., 2000). Park and Han (2000), used the Hasegawa's functionals and successive approximation in order to show the existence and uniqueness of fuzzy solutions of the equations $du(t)/dt = f(t,u(t)),\ u(0) = u_0 \in E^n$. New solutions for the first-order systems were introduced for the linear and nonlinear cases by (Bucley and Feuring, 2000a). The solution to the nonlocal fuzzy differential equation using the contraction principle was proved using the existence and uniqueness theorem by Park and partners (2000). Two solution methods of the n^{th}-order linear differential equation were presented in (Bucley and Feuring, 2001).

Galavec (2001), presented the necessary and sufficient conditions for the problem of solvability and the problem of unique solvability for a fuzzy relation equation. Vorobiev and Seikkala (2002) developed a comparative analysis about the two

theories of the fuzzy differential equations and several new definitions of solutions for the fuzzy differential equations. The study of unique solution or equilibrium point of the following fuzzy difference equation $x_{n+1} = A + x_n / x_{n-m}$, $n = 0, 1, \ldots$ *and* $m \in \{1, 2, \ldots\}$, with x_n and A are a sequence of fuzzy numbers and fuzzy number was made in (Papaschinopoulos and Papadopoulos, 2002).

Linear systems of fuzzy differential equations were used to present the theory of state transition matrices (Diamond, 2002). Xue and Fu, (2002) established the existence of solution using Caratheodory condition for fuzzy differential equations with right-hand side. If a tangency condition is satisfied and there exist a maximal solution to an appropriate differential equation then there is a viable solution to differential inclusions (Agarwal, et. al., 2005). Takagi-Sugeno-Kang models have been used for representing some linear models and it has been demonstrated to be more realistic and reliable models (Mastorakis, 2004).

2.6.2. Development of Neuro-Fuzzy Difference Equations (NFDE)

A previous work was the main motivation to find the Neuro-Fuzzy Difference Equation (NFDE) or Fuzzy Difference Equation (FDE) in the formal manner (Pinto, et. al., 2004). A formal NFDE (or FDE) was founded using the property of a universal approximator of the neuro-fuzzy systems and the NARX model structure of nonlinear model (Pinto, et. al., 2006). In this section the Neuro-Fuzzy Model was taken as a universal approximator and also as another alternative of solution for a difference equation in order to demonstrate its relationship with the formal mathematics.

Definition 1. A fuzzy model was defined without loss the generality as a multi-input single-output (MISO) system $f : U \subset R^n \mapsto V \subset R$, where the input space (Cartesian product) U is defined as $U = U_1 \times U_2 \times \cdots \times U_n = X_{j=1}^{n} U_j \subset R^n$ and the output space is defined as $V \subset R$ (Lee, 1990a).

Theorem 1 of the Universal Approximation Theorem (Wang, 1997). A smooth real continuous dynamic linear or nonlinear $g(\mathbf{x}(t))$ process was defined on the Universe of discourse U is a compacted set in R^n . Moreover, there exists a fuzzy system $f(\mathbf{x}(t))$ (for dynamic systems) and a small real constant $\varepsilon > 0$, such that (see Figures 2.4):

$$\sup_{\mathbf{x}(t)\in U} \left| f(\mathbf{x}(t)) - g(\mathbf{x}(t)) \right| < \varepsilon \quad \text{(for a dynamic function)} \tag{2.25}$$

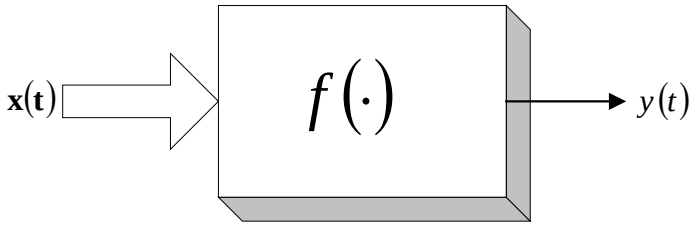

Figure 2.4 Universal Approximators for Dynamic Functions

where t is the time and $f(\bullet)$ is a dynamic function and $\mathbf{x}(t)$ is a regressor vector which contain dynamic information of process (states, inputs and outputs). This theorem is based on the proof of the Stone-Weierstrass Theorem (Wang, 1997). Proof: See Appendix A.4.

Theorem 2 (Stone-Weierstrass). Let Z be a set of teal continuous function on a compact set U. If (i) Z is an algebra, that is, the set Z is closed addition, multiplication, and scalar multiplication; (ii) Z separates points on U, that is, for every $x, y \in U$, $x \neq y$, there exist $f \in Z$ such that $f(x) \neq f(y)$; and (iii) Z vanishes at no point of U, that is, for each $x \in U$ there exist $f \in$ Z such that $f(x) \neq 0$; then for any real continuous function $g(x)$ on U and arbitrary $\in > 0$, there exists $f \in Z$ such that $\sup_{x\in U} \left| f(x) - g(x) \right| < \varepsilon$. Proof: See Rudin (1976).

Definition 2. A universal approximator called Neuro-Fuzzy (Takagi-Sugeno-Kang model) system $f(\mathbf{x}(t))$ is represented by fuzzy rules as follows (Pinto, 2004):

$$R_i: \text{If } \underbrace{\mathbf{x}(t) \text{ is } A_i}_{\text{antescedents}} \text{ then } \underbrace{y_i = a_i^T \mathbf{x}(t) + b_i}_{\text{consequent}} \quad , \quad i = 1, 2, \cdots, N \tag{2.26}$$

where R_i is the i-th fuzzy rule, A_i is the i-th fuzzy set, $\mathbf{x}(t)$ is the regressor vector $\left(\mathbf{x}(t) \in X \subset R^{Ny+Nu+1}\right)$, y_i is the i-th linear model $(y_i \in R)$, $\mathbf{a}_i$ is the i-th consequent parameter vector, b_i is the i-th scalar offset and K is the numbers of the rules.

Theorem 3. The Fuzzy system can approximate whatever smooth function if and only if it satisfies (Verdult, 2002):

$$y(t) = f\left(y(t-1),\ y(t-2),\ \cdots, y(t-Ny),\ u(t),\ u(t-1),\ \cdots,\ u(t-Nu)\right) \tag{2.27}$$

$$Nu \le Ny \le 2\,Nu + 1$$

where $y(t-1),\ y(t-2),\ \cdots, y(t-Ny),\ u(t),\ u(t-1),\ \cdots,\ u(t-Nu)$ are the time lagged inputs and outputs. *Ny* and *Nu* define the order of the some state-space system. Figure 2.5 shows the Universal Approximator with its input-output signals.

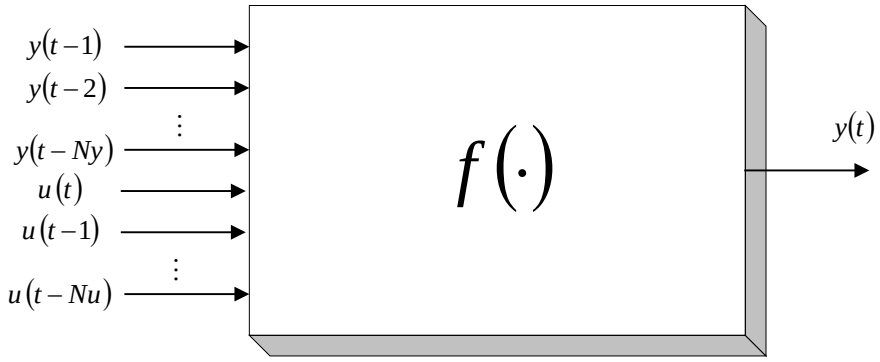

Figure 2.5 Fuzzy System as Universal Approximator

Note: Proof for Theorem 4 was developed in Appendix A.5.

Definition 5: A continuous nonlinear systems of the form (2.3) can be expressed as discrete nonlinear systems represented by the following:

$$\mathbf{x}^1(k+1) = \mathbf{F}_1\left(\mathbf{x}^1(k), \mathbf{u}(k)\right) \tag{2.28}$$

where $\mathbf{x}^1(k) \in R^{Ny}$, $\mathbf{u}(k) \in R^{Nu+1}$

Definition 6. A special type of Fuzzy system is the Neuro-Fuzzy system, which is a combination of a Fuzzy system and an Artificial Neural Network, which could be represented by following (Pinto, 2004):

$$y(t) = \sum_{i=1}^{K} \gamma_i(\mathbf{x}(t))\, y_i(\mathbf{x}(t)) \tag{2.29}$$

with

$$\gamma_i(\mathbf{x}(t)) = \frac{\prod_{j=1}^{p} \mu_{Aij}\left(x_i; c_{ij}; \sigma_{ij}\right)}{\sum_{i=1}^{K} \prod_{j=1}^{p} \mu_{Aij}\left(x_i; c_{ij}; \sigma_{ij}\right)} \tag{2.30}$$

and

$$\mu_{Aij}\left(x_i; c_{ij}, \sigma_{ij}\right) = \exp\left(-\frac{\left(x_j - c_{ij}\right)^2}{2\sigma_{ij}^2}\right) \tag{2.31}$$

and

$$y_i(\mathbf{x}(t)) = \mathbf{a}_i^T\, \mathbf{x}(t) + b_i \tag{2.32}$$

and

$$\mathbf{x}(t) = \left[y(t-1), \ldots, y(t-Ny), u(t), u(t-1), \ldots, u(t-Nu+1)\right]^T \tag{2.33}$$

where $\gamma_i(\mathbf{x}(t))$ is the i-th nonlinear function of the weighted average of the regressor, $\mathbf{x}(t)$ is the regressor vector and $\mu_{A_{ij}}(x_i; c_{ij}, \sigma_{ij})$ is the membership function with a Gaussian function and $y_i(x(t))$ is the i-th linear function, x_i is the i-th input and c_{ij} and σ_{ij} are the i-th set of fuzzy parameters in the j-th membership functions.

Theorem 4. A nonlinear plant is represented by a dynamic NARX model using a Neuro-Fuzzy system, which defines a Fuzzy Difference Equation, and an optimal solution for the dynamic system. The Fuzzy Difference Equation for SISO systems is represented as follows:

$$y(t) = \sum_{j=1}^{Ny} \sum_{i=1}^{N} \gamma_i \, a_i^j \, y(t-j) + \sum_{j=0}^{Nu} \sum_{i=1}^{N} \gamma_i \, c_i^j u(t-j) + \sum_{i=1}^{N} \gamma_i \, b_i \tag{2.34a}$$

or

$$y(t) = \sum_{i=1}^{N} \gamma_i \left(\mathbf{a}_i^T \, \mathbf{x}(t) + b_i \right) \tag{2.34b}$$

where a_i^j, c_i^j and b_i are the ij[th] optimal parameters of the affine-linear model. $y(t-j)$ and $u(t-j)$ are the delayed outputs and inputs. Ny and Nu define the order of the nonlinear system. N is the amount of the fuzzy rules. For simplicity the normalized degree of fulfilment $\gamma_i(\mathbf{x}(k))$ is expressed as γ_i.

In the case of MIMO systems the Fuzzy Difference Equation is expressed as follows:

$$y_M = \sum_{l=1}^{m} \sum_{j=1}^{N_y} \sum_{i=1}^{N} \gamma_{i,M} \, a_{i,l,M}^j \, y_l(t-j) + \sum_{z=1}^{n} \sum_{j=1}^{N_u} \sum_{i=1}^{N} \gamma_{i,M} \, c_{i,z,M}^j \, u_z(t-k) + \sum_{i=1}^{N} \gamma_{i,M} \, b_{i,M} \tag{2.35a}$$

or

$$y_M(t) = \sum_{i=1}^{N} \gamma_{i,M} \left(\mathbf{a}_{i,M}^T \, \mathbf{x}(t) + b_{i,M} \right) \tag{2.35b}$$

where M belongs to the M[th] output signal. m and n are the m[th] input signal and the n[th] output signal. N_y and N_u define the order of the nonlinear system. N is the numbers of the fuzzy rules.

See the proof of Theorem 4 in Appendix A.6.

Example 2.1. Fuzzy Difference Equation: Nonlinear SISO case

The nonlinear system is a Magnet suspended above an electromagnetic, where the allowed movement is vertical. It is shown in Figure 2.6.

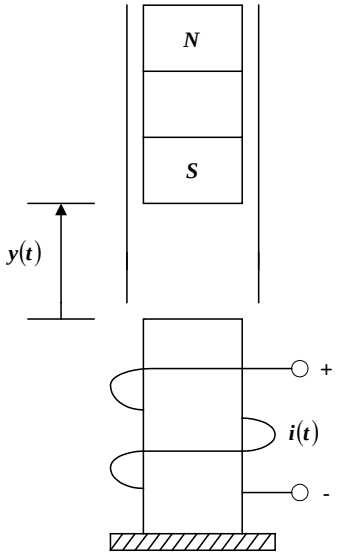

Figure 2.6 Magnet Suspended Above an Electromagnet

The dynamic equation, which describes the nonlinear system, is expressed as:

$$\frac{d^2 y(t)}{dt^2} = -g + \frac{\alpha}{M}\frac{i^2(t)}{y(t)} - \frac{\beta}{M}\frac{d\,y(t)}{dt} \tag{2.36}$$

where $y(t)$, $i(t)$, M, g, β and α are the distance of the magnet above the electromagnet, the current flowing in the electromagnet, the mass of the magnet, the gravitational constant, the viscous friction coefficient (depend of the material in which the magnet move) and the field strength constant, which is a function of the number of turns of wire on the electromagnet and the strength of the magnet. The values for the constants are as follows:

$M = 3kg;\ \ g = 9.8 m/s^2;\ \ \beta = 12;\quad \alpha = 15$

The nonlinear dynamic system describes the position of a magnet suspended above an electromagnet, where the movement of the magnet is only allowed vertically.

The input signal was generated (in a SIMULINK environment) by the addition and substraction of unit step signals combined with the white noise which covers all operating range as shown in Figure 2.7. The output signals obtained with the training data (red line), the ANFIS (blue line) and the fuzzy difference equation (dash-dot green line) are shown in Figure 2.8. The simulation results are very similar (lines overlapping between them) for the ANFIS and the fuzzy difference equation compared with the training on data. The accuracy of the solution for the fuzzy difference equation depends the amount of the input signal initially chosen for the neuro-fuzzy system (ANFIS), which will be transformed to a fuzzy difference equation using the procedure described in this section. Also, all the factors which affect the accuracy of the ANFIS, will also affect the solution of the fuzzy difference equation.

The block diagram of the Dynamic MISO Neuro-Fuzzy model is shown in Figure 2.9. The MISO Neuro-Fuzzy model takes the lagged of the input $\big(i(t)\big)$ and output $\big(y(t)\big)$ signals to obtain the nonlinear model. It was used to identify the SISO nonlinear plant represented by the Levitation System. After the training process, the dynamical behaviour of this structure should approximate the nonlinear plant.

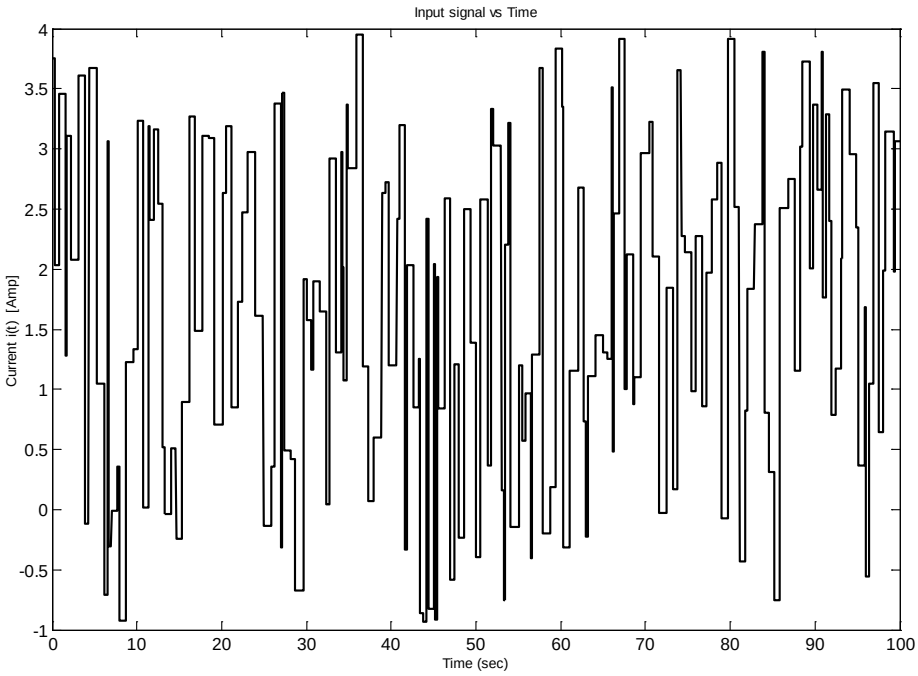

Figure 2.7 Input Signal Applied to the Open Loop System

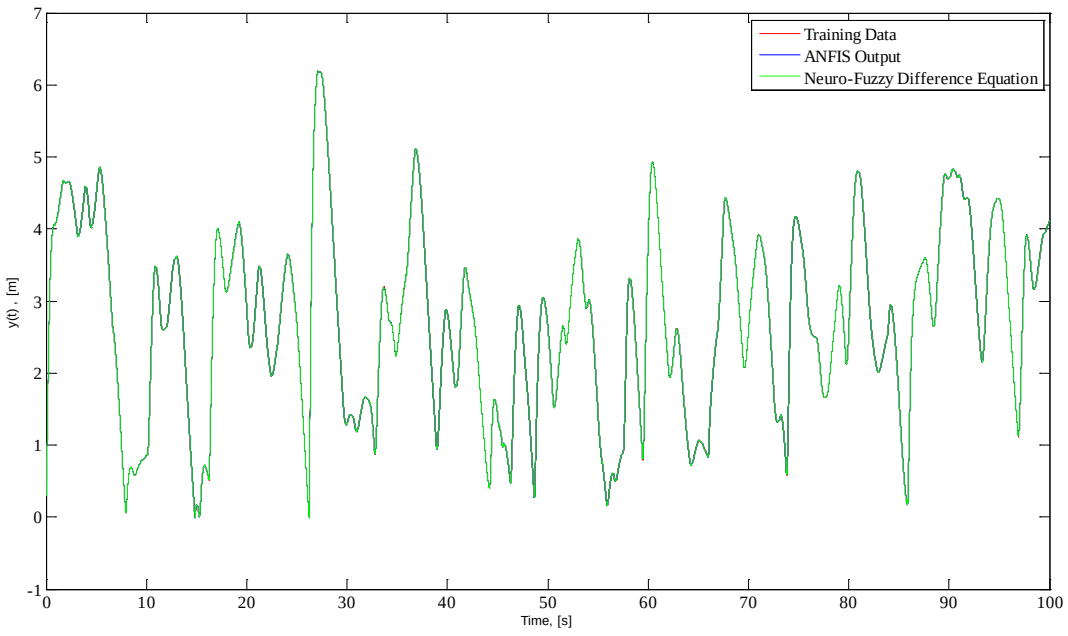

Figure 2.8 Output Signal of the Open Loop System

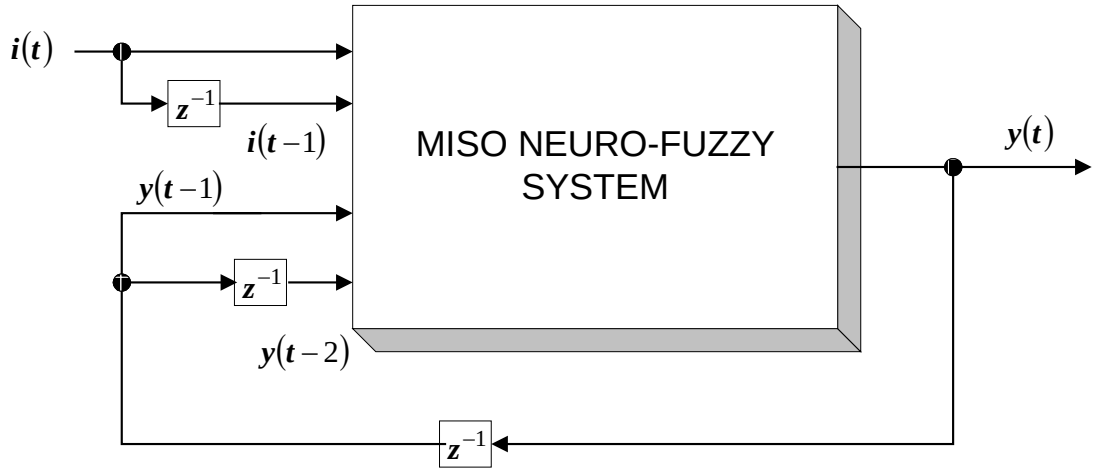

Figure 2.9 Block Diagram of the Dynamic MISO Neuro-Fuzzy Model

Membership functions build continuous nonlinear function by intervals (covering all operating range by sections of input space intervals). There are four inputs signals $\big(i(t), i(t-1),\ y(t)$ and $y(t-1)\big)$ shown in Figure 2.9. These membership functions develop the fuzzy mapping of the continuous (real) values and they are used implicitly in the normalised degree of fulfilment defined by the equation (2.39).

The regressor vector $\mathbf{x}(\mathrm{t})$ and the set of input variables x_j for the nonlinear plant are defined as follows:

$$\mathbf{x}(\mathrm{t}) = \left[i(\mathrm{t}), i(\mathrm{t}-1), y(\mathrm{t}-1), y(\mathrm{t}-2)\right]^T \tag{2.37}$$

$$x_j = \left\{i(\mathrm{t}), i(\mathrm{t}-1), y(\mathrm{t}-1), y(\mathrm{t}-2)\right\} \tag{2.38}$$

The normalised degree of fulfilment is expressed as follows:

$$\gamma_i(k) = \frac{\prod_{j=1}^{4} \exp^{-\frac{1}{2}\left(\frac{x_j - c_{ij}}{\sigma_{ij}}\right)^2}}{\sum_{i=1}^{16} \prod_{j=1}^{4} \exp^{-\frac{1}{2}\left(\frac{x_j - c_{ij}}{\sigma_{ij}}\right)^2}} \tag{2.39}$$

For simplicity $\gamma_i = \gamma_i(k)$

where the sets of nonlinear (antecedent) parameters are defined as follows:

c_{ij} = {-0.9349, 3.951, -0.001585, 6.19, 0.001279, 6.187, -0.9355, 39.5}

σ_{ij} = {2.075, 2.074, 2.627, 2.625, 2.631, 2.625, 2.076, 2.076}

i=1, 2, ..., 16; j =1, ..., 4.

Finally, the output signal of the Neuro-Fuzzy model can be expressed as follows:

$$y(t)=\sum_{i=1}^{16}\gamma_i\ y_i=\sum_{i=1}^{16}\gamma_i\left\{\begin{bmatrix}p_i & q_i & r_i & s_i\end{bmatrix}\begin{bmatrix}i(t)\\ i(t-1)\\ y(t-1)\\ y(t-2)\end{bmatrix}+t_i\right\} \tag{2.40}$$

with the sets of linear (consequent) parameters defined as follows:

p_i = {0.1945, -0.06183, 9.229, 3.829, -10.15, -3.579, 0.28, -0.04436, 0.4415, -0.2966, -5.966, 3.703, 4.814, -3.074, 0.4214, -0.1752}

q_i = {1.426, -2.0306, 3.878, -4.017, 1.572, 16.56, 2.176, 5.445, 10.6, 0.284, -32.79, 22.12, 4.792, -16.3, -4.008, 3.121}

r_i = {-0.404, 3.951, -1.697, 11.71, -1.557, -18.95, -1.129, -3.914, -10.34, 0.6775, 17.04, -17.17, 8.741, 13.33, 4.271, -2.118}

s_i = {-0.1427, -0.2246, -9.144, 0.9041, 9.922, -0.08219, -0.2224, -0.292, 0.1177, 0.3572, 4.708, -2.8, -5.263, 2.024, 0.1556, 0.2275}

t_i = {0.1274, 1.268, -2.359, -12, 1.61, -1.289, -0.2396, -2.925, -1.881, -0.2108, 19.81, -16.26, -2.893, 17.01, 3.902, -0.239}

Simplifying the equation (2.40) will lead to the following neuro-fuzzy difference equation:

$$y(t)=\left(\sum_{i=1}^{16}\gamma_i\, p_i\right)i(t)+\left(\sum_{i=1}^{16}\gamma_i\, q_i\right)i(t-1)+\left(\sum_{i=1}^{16}\gamma_i\, r_i\right)y(t-1)+\left(\sum_{i=1}^{16}\gamma_i\, s_i\right)y(t-2)+\left(\sum_{i=1}^{16}\gamma_i\, t_i\right) \tag{2.41}$$

or

$$y(t)=\frac{\left[\left(\sum_{i=1}^{16}\gamma_i\, p_i\right)+z^{-1}\left(\sum_{i=1}^{16}\gamma_i\, q_i\right)\right]i(t)+\left(\sum_{i=1}^{16}\gamma_i\, t_i\right)}{\left[1+z^{-1}\left(\sum_{i=1}^{16}\gamma_i\, r_i\right)+z^{-2}\left(\sum_{i=1}^{16}\gamma_i\, s_i\right)\right]} \tag{2.42}$$

Equations (2.41) and (2.42) represent the fuzzy (nonlinear) difference equations of the nonlinear system. The structure of the equation (2.42) was expressed like a fuzzy (nonlinear) filter. The fuzzy difference equation is a MISO Neuro-Fuzzy model with 16 fuzzy rules (called linguistic model) and it has the nonlinear dynamics of the target nonlinear plant (Pinto, 2006). Theorem 4 was used as the fundamental to develop the Fuzzy Difference Equation for the nonlinear system. For the particular nonlinear system were used only 2 membership functions, enough to obtain the Neuro-Fuzzy model. The shape of the membership function is not important.

Example 2.2 Fuzzy Difference Equation: Nonlinear MIMO Case – Real Time Application

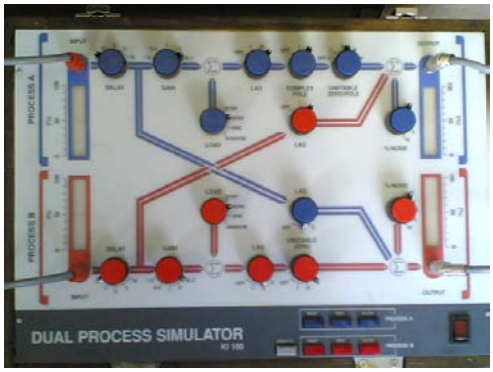

Figure 2.10 Dual Process Simulator KJ 100

The process selected is a MIMO nonlinear system, which was the *KRi Dual Process Simulator KI 100*, which is shown in Figure 2.10.

The simulator is able to produce a MIMO nonlinear process with several dynamic behaviours (KRI, 2006). For simplicity the variable "t" is the same as the sampling variable "k".

The input signals were generated combining a successive addition of unit steps signal with a white noise zero mean in order to produce the each input signal. The combination process of the input signals was developed in LabView. The input signals were feeding to each channel covering all operating range of the process (0-5 volts). Figures 2.11 and 2.12 show the inputs signals applied to process and the output signals produced for the process.

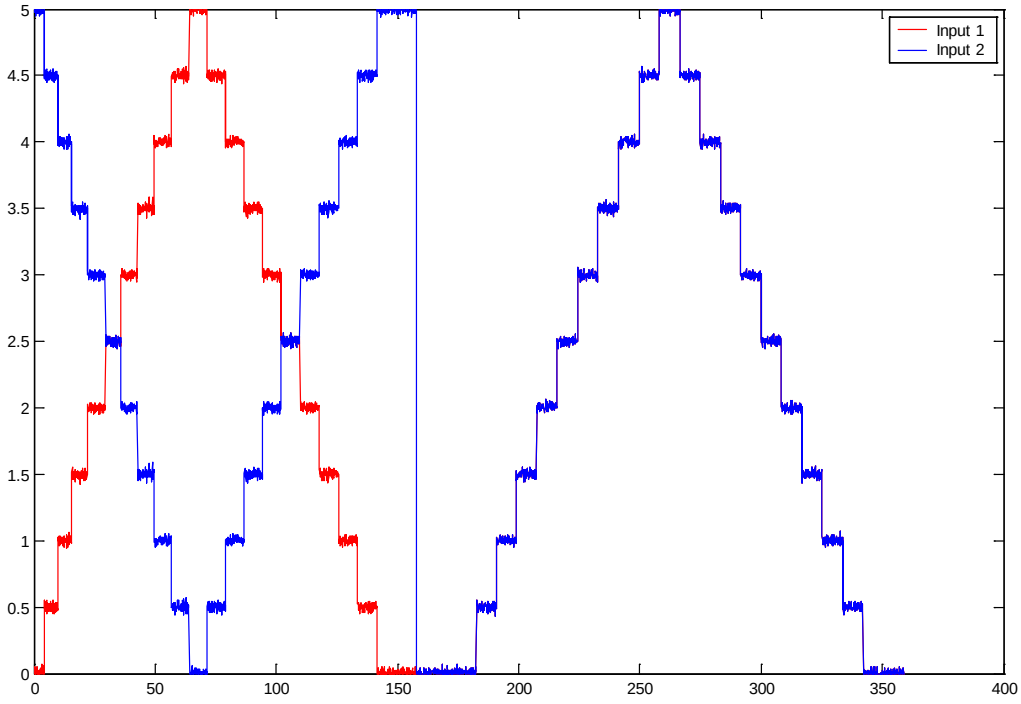

Figure 2.11 Inputs signals: Inputs u1(t) and u2(t) are the red line and the blue line, respectively.

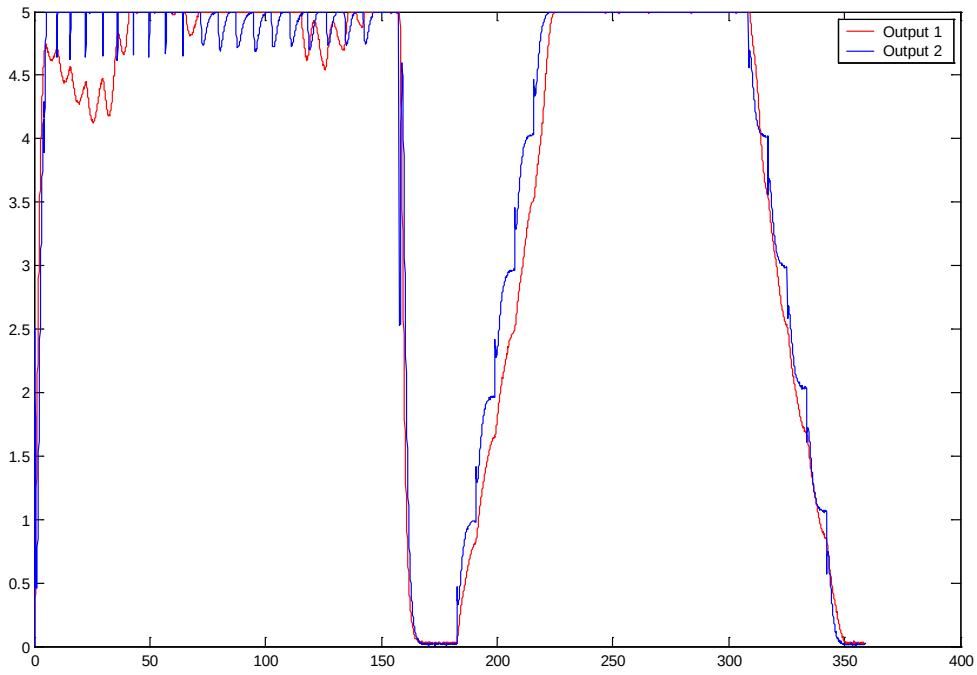

Figure 2.12 Outputs signals: Outputs u1(t) and u2(t) are the red line and the blue line, respectively.

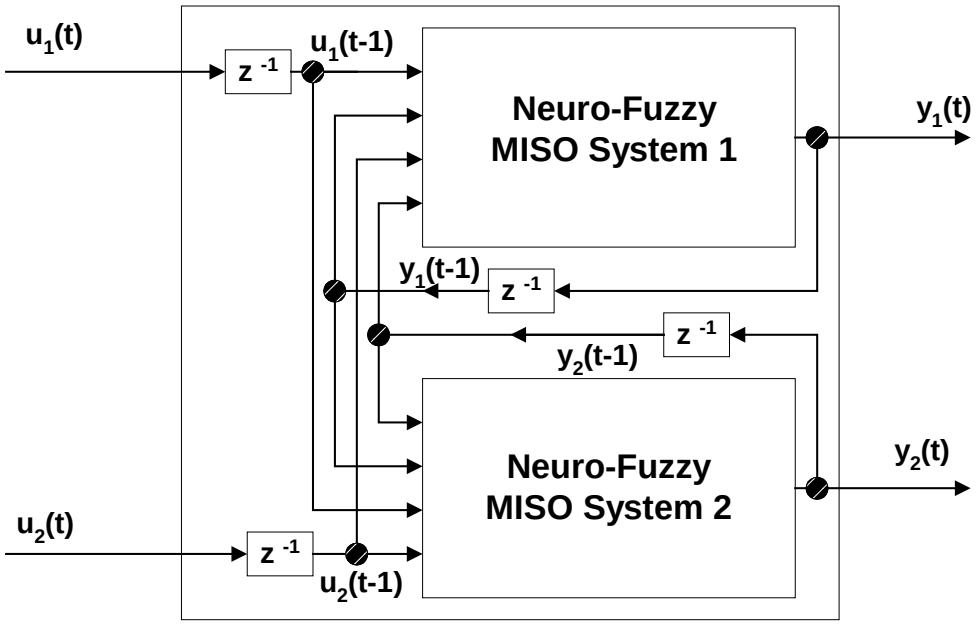

Figure 2.13 Block Diagram of the MIMO Neuro-Fuzzy Model

The MIMO NFS is divided in two MISO NFS, which interact with each other through the common delayed input and output signals. The input signals and outputs signal of the NFS are shown in Figure 2.13. Both MISO NFSs were training OFF-LINE, only using the common input-output data obtained from the measurement of the *KRi Dual Process Simulator KI 100*.

After the training process, the MIMO NFS was rebuilt with the structure shown in Figure 2.13. The output signal $y_1(t)$ of the *KRi Dual Process Simulator KI 100* is compared with the output signal obtained after the training process of the Neuro-Fuzzy MISO System 1 and the respective Fuzzy Difference Equation in Figure 2.14.

Individually, the Neuro-Fuzzy MISO System 2 was also trained with the corresponding input-output data and after that the output signal $y_2(t)$ of the *KRi Dual Process Simulator KI 100* was compared with the output signal obtained after the training process of the Neuro-Fuzzy MISO System 2 and the respective Fuzzy Difference Equation in Figure 2.15.

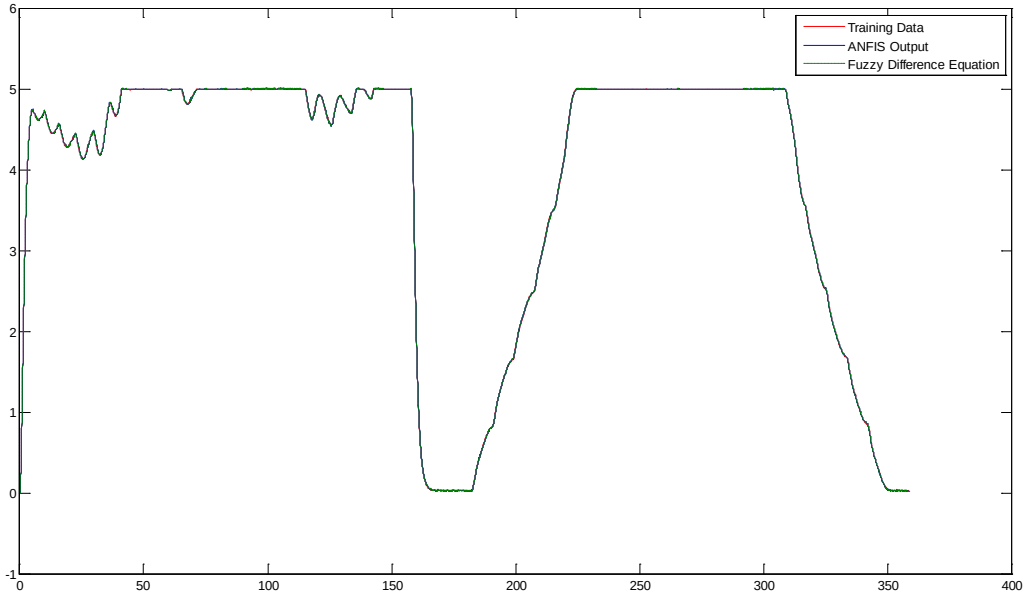

Figure 2.14. Output signal of the *KRi Dual Process Simulator KI 100* (y1(t), red line ,the output signal 1 (ANFIS-output, blue line) and the output signal 1 due to the Fuzzy Difference Equation (dash-dot green line)

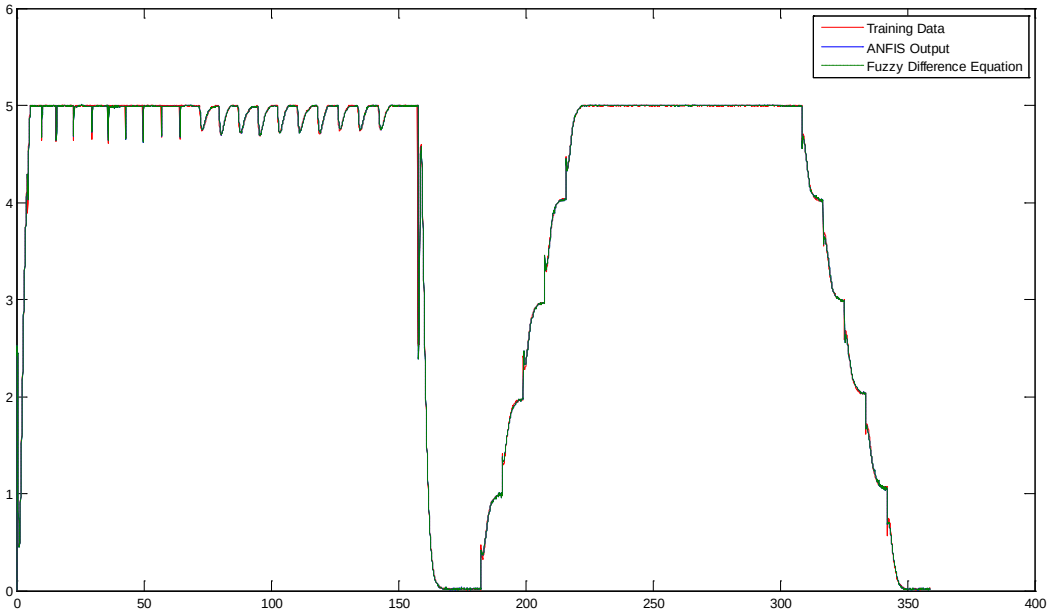

Figure 2.15. Output signal of the *KRi Dual Process Simulator KI 100* (y2(t)), red line and the output signal 2 (ANFIS-output, blue line) and the output signal 2 due to the Fuzzy Difference Equation (dash-dot green line)

The normalised degree of fulfilment for the m-th Neuro-Fuzzy System can be expressed as follows:

$$\gamma_i^m(k) = \frac{\prod_{j=1}^{4} \frac{1}{1+\left|\frac{x_j^m - c_{ij}^m}{a_{ij}^m}\right|^{2b_{ij}^m}}}{\sum_{i=1}^{16} \prod_{j=1}^{4} \frac{1}{1+\left|\frac{x_j^m - c_{ij}^m}{a_{ij}^m}\right|^{2b_{ij}^m}}} \qquad (2.45)$$

with $\gamma_i^m = \gamma_i^m(k)$ and $m = 1,2$

where the sets of the nonlinear (antescedent) parameters are the following:

$a_{ij}^1 = \{2.301, 2.728, 1.491, 0.8518, 2.166, 1.346, 2.839, 1.835\}$

a_{ij}^{2}={0.3721, 2.352, 1.095, 0.7676, 3.063, 2.483, 2.19, 1.802}

b_{ij}^{1}={3.059, 2.508, 2.294, 3.628, 2.25, 1.245, 4.172, 1.167}

b_{ij}^{2}={0.5992, 3.447, 2.682, 3.78, 2.699, 2.826, 2.581, 1.479}

c_{ij}^{1}={0.03985, 4.481, -0.4687, 3.89, 2.961, 4.949, 1.827, 4.984}

c_{ij}^{2}={-2.326, 3.992, -0.8245, 3.755, -1.083, 3.949, 1.653, 5.189}

The output signal of the m-th Neuro-Fuzzy system is expressed as follows:

$$y_m(t)=\sum_{i=1}^{16}\gamma_i^m\ y_i^m=\sum_{i=1}^{16}\gamma_i^m\left\{\begin{bmatrix}p_i^m & q_i^m & r_i^m & s_i^m\end{bmatrix}\begin{bmatrix}u_1(t-1)\\ u_2(t-1)\\ y_1(t-1)\\ y_2(t-1)\end{bmatrix}+t_i^m\right\} \tag{2.46}$$

with $m=1,2$

where the set of nonlinear (consequent) parameters are the following:

p_i^1 = {4.745, -6.339, -2.519, 3.533, 2.813, -1.186, -1.205, 0.5679, 3.489, -1.586, -1.835, 0.8524, 4.808, -0.7754, -2.575, 0.4456}

p_i^2 = {-2.043, 63.3, -50.85, 1.75, -52.81, 18.96, -1.007, -0.2248, 13.88, 36.02, -1.831, -0.7073, 99.4, -13.2, 0.07675, 0.07909}

q_i^1= {-4.517, 6.4, 2.713, -3.668, 1.63, -0.7615, -0.9473, 0.4463, -2.072, 0.2868, 1.313, -0.2061, -6.755, 3.238, 3.458, -1.78}

q_i^2 = {-4.317, 39.12, 40.87, -5.931, -6.602, 7.405, -5.999, 0.4839, -19.44, 33.87, -3.394, -0.3768, 25.08, -4.072, 1.61, -0.1389}

r_i^1 = {1.096, 0.9101, 0.7571, 1.452, 1.041, 1.046, 1.368, 1.084, -0.8136, 5.441, 4.125, 2.342, 0.2451, 1.325, -0.9127, 1.499}

r_i^2 = {3.167, -103.4, -1.998, -7.845, 28.09, 4.804, 3.889, -0.2515, 3.379, 0.5318, -0.4071, 0.8625, -108.6, -33.59, -16.1, 56.02}

s_i^1 = {-0.08116, 0.09364, 0.2906, 1.384, -0.00644, 0.4206, -0.2529, -0.4867, 1.562, -0.8069, -3.175, -1.054, 0.6867, -2.748, 1.079, 0.3265}

s_i^2 = {-0.2029, 49.46, 0.08933, -2.859, 16.1, -7.316, 3.572, 1.688, -2.787, -31.65, 2.916, 1.065, -58.63, 38.06, -8.195, -1.598}

t_i^1 = {0.2498, -0.431, 1.15, -9.384, -4.847, 0.7159, 1.773, 0.3515, -2.441, -5.45, -2.325, -7.306, -0.4976, 7.423, 3.946, -1.268}

t_i^2 = {2.295, 4.753, 9.094, 62.06, -10.26, -26.84, -2.145, -4.808, 4.43, 0.8439, 4.983, -1.77, 44.24, -28.07, 115.6, 13.51}

From equation (2.46) the Multivariable Fuzzy Difference Equation was obtained for the MIMO nonlinear plant which is expressed by the following equation:

$$\begin{bmatrix} y_1(t) \\ y_2(t) \end{bmatrix} = \begin{bmatrix} \left(\sum_{i=1}^{16} \gamma_i^1 r_i^1\right) & \left(\sum_{i=1}^{16} \gamma_i^1 s_i^1\right) \\ \left(\sum_{i=1}^{16} \gamma_i^2 r_i^2\right) & \left(\sum_{i=1}^{16} \gamma_i^2 s_i^2\right) \end{bmatrix} \begin{bmatrix} y_1(t-1) \\ y_2(t-1) \end{bmatrix} + \begin{bmatrix} \left(\sum_{i=1}^{16} \gamma_i^1 p_i^1\right) & \left(\sum_{i=1}^{16} \gamma_i^1 q_i^1\right) \\ \left(\sum_{i=1}^{16} \gamma_i^2 p_i^2\right) & \left(\sum_{i=1}^{16} \gamma_i^2 q_i^2\right) \end{bmatrix} \begin{bmatrix} u_1(t-1) \\ u_2(t-1) \end{bmatrix} + \begin{bmatrix} \left(\sum_{i=1}^{16} \gamma_i^1 t_i^1\right) \\ \left(\sum_{i=1}^{16} \gamma_i^2 t_i^2\right) \end{bmatrix} \quad (2.47)$$

Equation (2.47) defines the explicit Fuzzy Difference Equation (FDE) for the nonlinear plant produced by the *KRi Dual Process Simulator KI 100.* In this example and in Figures 2.11 and 2.12 the overlapping between the lines corresponding to the neuro-fuzzy systems and the fuzzy difference equations

expressed by the equation (2.47) were clearly observed. Finally, the Fuzzy Difference Equation takes information about the discrete states of nonlinear model based on Theorem 5.

2.7. Conclusions

Fuzzy Difference Equations (FDEs) are an alternative approach to represent a neuro-fuzzy system (NFS) with a good accuracy applied with the NARX models (with delayed inputs and outputs). The mathematical structure is clearer using the FDE than the NFSs. In addition, the only nonlinear term involved with the FDE is the normalized degree of fulfilment $\gamma_i = \gamma_i(\mathbf{x}(k))$. The linearization of the FDE by Taylor's series gives the possibility of stability and convergence analysis.

Chapter 3 Nonlinear Generalised Minimum Variance Controller Using Neuro Fuzzy Structures

3.1. Introduction

This chapter is concerned with the design of the Nonlinear Generalised Minimum Variance (NGMV) Controller using Neuro-Fuzzy technique to represent the process nonlinearities. The NGMV control algorithms described here are related with Artificial Neural Networks (ANNs) and Neuro-Fuzzy systems.

In the implementation of the NGMV controller, the Artificial Neural Networks (ANNs) or Neuro-Fuzzy systems (NFSs) were used to approximate the nonlinear part of the algorithm and the solution of a specific Diophantine equation was used in order to find the linear part of the NGMV controller. These are important parts of the implementation process for the NGMV control law. Specific nonlinear models have been used to design self-tuning MV/GMV controllers with an explicit nonlinear MV/GMV control law (Anbumani, et. al., 1981; Zhang and Lang, 1988; 1989; Dochain and Bastin, 1984; Svoronos, et. al., 1981; Agarwal and Seborg, 1987; Kung and Womack, 1984). NARMAX (nonlinear autoregressive moving average) polynomial models were developed in order to design a self-tuning GMV algorithm (Sales and Billings, 1990). A nonlinear control weighting is included in the control variable in order to include this in the GMV performance index.

This chapter describes the bases for several structures of the nonlinear generalised minimum variance (NGMV) controllers. It is based on the specific type of modelling used (i.e. linear affine models, neural networks and neuro-fuzzy systems) to obtain the parameters for the control design and the type of penalization used over the nonlinear control systems (Pinto, 2004a). The success of a control law depends on the accuracy and precision of the model obtained using physical laws, input-output data approaches and parameters optimization techniques. Finally, the Neuro-Fuzzy Generalised Minimum Variance (NFGMV) controller was designed and applied. The NFGMV controller was applied to a model of the Continuous Stirred Tank Reactor with a

Cooling Jacket. The NFGMV control was compared with a digital PI controller for tracking reference, perturbance rejection and robustness tests. Also, a fuzzy adaptive mechanism was developed in order to tune the NFGMV control system on line.

3.2. Nonlinear Generalised Minimum Variance Control System

Grimble (2003), developed the nonlinear generalised minimum variance (NGMV) controller (with dynamic weighting) for multivariable systems. This algorithm was developed for nonlinear minimum phase (or stable open-loop) systems with considerable time delays using a polynomial approach.

The NGMV controller was developed taking the theoretical foundation and the structure of the Smith Predictor. Separable linear and nonlinear components are assumed. In general, the nonlinear model was divided into three parts: the linear function, the nonlinear function and the time-delay. Appendix B.1. shows the basic concepts of the NGMV control law. Theorem 3.1 summarises the NGMV optimal control law.

Theorem 3.1 of the NGMV Optimal Controller (Grimble, 2003):
Following the derivation in Appendix B.1,

The selection of the dynamic weighting P_c and F_c ensures the time-varying operator $\left(P_c W_k - F_{ck}\right)$ is a stable causal inverse.

Diophantine equation:

The stability of the NGMV controller is based on the solution of $\left(G_0, F_0\right)$ with the $\deg\left(F_0\right) < k_j$ (minimum degree of F_0) for the following identity:

$$A_p P_{cd} F_0 + D_k G_0 = P_{cf} D_f \tag{3.1}$$

with the left coprime polynomial matrices A_p and P_{cf}:

$$A_p^{-1}\ P_{cf} = P_{cn}\ A^{-1} \tag{3.2}$$

and the spectral factor Y_f defined as follows:

$$Y_f = A^{-1}\ D_f \tag{3.3}$$

where D_f is a polynomial matrix strictly Schur. As a related formula the pseudo difference signal $f(t)$ can be expressed as follows:

$$f(t) = Y_f\ \varepsilon(t) \tag{3.4}$$

where $\varepsilon(t)$ is the zero-mean white noise of identity covariance matrix.

Optimal NGMV control signal:

The expression used in order to compute the optimal NGMV controller was expressed as follows:

$$u(t) = \left(F_0\ Y_f^{-1}\ W_k - F_{ck}\right)^{-1}\left(\left(A_p\ P_{cd}\right)^{-1}\ G_0\ Y_f^{-1}\right) e(t) \tag{3.5}$$

3.2.1. Steps for Computing of the Optimal NGMV Control System:

Step 1: Recalling equation (B.16) (from the Appendix B) of the optimal cost function:

$$\phi_0(t) = P_c\ e(t) + F_c\ u(t) \tag{B.16}$$

Step 2: Substituting equation (B.3) in equation (B.1) was obtained as follows:

$$e(t) = r(t) - W(t)u(t) - d(t) \tag{3.6}$$

Step 3: Substitution of equation (3.6) in equation (B.16) gives the following expression:

$$\phi_0(t) = P_c\,(r(t) - d(t)) + (F_c - P_c\,W(t))\,u(t) \tag{3.7}$$

Step 4: Substituting expressions (3.2), (3.3) and (3.4) in equation (B.18) gives:

$$\phi_0(t) = (A_p\,P_{cd})^{-1} P_{cf}\;\; D_f\;\varepsilon(t) + (F_c - P_c\,W(t))\,u(t) \tag{3.8}$$

Step 5: Substituting equation (3.2) for the product $P_{cf}\;D_f$ in equation (B.19) gives:

$$\phi_0(t) = F_0\,\varepsilon(t) + (A_p\,P_{cd})^{-1}\,D_k\,G_0\,\varepsilon(t) + (F_c - P_c\,W(t))\,u(t) \tag{3.9}$$

Step 6: Obtain the expression for the zero-mean white noise of the of identity covariance matrix $\varepsilon(t)$ from equation (3.4) with the substitution of the equations (B.3) and (B.5), to give:

$$\varepsilon(t) = Y_f^{-1}(e(t) + W(t)\,u(t)) \tag{3.10}$$

Step 7: Substituting equation (3.2) in equation (3.1) leads to:

$$\phi_0(t) = F_0\,\varepsilon(t) + (A_p\,P_{cd})^{-1}\,D_k\,G_0\,Y_f^{-1}(e(t) + W(t)u(t)) + (F_c - P_c\,W(t))\,u(t) \tag{3.11}$$

Re-arranging and factorizing the previous equation the following expression can be derived:

$$\phi_0(t) = F_0\,\varepsilon(t) + (A_p\,P_{cd})^{-1}\,D_k\,G_0\,Y_f^{-1}e(t) + \left(\left((A_p\,P_{cd})^{-1}\,D_k\,G_0\,Y_f^{-1} - P_c\right)W(t) + F_c\right)u(t) \tag{3.12}$$

or

$$\phi_0(t) = F_0\,\varepsilon(t) + (A_p\,P_{cd})^{-1}D_k G_0\,Y_f^{-1}e(t) + \left((A_p\,P_{cd})^{-1}(D_k\,G_0 - A_p\,P_{cd}\,P_c)Y_f^{-1}W(t) + F_c\right)u(t) \tag{3.13}$$

Combining the third term of equation (3.13) with equations (3.2) and (3.3) gives the following expression:

$$D_k G_0 - A_p P_{cd} P_c Y_f = D_k G_0 - A_p P_{cn} A^{-1} D_f = D_k G_0 - P_{cf} D_f = -A_p P_{cd} F_0 \quad (3.14)$$

Substituting equation (3.14) in the equation (3.13) yields:

$$\phi_0(t) = F_0 \varepsilon(t) + \left(A_p P_{cd}\right)^{-1} D_k G_0 Y_f^{-1} e(t) + \left(F_c - F_0 Y_f^{-1} W(t)\right) u(t) \quad (3.15)$$

Substituting equation (B.14) in equation (3.7) and after factorizing with D_k leads to:

$$\phi_0(t) = F_0 \varepsilon(t) + D_k \left(\left(A_p P_{cd}\right)^{-1} G_0 Y_f^{-1} e(t) + \left(F_{ck} - F_0 Y_f^{-1} W_k(t)\right) u(t)\right) \quad (3.16)$$

Computing the pseudo output k steps ahead predictor gives:

$$\phi_0(t+k) = F_0 \varepsilon(t+k) + \left(\left(A_p P_{cd}\right)^{-1} G_0 Y_f^{-1} e(t) + \left(F_{ck} - F_0 Y_f^{-1} W_k(t)\right) u(t)\right) \quad (3.17)$$

By definition, the pseudo predictor $\phi_0(t+k|t)$ is defined as follows:

$$\phi_0(t+k|t) = \left(\left(A_p P_{cd}\right)^{-1} G_0 Y_f^{-1} e(t) + \left(F_{ck} - F_0 Y_f^{-1} W_k(t)\right) u(t)\right) \quad (3.18)$$

In steady state, the value of the pseudo output $\phi_0(t+k)$ is expressed as follows:

$$\phi_0(t+k) = F_0 \varepsilon(t+k) \;\; or \;\; \phi_0(t) = F_0 \varepsilon(t) \quad (3.19)$$

When there is a minimum variance value then the pseudo predictor $\phi_0(t+k|t)$ is approximated to zero value, expressed as follows:

$$\phi_0(t+k|t) = \left(\left(A_p P_{cd}\right)^{-1} G_0 Y_f^{-1} e(t) + \left(F_{ck} - F_0 Y_f^{-1} W_k(t)\right) u(t)\right) = 0 \quad (3.20)$$

Finally, from equation (3.20) the optimal NGMV control law is defined as follows (Grimble, 2003):

$$u(t) = \left(F_0 Y_f^{-1} W_k(t) - F_{ck}\right)^{-1} \left(\left(A_p P_{cd}\right)^{-1} G_0 Y_f^{-1} e(t)\right) \tag{3.21}$$

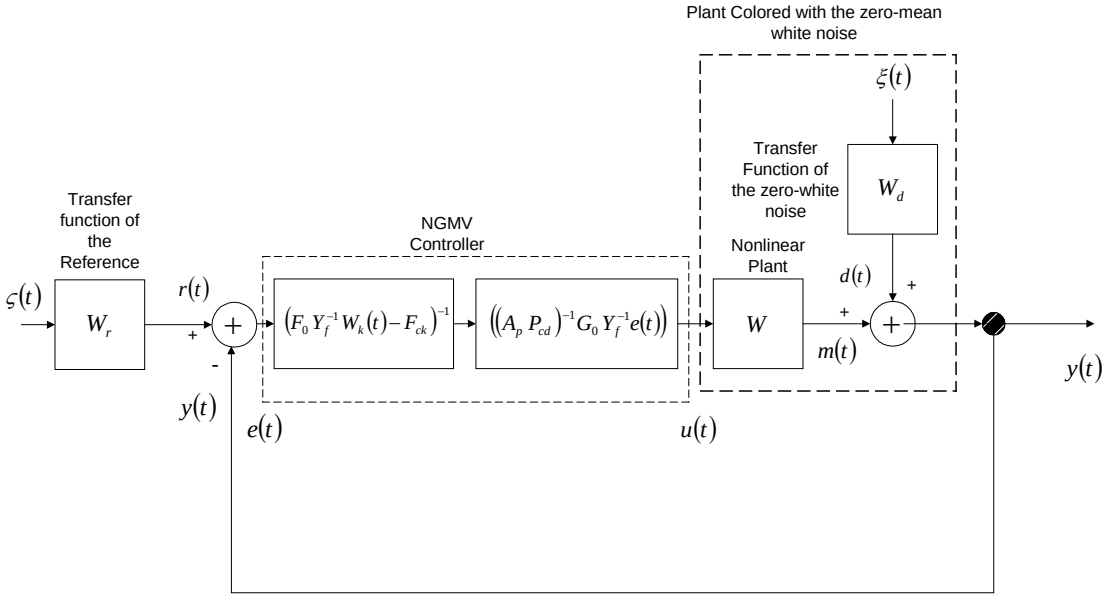

Figure 3.1 Structure of the NGMV Controller Revisited

Equation (3.21) represents the final structure of the NGMV controller as shown in Figure 3.1. The calculation of the inverse $\left(F_0 Y_f^{-1} W_k(t) - F_{ck}\right)^{-1}$ is not always possible, hence the control law should use concepts from the Smith predictor as follows:

$$u(t) = F_{ck}^{-1} \left(F_0 Y_f^{-1} W_k(t)\, u(t) - \left(A_p P_{cd}\right)^{-1} G_0 Y_f^{-1} e(t)\right) \tag{3.22}$$

The structure of the new controller is shown in Figure 3.2.

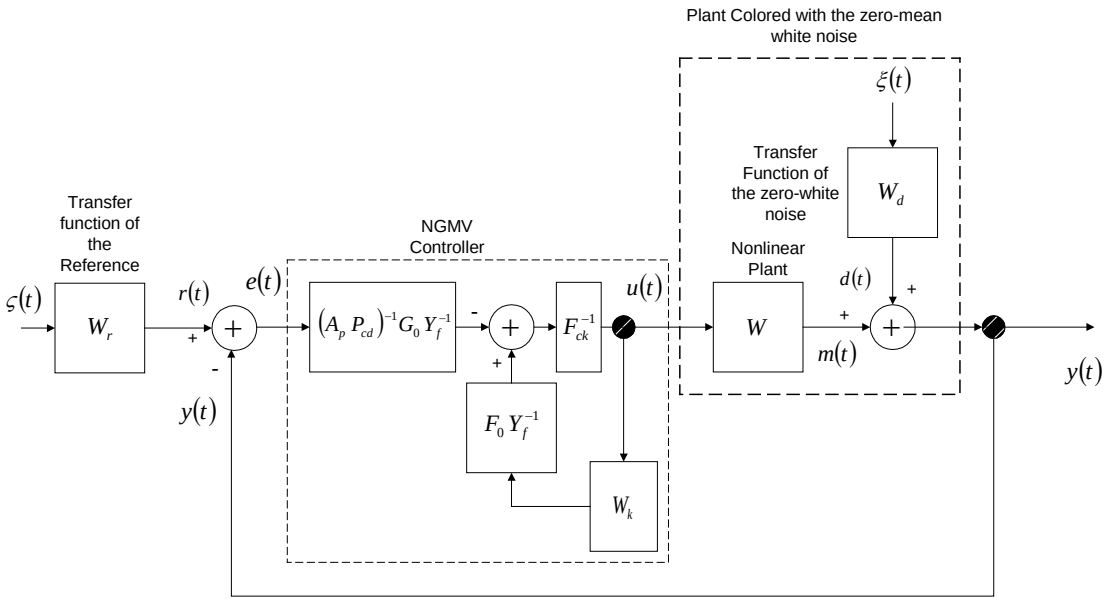

Figure 3.2 Final Structure of the NGMV Controller

In order to modify expression (3.22) for the NGMV controller, dynamic weightings were necessary to modify the equation to:

$$Y_f^{-1} = \left(A^{-1} D_f\right)^{-1} = D_f^{-1} A \tag{3.23}$$

substitute equation (3.6) in equation (3.22) to obtain:

$$u(t) = F_{ck}{}^{-1}\left(F_0 Y_f^{-1} W_k(t)\, u(t) - \left(A_p P_{cd}\right)^{-1} G_0 Y_f^{-1}\left(r(t) - W(t)\, u(t) - d(t)\right)\right) \tag{3.24}$$

Substituting equation (B.11) in equation (B.5) to obtain the following expression:

$$u(t) = F_{ck}{}^{-1}\left(F_0 Y_f^{-1} W_k(t)\, u(t) - \left(A_p P_{cd}\right)^{-1} G_0 Y_f^{-1}\left(r(t) - D_k W_k(t)\, u(t) - d(t)\right)\right) \tag{3.25}$$

By factorizing equation (B.6), a new structure is developed to make the application of the Neuro-Fuzzy systems possible as follows:

$$u(t) = F_{ck}{}^{-1}\left(\left(F_0 + \left(A_p P_{cd}\right)^{-1} D_k G_0\right) Y_f^{-1} W_k(t) u(t) - \left(A_p P_{cd}\right)^{-1} G_0 Y_f^{-1}\left(r(t) - d(t)\right)\right) \tag{3.26}$$

or

$$u(t) = F_{ck}^{-1}\left(\left(A_p\,P_{cd}\right)^{-1}\left(A_p\,P_{cd}\,F_0 + D_k\,G_0\right)Y_f^{-1}W_k(t)u(t) - \left(A_p\,P_{cd}\right)^{-1}G_0\,Y_f^{-1}\left(r(t) - d(t)\right)\right) \tag{3.27}$$

Substituting expression (3.15) in equation (B.20) gives:

$$u(t) = F_{ck}^{-1}\left(\left(A_p\,P_{cd}\right)^{-1}P_{cf}\,A\,W_k(t)u(t) - \left(A_p\,P_{cd}\right)^{-1}G_0\,Y_f^{-1}\left(r(t) - d(t)\right)\right) \tag{3.28}$$

or

$$u(t) = F_{ck}^{-1}\left(P_{cd}^{-1}\,A_p^{-1}\,P_{cf}\,A\,W_k(t)u(t) - \left(A_p\,P_{cd}\right)^{-1}G_0\,Y_f^{-1}\left(r(t) - d(t)\right)\right) \tag{3.29}$$

The control law defined by the equation (3.28) is shown in Figure 3.3.

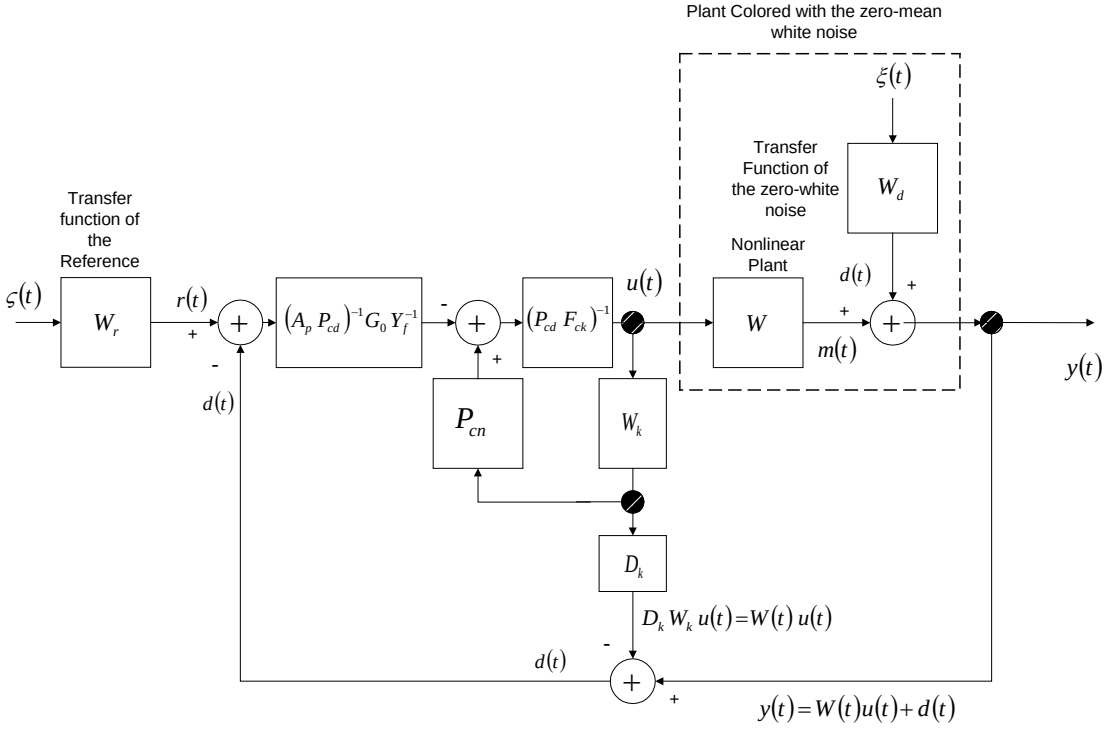

Figure 3.3 Second Structure of the Nonlinear Generalised Minimum Variance Controller with Dynamic Weighting as a Nonlinear Smith Predictor with Internal Model.

Substituting identity (B.18) in equation (3.29) to obtain u(t):

$$u(t) = F_{ck}^{-1}\left(P_{cd}^{-1}\,P_{cn}\,W_k(t)u(t) - \left(A_p\,P_{cd}\right)^{-1}G_0\,Y_f^{-1}\left(r(t) - d(t)\right)\right) \tag{3.30}$$

or

$$u(t) = F_{ck}^{-1}\left(P_c W_k(t)u(t) - \left(A_p P_{cd}\right)^{-1} G_0 Y_f^{-1}\left(r(t) - d(t)\right)\right) \tag{3.31}$$

Equation (3.31) is the representation of the first structure of the *NGMV control dynamically weighted* as a *nonlinear Smith Predictor with an internal model structure*, which is shown in Figure 3.5. This structure was obtained by introducing the disturbance model $d(t)$ and the delay matrix D_k in the feedback loop.

Taking equation (3.30) and factorizing with the factor P_{cd}^{-1} to obtain another expressions for the representation of the second structure of the *NGMV control dynamically weighted* as a *nonlinear Smith Predictor with an internal model structure* (see Figure 3.2):

$$u(t) = F_{ck}^{-1} P_{cd}^{-1}\left(P_{cn} W_k(t)u(t) - A_p^{-1} G_0 Y_f^{-1}\left(r(t) - d(t)\right)\right) \tag{3.32}$$

or

$$u(t) = \left(P_{cd} F_{ck}\right)^{-1}\left(P_{cn} W_k(t)u(t) - A_p^{-1} G_0 Y_f^{-1}\left(r(t) - d(t)\right)\right) \tag{3.33}$$

Another alternative of the controllers were developed by factorizing equation (3.22) with the common factor $\left(A_p P_{cd}\right)^{-1}$, i.e.:

$$\begin{aligned} u(t) &= F_{ck}^{-1}\left(A_p P_{cd}\right)^{-1}\left(A_p P_{cd} F_0 Y_f^{-1} W_k(t)\, u(t) - G_0 Y_f^{-1} e(t)\right) \\ &= \left(A_p P_{cd} F_{ck}\right)^{-1}\left(A_p P_{cd} F_0 Y_f^{-1} W_k(t)\, u(t) - G_0 Y_f^{-1} e(t)\right) \end{aligned} \tag{3.34}$$

By substituting equation (3.2) in equation (3.34):

$$\begin{aligned} u(t) &= F_{ck}^{-1}\left(A_p P_{cd}\right)^{-1}\left(\left(P_{cf} D_f - D_k G_0\right) Y_f^{-1} W_k(t)\, u(t) - G_0 Y_f^{-1} e(t)\right) \\ &= \left(A_p P_{cd} F_{ck}\right)^{-1}\left(\left(P_{cf} D_f - D_k G_0\right) Y_f^{-1} W_k(t)\, u(t) - G_0 Y_f^{-1} e(t)\right) \end{aligned} \tag{3.35}$$

Replacing equation (3.35) in equation (B.11) is obtained the following expression:

$$
\begin{aligned}
u(t) &= F_{ck}^{-1}\left(A_p\, P_{cd}\right)^{-1}\left(\left(P_{cf} D_f W_k(t) - G_0 W(t)\right) Y_f^{-1}\; u(t) - G_0 Y_f^{-1} e(t)\right) \\
&= \left(A_p\, P_{cd} F_{ck}\right)^{-1}\left(\left(P_{cf} D_f W_k(t) - G_0 W(t)\right) Y_f^{-1}\; u(t) - G_0 Y_f^{-1} e(t)\right)
\end{aligned}
\tag{3.36}
$$

Equation (3.36) shows the second case for the final structure of the NGMV controller dynamically weighted as shown in Figure 3.4.

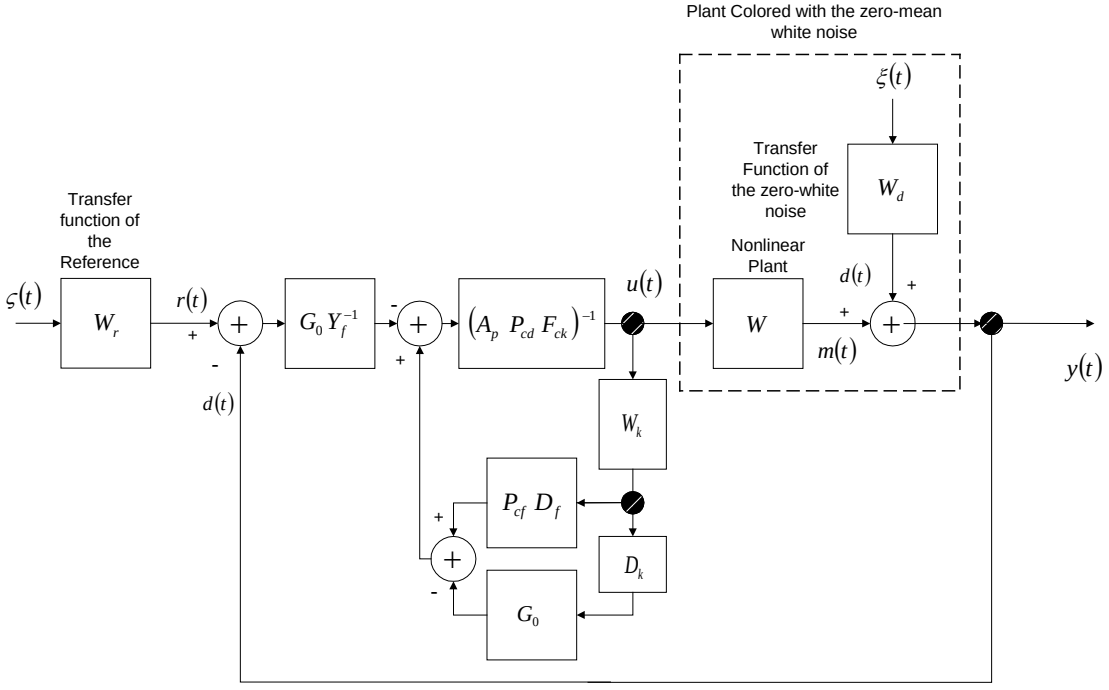

Figure 3.4 Final Structure of the Nonlinear Generalised Minimum Variance Controller Dynamically Weighted (Second Case)

Substituting equation (B.17) in equations (3.34) and (3.35) gives:

$$
\begin{aligned}
u(t) &= F_{ck}^{-1}\left(A_p\, P_{cd}\right)^{-1}\left(P_{cf} D_f\, Y_f^{-1} W_k(t)\, u(t) - G_0 Y_f^{-1}\left(r(t) - d(t)\right)\right) \\
&= \left(A_p\, P_{cd} F_{ck}\right)^{-1}\left(P_{cf} D_f Y_f^{-1} W_k(t)\, u(t) - G_0 Y_f^{-1}\left(r(t) - d(t)\right)\right)
\end{aligned}
\tag{3.37}
$$

Expressions (3.14)-(3.37) include the free delay nonlinear model $W_k(t)$, which could be obtained by Look-up Tables, Neural Networks and Neuro-Fuzzy systems (Pinto, et. al., 2004a; 2004b; 2005).

Figure 3.5 shows the *third structure of the NGMV controller dynamically weighted as a nonlinear Smith Predictor with Internal Model*, which belongs to equation (3.36). The previous structure was developed as a part of this research and it was not included in (Grimble, 2003).

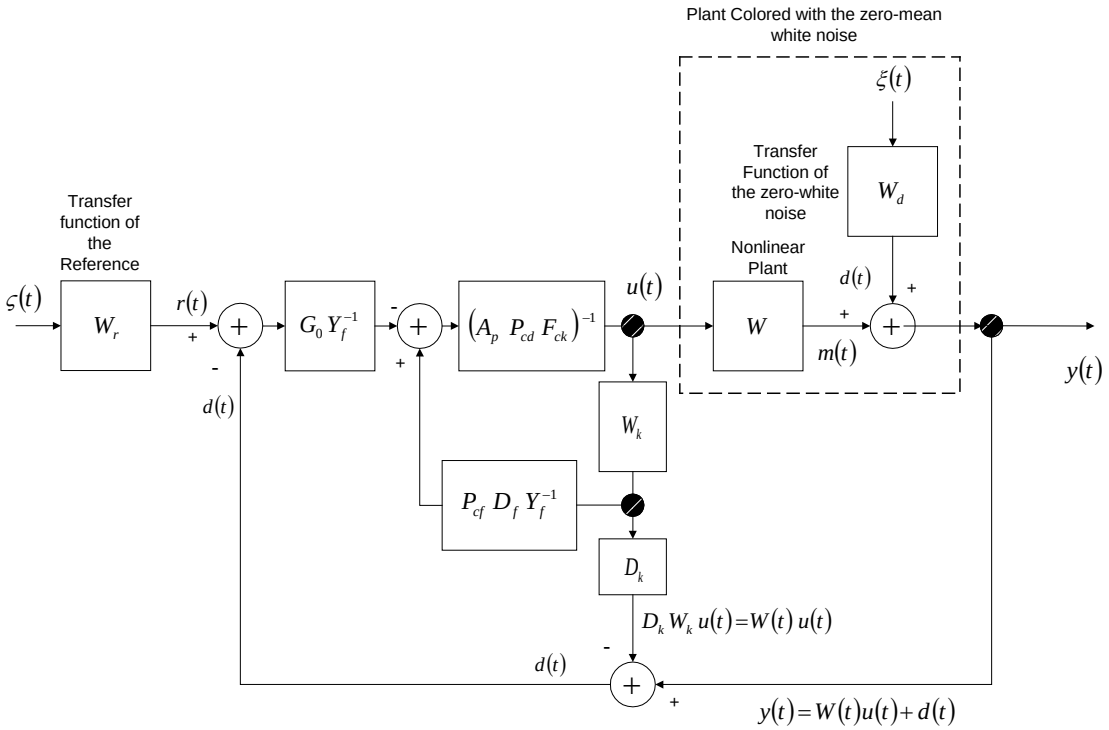

Figure 3.5 Third Structure of the Nonlinear Generalised Minimum Variance Controller Dynamically Weighted

Step 8:

The dynamic control weighting was parameterized as follows (Grimble, 2008):

$$F_{ck} = \begin{bmatrix} \rho_{11} & 0 & \cdots & 0 \\ 0 & \rho_{22} & \cdots & 0 \\ \vdots & \vdots & \ddots & \vdots \\ 0 & 0 & \cdots & \rho_{r\,m} \end{bmatrix} = Diag\left[\rho_{11}, \rho_{22}, \cdots, \rho_{r\,m}\right] \tag{3.38}$$

$$F_{cd} = \begin{bmatrix} 1 & 0 & \cdots & 0 \\ 0 & 1 & \cdots & 0 \\ \vdots & \vdots & \ddots & \vdots \\ 0 & 0 & \cdots & 1 \end{bmatrix} = I_{(r \times m)} \tag{3.39}$$

where $\rho_{ij} < 0 \ (i = 1, \cdots, r \ ; j = 1, \cdots, m)$

The structure of the dynamic error weighting belongs to a decoupled MIMO PID controller and it has the following form:

$$\begin{aligned} P_{cn} &= \begin{bmatrix} a_{11} - b_{11} z^{-1} & 0 & \cdots & 0 \\ 0 & a_{22} - b_{22} z^{-1} & \cdots & 0 \\ \vdots & \vdots & \ddots & \vdots \\ 0 & 0 & \cdots & a_{rm} - b_{rm} z^{-1} \end{bmatrix} \\ &= Diag\left[\left(a_{11} - b_{11} z^{-1}\right), \left(a_{22} - b_{22} z^{-1}\right), \cdots, \left(a_{rm} - b_{rm} z^{-1}\right)\right] \end{aligned} \tag{3.40}$$

where a_{ij} and b_{ij} $(i = 1, \ldots, r; j = 1, \ldots, m)$ are constants greater than zero.

$$\begin{aligned} P_{cd} &= \begin{bmatrix} \delta_{11}\left(1 - z^{-1}\right) & 0 & \cdots & 0 \\ 0 & \delta_{22}\left(1 - z^{-1}\right) & 0 & \vdots \\ \vdots & 0 & \ddots & 0 \\ 0 & 0 & \cdots & \delta_{rm}\left(1 - z^{-1}\right) \end{bmatrix} \\ P_{cd} &= Diag\left[\delta_{11}\left(1 - z^{-1}\right), \delta_{22}\left(1 - z^{-1}\right), \cdots, \delta_{rm}\left(1 - z^{-1}\right)\right] \end{aligned} \tag{3.41}$$

where $\delta_{ij} > 0 \ (i = 1, \ldots, r; j = 1, \ldots, m)$.

An initial point of the selection for the dynamic weightings is a PID control system applied with success to the free delay nonlinear plant. In other words, the PID controller keeps the output signal stable. The dynamic error weighting belongs to a decoupled MIMO PID controller because the internal interactions and nonlinearities were included in the free delay Neuro-Fuzzy model of the nonlinear process (Pinto, et.

al., 2004). The main weakness of this technique is the fact that the exact free delay nonlinear model and the time-delay have to be known in advance.

3.3. Neuro-Fuzzy Generalised Minimum Variance Controller

The Neuro-Fuzzy GMV (NFGMV) controller was developed by Pinto, Grimble and Katebi (2004a; 2004b) based on the initial idea of Grimble (2003). It was described in the previous section and also included several additional analyses in Appendix B.1. The NFGMV control law was based on the assumption that all nonlinear plants with delays could be represented by the product between a linear block and a nonlinear block affected in each output path by a common or minimum delay. The important part of the algorithm is to know in advance: the common delay of each path and identify the free delay nonlinear model of the plant using Neuro-Fuzzy Systems.

Nowadays, techniques for designing nonlinear controllers shown to have a radical improvement in the performance of conventional (linear PID) controllers because they are designed for the full operating range of the plant, instead of a specific operating point (Pinto, et. al., 2004a).

The need to provide improved scalar and particularly multivariable control techniques has led to the wider use of optimal control design approaches, such as LQ, LQG and H_∞ (Grimble, 1994). The controllers were obtained by minimizing a cost function and have the advantage that the control signal can be weighted to obtain a more realistic design (Çağlayan, 1997). A simple Minimum Variance (MV) controller was developed by Åström and Wittermark for linear minimum-phase plants and later generalized to non-minimum phase, time varying and nonlinear plants (Åström, 1979; 1995; Huang, 2002; Grimble, 2003).

The cost function for the MV controller includes only the error signal (Åström, 1995; Karagöz, 2000) and it is defined as follows:

$$J = E\left\{\left(r_t - y_t\right)^2\right\} \tag{3.42}$$

where $E\{\cdot\}$ is the expectation operator. The Minimum Variance cost function was modified by Clarke and Gawthrop (1975) in order to obtain the Generalised Minimum Variance (GMV) controller, where the cost function includes the variances of both the error and control signals. Two possible definitions of the cost function are (Karagöz, 2000):

$$J = E\left\{\left(r_{t+k} - y_{t+k}\right)^2 + \lambda u_t^{\,2}\right\} \tag{3.43}$$

and

$$J = E\left\{\left(r_{t+k} - y_{t+k}\right)^2 + \lambda \Delta u_t^{\,2}\right\} \tag{3.44}$$

Grimble (2001) introduced a slightly more general cost function, defined by:

$$J = E\left\{\left(P_c\ e(t) + F_c\, u(t)\right)^2\right\} \tag{3.45}$$

where P_c and F_c are the error and control weightings, respectively.

The control costing term enables the GMV controller to be used for non-minimum phase systems, whilst using a k-steps-ahead optimal control law (Pinto, et. al., 2004). The MV and GMV controllers have been commonly used to assess the performance of controllers by means of benchmarking techniques (Grimble 2002; 2003; 2004; Huang2002). The GMV control law is also applicable for self-tuning control systems.

Neuro-fuzzy modelling has proved to be successful for process modelling due to the robustness and fault-tolerance required for industrial applications. This technique is appropriate for systems with strong nonlinear behaviour, high degree of uncertainties or systems without explicit mathematical model, or time-varying characteristics (Pinto, 2001; Pinto and Madrigal, 2001). In addition, the technique makes it easy to develop models by means of a combination of empirical models, heuristics and real data. A neuro-fuzzy model is a type of hybrid fuzzy system which is represented by fuzzy *if-then* rules in a neural network. Neuro-Fuzzy systems can be interpreted and

analyzed as a Fuzzy system and trained as a neural network. Neuro-Fuzzy modelling uses local linear model in order to represent operating regime decomposition of the nonlinear plant (Verdult, 2002).

In this algorithm the Neuro-Fuzzy Generalized Minimum Variance (NFGMV) controller, which is a combination of the GMV polynomial control approach and Neuro-Fuzzy based identification was designed and applied.

3.3.1. NGMV Control Law Dynamically Weighted

The complete theoretical explanation and development about the NGMV controller dynamically weighted was developed in the Appendix B.1. and Section 3.2.

The final expression used in the controller was described in the equation (3.22) as follows:

$$u(t) = F_{ck}{}^{-1}\left(F_0 Y_f^{-1} W_k(t)\, u(t) - \left(A_p P_{cd}\right)^{-1} G_0 Y_f^{-1} e(t)\right) \tag{3.22}$$

Also, the control structure used was show in Figure B.2 of Appendix B.1.

3.3.2. Design of the Neuro-Fuzzy Generalised Minimum Variance Controller

3.3.2.1. Neuro-Fuzzy Modelling

The Neuro-Fuzzy Generalized Minimum Variance Controller is considered nonlinear due to the contribution of the dynamic nonlinearities of the model used. The fuzzy membership functions were defined by the weighted combination of the local models in order to approximate the nonlinear behaviour of the plant. The weighted validation describes which model or combination of model is active and appropriate in a certain operating regime of the plant. This universal approximator is the most used in nonlinear identification.

In order to obtain the dynamic model of equation (B.14) of Appendix B.1., the NARX input-output model was used:

$$y(t) = f(\mathbf{x}(t)) \tag{3.46}$$

where $y(t)$ denotes the *output predicted* at the future time instant and $\mathbf{x}(t)$ is the *regressor vector*, consisting of a finite number of past inputs and outputs:

$$\mathbf{x}(t) = \left[y(t-1) \ \cdots \ y(t-n_y) \ \ u(t) \ \ u(t-1) \ \cdots \ u(t-n_u) \right]^T \tag{3.47}$$

where the dynamic order of the system was represented by the number of lags n_u and n_y. Neuro-Fuzzy model is defined also as Takagi-Sugeno-Kang (TSK) model (Pinto, 2001). This model is defined by expert rules that describe the behaviour of the nonlinear system. The rules have antecedents and consequents parts with a linear function of the input variables (Pinto, et. al., 2004):

$$\begin{aligned} &R_i : \text{If } \mathbf{x}(t) \text{ is } A_i \text{ then } \ y_i = a_i^T \mathbf{x}(t) + b_i \ , \\ &i = 1, 2, \cdots, N \end{aligned} \tag{3.48}$$

where R_i is the i[th] fuzzy rule, A_i is the i[th] fuzzy set, $\mathbf{x}(t)$ is the regressor vector, y_i is the i[th] linear model, $\mathbf{a}_i$ is the i[th] consequent parameter vector, b_i is the i[th] scalar offset and K is the numbers of the rules.

The individual rules define the output $y(t)$ by means of the weighted average of the rules. It was defined by recalling equation (2.13) of Section 2.5.2.1:

$$y(t) = \frac{\sum_{i=1}^{N} \beta_i(\mathbf{x}) y_i}{\sum_{i=1}^{N} \beta_i(\mathbf{x})} = \frac{\sum_{i=1}^{N} \beta_i(\mathbf{x}) (\mathbf{a}_i^T \mathbf{x} + b_i)}{\sum_{i=1}^{N} \beta_i(\mathbf{x})} \tag{2.13}$$

where the $\beta_i(\mathbf{x})$ is the degree of membership of the i[th] rule. The input space was defined using different partly overlapping regions by means of the antecedent fuzzy sets. These are local lineal models or local linear approximations of the nonlinear

system defined for the parameters $\mathbf{a}_i$ and b_i. The (Neuro-Fuzzy model) dynamic input-output model was also defined by the first-order TSK model, expressed by equations (2.11), (2.12) and (2.17) of the Section 2.5.2.1.:

$$y(t) = \sum_{i=1}^{N} \gamma_i(\mathbf{x}(t))\, y_i \tag{2.11}$$

with

$$\gamma_i(\mathbf{x}) = \frac{\prod_{j=1}^{p} \exp\left(-\frac{(x_j - c_{ij})^2}{2\sigma_{ij}^2}\right)}{\sum_{i=1}^{K}\prod_{j=1}^{p} \exp\left(-\frac{(x_j - c_{ij})^2}{2\sigma_{ij}^2}\right)} \tag{2.12}$$

and

$$y_i = \mathbf{a}_i^T\, \mathbf{x}(t) + b_i \tag{2.17}$$

where $\gamma_i(x(t))$ is the i[th] nonlinear function and y_i is the i[th] linear function.

Nevertheless, we can take the equations (B.14) and (3.47) and define the free time-delay nonlinear model as follows:

$$y_m(t) = W_{0k}\,(W_{1k}\,u)(t) = \sum_{i=1}^{N} \gamma_i(\mathbf{x}(t))\, y_i \tag{3.49}$$

This equation justifies the use of the Neuro-Fuzzy systems and it was the best model technique to use for this approach (Pinto, et. al., 2004). Identifying the nonlinear model without delay using the Neuro-Fuzzy model in open-loop represented the first step of the controller formulation. It was necessary to obtain expert knowledge and register data of the system in order to obtain an acceptable operation surface by means of the Neuro-Fuzzy model. The training method used was offline learning using the ANFIS Toolbox of MATLAB® (Matlab, 1999).

After training the Dynamic Neuro-Fuzzy model, it was compared with the plant to obtain the best model $\left(y_p(t) - y_m(t) \cong 0\right)$ as shown in the Figure 3.6.

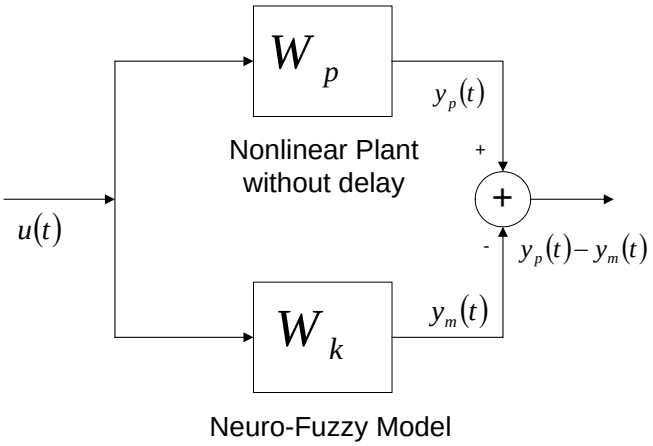

Figure 3.6 Comparison Between the Nonlinear Plant without Delay and The Neuro-Fuzzy Model

3.3.3. Computing of Parameters for the Neuro-Fuzzy GMV Controller

To compute the parameters of the Neuro-Fuzzy GMV controller, the transfer functions of the reference and disturbance using equations (B.8) and (B.9) of Appendix B.1. are used and the power spectrum for the combined noise signal computed using equations (3.2), (3.3), (B.6) and (B.7) in order to obtain the strictly Schur polynomial D_f .

The control weighting was parameterized as follows:

$$F_{ck} = \frac{F_{cn}}{F_{cd}} = \rho \times \frac{\left(1 - \mathrm{a}\, z^{-1}\right)}{\left(1 - \mathrm{b}\, z^{-1}\right)} \tag{3.50}$$

where ρ , a and *b* are constants used to tune the high-pass filter (invertible and stable). The error weighting has the following form:

$$P_c = \frac{P_{cn}}{P_{cd}} = k_p + \frac{k_I}{1 - z^{-1}} + k_d \left(1 - z^{-1}\right) \tag{3.51}$$

where k_p, k_I, k_d are the proportional, integral and derivative gains of a PID controller. When this PID controller stabilizes the free delay nonlinear plant, it was considered a starting point for the weighting selection.

The next step is to define the Diophantine equation in equation (3.1) and solve it. The final step was to calculate the values of the blocks shown in Figure 3.7, which represents the structure of the Neuro-Fuzzy GMV controller.

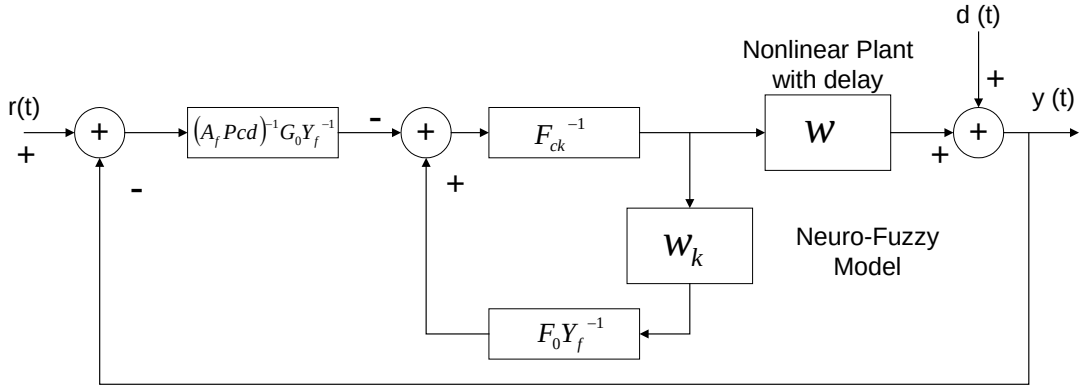

Figure 3.7 Structure of the Neuro-Fuzzy GMV (NFGMV) controller.

3.4. Simulation Example

The example used was a Continuous Stirred Tank Reactor with Cooling Jacket (CSTRCJ) model as shown in Figure 3.8.

An irreversible exothermic reaction occurs in the model of a continuous reactor used for testing the performance of the Neuro Fuzzy Generalize Minimum Variance (NFGMV). The reaction was expressed as follows:

$$A \rightarrow B \tag{3.52}$$

with a constant volume reactor cooled by a single coolant stream. The Nonlinear model of the Reactor was expressed by:

Energy Balance Equation

$$\frac{dT(t)}{dt} = \frac{q(t)}{V}[T_0(t) - T(t)] - \frac{k_0 \Delta H}{\rho C_p} C_a(t + k_d) \exp\left(-\frac{E}{RT(t)}\right) + \frac{\rho_c C_{pc}}{\rho C_p V} q_c(t) \left[1 - \exp\left(-\frac{hA}{q_c(t) \rho_c C_{pc}}\right)\right] [T_{C0}(t) - T(t)] \tag{3.53}$$

and

Mass Balance Equation

$$\frac{dC_a(t + k_d)}{dt} = \frac{q(t)}{V}[C_a^0(t) - C_a(t + k_d)] - k_0 C_a(t + k_d) \exp\left(-\frac{E}{RT(t)}\right) \tag{3.54}$$

Table 3.1 shows the nominal parameter values in the model of the Reactor. For manipulating the Coolant flow rate $q_c(t)$ is controlled the measured concentration of the reactive A at the outlet stream $C_a(t)$. The time delay of the concentration is $k_d = 0.5 \text{ min}$.

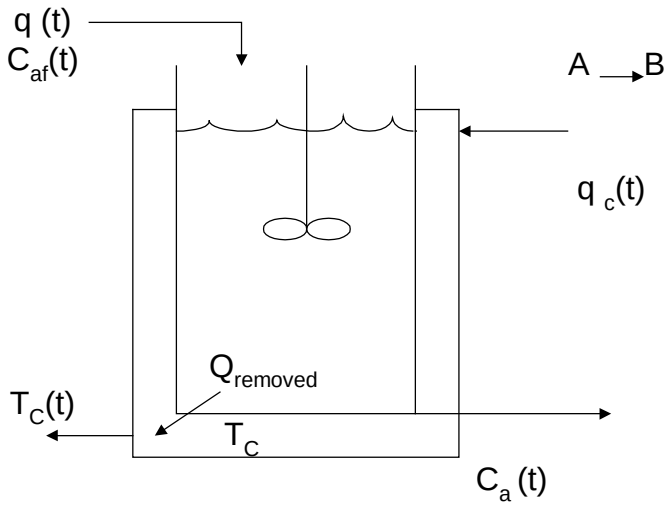

Figure 3.8 Continuous Stirred Tank Reactor with Cooling Jacket

Table 3.1 **Nominal CSTR Parameters Value**

Parameter	Nomenclature	Value
Measured concentration	C_a	0.1 mol L^{-1}
Reactor temperature	T	438.5 K
Coolant flow rate	q_c	103.41 L min^{-1}
Process flow rate	q	100 L min^{-1}
Feed concentration	C_{a0}	1 mol L^{-1}
Feed temperature	T_0	350 K
Inlet coolant temperature	T_{c0}	350 K
CSTR volume	V	100 L
Heat-transfer term	hA	7.0 x 10^5 cal min^{-1} K^{-1}
Reaction rate constant	k_0	7.2 x 10^{10} min^{-1}
Activation energy	E/R	1.0 x 10^4 K^{-1}
Heat of reaction	ΔH	-2.0 x 10^5 cal mol^{-1}
Liquid densities	ρ, ρ_c	1.0 x 10^3 g L^{-1}
Specific heats	C, C_{pc}	1.0 x 10^3 cal K^{-1}
Sampling Time	Ts	0.01s

3.4.1. Design of the Neuro-Fuzzy Model

The model of the reactor CSTRCJ was excited in open-loop with the function as shown in Figure 3.20.

Figure 3.9 includes the training data of the Neuro-Fuzzy model. In the process of training, it was necessary to select adequate training data choosing an input in open-loop that covered the operating range to ensure a correct Neuro-Fuzzy modelling.

In addition, the training process required the type membership function to be selected for the inputs and output and the number of fuzzy set per inputs, step size of training, enough number of pair of data for convergence, number of epoch (iteration), type of

optimization algorithm. The general information of the Neuro-Fuzzy model is shown in Table 3.2.

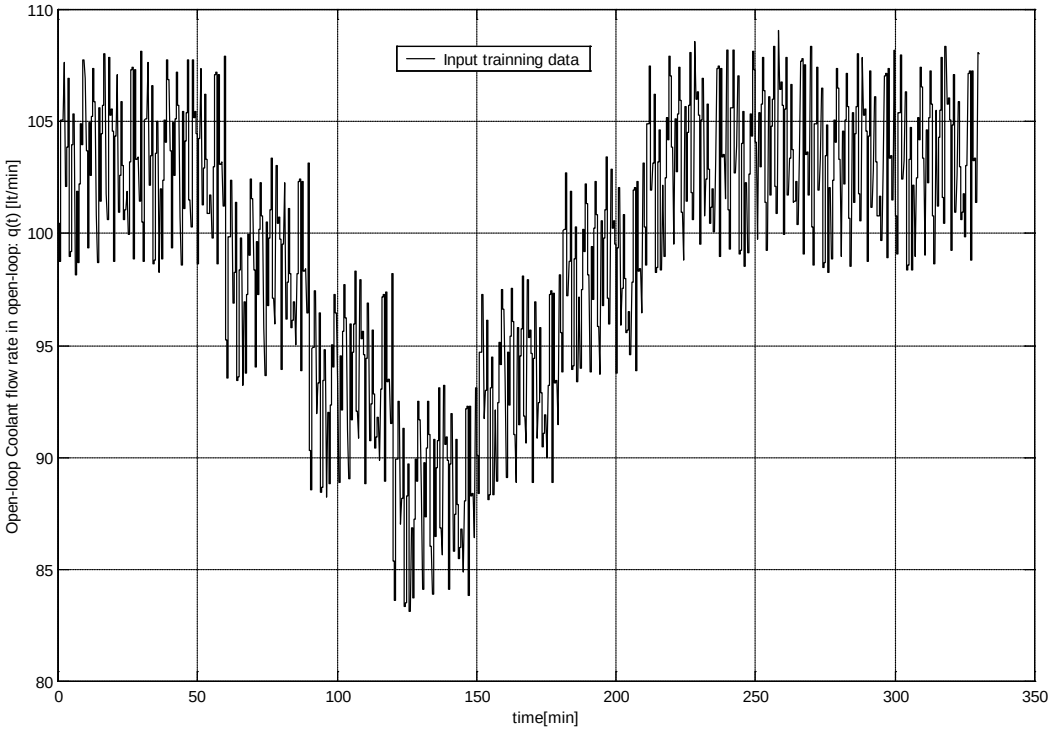

Figure 3.9 Input Training Data in Open-Loop

Table 3.2 General Information of the Neuro-Fuzzy Model

Parameter	***Description***
Number of nodes	55
Number of linear parameters	80
Number of nonlinear parameters	24
Total number of parameters	104
Number of training data pairs	3000
Number of checking data pairs	0
Number of fuzzy rules	16
Type of input membership function	*gbellmf*: Generalized bell curve membership function.

And method	Product
Or method	Maximum
Type of Fuzzy System	Takagi-Sugeno-Kang
Type of output membership function	First order and linear
Defuzzification method	Weigthed average

After training the best model was obtained and the responses are shown in Figures 3.10 and 3.11. The Reactor Temperature was not taking as output signal of the nonlinear plant because for this case the system is not a SISO system.

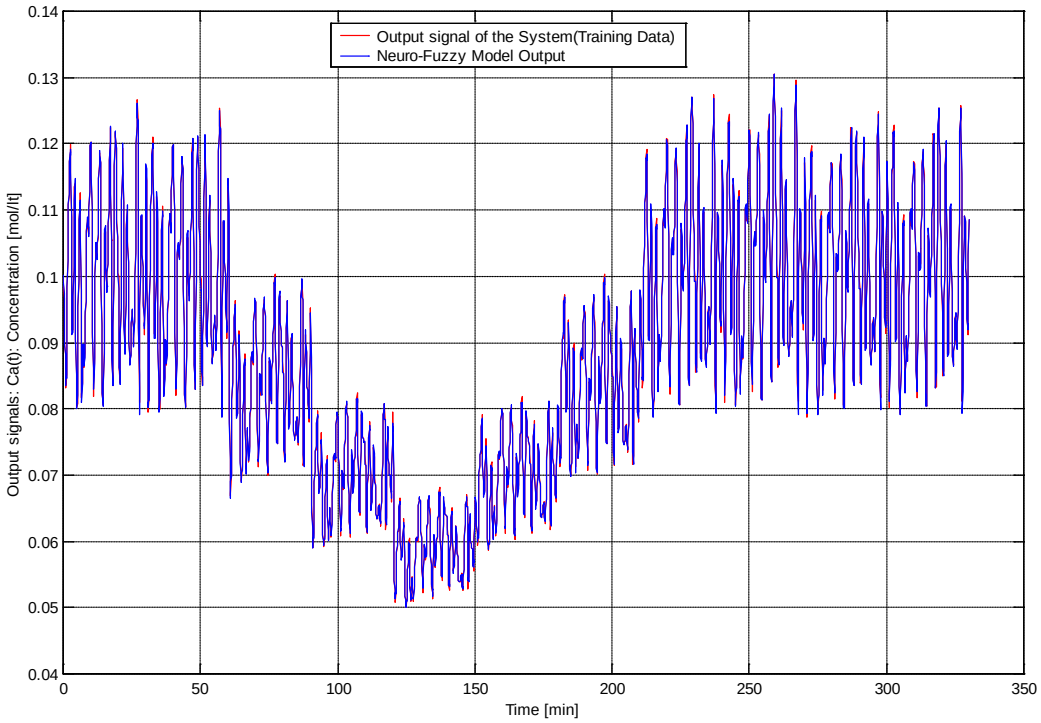

Figure 3.10 System Output (training Data) and Neuro-Fuzzy Model Output

In the training process, it is very important to select the appropriate data for identifying the best model without the problem of convergence in the optimization method. The error between the plant and the Neuro-Fuzzy model should be a minimum or approximately zero. After the training process, all the parameters of the Neuro-fuzzy model were found. The difference between the correct model of the Reactor and the Neuro-Fuzzy model is shown in Figure 3.11.

3.4.2. Membership Functions and Fuzzy Sets of the Inputs

The type of fuzzy sets for the membership functions of the inputs is the "generalized bell curve membership function". These were defined as follows:

$$gbellmf\left(x,\left[a \quad b \quad c\right]\right)=\frac{1}{\left(\left(1+\left|\frac{x-c}{a}\right|\right)^{2b}\right)} \tag{3.55}$$

where a, b, and c are the nonlinear parameters of the antecedent part of the fuzzy rules. x is the input signal to be mapped into the fuzzy domain.

The *fuzzy sets of the layer 1 (fuzzy interfaz input)* are defined as follows

$$G_{11}=gbellmf\left(q_c\left(t\right),\left[12.96 \quad 2 \quad 83.12\right]\right) \tag{3.56}$$

$$G_{12}=gbellmf\left(q_c\left(t\right),\left[12.96 \quad 2 \quad 108.9\right]\right) \tag{3.57}$$

The operating range for the input1 $q_c\,(t)$ (covered by G_{11} and G_{12}) is the interval [83.12 109].

$$G_{21}=gbellmf \quad \left(C_a\left(t-1\right),\left[0.06635 \quad 2 \quad 5.071\,e-05\right]\right) \tag{3.58}$$

$$G_{22}=gbellmf \quad \left(C_a\left(t-1\right),\left[0.06627 \quad 2 \quad 0.1326\right]\right) \tag{3.59}$$

The operating range for the input2 $C_a\,(t\text{-}1)$ (covered by G_{21} and G_{22}) is the interval [0 0.1326].

$$G_{31}=gbellmf \quad \left(C_a\left(t-2\right),\left[0.06623 \quad 2 \quad -4.77\,e-05\right]\right) \tag{3.60}$$

$$G_{32}=gbellmf \quad \left(C_a\left(t-2\right),\left[0.06629 \quad 2 \quad 0.1326\right]\right) \tag{3.61}$$

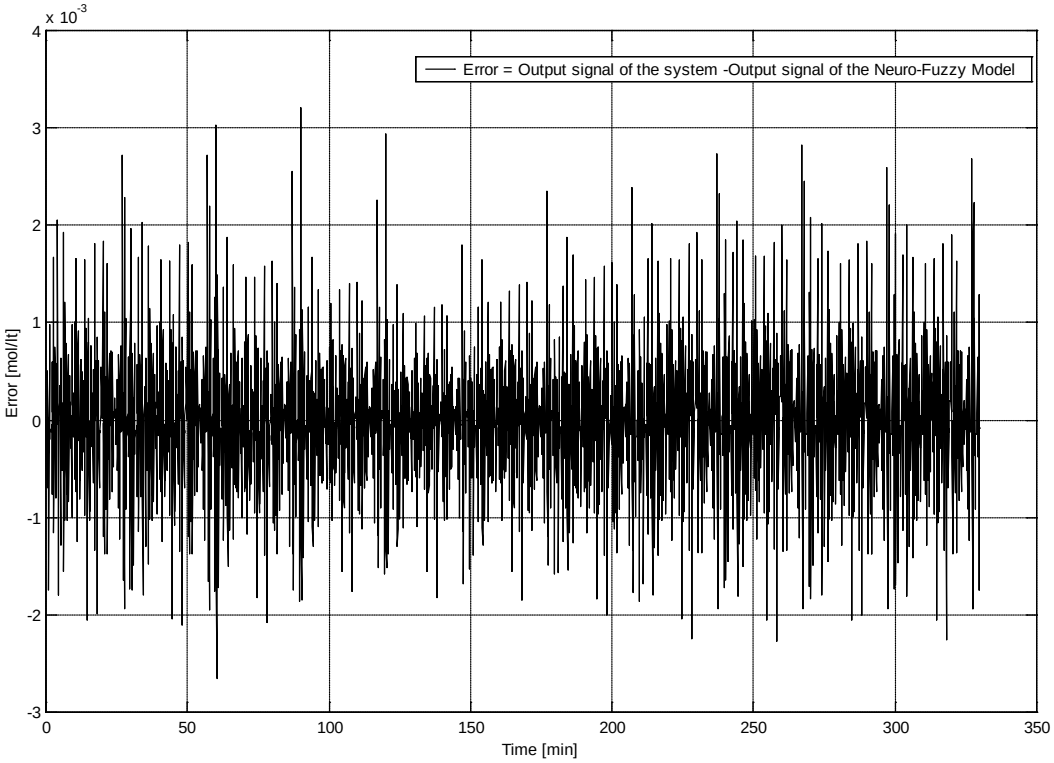

Figure 3.11 Error Signal between the Training Output Data and the Neuro-Fuzzy Model

The operating range for the input3 C_a *(t-2)* (covered by G_{31} and G_{32}) is the interval [0 0.1305].

$$G_{41} = gellmf\ \left(q_c\left(t-1\right),\left[54.45 \quad 2 \quad -1.794e-08\right]\right) \tag{3.62}$$

$$G_{42} = gbellmf\left(q_c\left(t-1\right),\left[54.45 \quad 2 \quad 108.9\right]\right) \tag{3.63}$$

The operating range for the input 4 *qc (t-1)* (covered by G_{41} and G_{42}) is the interval [0 108.9].

The fuzzy sets G_{11} and G_{12} are part of input1 q_c *(t).* The fuzzy sets G_{21} and G_{22} are part of the input2 C_a *(t-1).* The fuzzy sets G_{31} and G_{32} are part of the input3 C_a *(t-2).* The fuzzy sets G_{41} and G42 are part of the input 4 q_c *(t-1).*

3.4.3. Output Local Linear Models

The membership functions of the local outputs were defined by local linear models for the Takagi-Sugeno-Kang Model (Pinto, 2001; Pinto, et. al., 2004). The output local linear models were found after the training process and they are described using the equation (3.64). The output linear models were used in combination to represent a nonlinear sub-operation range of the model output. These models are similar to the difference equation (discrete state) and they are activated by means of the fuzzy rules. The operating range of the output linear model was the interval [0.05004 0.1326].

The general structures of the output local linear models are:

$$C_{ai}(t) = p_i\, q_c(t) + q_i\, C_a(t-1) + r_i\; C_a(t-2) + s_i\; q_c(t-1) + t_i \qquad (3.64)$$

i = 1,2, … N.

where $C_{ai}(t)$ is the n-ith linear output model, p_n, q_n, r_n, s_n , t_n are the nth parameters of the linear model and N defines the number of the fuzzy rules (i.e. N = 16 fuzzy rules in this case). The symbol "t" was chosen as a discrete time to avoid confusion with the time delay "*k*" of the nonlinear system.

The output local linear models are represented by means of the equations (3.64) substituting with the following parameter sets:

p_i ={-0.636, -0.0006988, -0.1472, -0.00235, 0.07001, -0.00224, -0.0003219, 0.0002053, 0.004346, 0.0006502, 0.01522, 0.0005565, -0.05639, 0.002772, -0.00194, 0.000009219}

q_i = {0.05138, 0.9238, -0.1259, -0.6986, 0.1722, 1.077, 0.292, 2.482, 0.09943, 1.004, 0.04869, 0.5394, -0.02905, -0.5314, 0.09263, 2.371}

r_i = {-0.04837, -0.532, 0.1317, 1.51, -0.06777, -0.7305, -0.2191, -1.564, -0.03413, -0.4555, 0.1546, 1.683, 0.05032, 0.6653, -0.2292, -1.344}

s_i = {0.0099882, 0.000284, 0.01148, 0.001514, -0.0637, 0.001996, -0.001681, -0.01311, -0.002559, 0.001428, -0.008084, 0.0004889, 0.07041, 0.0000616, 0.0007668, -0.0003219}

t_i = {0.03116, -0.2101, -0.02125, 0.1018, -0.0151, 0.05655, -0.04142, 0.1727, 0.04353, -0.1858, 0.04075, -0.2947, 0.0464, -0.3323,-0.0203, 0.04551}

3.4.4. Fuzzy Rules of the Neuro-Fuzzy Model

The fuzzy rules are the fuzzy equations for representing the free delay nonlinear model of the Reactor (CSTRCJ). They are the kernel of the Fuzzy systems because they define the fuzzy model and the operation surface of the nonlinear system. The fuzzy rules were expressed as follows:

R_i: If **x(t)** is A_i then $C_{ai}(t) = p_i\, q_c(t) + q_i\, C_a(t-1) + r_i\, C_a(t-2) + s_i\, q_c(t-1) + t_i$

i = 1,2, … N. (3.65)

where

$\mathbf{x}(t) = [q_c(t), C_a(t-1), C_a(t-2), q_c(t-1)]^T$: is the regressor vector. $q_c(t)$, $C_a(t-1)$, $C_a(t-2)$, $q_c(t-1)$ are the inputs signal of the Neuro-Fuzzy system. A_i is the i^{th} membership function and N defines the amount of the fuzzy rules.

The inputs signals are part of the antecedent (membership function) and consequent (local linear models) parts of the fuzzy rules.

Finally, the fuzzy model of the Continuous Stirred Tank Reactor with Cooling Jacket (CSTRCJ) was defined by the summarized fuzzy model (fuzzy rules) represented in Table 3.3.

Table 3.3 Summarised Fuzzy Rules

	$C_a(t-2), q_c(t-1)$	G_{31}, G_{41}	G_{31}, G_{42}	G_{32}, G_{41}	G_{32}, G_{42}
$q_c(t), C_a(t-1)$					
G_{11}, G_{21}		$C_{a1}(t)$	$C_{a2}(t)$	$C_{a3}(t)$	$C_{a4}(t)$
G_{11}, G_{22}		$C_{a5}(t)$	$C_{a6}(t)$	$C_{a7}(t)$	$C_{a8}(t)$
G_{12}, G_{21}		$C_{a9}(t)$	$C_{a10}(t)$	$C_{a11}(t)$	$C_{a12}(t)$
G_{12}, G_{22}		$C_{a13}(t)$	$C_{a14}(t)$	$C_{a15}(t)$	$C_{a16}(t)$

As an example of Table 3.3 can be observed in the following fuzzy rule:

Rule1: If $q_c(t)$ is G_{11} and $C_a(t-1)$ is G_{21} and $C_a(t-2)$ is G_{31} and $q_c(t-1)$ is G_{41} then

$C_{a1}(t) = -0.6326q_c(t)+0.05138C_a(t-1) -0.04837C_a(t-2)+0.0099882\, q_c(t-1)+0.03116$ (3.66)

Another way to represent the fuzzy model is by using its fuzzy difference equation as follows:

$$\gamma_i = \frac{\prod_{j=1}^{4} \frac{1}{\left[1+\left|\frac{x_j - c_{ij}}{a_{ij}}\right|\right]^{2b_{ij}}}}{\sum_{i=1}^{16} \prod_{j=1}^{4} \frac{1}{\left[1+\left|\frac{x_j - c_{ij}}{a_{ij}}\right|\right]^{2b_{ij}}}} \tag{3.67}$$

With

$x_j = \{q_c(t), C_a(t-1), C_a(t-2), q_c(t-1)\}$: is the set of input signals.

where a_{ij}, b_{ij}, and c_{ij} are the nonlinear parameters.

The set of nonlinear parameters are:

a_{ij} = {12.96, 12.96, 0.06635, 0.06627, 0.06623, 0.06629, 54.45, 54.52}

b_{ij} = {2, 2, 2, 2, 2, 2, 2, 2}

c_{ij} = {83.12, 108.9, 5.071e-05, 0.1326, -4.77e-05, 0.1326, -1.794e-08, 108.9 }

Finally, repeating the procedure developed in Section 2.6.2. of Chapter 2, the fuzzy model (fuzzy difference equation) was represented as follows:

$$C_a(t)=\left(\sum_{i=1}^{16}\gamma_i\, p_i\right) q_c(t)+\left(\sum_{i=1}^{16}\gamma_i\, q_i\right) C_a(t-1)+\left(\sum_{i=1}^{16}\gamma_i\, r_i\right) C_a(t-2)+\left(\sum_{i=1}^{16}\gamma_i\, s_i\right) q_c(t-1)+\left(\sum_{i=1}^{16}\gamma_i\, t_i\right) \tag{3.68}$$

Figure 3.12 shows the nonlinear operating surface of the Neuro-Fuzzy model. Figure 3.13 shows the nonlinear trajectory of the Continuous Stirred Tank Reactor with Cooling Jacket in the operation range.

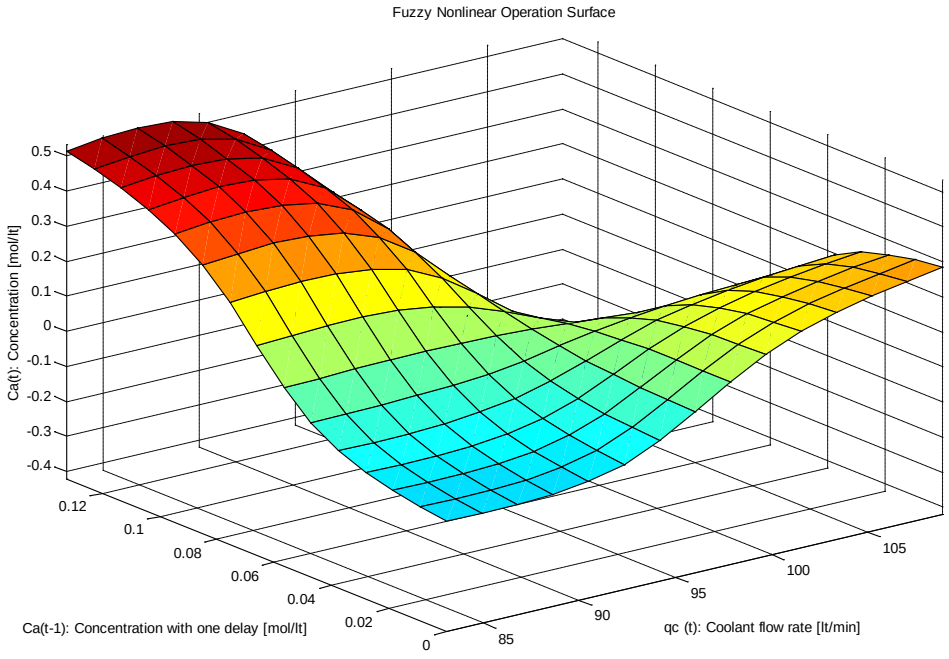

Figure 3.12 Nonlinear Operating Surface of the Neuro-Fuzzy Model

The nonlinear operating surface of the Neuro-Fuzzy model tries to set the real operation data over nonlinear fuzzy surface (smooth nonlinear surface), which emulates the real operation surface of the nonlinear plant.

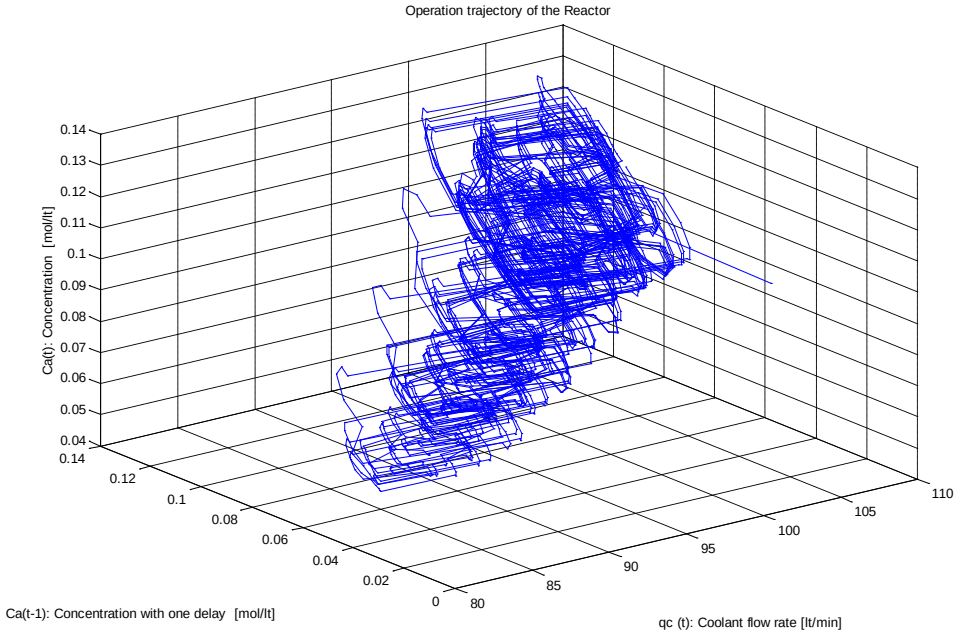

Figure 3.13 Operation of the Nonlinear Trajectory of the Continuous Stirred Tank Reactor with Cooling Jacket

Figure 3.12 describes a nonlinear surface using the Neuro-Fuzzy Model of the Reactor. The nonlinear surface includes the nonlinear trajectory of the Continuous Stirred Tank Reactor with Cooling Jacket shown in Figure 3.13. Certainly, Figures 3.12 and 3.13 are differents but the fact is that the nonlinear trajectories described by the nonlinear system in Figure 3.13 are over the nonlinear surface described by the Neuro-Fuzzy system of Figure 3.12. The previous comment is true when the Neuro-Fuzzy is able to reproduce the nonlinear plant.

Figure 3.14 shows the final structure of the Neuro-Fuzzy model of the CSTRCJ.

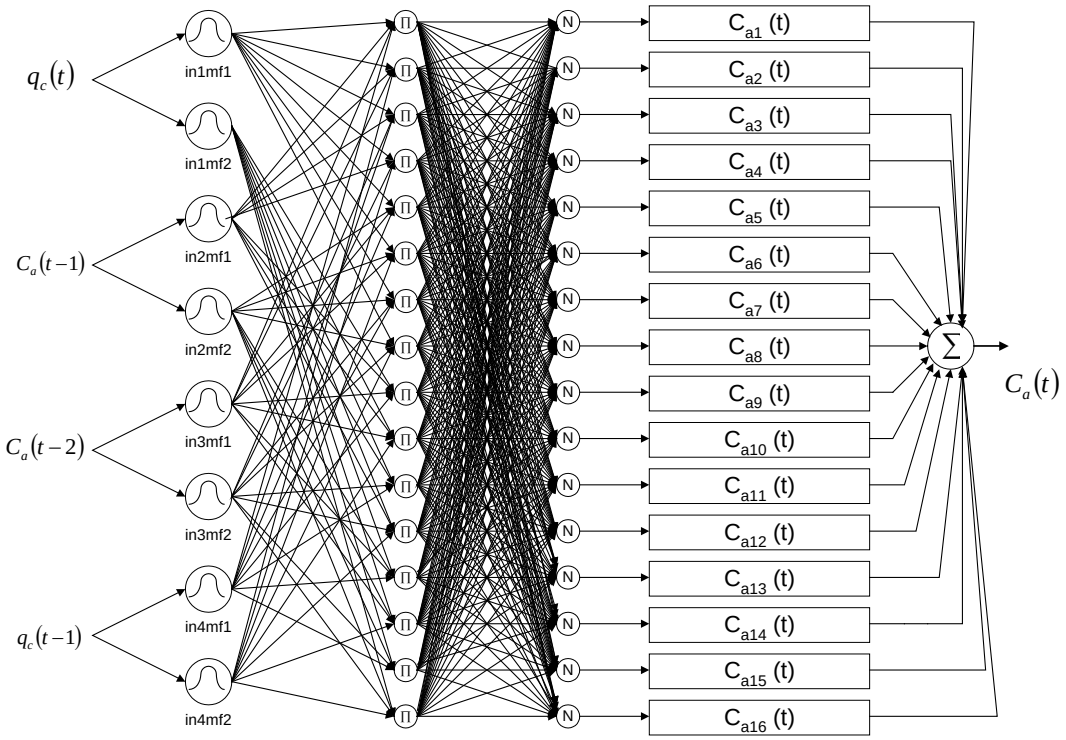

Figure 3.14 Neuro-Fuzzy Model of the Continuous Stirred Tank Reactor with Cooling Jacket

Figure 3.15 shows the final structure of the Neuro-Fuzzy Generalise Minimum Variance Controller which is a combination of the stochastic control and neuro-fuzzy control. To design, the parameters of the controller:

k =3; A_f =1 -0.8z^{-1} ; C_d = 0.005; E=0; k_p = 9;
k_i = 20; k_d = 0; ρ = 5.5; a= 0.785 ; b =1.

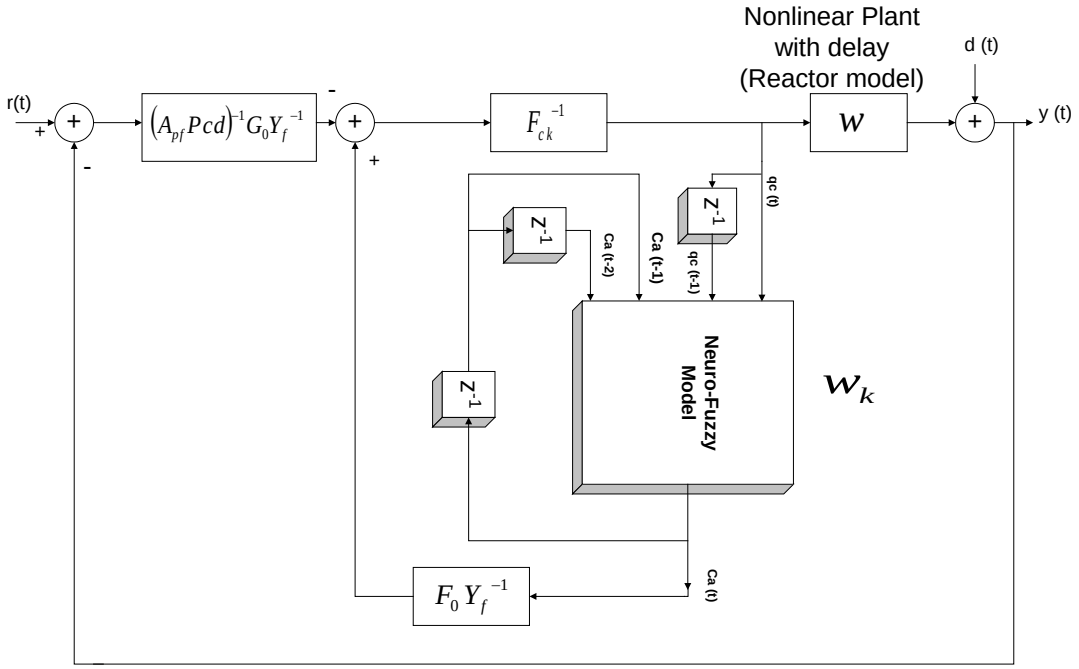

Figure 3.15 Final Structure of the Neuro-Fuzzy Generalise Minimum Variance Controller

The nominal parameter values in the model of the Reactor are described in Table 3.1 The time delay of the concentration is $k_d = 0.5$ min. The digital filter (PI controller) was defined by: $k_p = 10$ and k_i =10.

3.4.5. Tracking Reference Test

In this test the reference signal was changed in the extremes of operation range of the CSTRCJ. The reference signal Fc_{ref} is varying from to 0.1 mol L^{-1} to 0.055 mol L^{-1}, from 0.055 mol L^{-1} to 0.125 mol L^{-1} , and from 0.125 mol L^{-1} to 0.1 mol L^{-1} in intervals of 10 min. The results of this test are shown from Figures 3.16 to 3.18. The results shows the responses of the output signal between the GMV with the correct model and the NFGMV are almost similar. It means the Neuro-Fuzzy model is a good approximation for the nonlinear plant. Both of them show better performance than the PI controller in the tracking reference test.

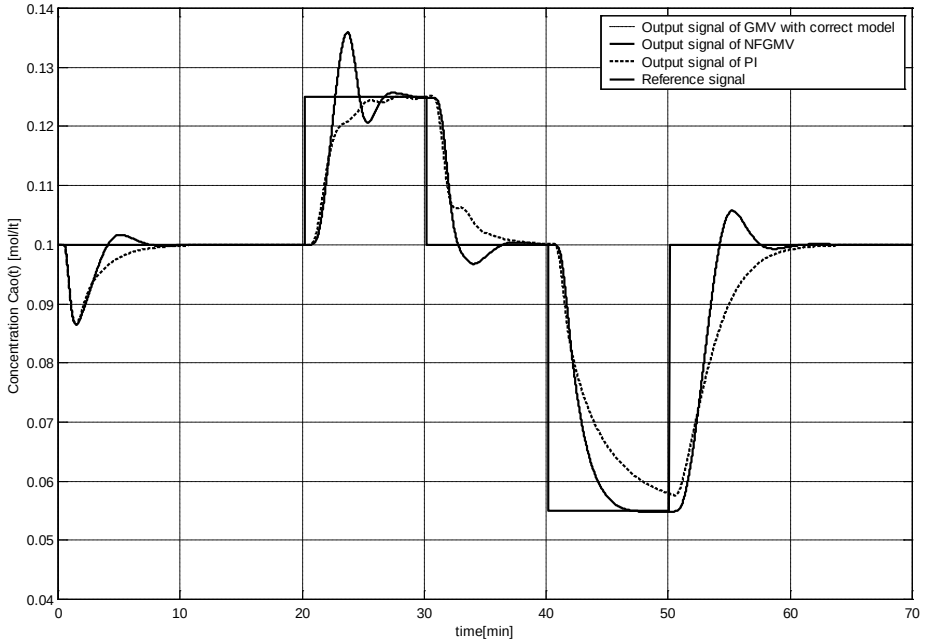

Figure 3.16 Output Signals of the Filter and NFGMV in the Tracking Reference Test

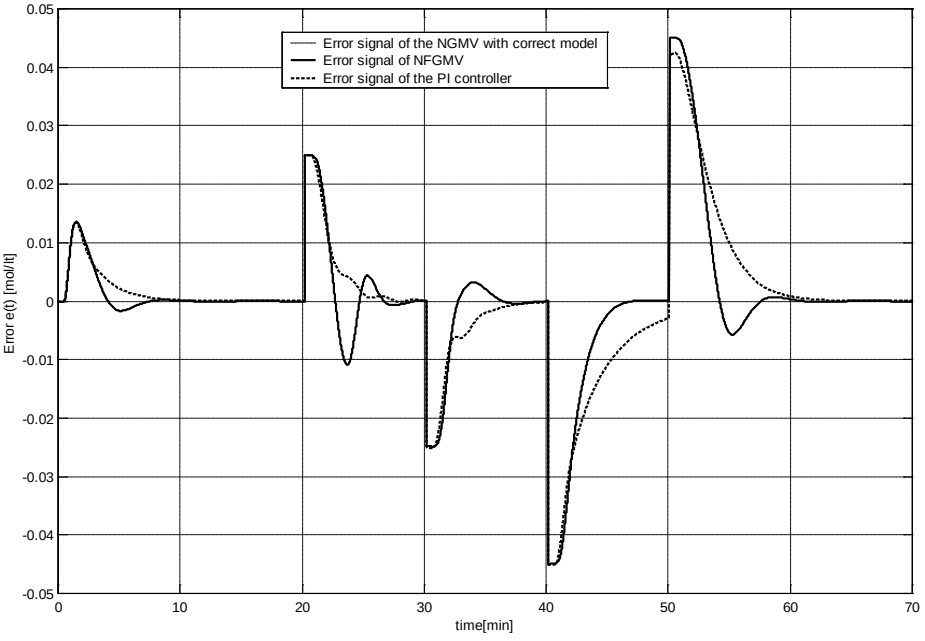

Figure 3.17 Error Signals of the Digital Filter and NFGMV in the Tracking Reference Test

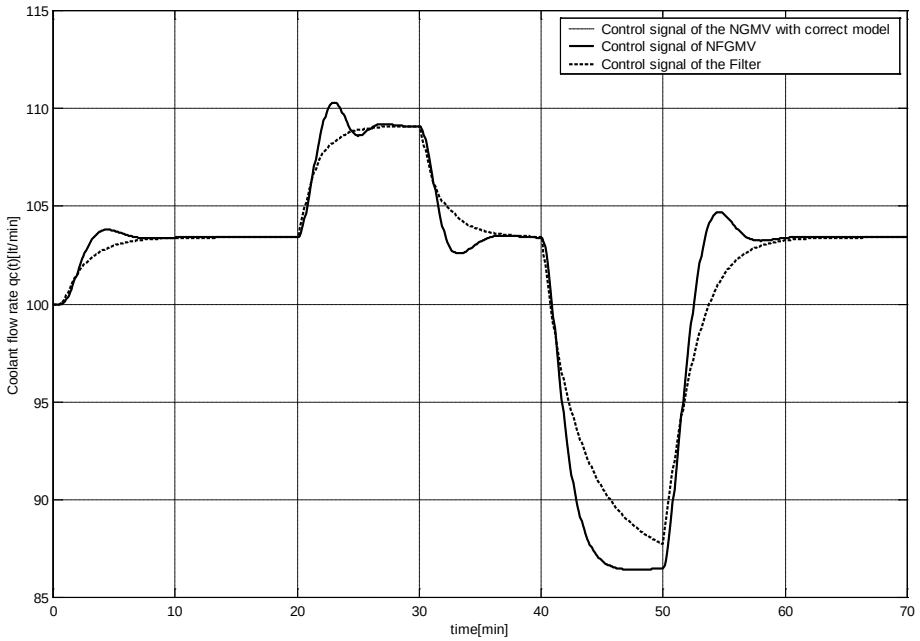

Figure 3.18 Control Signals of the Digital Filter and NFGMV in the Tracking Reference Test

The error signal is higher in the PI controller than the error signal than the GMV with the correct model and the NFGMV controller (the area covered by the Error signal of the PI is bigger than the NFGMV controller). The control signal of the PI controller is very slow and limited in several intervals because of the strong nonlinearities of the plant.

3.4.6. Disturbance Rejection Test

In this text the reference signal Fc_{ref} was maintained constant in 0.1mol L^{-1}. Here, one disturbance was applied to the CSTRCJ. The disturbance was applied to the 130 seconds of the simulation. It was also applied in steady state conditions.

The results of this test are shown from Figures 3.19 to 3.21. The responses of the GMV controller with the correct model and the NFGMV are faster to reject a disturbance than the PI controller because of the limitations in speed and amount of the control signal. Moreover, this effect is also shown in the error signal.

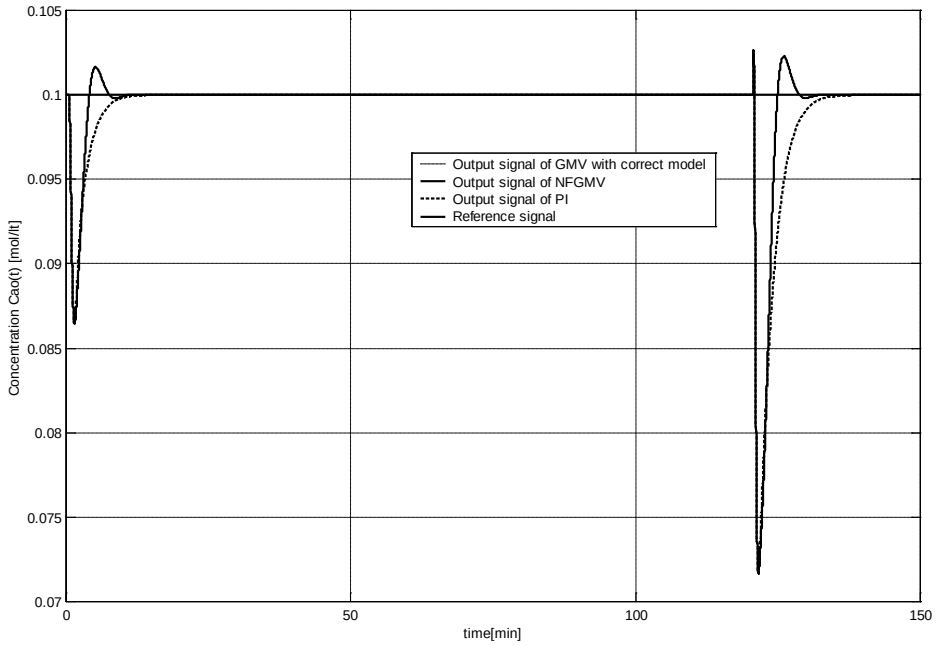

Figure 3.19 Output Signals of the Digital Filter and NFGMV in the Perturbance Rejection Test

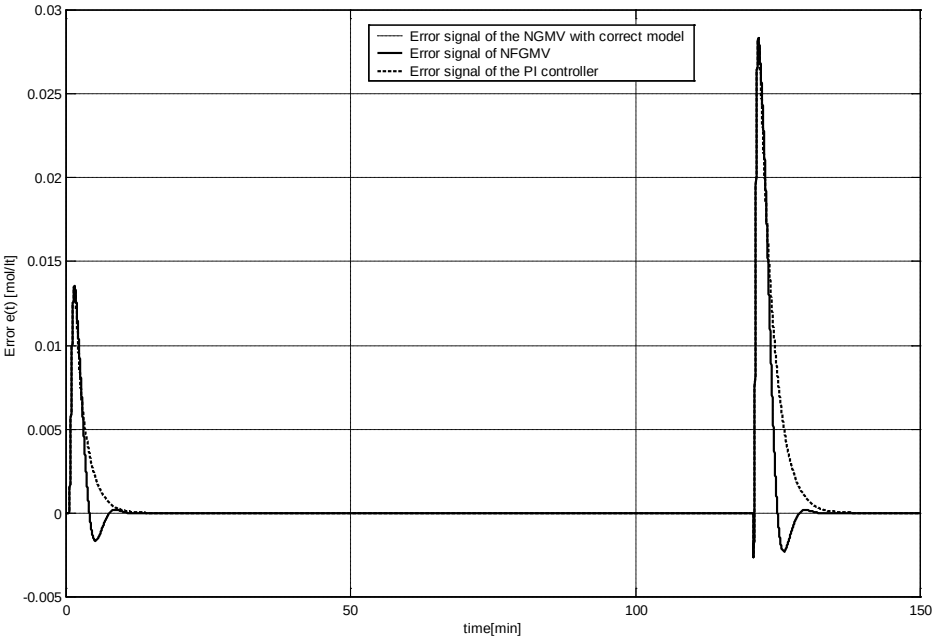

Figure 3.20 Error Signals of the Digital filter and NFGMV in the Perturbance Rejection Test

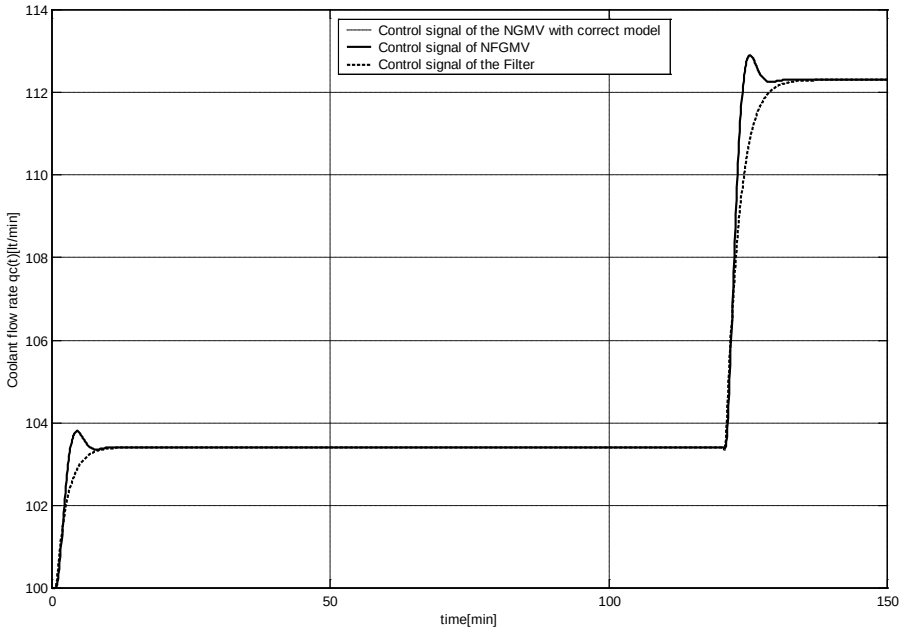

Figure 3.21 Control Signals of the Digital Filter and NFGMV in the Perturbance Rejection Test

3.4.7. Robustness Test

In this test, the reference signal Fc_{ref} was varied from to 0.1 mol L^{-1} to 0.125 mol L^{-1}, from 0.125 mol L^{-1} to 0.055 mol L^{-1}, and from 0.055 mol $L^{-1}$to 0.1 mol L^{-1}. The results of this test are shown in Figures 3.22 to 3.24.

The variation of the nominal CSTR parameters are the following:

V=95 L, hA=6.95e5 cal min^{-1} K^{-1}, k_0=7.25 x 10^{10} min^{-1}, E/R=1.0 x 10^4 K^{-1}, ΔH = -2.2 x 10^5 cal mol^{-1}, $\rho = \rho_c = 1.04$ x 10^3 g L^{-1} and $C = C_{pc} = 1.0$ x 10^3 cal K^{-1}.

The variations for the nominal CSTR parameters can be observed comparing the previous values with the values in Table 3.1.

The results of this test are shown in Figures 3.22 to 3.24. The GMV controller with the correct model and the NFGMV controller have a robustness better dynamical

behaviour than the PI controller. The reaction of the PI controller is very limited in amount and speed of reaction.

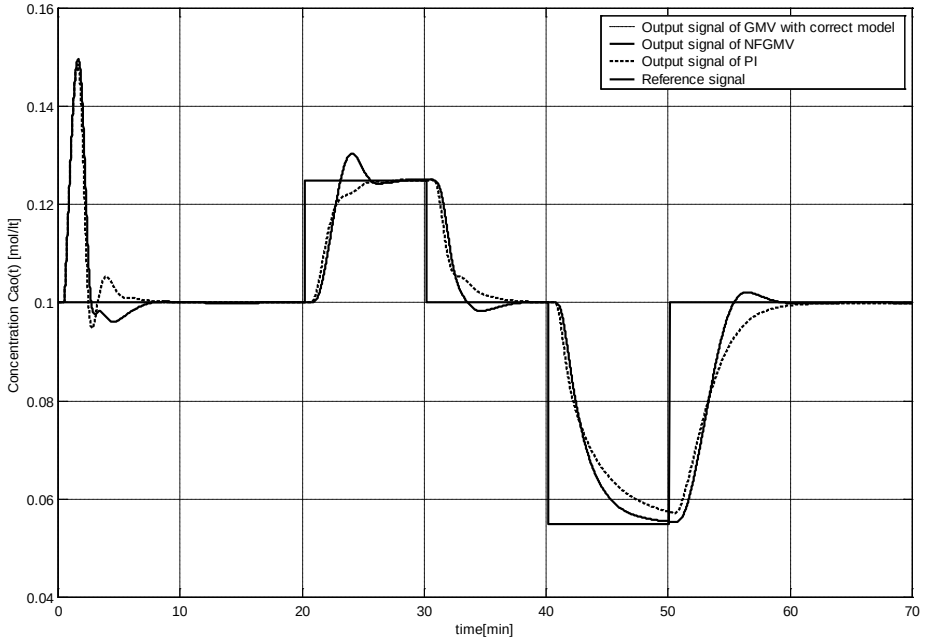

Figure 3.22 Output Signals of the Digital Filter and NFGMV in the Robustness Test

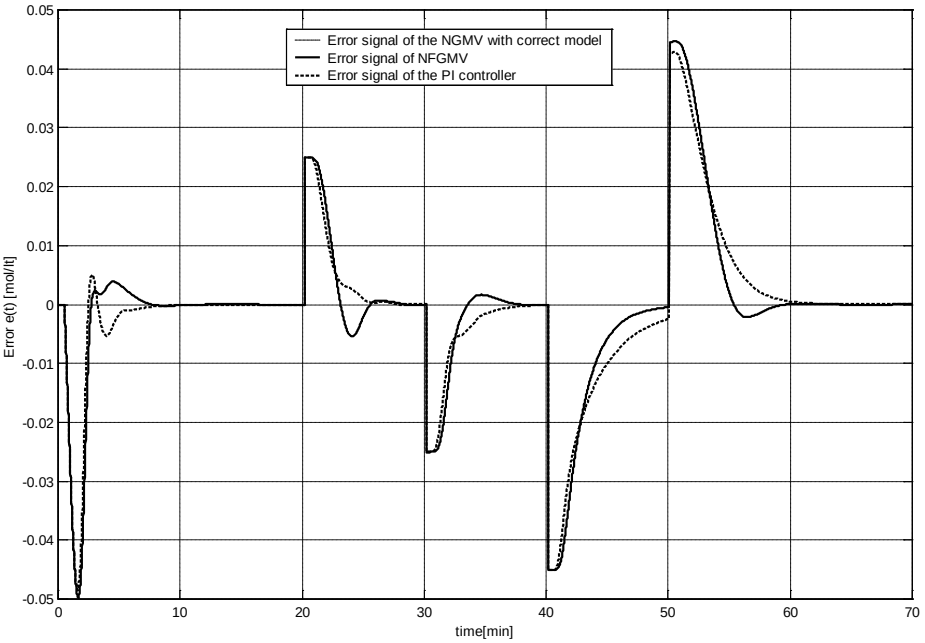

Figure 3.23 Error Signals of the Digital Filter and NFGMV in the Robustness Test

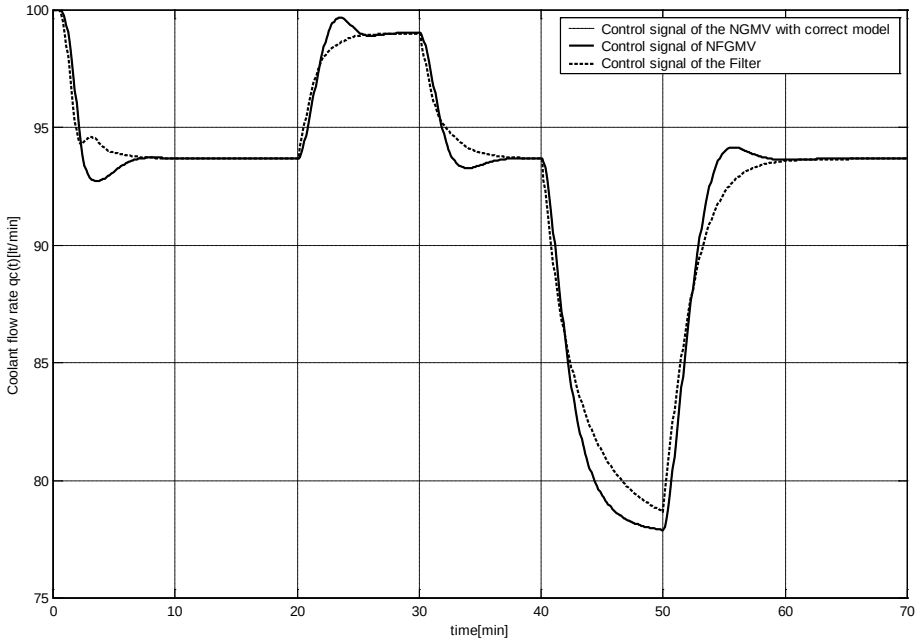

Figure 3.24 Control Signals of the Digital Filter and NFGMV in the Robustness Test

The tests above showed that the Neuro-Fuzzy Generalized Minimum Variance controller had the best dynamic behaviour from the point of view of tracking reference, disturbance rejection and robustness. On the other hand, the Neuro-Fuzzy Generalized Minimum Variance controller shown a faster dynamic response. This approach is easy to design, interpret and analyse. This hybrid system (Generalised minimum variance and Neuro-Fuzzy system) has been shown to give the same results (for practical purposes) as the GMV with the correct model. In addition, the Fuzzy model obtained for the Reactor has shown that this approach has a simple interpretation in the manner of data processing different to black box.

3.5. Self-Tuning Neuro-Fuzzy Generalised Minimum Variance Controller

The Self- Tuning Neuro-Fuzzy GMV control law was also developed by Pinto, Grimble and Katebi (2005) inspired by the initial idea developed by Pinto and co-workers (2004). The adaptive mechanism was developed using a Mamdani's Fuzzy model.

Fuzzy Logic has been applied in many areas with success. It is a qualitative representation of the natural process using fuzzy rules (Pinto, 2001). Fuzzy identification uses also fuzzy rules to identify the objective model. This model has been used to control plants using adaptive Neuro-Fuzzy (NF) controllers and models (Pinto, et. al., 2005). The Tuning of controllers has always represented a challenge because it is usually heuristic and trial-error based. The fuzzy tuning mechanism has been reported before in some previous works in order to tune several types of controllers (He et all. , 1993; Molengraft, 1995; Wang , 1997; Mudi and Nikhil ,1999; Pinto ,2001a; Babuška et. all., 2002). The advantages of these structures are the capacity to adapt the parameters of the controller to the changes of the parameters of the plant and also save time in the tuning procedure of the controller.

The main contribution of this development was to design and apply the Self-Tuning Neuro-Fuzzy GMV (STNFGMV), which uses the fuzzy expert knowledge of dynamical weightings (Error Weighting and Control Weighting) to tune the controllers. Also, other important feature of this controller is that we only need input-ouput data of the plant in order to identify the nonlinear model. This controller was based on a polynomial system approach combined the Neuro-Fuzzy (NF) model and the Fuzzy Self-Tuning Mechanism. The STNFGMV was applied to a model of the Continuous Stirred Tank Reactor with Cooling Jacket and it was compared to a PI controller, GMV controller with the correct model and the Fuzzy-PI controller heuristically designed and used in (Pinto 2001, Pinto and Madrigal, 2001). Also this controller gives us the possibility to control nonlinear systems with delay. Simulation results are presented to demonstrate the performance of the proposed method.

3.5.1. STNFGMV CONTROL LAW

The STNFGMV controller has a structure formed by the Neuro-Fuzzy GMV controller and the Fuzzy Self Tuning Mechanism. The general structure of the STNFGMV is shown in Figure 3.25. This NFGMV is a hybrid controller that combines the stochastic control (controller colored by white noise zero-mean) with the NF modeling.

The hybrid algorithm takes advantage of the individual characteristics of the ANN and FL in order to make the physical meaning clear, using the fuzzy rules and the acquisition of the expert knowledge by the training as an ANN. To tune the NFGMV controller by trial and error, much time was spent in order to obtain appropriate values for the control weighting P_c .and error weighting F_c .

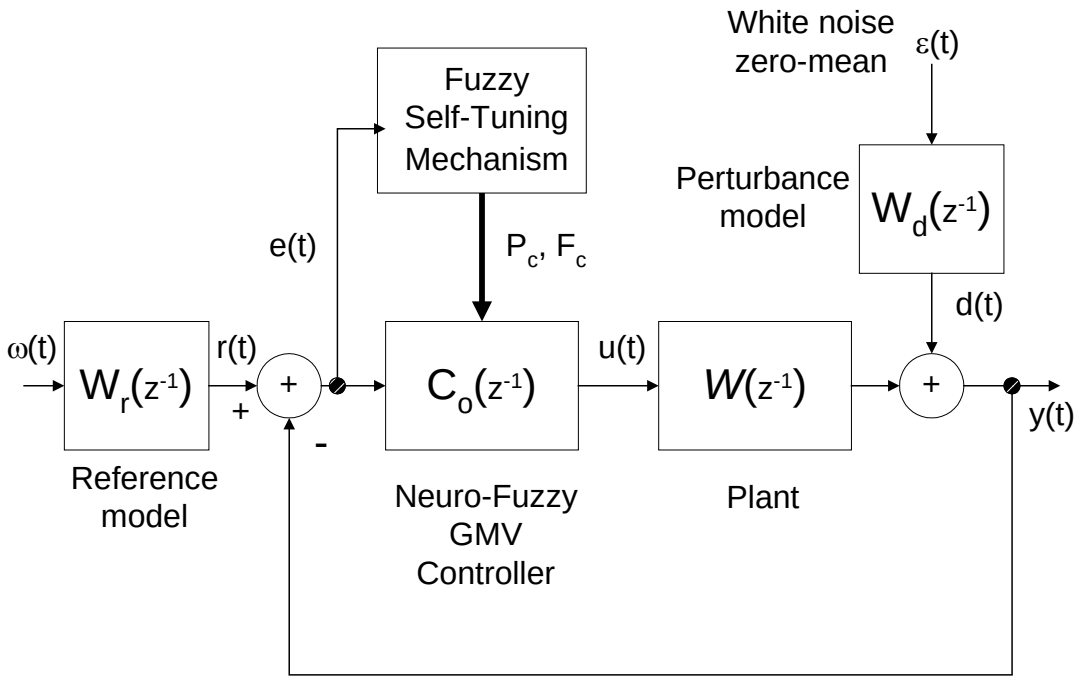

Figure 3.25 General Structure of the Self-Tuning Neuro-Fuzzy Generalised Minimum Variance Controller

The models and signals present in the STNFGMV controller are the same as those of the NGMV controller and the NFGMV controller (see Appendix B.1.). The new block included in the STNFGMV control law is the block of the Self-tuning Mechanism.

3.5.2. Neuro-Fuzzy Models

The Takagi-Sugeno-Kang (TSK) model uses the principle of "divide and conquer" by using overlapping local linear models to approximate the behaviour in the operating range of nonlinear plants. These local linear models are linear models or piece-wise linear models that are locally stables, which produce the stability of the TSK model (Pinto, et. al., 2004). The TSK model uses an NARX (nonlinear autoregressive with exogenous input) input-output model. The modeling process is the same developed in the previous section, which is described by equations (3.52)-(3.54).

3.5.3. The Error and Control Weighting

The Error Weighting P_c and Control Weighting F_c were defined initially in equations (B.18) and (B.19) of Appendix B. The Error Weighting was expressed as follows:

$$P_c = \frac{P_{cn}}{P_{cd}} = \frac{(k_{P0} + k_P)(k_{I0} + k_I) - (k_{P0} + k_P)z^{-1}}{1 - z^{-1}} \tag{3.69}$$

where k_{P0} and k_{I0}, are the proportional and integral gain of the PI controller that can initially stabilize the nonlinear plant, respectively. The variables k_P and k_I are the gains computed by the Fuzzy Self-Tuning Mechanism and take the initial value of zero.

The Control Weighting was expressed as follows:

$$F_{ck} = \frac{F_{cn}}{F_{cd}} = (\rho + \rho_0) \times \frac{(1 - a\, z^{-1})}{(1 - b\, z^{-1})} \tag{3.70}$$

where ρ_0, a and b are constants for tuning the Control Weighting without delay F_{ck}. The variable ρ is a gain introduced by the Self-Tuning Mechanism. The Error Weighting P_c and Control Weighting F_{ck} are nonlinear filters due to their adaptation on-line in each sample time.

3.5.4. Self-Tuning Mechanism

The Fuzzy Self-Tuning Mechanism of the controller has been built using expert knowledge to tune the gains in the PI controller (heuristically designed) for the Error Weighting P_C and in the dynamic effect over the response of ρ for the Control Weighting F_c. The expert knowledge was defined using Fuzzy rules with a structure represented by Mamdani Fuzzy System (Pinto, 2001; Pinto, et. al., 2004). The rules definition was obtained using the error signal $e(k)$ and increment of the error signal

$\Delta e(k)$ as indicators of the dynamic behaviour of the output. The fuzzy rules for the Fuzzy Self-Tuning Mechanism have the following structure:

$$IF\ e(k)\ is\ Z\ and\ \Delta e(k) is\ Z\ \ Then\ k_p\ is\ Z\ and\ k_i\ is\ Z\ and\ \rho\ is\ Z \tag{3.71}$$

The Fuzzy Rules Base for the variables k_p and ρ are the same and are defined in Table 3.4. The Fuzzy Rules Base for the variable k_I is defined in Table 3.5.

Table 3.4. Fuzzy Rule of the Variables e(k), Δe(k), k_P and ρ

$\Delta e\ /e$	***MN***	***N***	***Z***	***P***	***MP***
MN	MN	MN	MN	N	MN
N	MN	N	N	N	MP
Z	MN	N	Z	P	MP
P	P	P	P	P	MP
MP	MP	MP	MP	MP	MP

Table 3.5 Fuzzy Rule of the Variable k_I

$\Delta e\ /e$	***MN***	***N***	***Z***	***P***	***MP***
MN	MP	MP	MP	MP	MP
N	MP	P	P	P	P
Z	P	Z	Z	Z	P
P	P	P	P	P	MP
MP	MP	MP	MP	MP	MP

The variables k_p, k_i and ρ are nonlinear functions of the error and the difference of the error, expressed by the next equations:

$$k_p(k) = f(e(k), \Delta e(k)) \tag{3.71}$$

$$k_I(k) = g(e(k), \Delta e(k)) \tag{3.72}$$

$$\rho(k) = h(e(k), \Delta e(k)) \tag{3.73}$$

Equations (3.71), (3.72) and (3.73) are nonlinear digital filters. The membership functions for the error signal $e(k)$, increment of the error $\Delta e(k)$, proportional gain k_P and control weighting ρ are shown in Figure 3.26. The membership function for the integral gain k_I is shown in Figure 3.27.

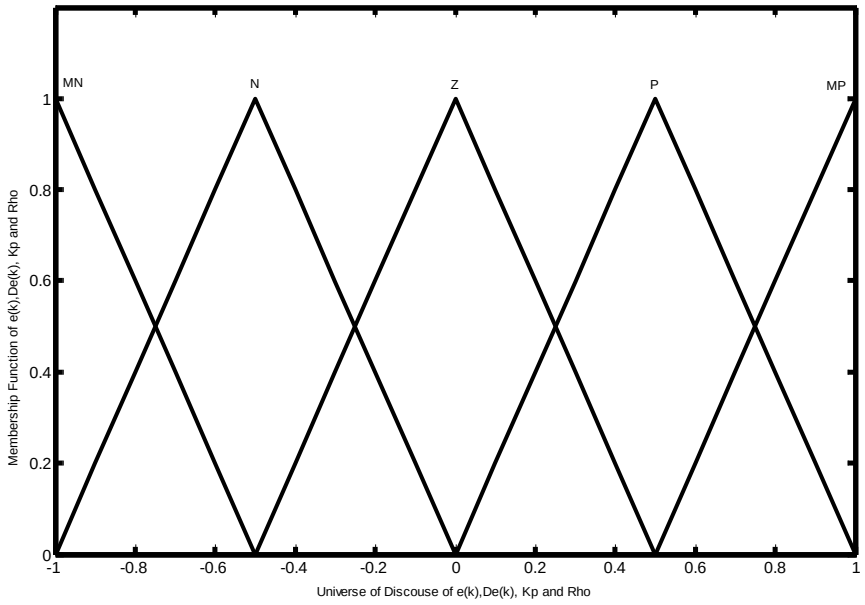

Figure 3.26 Membership Function of the Variables $e(k), \Delta e(k)$, k_P and ρ

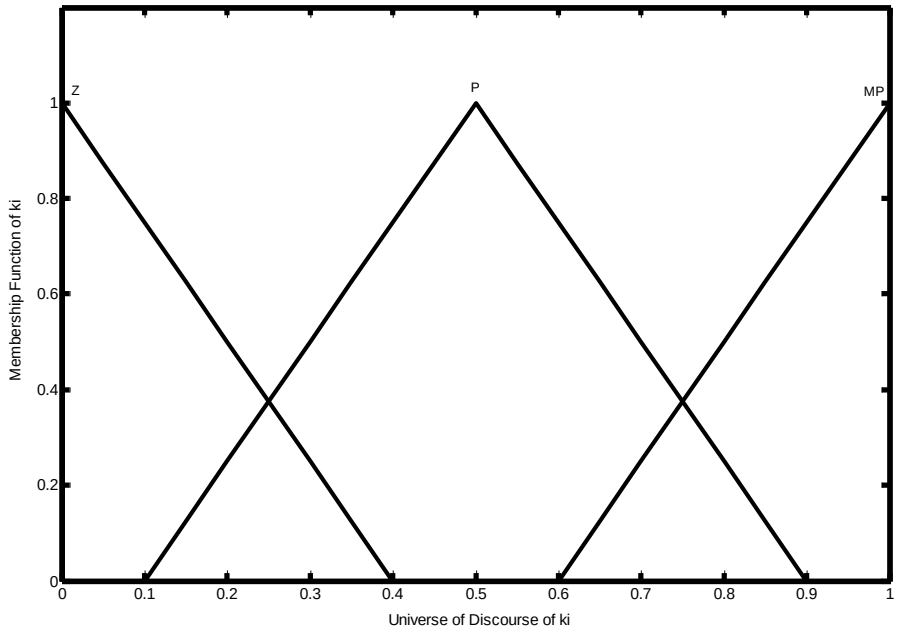

Figure 3.27 Membership Function of the Variable k_I

There are 25 fuzzy rules for each variable (k_p, k_i and ρ). The expert knowledge of the process variable was obtained from the dynamic analysis of the NGMV developed in (Pinto, et. al., 2004).

For the variable k_i positives values were selected because is the variable can only be positive. In Tables 3.4-3.5 the names of the Fuzzy set are More Negative (MN), Negative (N), Zero (Z), Positive (P) and More Positive (MP). The fuzzy sets are defined in Figure 3.26 and 3.27.

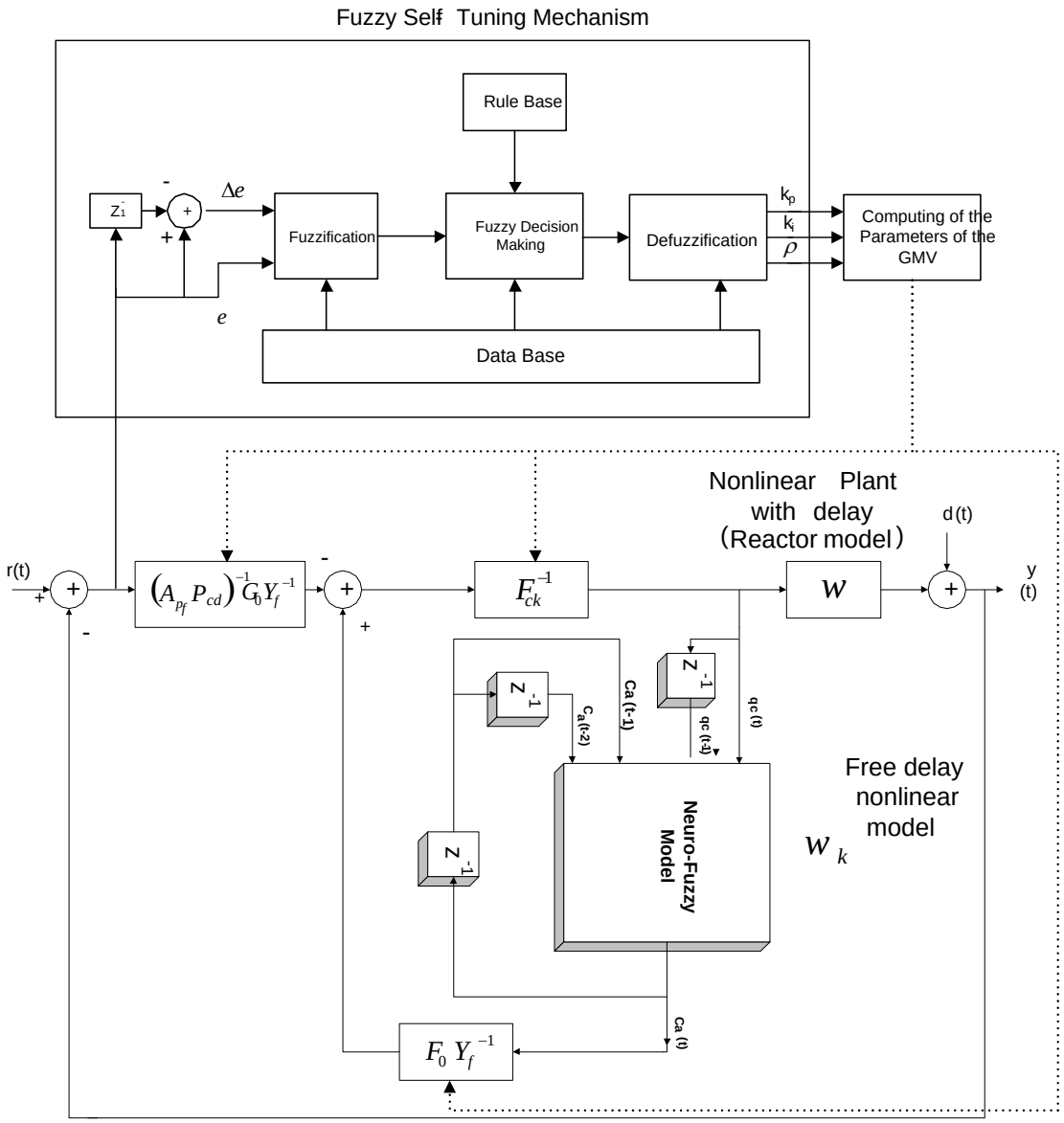

Figure 3.28 Final Structure of the Self-Tuning Neuro-Fuzzy Generalized Minimum Variance Controller

3.5.5. APPLICATION OF THE STNFGMV CONTROLLER

The simulation example selected is the same selected in Section 3.4 for the NFGMV controller (i.e. irreversible exothermic reaction that occurs in the Continuous Stirred Tank Reactor with Cooling Jacket). The Model of the Continuous Stirred Tank Reactor with Cooling Jacket was described previously with equations (3.51)-(3.54).

The initial parameters for the STNFGMV controller are as follows:

k =3; A_f =1 -0.8z^{-1} ; C_d = 0.005; E=0; k_p = 9;

$k_{i\,0}$= 20; k_{d0} = 0; ρ_0 = 6.5; a= 0.785 ; b =1.

3.5.5.1. The Neuro-Fuzzy Model of the Nonlinear Plant

The Neuro-Fuzzy model used was the same model used in the previous Section 3.4. described for equations (3.55)-(3.68) and described from Figures (3.15) to (3.21).

3.5.6. Tests

The tests have been carried on by comparing the dynamical behaviour to tracking reference and robustness of the GMV controller with correct model, Self-Tuning NFGMV controller, PI controller and PI fuzzy controller (Pinto and Madrigal, 2001).

3.5.6.1. Tracking Reference Test

In this test the reference signal was changed in the extremes of operation range of the CSTRCJ. The reference signal Fc_{ref} varies from to 0.1 mol L^{-1} to 0.125 mol L^{-1}, from 0.125 mol L^{-1} to 0.1 mol L^{-1} , and from 0.1 mol L^{-1} to 0.055 mol L^{-1} in intervals of 10 min. The results of this test are shown in Figure 3.29.

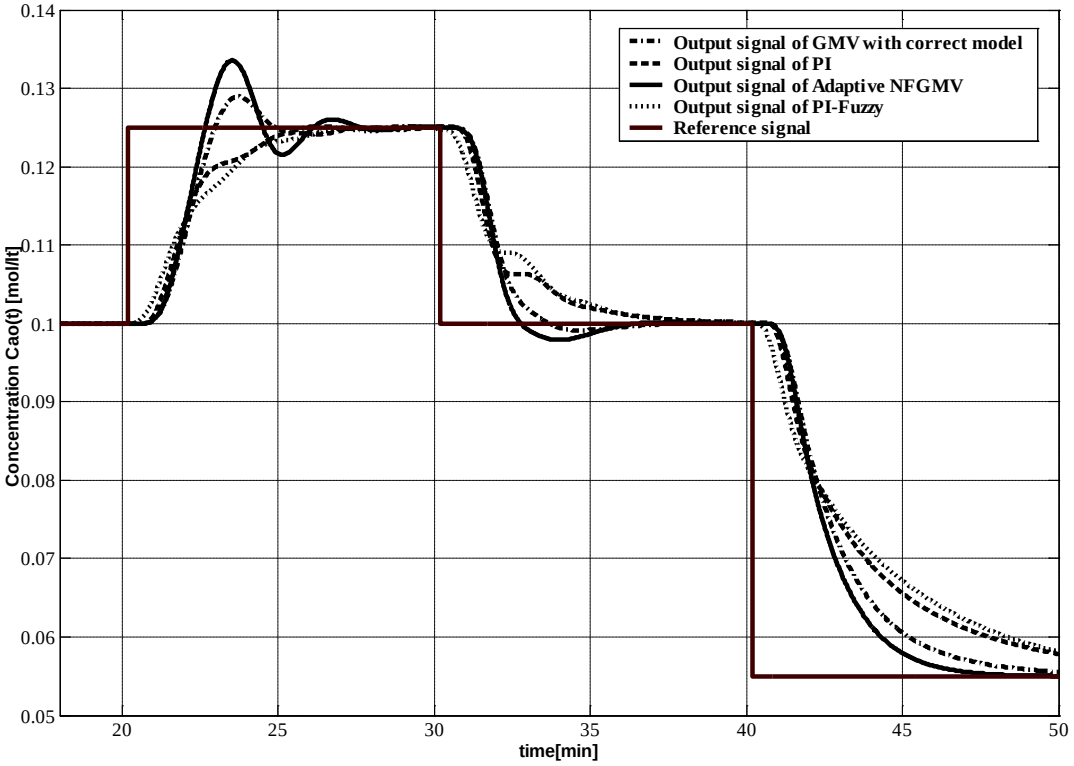

Figure 3.29 Output Signals of the Digital Filters and Self-Tuning NFGMV in the Tracking Reference Test

3.5.6.2. Robustness Test

In this test, the reference signal Fc_{ref} was varied from to 0.1 mol L^{-1} to 0.125 mol L^{-1}, from 0.125 mol L^{-1} to 0.1 mol L^{-1} , and from 0.1 mol $L^{-1}$to 0.055 mol L^{-1} in intervals of 10 min. The results of this test are shown in figures 3.30.

The variations of the nominal CSTRCJ parameters are:

V=95 L, hA=6.95e5 cal min^{-1} K^{-1}, k_0=7.25 x 10^{10} min^{-1}, E/R=1.0 x 10^4 K^{-1}, ΔH = -2.2 x 10^5 cal mol^{-1}, $\rho = \rho_c = 1.04$ x 10^3 g L^{-1} and $C = C_{pc} = 1.0$ x 10^3 cal K^{-1}.

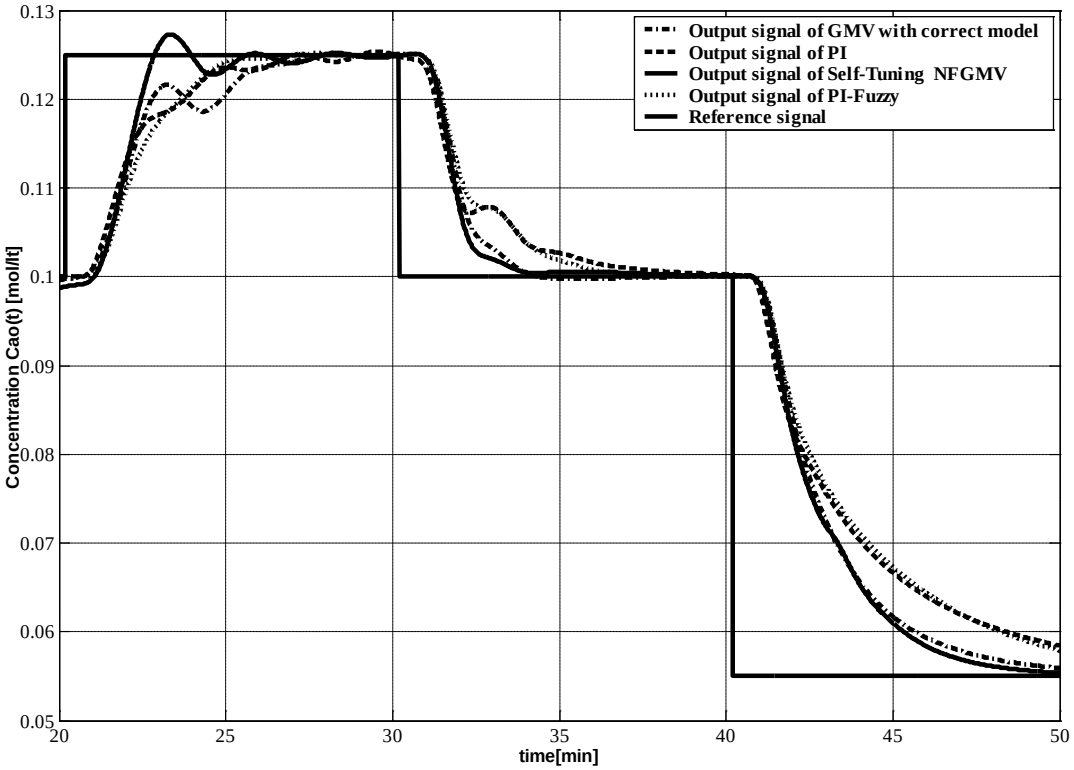

Figure 3.30 Output Signals of the Digital Filters and NFGMV in the Robustness Test

3.5.6.3. Conclusions

The STNFGMV simplifies the time consuming for the tuning process of the NFGMV controller, because it is automatic. The dynamic behaviour of the STNFGMV is better than the GMV controller with the correct model and the PI controller and the PI fuzzy controller in the complete operation range for the Continuous Stirred Tank Reactor with Cooling Jacket (nonlinear process). The PI shown a poor performance when the reference signal was changed between different levels.

Chapter 4 Powertrain Neuro-Fuzzy Control Systems

4.1. Introduction

This chapter is concerned with the automotive powertrain engine Neuro-Fuzzy control systems and the automotive powertrain system. It includes an historical introduction of the development of the car engine system, state of the art of the car engine applications, and basic concepts of the automotive powertrain. The basic concepts include a complete explanation about the dynamical behaviour of the car engine, including its characteristics and challenges for the control engineers. Also, this chapter aims are the control objective in the car engines and the current developments in the automotive industry using neural networks and the neurofuzzy control systems applied to the car engine. Finally, this chapter has several conclusions, which include a discussion about the experiments and future research in order to solve the car engine problem (see Chapter 7).

Every country is affected by the automotive technology, with respect to the economic, environmental and human conditions (Powers and Nicastri, 2000). The automotive industry has to keep a balance of personal mobility against the environment, traffic congestion and energy availability. The pollution caused by an incomplete combustion process exists in the majorities of industries that use oil to convert the chemical energy to other forms of energy, such as electrical, mechanical, etc. Most of these processes have emissions regulated but the pollution is still present due to the low performance control systems used in the combustion process.

In the USA, the fuel economy and the pollutant emission as carbon monoxide (CO), oxides of nitrogen (NO_x) and hydrocarbons (HC) are restricted by federal regulations (He and Jagannathan, 2005). The automobile production with catalytic converters was introduced in 1975 in order to satisfy the emission control regulation (Brandt, et. al., 2000). Less harmful components are normally produced by passing the CO, NO_x

and HC through a three-way catalytic converter. This complex process is currently managed in spark ignition (SI) engines with sophisticated microprocessors and control algorithms. The automotive industry has itself spent much research in improving the control systems in the combustion of the fuel during the process of the spark ignition engine (Tseng and Cheng, 1999).

The throttle maneuvers in transient conditions is a very complex task which try to keep the stoichiometric mixture near to 14.7, in the SI engine using a control system (Weeks and Moskwa, 1995). An accurate estimation or measurement of the airflow rate in an engine is key to a good stoichiometric air-fuel ratio control system. In order to satisfy the previous constraints, it is necessary to develop vehicles that reduce the negative impact on the environment and maximize fuel resources while covering the safe, secure and comfortable cars.

The automotive system is a real application of the mechatronic systems because it includes applications of electronics, sensors, actuators and microprocessor-based control system to obtain a suitable performance, to decrease the fuel consumption, to reduce emission level, and ensure safety and driving comfort (Conatser, et. al., 2004). In other words, the integration of electronic sensors, actuators, microprocessors, software, information processing for single components, and engine, drive-train, suspension and brake systems in a automotive powertrain system is a strict example of a mechatronic systems (Isermann, et. al., 2002).

4.1.1. Objective

To develop new neurofuzzy control structures in order to increase the performance of the automotive powertrain by improving the air to fuel ratio output signal. Direct benefits of this control are the reduction of the fuel consumption and the amount of pollutant emissions. Reducing the fuel consumption will be reflected in saving money by the owner of the car and ensure the life extension of the natural reserves of oil. The reduction of pollutants helps to preserve the environment an adequate way in

order to avoid natural disasters (i.e. global warming) because most of the pollutants presents in the environment are produced by cars using fossil fuel as an energy source.

4.1.2. Basic Concepts of Automotive Powertrain Engines

There are three types of engine control algorithms namely: the spark advance (SA) control, the air-fuel (A/F) ratio control and the exhaust gas recirculation (EGR) control (He and Jagannathan, 2005). The complete combustion with stoichiometric condition is the operating condition for all the engine control systems (ECS). Greenhouse gases are one of the most important factors in the current regulations for the combustion control. The design of ECS is strongly related to the study of transient phenomena (Arsie, et. al., 2002). The ECS is a control of mixture which needs to be accurately developed to guarantee a proper efficiency of the three way catalytic converters with the previous knowledge of the exhaust regulations. In addition, the control targets have to be known with the steady state and transient conditions. The key is the estimation of the air mass flow in the injector in order to know the correct proportion of the air-to-fuel ratio $(\beta = 14.7)$ and with the appropriate time dependency.

The basic configuration for the SI engines can be divided into three subsystems (Nyberg and Nielsen, 1997) (see Figure 4.1):

a) Air intake system: air mass flow meter, throttle, manifold pressure sensor and engine speed sensor.

b) Fuel/Combustion system: fuel injector, spark plug and misfire.

c) Exhaust after-treatment system: lambda sensors and catalyst.

d) Evaporation system.

e) Exhaust gas recirculation system.

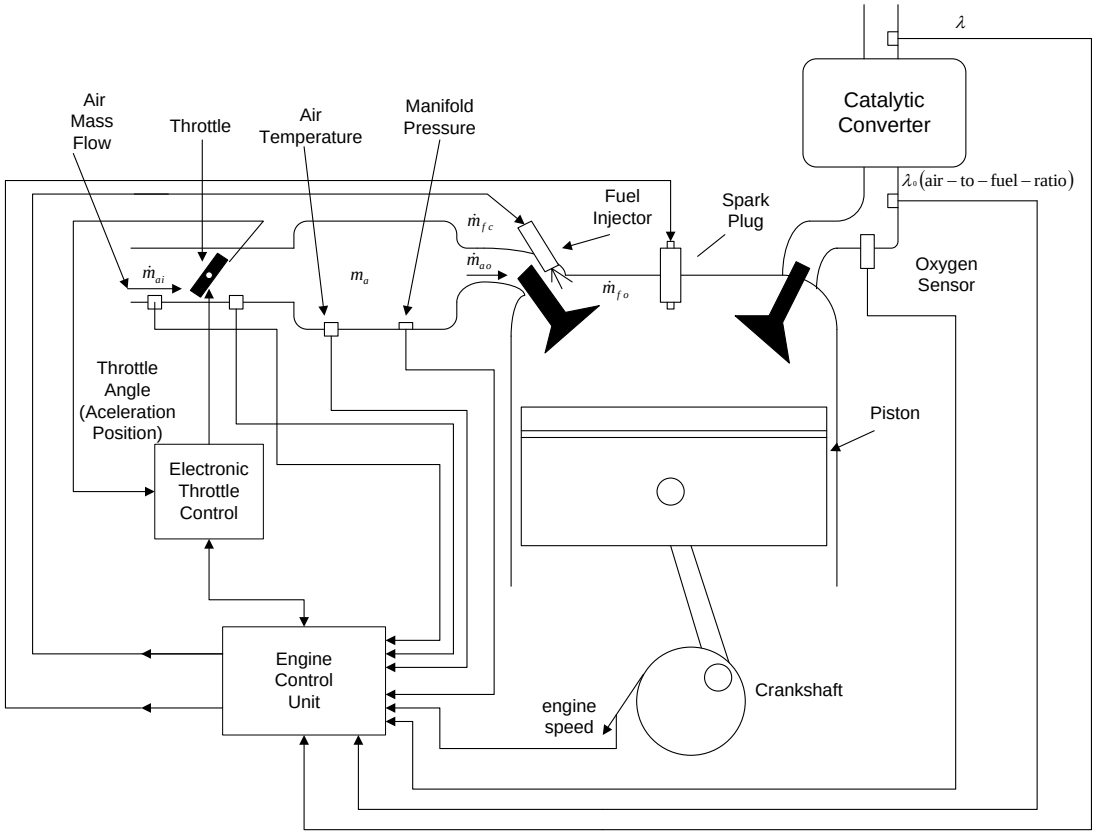

Figure 4.1 Basic Structure for a Spark Ignition Engine

The variables are defined as follows: the mass airflow (MAF) or measured throttle flow rate $\dot{m}_{ai}$ and throttle position TPS (or throttle angle, TA) in the inlet, manifold air mass m_a, output airflow rate $\dot{m}_{ao}$, fuel mass flow rate through the injector $\dot{m}_{fi}$ and the fuel mass flow rate into the cylinder $\dot{m}_{fc}$. Manifold air pressure MAP or intake manifold pressure P_{im} and the temperature T_{im} in the intake manifold, exhaust manifold pressure P_{em} and temperature T_{em}. The measurement of the normalized air-fuel ratio before and after the exhaust manifold are λ_0 and λ. The measurement of the engine speed is expressed as N.

The Electronic Throttle Control (ETC) regulates the servo-motor voltage after processing the driver's command and the throttle position (Conaster, et. al., 2004). The real objective is to increase or decrease the engine speed by modifying the throttle angle with a servo-controller called ETC, which regulate the throttle angle using a Direct Current (DC) servo-motor to adjust the inlet airflow rate. The fuel is spread by a pump and the air is feed to the intake manifold. The fuel is partially distributed as an spray near to the spark plug and also a fuel film in the walls of the engine.

The Engine Control Unit (ECU) is the controller to send the signals to the fuel injector (pump) and the timing signal for the spark plug. In other words, based on the commanded throttle position, the engine speed and the engine load, the ECU regulates the spark and fuel delivery processes. The ECU has to work in unison with the ETC. After several time delays, the explosion happens by the combustion of the air and fuel. The explosion produces a pressure which pushes the piston to move with an unknown air mass. The piston moves the crankshaft producing a torque, which produces the engine speed. After some delays the burned gases are detected by the oxygen sensor and the air-fuel (A/F) ratio sensor. The A/F ratio signal is one of the main control variables which should be near to the value of 14.7. A block diagram of automotive powertrain engine is shown in Figure 4.2.

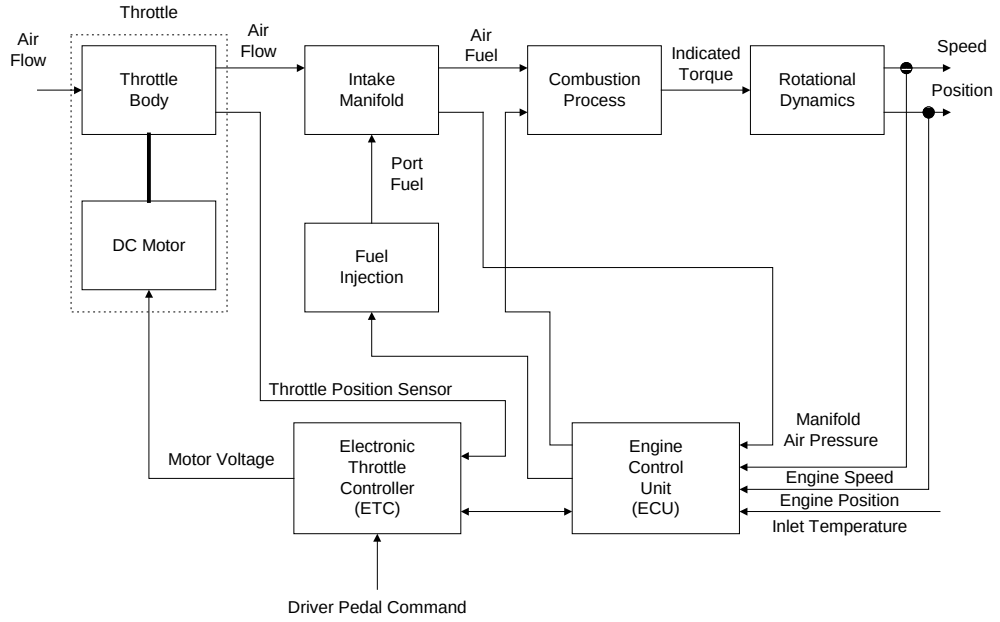

Figure 4.2. Block Diagram of Automotive Powertrain Engine

The regulation of the A/F ratio is the main objective of the fuel injection controllers with specific ratio in accordance to the type of the engine operations as warming up, constant high speed operation, and the urban traffic mode with recurrent tip-in and tip-out movement of the throttle (Won, et. al., 1998). The main requirements for a car are the desired driveability, the economic fuel consumption and the emission levels, which are reached by regulation of a desired A/F ratio.

Car engines with spark ignition (SI) system commonly have the three-way catalytic (TWC) converters, which oxidize the pollutants in the tail pipe such as CO, HC and NO_X. The TWC has a pretty high efficiency in a very small range around the complete stoichiometry combustion (A/F ratio equal to 14.7) where the pollutants will be reduced. The TWC have shown to be very sensitive to the variation of the A/F ratio which is the main target for control systems of the Spark Ignition (SI) engines. The objective is to keep the A/F ratio near to 14.7 either in steady state or transient operation mode to reach the full stoichiometry reaction. The transients control is more complicated than the steady state control because the air-induction and fuel dynamics vanish in steady state (Choi and Hedrick, 1998). In urban traffic condition, the SI engine is used in transient condition most of the time and that is why the transient control is a very hard task. The transient conditions are produced by the continuous movement of the throttle by the driver and the speed demanded by the SI engine.

4.1.3. Problem to Solve

The oxygen sensor of the exhaust used in the A/F ratio regulation has a considerable sensing time delay (Canale, et. al., 1978). The transient A/F ratio values are affected by three characteristics delays known as time-delay of the computer control system, a transport delay in the intake manifold and a physical delay of the fuel flow as a result of the fuel film evaporation on the intake manifold and port walls (Aquino, 1981; Baruah, 1990; Chang, et. al., 1993; Won, et. al., 1998; Choi and Hedrick, 1998). In other words, the problem related to the large modeling uncertainties in the fuel-

injection subsystem and the unavoidable time-delay between the control action and measurement cause the chattering problem of the air-to-fuel ratio (Choi and Hedrick, 1998).

A better way to fuel management in the spark ignition (SI) engines is key for car driveability and high reduction of pollutant emissions (Tseng and Cheng, 1998). The optimum catalyst performance has a direct dependence on the dynamic behaviour of the air/fuel ratio control system. The dynamic transient influence is mainly explained as follows (Choi and Hedrick, 1998; Brandt, et. al., 2000; Arsie, et. al., 2002; Arek, 2005):

a) Air induction dynamics is produced by the mass of air inducted into the individual cylinder which is the most important variable for the fuel metering control. When the intake valve is closed there is not flow entering but there is a flow in the reverse direction during part of the intake processes, making the flow into the cylinder not continuous. The measurement of the induced air is not possible to be made directly. Airflow is feeding to a bank of cylinders through the throttle into the manifold plenum, where the airflow is measured with an airflow sensor. Obviously, the filling and emptying dynamics of the plenum produce a great difference between the airflow measurement into the manifold and each actual flow measurement into the individual cylinders.

b) The fuel used in the combustible mixture for a cycle is not the same amount as the fuel injected during transient conditions because of the finite rate of fuel evaporation and the dynamic behaviour of the liquid fuel film in the port. As a consequence of this fuel lag there are spikes present in the A/F ratio output signal.

c) The A/F ratio control system receives one of the most important information from the exhaust oxygen sensor. Signal compensation is necessary in engine transient operations because of the finite response of the sensor (~100 ms), a time-delay for the transport produced for the exhaust and the arrival of the gas at

the sensor and finally the existence of a mix of the exhaust gas between all the cylinders.

d) There are different events which require correction, i.e. the events of the fuel injection and intake exhaust. The air induction of the cycle is made after the fuel injection. Consequently, the A/F ratio signal is delayed as well.

In order to optimize the engine's performance the following variables are selected (Flynn, et. al., 1997; Dutka, 2005): injected fuel, injection angle, variable turbine geometry of turbochargers (VTG), exhaust gas recirculation (EGR) and common rail injection (CRI) should be controlled. All these variables have a strong influence on the engine torque, the fuel consumption and the pollutant emissions.

In addition, the demands on the behaviour of automotive powertrain and the complexity of vehicle systems make the control design complex (Winsel, et. al., 2004). The physical SI engine models usually are not good for real-time applications, and it is mainly used for the cold start and warm-up dynamics.

Cold start and warm-up represent the challenges in control application but exhaust purification in hot engines is well controlled (Pischinger, et. al., 2004). The calibration of the exhaust after treatment and engine control strategies are the challenges mentioned before. After each test of cold start, the vehicle and the engine have to be returned to the prescribed start temperature and because of that these experiments are really expensive. The hardware and the downtime ties up are the expensive test equipment. The first three minutes of operation for a SI engine have the most significant changes in engine temperature. If the surface temperature is treated as a time-varying variable then its influence over intake/exhaust gas temperatures and combustion heat losses can be captured.

4.1.4. State of the Art of Car Engine Applications

Weeks and Moskwa (1995a), designed a nonlinear observer which was developed using the model of the process estimating the flow rates at the throttle and the intake ports flow rate of an SI engine using a speed-density type sensor.

A nonlinear mean-torque predictive engine model using MATLAB/SIMULINK was developed by Weeks and Moskwa (1995b), which simulates a port-fuel-injected, spark ignition engine including air, fuel and EGR dynamics in the intake manifold including the process delays present in the four-stroke cycle engine.

Nyberg and Nielsen (1997), designed a model-based diagnosis for the air intake system of the spark ignition engine based on the nonlinear semi-physical model and used a combination of different residual generation methods.

An observer-based control law was developed by Choi and Hedrick (1998) in order to solve the transient operation and chattering of the air-to-fuel ratio in the spark ignition engines.

Pefefferl and Färber (1998) developed an intelligent and flexible algorithm applied in a vehicle control system with multiple algorithms of different complexities.

Tseng and Cheng (1998), developed an adaptive A/F ratio control algorithm for throttle transient operations. Using modern estimation technique, a single port fuel parameter is identified on-line. This was based on the fact that the time of one engine cycle is shorter compared with the time scale for change of the fuel dynamics parameter. However, it was possible to identify the parameter over several cycles. The engine aging is compensated by the control algorithm. The components of the control algorithms are: airflow estimator, the A/F ratio observer, the port liquid fuel dynamics model/ model parameter identifier, and the control algorithm which take all the information in order to compute the adequate injector pulse width.

Won and partners (1998), used the Gaussian Neural Network (GNN) to develop a direct adaptive control law (for air-to-fuel ratio of a spark ignition engine) for compensation of transient fuel dynamics and the measurement bias of mass airflow rate into the manifold. The transient fueling compensator is coupled to a dynamic sliding mode controller, which governs fueling rate when the throttle variation is slow. The computations were made on-line because of the simplicity of the control law.

Nyberg (1999), designed a model-based diagnosis system founded on structured hypothesis tests, which were applied to the air-intake system of an automotive engine.

Hafner and partners (2000), applied a fast neural network model for engine control design. The fast neural network has a special local linear radial basis function network (LOLIMOT).

The exhaust of cars in 1990 were at least 10 times cleaner and twice as fuel efficient than the automobiles of the 1970s (Powers and Nicastri, 2000). The improvements were due to the inclusion of microprocessor, electronic sensors, electronic actuators and digital computation. The notable improvements in the cars due to the current technological advances increase the fuel efficiency, notable reduction of pollutants; vehicles are safer, more comfortable, and more maneuverable. The improvements of the 21st century have to be in the same proportion. The control systems and design techniques will be implemented in the next generation of vehicles, which will be electric and hybrids (SI engine and Electric) designed by total systems approaches with new materials, alternative energy sources (aeolic, solar and nuclear) and more sophisticated powertrains. Even with more improvements in the mechanical designs of the engines.

An automotive powertrain of direct compression ignition (diesel) equipped with exhaust gas recirculation (EGR) and a variable geometry turbocharger (VGT) was developed to solve an emission control problem (Stefanopoulou, et. al., 2000). The

control objectives were driver's control demand and the minimization of NO_x avoiding the visible smoke generation. The EGR and VGT actuators have redundant effect over the emissions in steady state optimization. With this actuator redundancy a multivariable feedback controller was designed coordinating the two actuator to fully uses of the joint effect on engine emission performance.

Kolmanovsky and Stefanopoulou (2001), designed an optimal control system and showed how the optimal control techniques have to be used against the feasibility assessment with novel powertrains, determination of system configuration and subsystem requirement and operating strategy. A turbocharger power assist system was used as the case study. The diesel engine turbo-lag was reduced with the optimal control law by a numerical solution of a minimum-time optimal control problem.

An adaptive estimator based on the extended Kalman filter for the fuel film dynamics in the intake port of a spark ignition engine was designed by Arsie and partners (2002). The states of the observer were the impingement of the injected fuel on the manifold and the evaporation process.

The use of adaptive extended Luenberger state estimator for general nonlinear and possibly time-varying systems was investigated by Erdogmus and partners (2002). An artificial neural network was used as nonlinear mapping in order to approximate the nonlinear functions included in the general structure of the nonlinear plant. The extended Luenberger observer was applied to a realistic partial gasoline engine model.

Mollov (2002), designed a nonlinear fuzzy predictive controller for a Gasoline Direct Injection (GDI) engine determining the optimal setting for the start of injection, the amount of injected fuel, the ignition advance angle and the amount of fresh air introduced into the cylinders. A system identification was developed using a nonlinear fuzzy models predicting the state and output variables. Quadratic approximation using successive linearization of the prediction model along the

current operation trajectory was used as optimization algorithm. In order to minimize the torque oscillation, several mode-dependent constraints and weights were introduced in the cost function. Mollov noted that most of the nonlinearities of the GDI engines were related to the engine speed.

Stotsky and Kolmanovsky (2002), developed a nonlinear observer using input estimation techniques for charge estimation and control of gasoline and diesel engines with the conclusions founded in the real application on a vehicle and from an engine dynamometer.

Isermann and partners (2002), reviewed the state of the art for fault tolerant systems applied to different subsystems of the automotive powertrain systems.

Kolmanovsky and partners (2002), designed a model-base Lyapunov technique, called speed-gradient (SG) approach, which was applied to an advance technology gasoline direct injection stratified charge (DISC), solving specifically the air-to-fuel ratio and torque control problems. An scalar performance function was used to catch transient and steady state tracking requirements and constrains. The control action was obtained by decreasing the value of the performance function.

Liu and Stefanopoulou (2002), developed a two-input-two-output (TITO) control algorithm in order to deal with the nonminimum phase zero producing a minimum phase behaviour without transient deviations from the optimal fuel economy operation.

Vaes and partners (2002), developed a new control strategy applicable to square multiple-input-multiple-output (MIMO) systems with certain degree of symmetry. The control law was applied to the tracking problem on an automotive vibration rig. The controller was designed using the following steps: response measurement, almost decoupling of the MIMO system into multiple single-input-single-output (SISO) systems by transformations of the inputs and the outputs, SISO-identification of the decoupled systems and multiple SISO-controller design. A decoupled model

of the automotive vibration test rig could accurately approximate the full MIMO model.

Pichinger and partners (2004), made an experimental investigation and physical modeling of the port fuel injected SI engine using an Artificial Neural Network to develop a hybrid model.

A hybrid model using physical and neural network (NN) models was developed by Winsel and co-workers (2004) with the real-time capability and enough accuracy. They took advance of the NN prediction capability as a response of a real physical system after a previous training process. Because of this, the hybrid model was able to describe and simulate the dynamic behaviour of the SI engine in transients and steady state nonlinear conditions.

Evans-Pughe (2006), developed a synthesis of the current state of the art for the artificial neural networks applied to the automotive powertrain engines by the main automotive industry companies.

In general, the evolution of the research using nonlinear techniques was from the observer-based controllers and sliding mode control techniques to the use of adaptive extended Luenberger state estimator with artificial neural networks and neural network based automotive controller in order to solve the transient control problem. Also, until now several hybrid models has been developed using the physical laws and the neural networks shown a good approximation of the automotive car engine. The automotive powertrain control system is an interesting and promising area where there is more research work to be done.

4.1.5. How to Solve the Automotive Powertrain Problem?

Most of the control techniques applied to the automotive powertrain car engines are the observed based and sliding mode controllers or a combination with an artificial

intelligence approaches (artificial neural networks and fuzzy systems). All these techniques (in the step design) do not take into account the time-varying delay present in the measurement of the air to fuel ratio. Nevertheless, it is well known that neurofuzzy systems (on-line training) have the ability to deal with time-varying delay and nonlinearities due to their particular nonlinear adaptive structure (Pinto, et. al., 2004). The time-varying delay of the automotive powertrain process and the processing speed of the global minimum tracking solution are the boundary and weaknesses of the control algorithms currently applied in the car industry.

After developed the literature review of the car engine problem was decided to solve the car engine problem using a combination of transient and steady state neurofuzzy controllers, assuming that the car engine system can be treated such a multivariable nonlinear differential equation which has transient and steady state responses.

In Chapter 2, it was shown that neurofuzzy systems are a nonlinear differential equation (Pinto, et. al., 2011). The transient neurofuzzy controller is the homogeneous solution, the steady state is called non-homogeneous solution and the addition of both is the general solution for the multivariable nonlinear differential equation.

4.1.6. Structure of this Chapter

The remainder of this chapter start with a brief introduction section, which concerns the objective, the problem to solve, the state of the art, and the solution proposed to solve this problem. The second section summarizes the modelling of the engine used in the chapter. The last section describes the new neurofuzzy control structures applied to the car engine model. The optimization algorithms used in the chapter were related to the Backpropagation (BP) and to the Gradient Descent (GD).

4.2. Modelling of the Engine

The combustion engine model is a complex MIMO nonlinear plant with time-varying delays. It was developed by combining physical models (white-box), parameters identification (white-box) and look-up table techniques (black-box) with experimental data collected from the driving cycle (Dutka, 2005). Because of this, the model is considered to be a complex nonlinear hybrid (grey-box) model (see the Appendix D).

The main components of the automotive powertrain system are the driver dynamic, ETC, engine control units (ECU), physical model of the spark ignition, fuel injector dynamics, combustion process model, TWC model, variable field alternator, dynamic lead acid battery, dry clutch, automated layshaft transmission, brake system, complete vehicle longitudinal dynamics with tire-road interface characterization, and an ac-induction motor electric drive system.

4.3. Neurofuzzy Control Application to Car Engine

The neurofuzzy systems were used to develop several control structures in order to solve the problem for the control of the normalized air-fuel ratio, looking forward to improve the dynamical behaviour of the feedforward control system. The neurofuzzy control systems were applied in the car engine based on the principle of ″divide and conquer″ the total response of the nonlinear system in two parts, the transient and the steady state responses. A single neurofuzzy controller controlled each response in order to complement the total response reaching the set point of lambda λ (or the normalized air-fuel ratio).

4.3.1. Control Objectives

Torque and pollutants regulation are the main objectives in the automotive powertrain control problem. The model developed by Dutka (2005) did not

considers the spark advance because it was assuming to be a function of the current engine state, regulated by a local controller. The variation of the amount of combustible and air in the cylinders is the direct responsible for torque regulation. Either the amount of torque generated in the engine or the pollutants produced were determined by the composition of the combustible and air.

The most common measurements in the car engine are the ambient pressure P_{amb} and temperature T_{amb} in the inlet, mass airflow (MAF) or measured throttle flow rate $\dot{m}_{ai}$ and throttle position TPS in the inlet, manifold air pressure MAP or intake manifold pressure P_{im} and the temperature T_{im} in the intake manifold, exhaust manifold pressure P_{em} and temperature T_{em}. Finally, the measurement of the normalized air-fuel ratio before and after the exhaust manifold are λ_0 and λ. The measurement of the engine speed is expressed as N. Exhaust manifold contains the Three Ways Catalysis Converter (TWCC), which reduce the amount of emission. All The variables are shown in Figure 4.3.

For a multivariable control system, the throttle position command (SP: Set point of the throttle position) and fuel pulse width (*FPW*) are the manipulated variables. The FPW is a time period when the fuel injector is opened by an electric pulse in a solenoid valve. There is a proportional relationship between the pulse width and the amount of fuel injected. The driver defines the SP by making variable the amount of air feeds in the intake manifold affecting in the same manner the air injected into the cylinders.

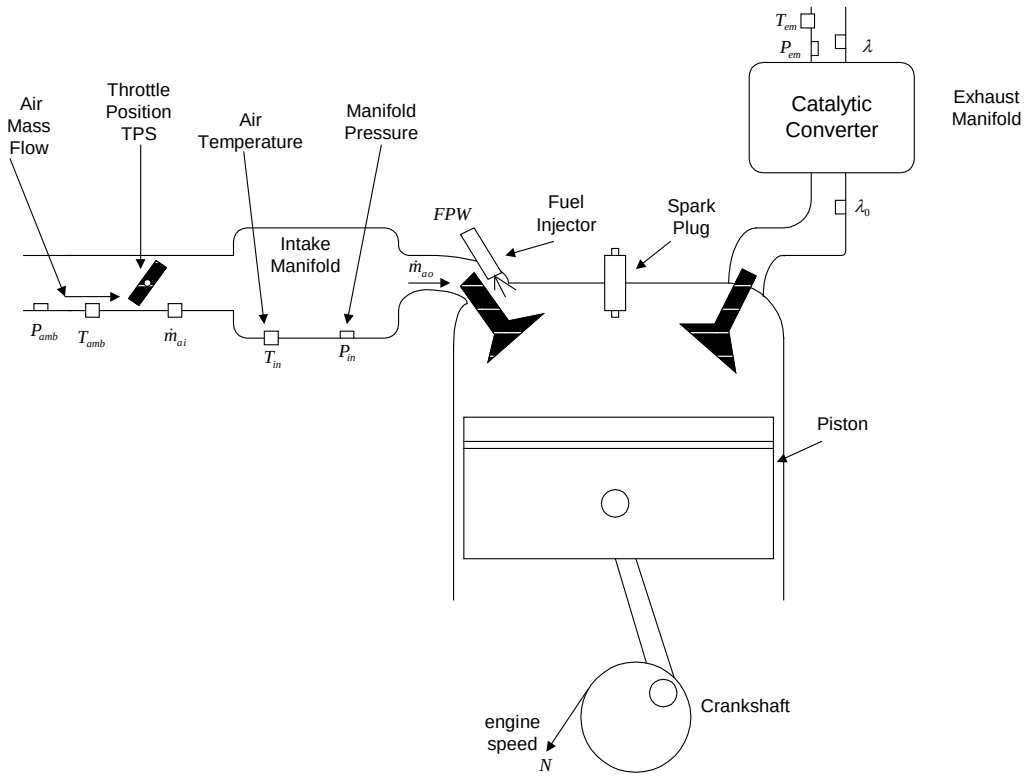

Figure 4.3 Automotive Powertrain Engine Diagram

Actually, the accelerator pedal driver (or the driver) can be decoupled from the dynamics of the engine (or the position of the throttle plate - throttle angle) because of the modern mechanism of the electronically actuated throttle. Also, a faster torque response is possible and a compensation of the intake manifold. Usually, when the driver took control of the throttle position (as in conventional control), it belongs to a faster movement of the throttle position without an smooth excursion to the complete stoichiometry of the air-fuel ratio. Injecting a bigger amount of fuel can help to deal with this effect but at the same time increases the amount of pollutants.

In general, the current engine speed was sampled at every 90 degrees of the crankshaft by sampling the driving cycle data in a specific frequency. If the previous sampling technique is used then several components of system's time delay can be considered constants. The nonlinear dynamics of the intake manifold were in function of the engine speed with a sampling rate variable, which became the best discretization of the model.

4.3.2. Control Objectives in the Automotive Spark Ignition Engines

Due to the nature of the automotive powertrain systems, it is necessary to obtain accuracy and adaptive behaviour in order to minimize the exhaust emissions and fuel consumption. In addition, for all operating conditions it is necessary to obtain the optimal driveability, minimization of evaporative emissions and fault diagnosis-health-monitoring systems to prevent malfunctions and accidents with an engine control system. The exhaust emissions and fuel consumption are closely related to each other with a trade-off between them due to the air-to-fuel ratio and brake torque control targets.

Stricter emission regulations, growing customer fuel economy and driveability requirements are making the modern powertrain control systems more complex (Kolmanovsky, et. al., 2002). Safety and security are other important targets included in the new models of automobiles covers with the addition of functions as aid in collision warning and avoidance, lateral control issues for steering assist and lane keeping, and personal and vehicle security issues (Powers and Niscatri, 2000). To control the combustion process in the car engine is necessary to regulate the set point of the torque demand and the A/F ratio with a minimization of fuel consumption. Also, it is required the driving comfort in the Engine Management System (EMS).

4.3.3. Neurofuzzy Control Techniques Applied in the Car Engine

As it is well known, the powertrain car engine system is a very complex multivariable system with high nonlinearities, coupling loops, time-varying delays and many internal uncertainties (i.e. the amount of fuel in the chamber combustion and the amount of the air in the cylinders). The car engine problem is governed most of the time by transient operation conditions rather than the steady state conditions. This problem is even more complicated with the additional limitations of the optimization techniques finding the global minimum and the delays introduced by the computing process. The technique used in this application was the *Gradient*

Descent (GD) or the *Back Propagation* (BP) algorithm. The GD algorithm has a poor performance in the optimization because its slow speed of convergence (Erdogmus, et. al., 2002). Moreover, there are several applications of the artificial neural networks and fuzzy systems in the car engine systems (Hafner, 2000; Mollov, 2002; Erdogmus, et. al., 2002). Mollov developed a nonlinear predictive controller, which did not lead to the expected results. Additionally, the most successful and common techniques applied have been the observers-based control system (Weeks and Moskwa, 1994; Tseng and Cheng, 1999; Stotsky and Kolmanovsky, 2002), sliding mode control (Choi and Hedrick, 1998), a combination of the artificial neural network with the sliding mode control (Won, et. al., 1998) and a combination of the observer with the neural networks (Erdogmus, et. al., 2002).

The car engine model was developed by Dutka (2005) using a MIMO feedforward controller. The powertrain model was developed using the physical rules, which govern the real car engine process. The MIMO feedforward controller was designing using the car engine model. The car engine model is a multivariable model with the following input signals: ambient temperature (Tamb), ambient pressure (Pamb), coolant temperature (Tcool), engine speed set point (RPM_sp), normalized air to fuel ratio set point (Lambda_sp), the throttle position (TP) or throttle angle (TA), fuel pulse width (FPW) and the perturbances.

The outputs signals of the car engine model are: mass airflow (MAF), manifold air pressure (MAP), engine speed (RPM) and normalized air to fuel ratio (Lambda), intake air temperature (Tman) and brake torque (BT). The input variable AF_sp is defined as the air-to-fuel ratio set point equal to 14.7 (complete combustion point).

The complete mathematical model of the car engine is a quite complicated model because of its degree of complexity, and several model uncertainties. Because of these characteristics, it was chosen to use the neurofuzzy systems in order to develop a control system.

4.3.4. State of the Art of Neural Network Applied on Car Engines

Most of the automotive firms are looking to use the Artificial Neural Network (ANN) to solve problems related with the demanding engine control and fault diagnostic requirements produced by tightening emissions regulations and the necessity for fuel economy (Evans-Pughe, 2006). Ford has introduced the second production of car model with ANN technology in the Econoline van. The ANN detects misfire first in its V12 engine (2004 Aston Martin DB9) and after that in its V10 engine. From now all Aston Martin engines will have this technology included.

Powertrain applications are the main target of the Chrysler since three years ago. It is the reason they developed an ANN approach in order to control the variable valve timing in the next-generation-fuel-efficient engines. Moreover, the UK neural network company Axeon developed a sensor replacement application for the General Motors in order to increase the speed of measurement using a virtual sensor. Also, the ANNs have been used by Ford in applications such as idle speed control, misfire detection and a form of fuel control used in a neural net chip (designed by the Jet Propulsion Lab (JPL)). Actually, those three applications have been used together in the last model of cars. Recently, due to the way in dealing with misfire detection in DB9, then Aston Martin got stuck and because of that they approved more production with the ANN technology.

4.3.4.1. Controlling Emissions

Higher hydrocarbon emissions are produced when there is an incomplete combustion (incomplete chemical reaction between the air and the fuel) as result of misfiring. The new legislation requirements in countries such as US and Europe (since 2004 On-board diagnostics), they have to include in all engine control units (ECU) a misfire detector inside of each single cylinder.

In engines with higher cylinder-counts the misfire detection is a very complicated task because a great amount of revolutions in small period of time leave to have the

possibility to discriminate between a fire and a misfire before the next set of information comes in. For example, Alan Beneth (Aston's Martin Chief Engineer, (Evans-Pughe, 2006)) says: "at the Aston Martine engine with 7500 rpm there is only 1.33 ms in order to decide about the fire or misfire for each cylinder". Also, he added that: "ANN has a faster respond because data are not processed so much as steered in the manner to produce an specific output".

Measurements of the crankshaft acceleration detect the misfire because of the acceleration "dips" where the cylinder produces a reduced pressure. The high level of vibration noise from the crankshaft makes impossible to detect the acceleration dips at high speed. The ANNs can learn the pattern of the noise and dig on the very noisy data collection in order to extract the real information decoding those in pieces.

Ford's ANN algorithm is running on an standard 16-bit microcontroller into the powertrain control module. The ANN will run on the main engine computer in the future. The inputs used in the ANN are engine speed, the engine acceleration, engine load and the cylinder position. The engine speed is measured from the crankshaft sensor and the engine acceleration is computed from the engine speed. The engine load is measured similarly to the throttle opening. The cylinder position is measured from the camshaft sensor which shows the cylinder in misfire. The ANN has two outputs: misfire and no misfire. At Ford's Powertrain Research and Advanced Engineering facility in Dearborn, Michigan the network training was carried out which has proved to be robust and easy to use for all Ford´s cars.

4.3.4.2 Fuel Efficiency

Ford is expecting to develop other applications. Large engines are the adequate environment for the ANN misfire application commonly in the family car without attempt to improve the fuel efficiency. ANNs have the possibility to be used in all types of vehicles in efficiency-boosting application such as controlling multiple displacement systems and variable valve timing (VVT).

Some of the cylinders are turning off in the multiple displacement system when there exist a small load and turning on when the load increase. The timing regime governs the opening and closing of the valves responsible for the flows at the cylinders (in the variable valve actuation). The flow of air, fuel and exhaust in and out of the cylinders are varied in order to maximize the efficiency without taken care of the operating conditions of the engines. The optimum performance in terms of the torque, fuel consumption and pollutant emissions at all speeds and conditions are provided by the previous systems.

To solve a real highly complex multivariable control problem it is necessary to use the complete capacity of solution of the control algorithm and the hardware. The usual list of spark-timing and air/fuel ratio plus intake cam-phasing and exhaust cam-phasing represent the previous multidimensional (or multivariable) control problem. This control problem has the following characteristics: multiple inputs-multiple outputs (MIMO), internal interaction between loops, high nonlinearities, several time-delays, faster dynamic behaviours and uncertainties in the physical modelling.

Denise Kramer (product development engineer at Daimler Chrysler's technical centre in Auburn Hills, Michigan) said (Evans-Pughe, 2006): "the optimization and characterization problems become more complex when you add extra actuators. However, in this case is necessary to control additional variables to the position of the actuators". Kramer and partners with collaboration with the University of Michigan optimized the actuator set points for a variable valve technology using ANNs which go under the label of continuous dual independent cam-phasing. They were looking for methods with ANNs, including additional sensors, multiple surfaces and polynomial fitting, but the ANNs have demonstrated to be the best, the fastest working in all the operating points (nonlinear operating surface) with a considerable reduction in the effective cost (explained by Kramer).

The ANNs convert global optimization problems into several local optimization problems. The camshaft position and the spark timing are the first optimized in order to obtain the best fuel economy, after that were adds NO_x emission targets and

finally were taken into account the close compromise between the fuel consumption and NO_x emissions. In the same manner, the Chrysler team developed a way of generating a map of optimised VVT set points and the characterization of the engine airflow across all dynamic operating range using a corresponding ANN weighting factors. Finally, they are using a type of neural network control algorithm programming and running on the central ECU with the possibility to be used in all engine families.

4.3.4.3 Hardware Acceleration

In order to compensate for the time-delays which are implicit on the faster engines, the high speeds conditions were a necessary mechanism to obtain the hardware acceleration. Axeon Company (Aberdeen-based) with General Motors showed how the mass airflow sensor function could be replaced by the Axeon's Vindax chip, which accelerates the execution of the ANN algorithm with the hardware. Vindax chip has the following secondary data inputs as the engine speed; throttle position, intake manifold air temperature and pressure. The Vindax chip output is a virtual version of the mass air function, which corresponds to the amount of air sucked in through the manifold. The cost of the system was reduced and the performance was improved because of the function approximation generated by the Axeon's Vindax chip.

The current ANN applications run on hardware, software, on a central ECU or any add-on chip.

4.3.5. Multivariable Neurofuzzy Generalised Minimum Variance Controller

The multivariable neurofuzzy generalised minimum variance (NFGMV) Controller was designed using the concepts described in the Chapter 3, Section 3.4.6. Figure 4.4 shows the block diagram of the car engine model with a multivariable NFGMV controller.

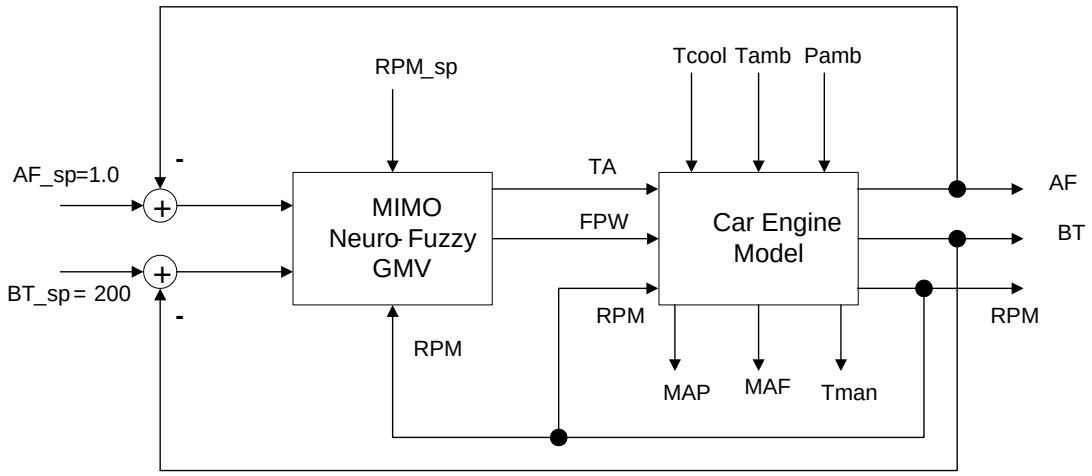

Figure 4.4 Block Diagram of the Car Engine Model with a Multivariable Neurofuzzy Generalised Minimum Controller

The application was designed assuming that the lower common delay in the entire path has to be removed to identify the free delay neurofuzzy car engine model (see Figure 4.5).

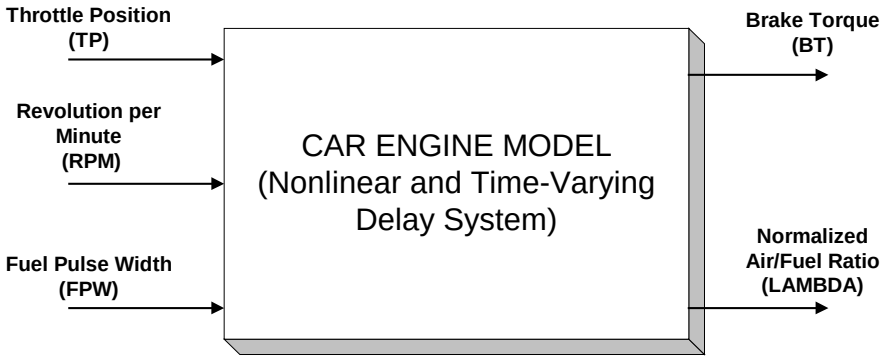

Figure 4.5 Open-Loop Car Engine Model Without the Lower Common Delay

The internal structure of a MIMO neurofuzzy model contains internally multiple-input-single-output (MISO) neurofuzzy models. The internal structure of the free delay neurofuzzy car engine model has two MISO neurofuzzy models (see Figure 4.6).

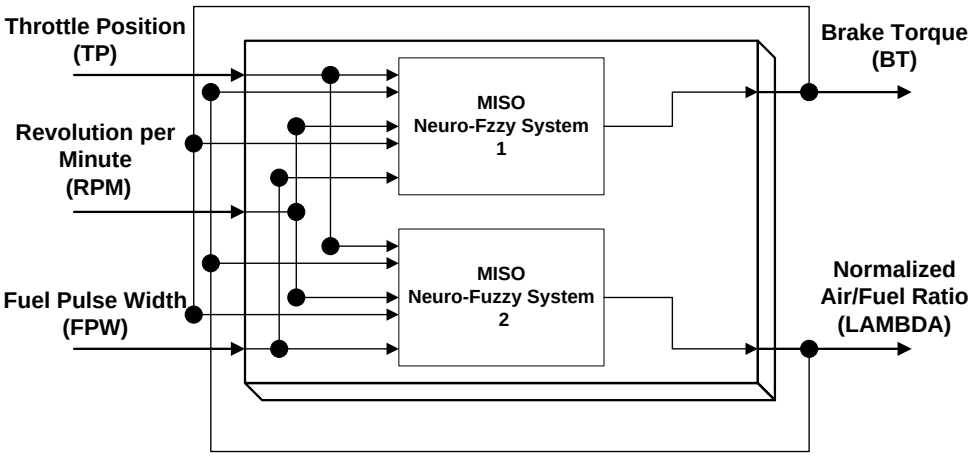

Figure 4.6 Internal Structure of the Free Delay Neurofuzzy Model of the Car Engine

The input signals were generated in order to cover all the operating range for the TP, RPM and FPW. TP was selected from 10% to 90% and 90% to 10% in order to cover the complete operating range. RPM was selected from 90 rpm (revolutions per minutes) to 2000 rpm. FPW was selected from 4 ms (10^{-3} seconds or milliseconds) to 10 ms. Additionally, the signals were combined in order to have all the possible combinations which can occur in real conditions in order to produce all dynamic behaviours.

The training process of the Neurofuzzy System was developed off-line and applied to the input signals shown in Figure 4.7 and the output signals expected in Figure 4.8. The output signals generated by the car engine model (thick line) and the output signals produced by its Free Delay Neurofuzzy Model (thin line) are shown in Figure 4.8.

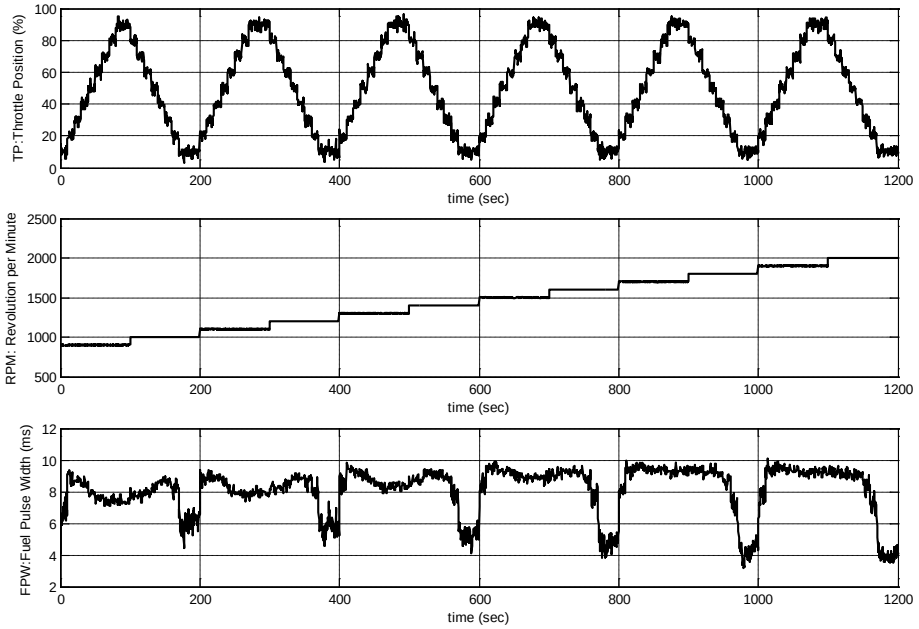

Figure 4.7 Input Signals Used to Identify of the Free Delay Neurofuzzy Model of the Car Engine

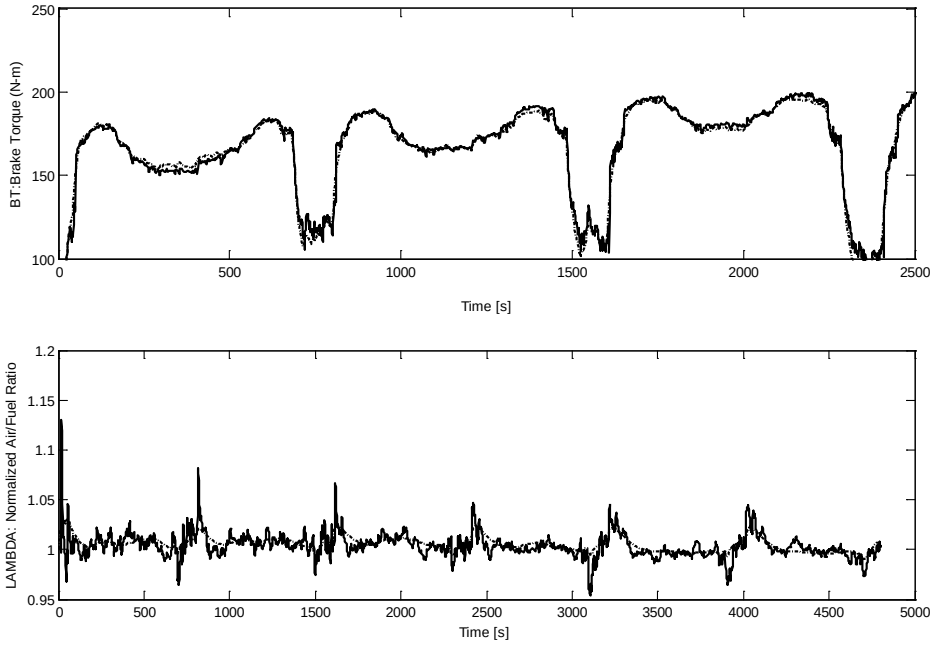

Figure 4.8 Output Signals Generated by the Car Engine Model (Thick Line) and the Output Signals Produced by its Free Delay Neurofuzzy Model (Thin Line)

Finally, either the free delay correct model or the free delay car engine neurofuzzy model were used in the implementation of the NFGMV controller and applying the concepts developed by Pinto, et al (2004b). Unfortunately, the control algorithm did not perform well for the car engine system because it was driving the system to instability under normal operation. This was because of the time delay effects combined with the sampling time (see Chapter 3).

4.3.6. Feedforward and Neurofuzzy Feedback Controllers

The feedforward and neurofuzzy controllers were used in this section as a complement in order to improve the performance and robustness of the complete control system by implementing a multiplicative adaptive nonlinear gain or a transient state controller with an addition to the output signal of the feedforward (steady state) controller.

In the first case, a multiplicative operation between the output signal of the feedforward controller $FPW_{ss}(k)$ and the output signal (nonlinear adaptive gain) of the neurofuzzy controller $G(k)$ was implemented as the control signal $FPW(k)$ defined as follows:

$$FPW(k) = G(k) \times FPW_{ss}(k) \quad [10^{-3}\text{sec}] \tag{4.1}$$

Based on the equation (2.56), the nonlinear adaptive neurofuzzy gain $G(k)$ was defined as follows:

$$G(k) = \sum_{i=1}^{N1} \gamma_i\big(\boldsymbol{x}(k)\big)\, y_i\big(\boldsymbol{x}(k)\big) \tag{4.2}$$

where $\gamma_i\big(\boldsymbol{x}(k)\big)$ and $y_i\big(\boldsymbol{x}(k)\big)$ are the ith normalized degree of fulfilment and the ith local lineal model. $\boldsymbol{x}(k)$ is the input (state or regressor) vector. *N1* are the amount of fuzzy rules. The normalized degree of fulfilment $\gamma_i\big(\boldsymbol{x}(k)\big)$ and the local lineal model $y_i\big(\boldsymbol{x}(k)\big)$ are defined by equation (2.57) and (2.62).

On the other hand, if there is an addition operation between the output signal of the feedforward controller $FPW_{ss}(k)$ and the output signal of the neurofuzzy controller $FPW_{ts}(k)$ then the control signal $FPW(k)$ is defined by the following:

$$FPW(k) = FPW_{ts}(k) + FPW_{ss}(k) \qquad [10^{-3}\text{s}] \qquad (4.3)$$

Using equation (2.56), the output signal of the neurofuzzy controller $FPW_{ts}(k)$ is expressed as follows:

$$FPW_{ts}(k) = \sum_{i=1}^{N2} \gamma_i\big(\boldsymbol{x}(k)\big)\, y_i\big(\boldsymbol{x}(k)\big) \qquad [10^{-3}\text{s}] \qquad (4.4)$$

where *N2* are the number of fuzzy rules.

Equations (4.2), (4.3) and (4.4) will be used in the experiments developed in the following sub-sections. Due to the characteristic of the car engine problem the optimization algorithm selected was the Gradient Descent (or Back propagation) algorithm.

4.3.6.1. Feedforward and Neurofuzzy Controller with 3 Inputs and 2 Fuzzy Sets per Input with Product Operation

The idea behind the structure of the multivariable feedforward controller and feedback neurofuzzy controller with product adaptable operation is to take advantage of the adaptation capability of the neurofuzzy systems to increase the performance and robustness of the control system. Figure 4.9 shows the block diagram of the car engine model with multivariable feedforward controller and feedback neurofuzzy controller with product adaptable operation. The output of the neurofuzzy controller is an adaptive nonlinear gain. The input signals selected for the feedback neurofuzzy controller were MAF, MAP and TP.

The fuzzy sets per input signal were equal to 2. Because of this, the number of the fuzzy rules was equal to 8 (with 8 local linear models). See Chapter 2 for a better and further explanation of these concepts. For the experiment were selected several values for the step size k in order to tune the feedback neurofuzzy controller.

The values selected for the step size k were lower than the maximum step size k_{CE} ($k < k_{CE} = 0.01$) of the car engine simulation (Dutka, 2002). The step size k defines the sampling time of the neurofuzzy controller and plays an important role in the tuning, stability and convergence of the neurofuzzy system (Pinto, 2001).

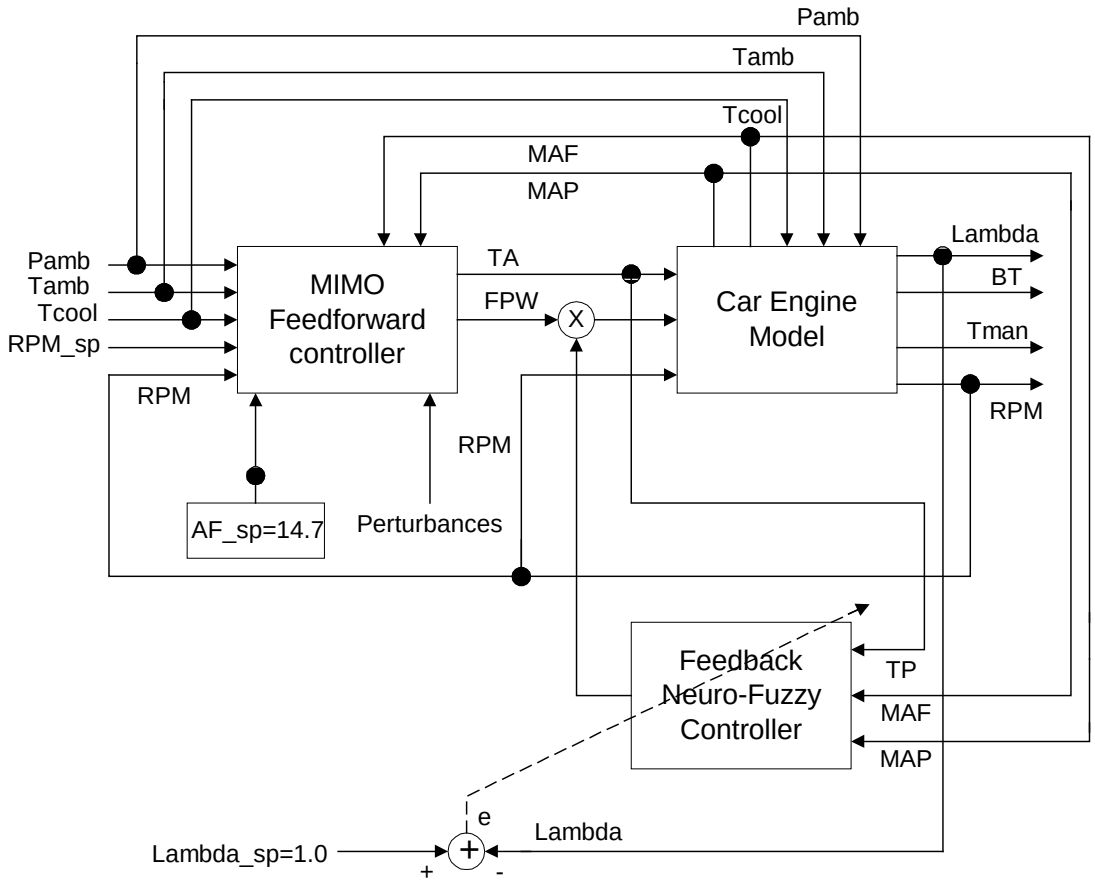

Figure 4.9 Block Diagram of the Car Engine Model with Multivariable Feedforward Controller and Feedback Neurofuzzy Controller No.1

As mentioned before, if the step size k was decreased then the convergence speed of the optimization algorithm increases.

The previous values of the specific step size are shown in Figures 4.10 and 4.11 where the input and output signals of the car engine model are shown. The neuro-fuzzy controller was designed with 8 fuzzy rules. Figure 4.10 shows TP, RPM and FPW have unstable dynamic behaviours which depends on step size k. In the output signals Lambda and BT (in the Figure 4.11) are also shown the unstable dynamic behaviours produced by unstable inputs. In general, there is no improvement in the performance of the control system with inclusion of the neurofuzzy controller.

The feedforward control (FFC) response was taken as the reference signal to be improved with the application of the neurofuzzy control systems varying the step sizes. The following values of step size k were used:

$$k1 = 1.25 \times 10^{-4};\ k2 = 1.25 \times 10^{-5};\ k3 = 1.25 \times 10^{-6};\ k4 = 1.25 \times 10^{-7};$$
$$k5 = 1.25 \times 10^{-8};\ k6 = 1.25 \times 10^{-9};\ k7 = 1.25 \times 10^{-10};\ k8 = 2.5 \times 10^{-7};$$
$$k9 = 2.5 \times 10^{-8};\ k10 = 2.5 \times 10^{-9};\ k11 = 5.0 \times 10^{-7};\ k12 = 5.0 \times 10^{-8};$$
$$k13 = 5.0 \times 10^{-9}$$

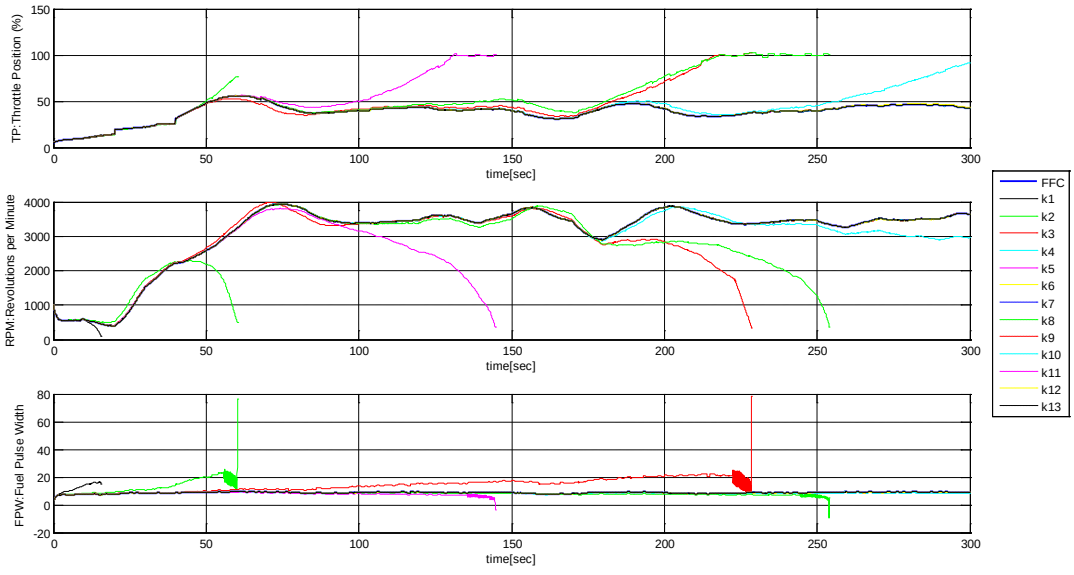

Figure 4.10 Input Signals of the Car Engine Model with Feedforward Controller and a Neurofuzzy Controller No.1

Each step size (from *k1* to *k13*) belongs to a different experiment.

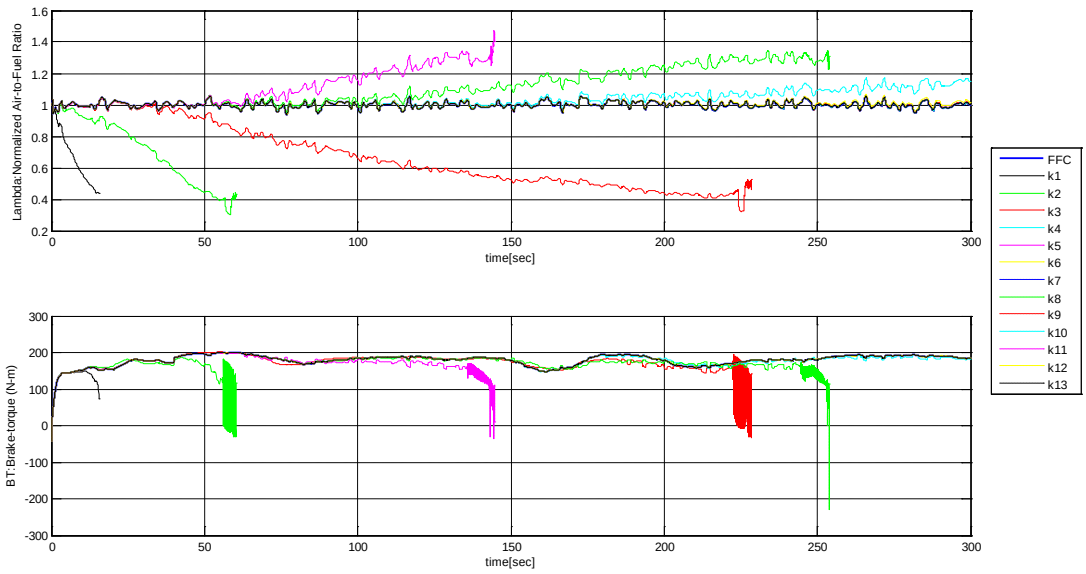

Figure 4.11 Output Signals of the Car Engine Model with Feedforward Controller and a Neurofuzzy Controller No.1

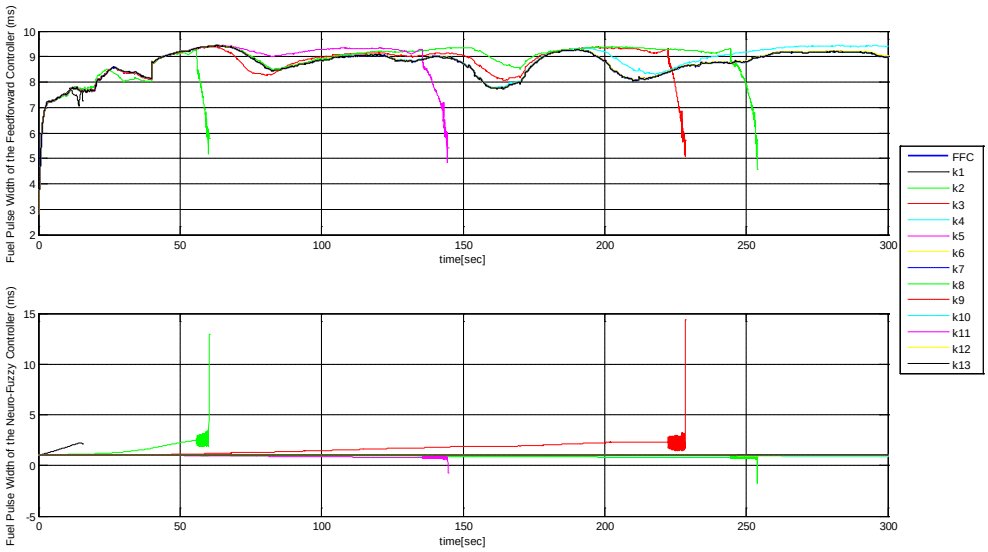

Figure 4.12 Output Signals of the of the Feedforward Controller and Neurofuzzy Controller No.1

The signals produced by using the step sizes from k1 to k4 was unstable (see Figures 4.10, 4.11 and 4.12) because the nonlinear surface of the car engine has too many local minimum and also the car engine dynamics are too fast compared with the slow speed of convergence of the gradient descend algorithm, which prevents the optimization algorithm for reaching the global solution.

The unstable behaviours are caused by the optimization (GD or BP) algorithm of the neurofuzzy controller. The output signal of neurofuzzy controller is an adaptive gain, which is multiplied by the output signal of the feedforward controller. As it is well known, the Gradient Descent algorithm has a bad reputation when it is searching the global minimum also the convergence which prevent to the algorithm from converging to the global solution (Mollov, 2002; Erdogmus, et. al., 2002).

For the signals produced by the step sizes between k5 to k13 the responses were overlapped with the response of the feedforward control system FFC, shown a stable behaviour without improvements. The experiment was also repeated using the neurofuzzy controller with the following signals inputs:

a) MAF, MAP and Lambda
b) MAF MAP and RPM
c) BT, RPM and Lambda

After concluding this part of the experiment, the results were not better than the previous one because in the majorities of the cases the control system became unstable with even worst results.

4.3.6.2. Feedforward and Neurofuzzy Controller with 3 Inputs and 3 Fuzzy Sets per Input with Product Operation

The previous experiment was repeated with the inclusion of an additional fuzzy set per input (in total 3 fuzzy sets per input signal). In this case, the neurofuzzy system has 27 fuzzy rules in order to specify the adaptive gain in the output of the neurofuzzy controller. The decision to increase the number of the fuzzy rules was taken based on the fact that the performance of the neurofuzzy system could be improved by adding more fuzzy rules which define the dynamical nonlinear behaviours (Pinto, 2001; 2004b). The control structure used was the same as that of Figure 4.9.

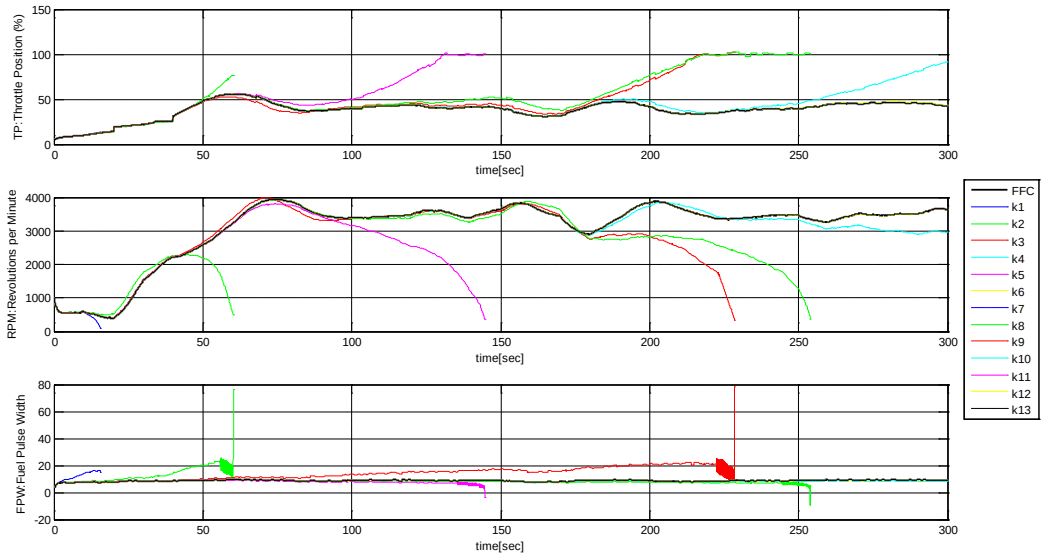

Figure 4.13 Input Signals of the Car Engine Model with Feedforward Controller and a Neurofuzzy Controller No.2

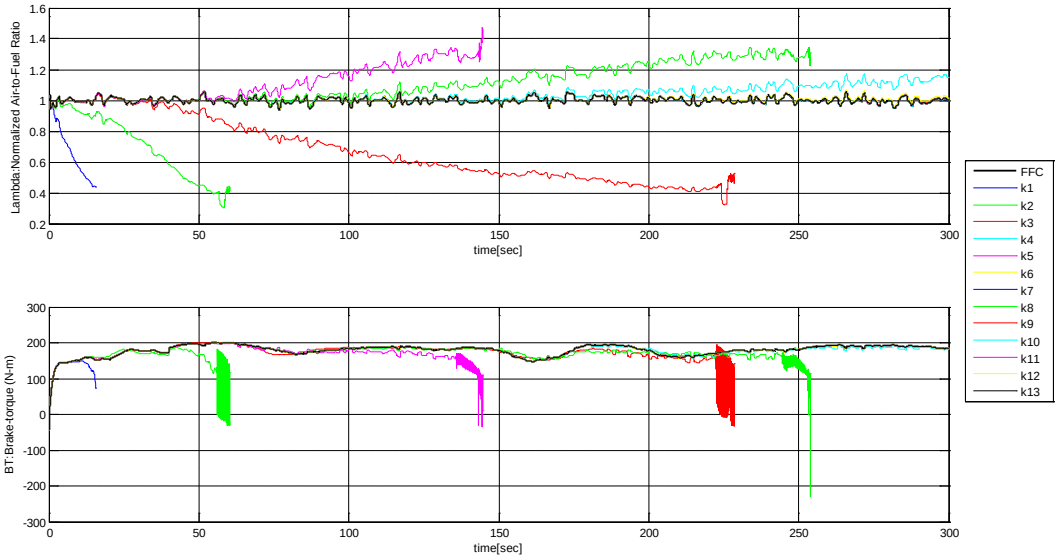

Figure 4.14 Output Signals of the Car Engine Model with Feedforward Controller and a Neurofuzzy Controller No.2

The results belonging to this experiment are Figures 4.13, 4.14 and 4.15. The input and output signals are shown in Figures 4.13 and 4.14. The output signals of the feedforward controller and neurofuzzy Controller with 8 Fuzzy Rules are shown in Figure 4.15. The values for the step size k used in Section 2.7.2.1 were again used in this experiment with the only variation of the amount of fuzzy rules.

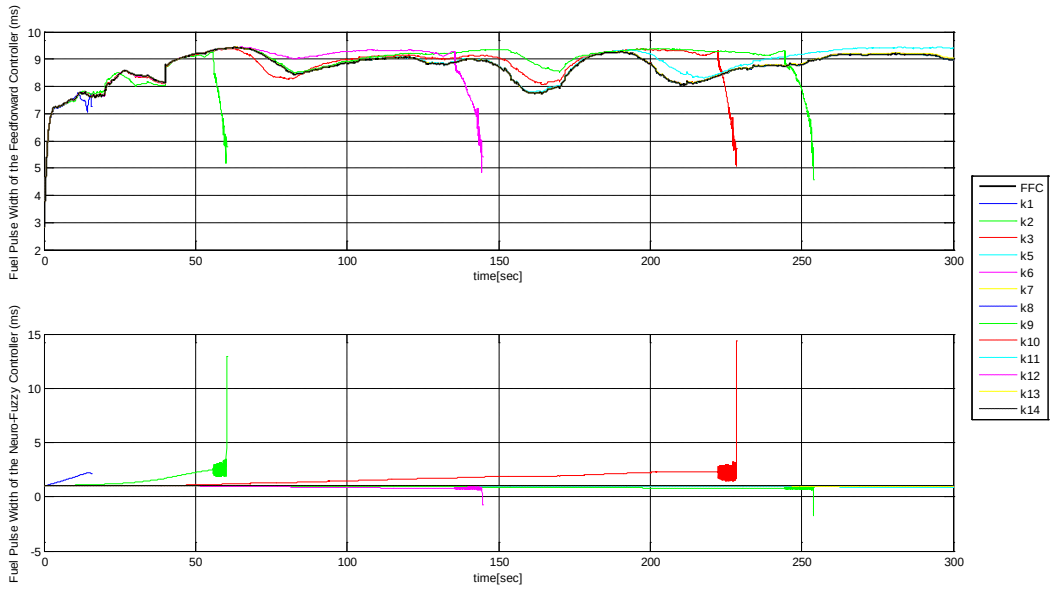

Figure 4.15 Output Signals of the of the Feedforward Controller and Neurofuzzy Controller No.2

The neuro-fuzzy controller was designed with 27 fuzzy rules. Unfortunately, even with the increment of fuzzy rules, combining of the feedforward controller with the neurofuzzy controller has not improved the performance of the feedforward controller because of the weakness of the GD algorithm.

4.3.6.3. Feedforward and Neurofuzzy Controller with 3 Inputs and 2 Fuzzy Sets per Input with Addition Operation

The reason for this structure was based on the fact the neurofuzzy controller acts as dynamic controller while the feedforward controller acts as a steady state controller. In this case, the output of the neurofuzzy controller is the transient fuel pulse width in milliseconds (10^{-3} seconds).

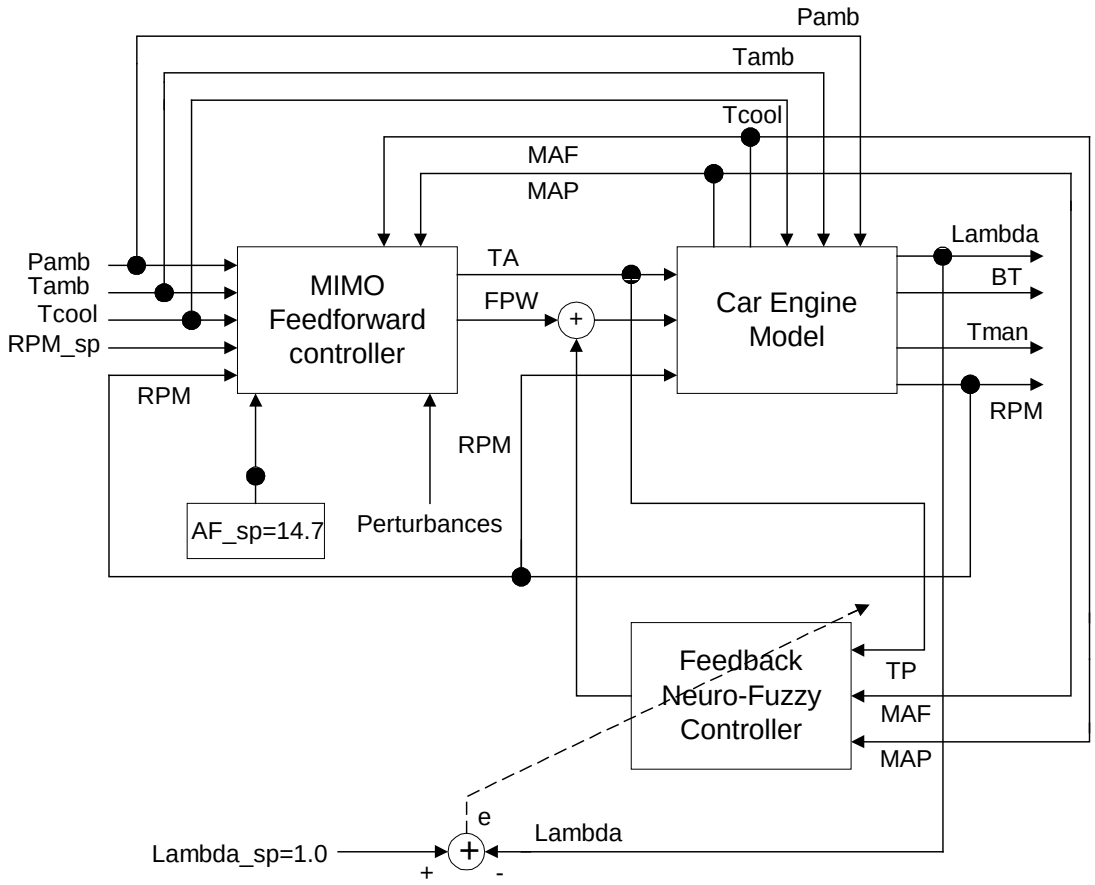

Figure 4.16 Block Diagram of the Car Engine Model with Multivariable Feedforward Controller and Feedback Neurofuzzy Controller No.3

Figure 4.16 shows the block diagram of the car engine model with multivariable feedforward controller (FFC) and feedback neurofuzzy controller with addition adaptable operation. The neuro-fuzzy controller was designed with 8 fuzzy rules. In this experiment, the values of step size k used were:

$$k1a = 1.25 \times 10^{-4};\ k2a = 1.25 \times 10^{-5};\ k3a = 1.25 \times 10^{-6};\ k4a = 1.25 \times 10^{-7}$$

The reason for selecting only these values of *k* was because these represent the more representative results for these experiments.

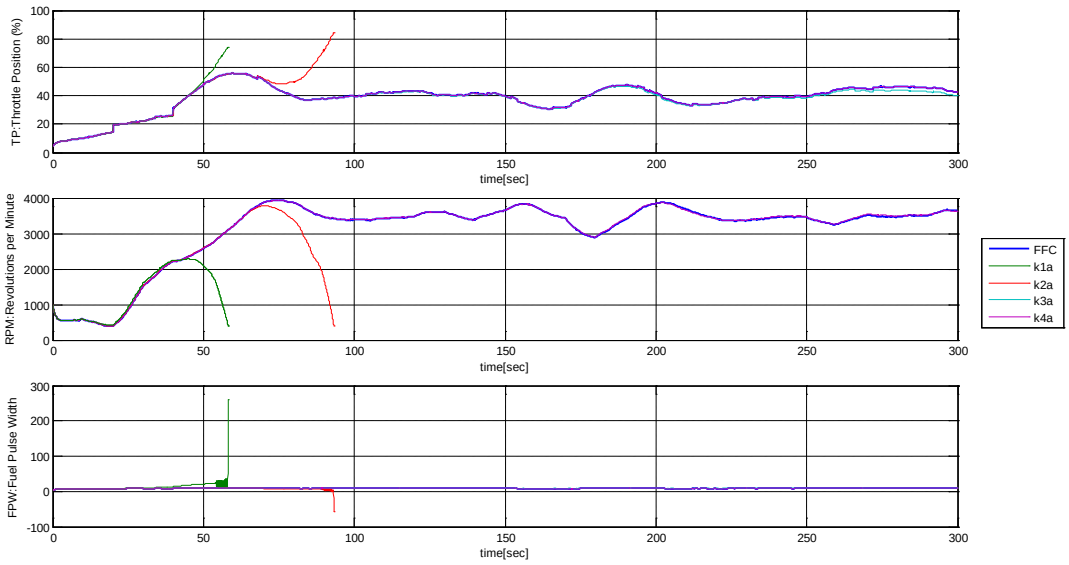

Figure 4.17 Input Signals of the Car Engine Model with Feedforward Controller and a Neurofuzzy Controller No.3

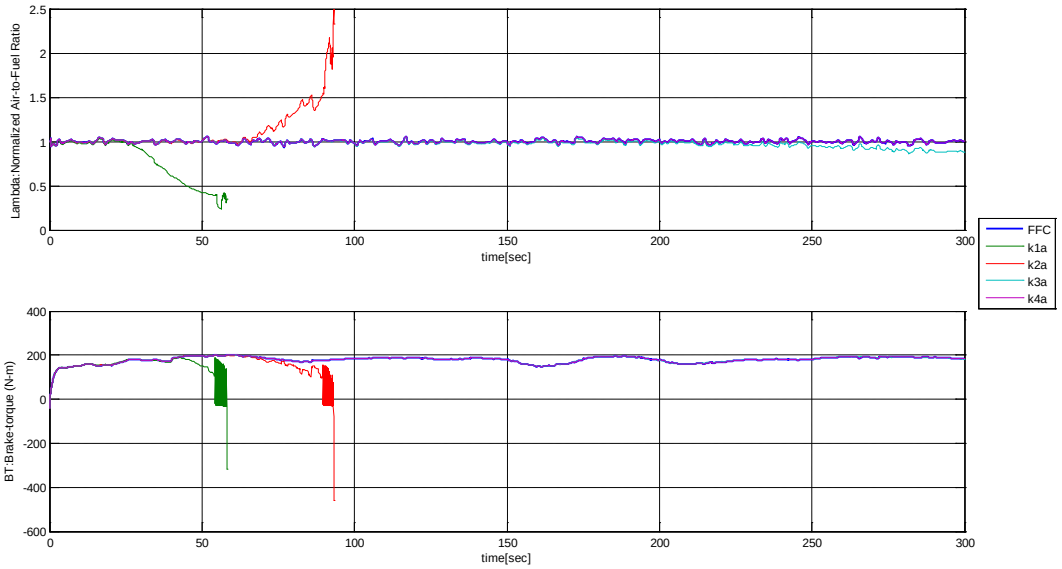

Figure 4.18 Output Signals of the Car Engine Model with Feedforward Controller and a Neurofuzzy Controller No.3

The input signals of the car engine model with a neurofuzzy controller including 8 fuzzy rules and addition adaptive operation are shown in Figure 4.17. Also the output signals are shown in Figure 4.18. Figure 4.19 shows the control signals of the feedforward controller and the neurofuzzy controller. The lines belonging to the step sizes *k1a* (green line) and *k2a* (red line) shown an unstable behaviour, which is caused by the unstable behaviour in the neurofuzzy controller shown in Figure 4.19. The lines with sky blue (step size *k3a*) and magenta (step size *k4a*) show an stable behaviour, which is also evident in the stable behaviour of the neurofuzzy controller which has an output signal approximated to zero compared with the output signal of the feedforward controller FFC.

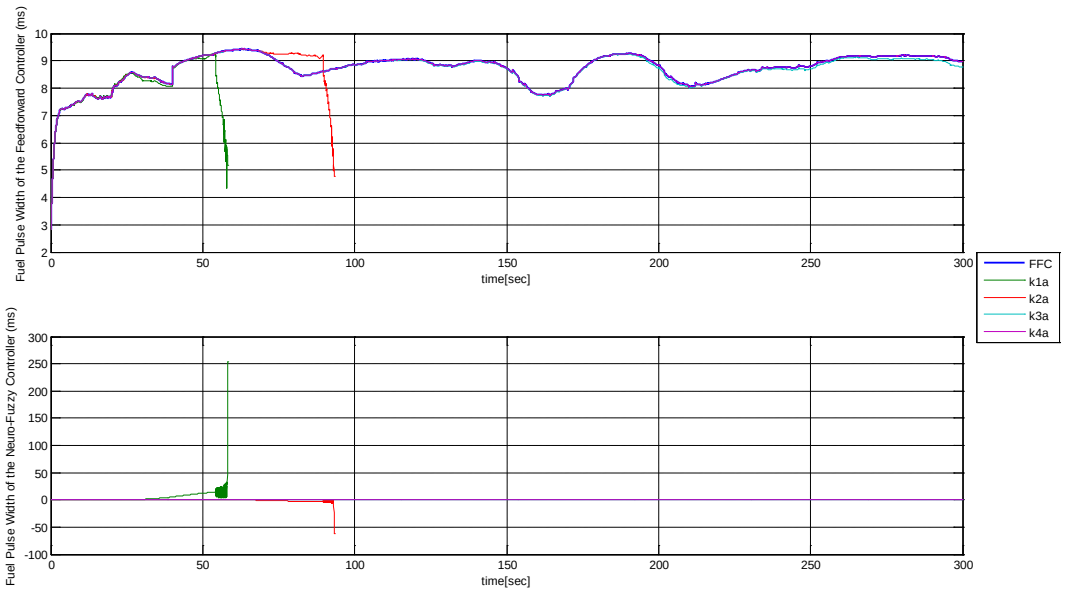

Figure 4.19 Output Signals of the of the Feedforward Controller and Neurofuzzy Controller No.3

One more time, the weaknesses of the GD algorithm is evident using a different structure of the neurofuzzy controller. The magenta and blue lines shown a good behaviour but it is not better than the feedforward controller which looks exactly the same to the result of the magenta line.

4.3.6.4. Feedforward and Neurofuzzy Controller with 3 Inputs and 3 Fuzzy Sets per Inputs with Addition Operation

In this experiment, the neurofuzzy controller was defined by 27 fuzzy rules with addition adaptive operation in order to produce an adaptive fuel pulse width (in milliseconds), which modifies the control output signal by addition to the fuel pulse width generated by the feedforward controller. The step sizes used in this experiment were the same values used for the experiment described above in the Section 4.3.6.1 and they were the following:

$$k1 = 1.25 \times 10^{-4};\ k2 = 1.25 \times 10^{-5};\ k3 = 1.25 \times 10^{-6};\ k4 = 1.25 \times 10^{-7};$$
$$k5 = 1.25 \times 10^{-8};\ k6 = 1.25 \times 10^{-9};\ k7 = 1.25 \times 10^{-10};\ k8 = 2.5 \times 10^{-7};$$

$k9 = 2.5 \times 10^{-8}$; $k10 = 2.5 \times 10^{-9}$; $k11 = 5.0 \times 10^{-7}$; $k12 = 5.0 \times 10^{-8}$; $k13 = 5.0 \times 10^{-9}$

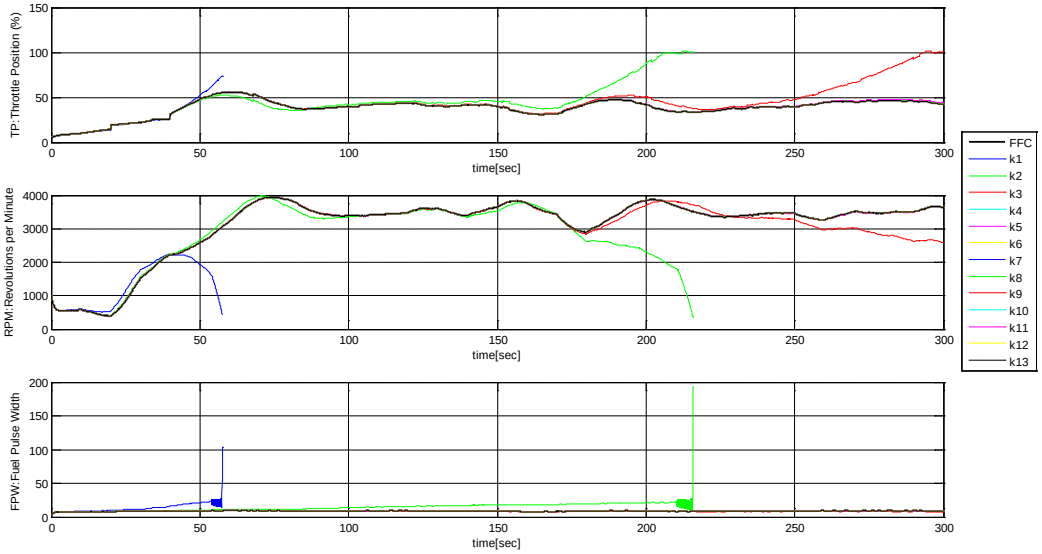

Figure 4.20 Input Signals of the Car Engine Model with Feedforward Controller and a Neurofuzzy Controller No.4

The input (TP, RPM and FPW) and output (Lambda and BT) signals are shown in Figures 4.20 and 4.21. Figure 4.22 shows the control signals of the feedforward controller and the neurofuzzy controller.

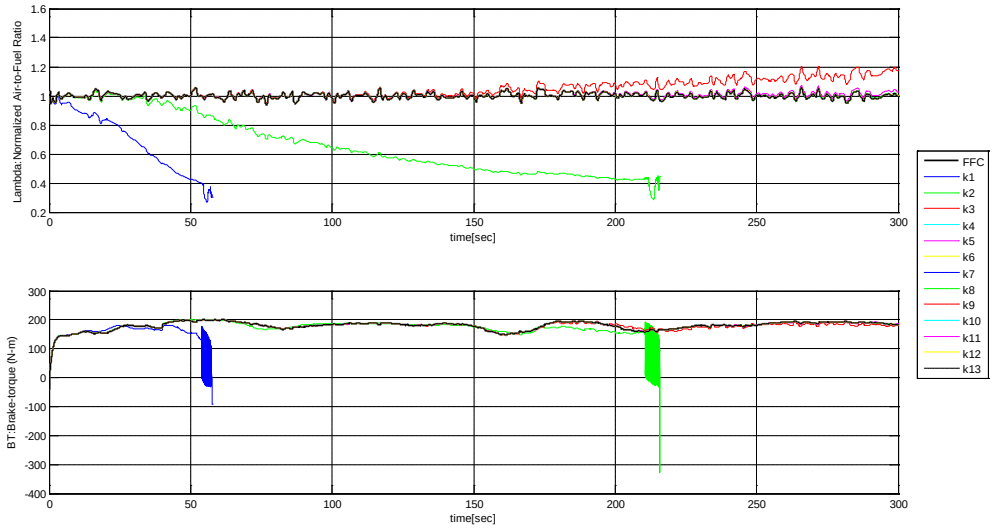

Figure 4.21 Output Signals of the Car Engine Model with Feedforward Controller and a Neurofuzzy Controller No.4

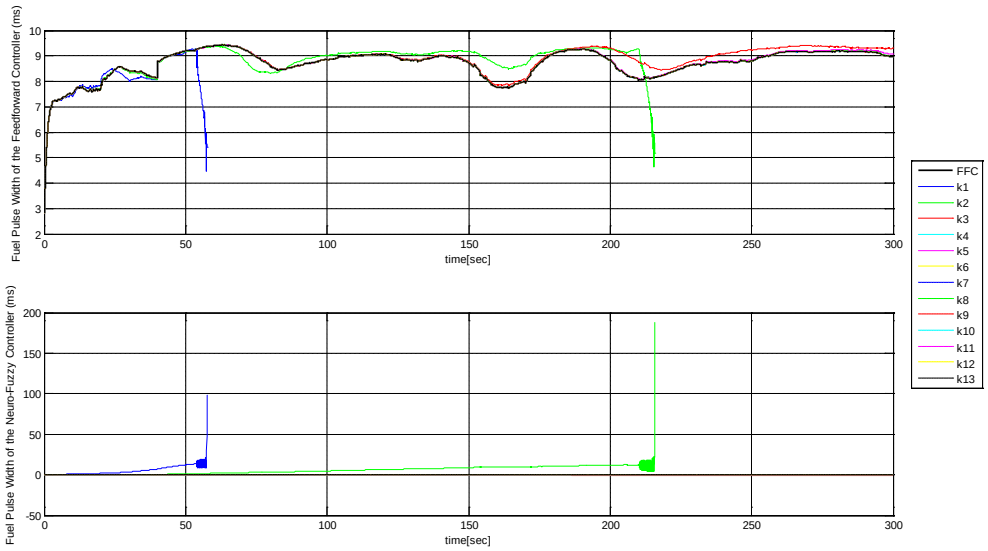

Figure 4.22 Output Signals of the of the Feedforward Controller and Neurofuzzy Controller No.4

The block diagram of the car engine model with multivariable feedforward controller and feedback neurofuzzy controller (4 inputs and 1 output) with the adaptive feature is shown in Figure 4.16. The simulation was developed from 0 to 300 [s]. In this test was used as a reference signal the response of the FFC system for the normalized air-fuel ratio signal. After the step sizes *k1* and *k2* were used in the neurofuzzy controller, the process became unstable. The response of the control system (FFC and the neurofuzzy controller) with step size *k3* was unstable from 0 to 150 [s] and after that the system was stabilised.

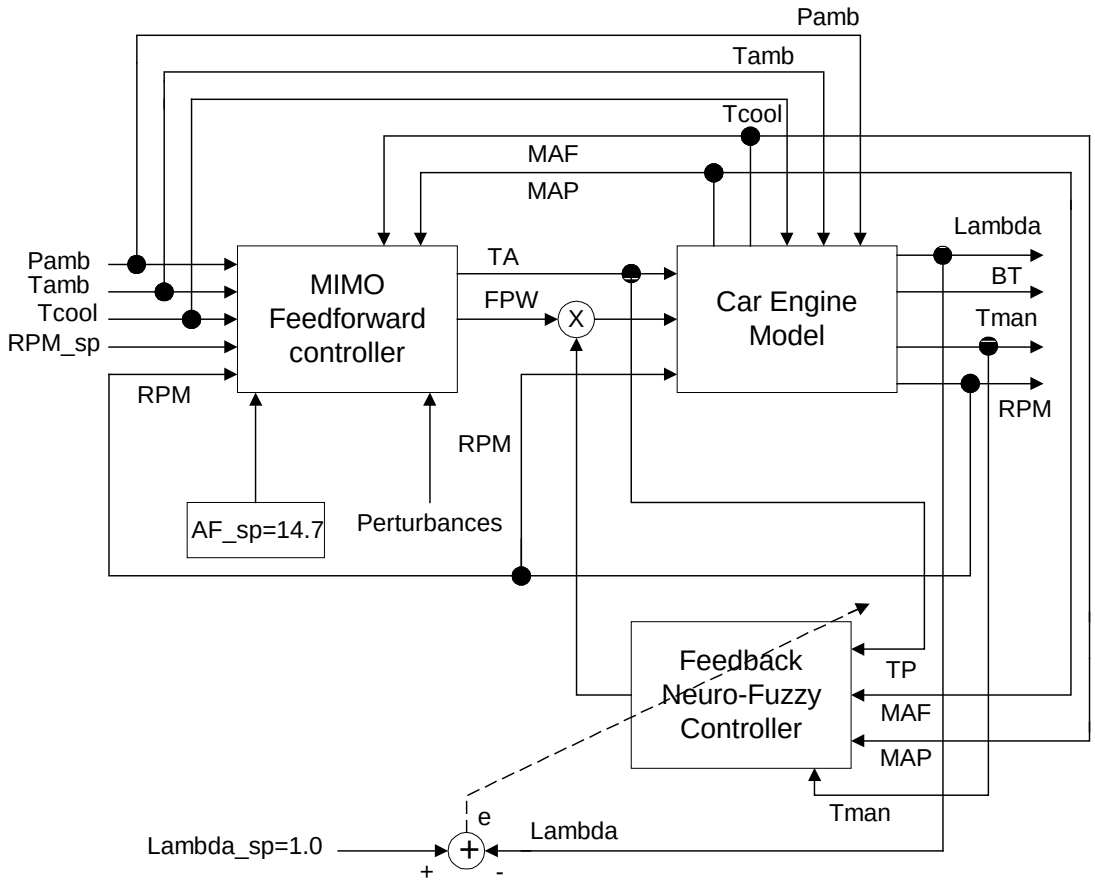

Figure 4.23 Block Diagram of the Car Engine Model with Multivariable Feedforward Controller and Feedback Neurofuzzy Controller No.5

The control systems developed using the step sizes from *k4* to *k13* shows a stable dynamic behaviour without any improvement compared with the feedforward controller (FFC) system. The performance of the FFC has not been improved by this experiment using a neurofuzzy controller with 27 fuzzy rules and addition adaptive operation with the FFC.

4.3.6.5. Feedforward Controller and Neurofuzzy Controller with 4 Inputs and 2 Fuzzy Sets per Input with Product Operation

The feedforward controller and neurofuzzy controller with 4 inputs and 2 fuzzy sets per Inputs with 16 fuzzy rules and product Operation are shown in Figure 4.23. The values of step size k used in the experiment were:

$$k1 = 1.25 \times 10^{-4};\ k2 = 1.25 \times 10^{-5};\ k3 = 1.25 \times 10^{-6};\ k4 = 1.25 \times 10^{-7};$$
$$k5 = 1.25 \times 10^{-8};\ k6 = 1.25 \times 10^{-9};\ k7 = 1.25 \times 10^{-10}$$

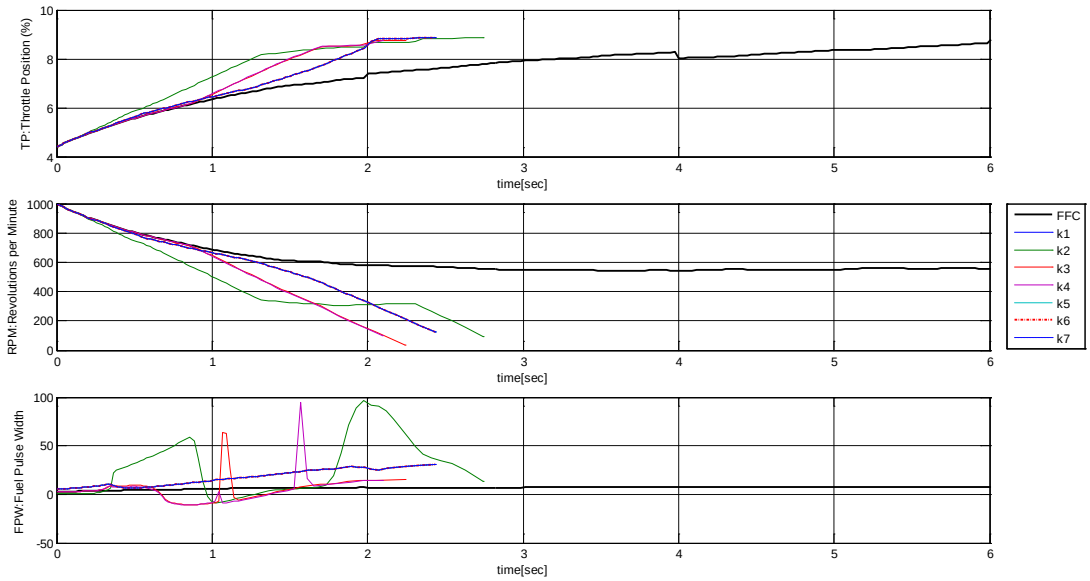

Figure 4.24 Input Signals of the Car Engine Model with a Feedforward Controller and Neurofuzzy Controller No.5

Input and output signals of the car engine model are shown in Figures 4.24 and 4.25. The output signal for the feedforward controller and the neurofuzzy controller with 4 inputs and 16 fuzzy rules are shown in Figure 4.26. All the results obtained were unstable because of the poor performance obtained with the Gradient Descend optimization algorithm. The black lines in the Figures 4.24, 4.25 and 4.26 are the input and output signals belong to the car engine model with the feedforward controller.

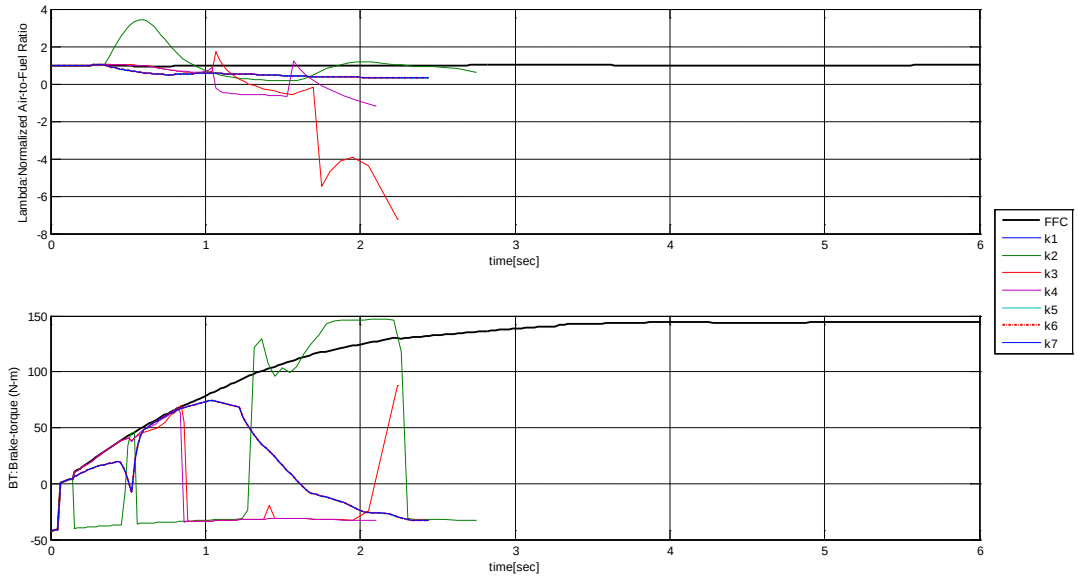

Figure 4.25 Output Signals of the Car Engine Model with a Feedforward Controller and Neurofuzzy Controller No.5

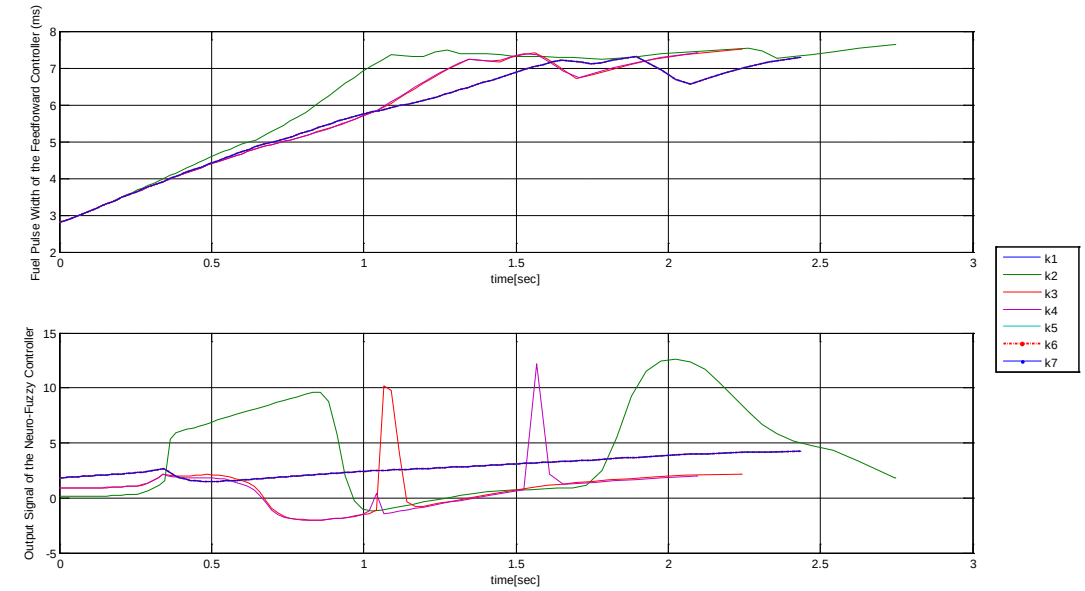

Figure 4.26 Output Signals of the of the Feedforward Controller and Neurofuzzy Controller No.5

4.3.7. Neurofuzzy Control System

The neurofuzzy control system was ideally designed based on the ideas of the general solution for a continuous differential equation, which has its general solution defined as the addition between the transient and steady state solutions. The solution was inspired also in the previous solutions for the car engine problem which combine a steady state controller with a transient state controller (Won, et. al.,1998).

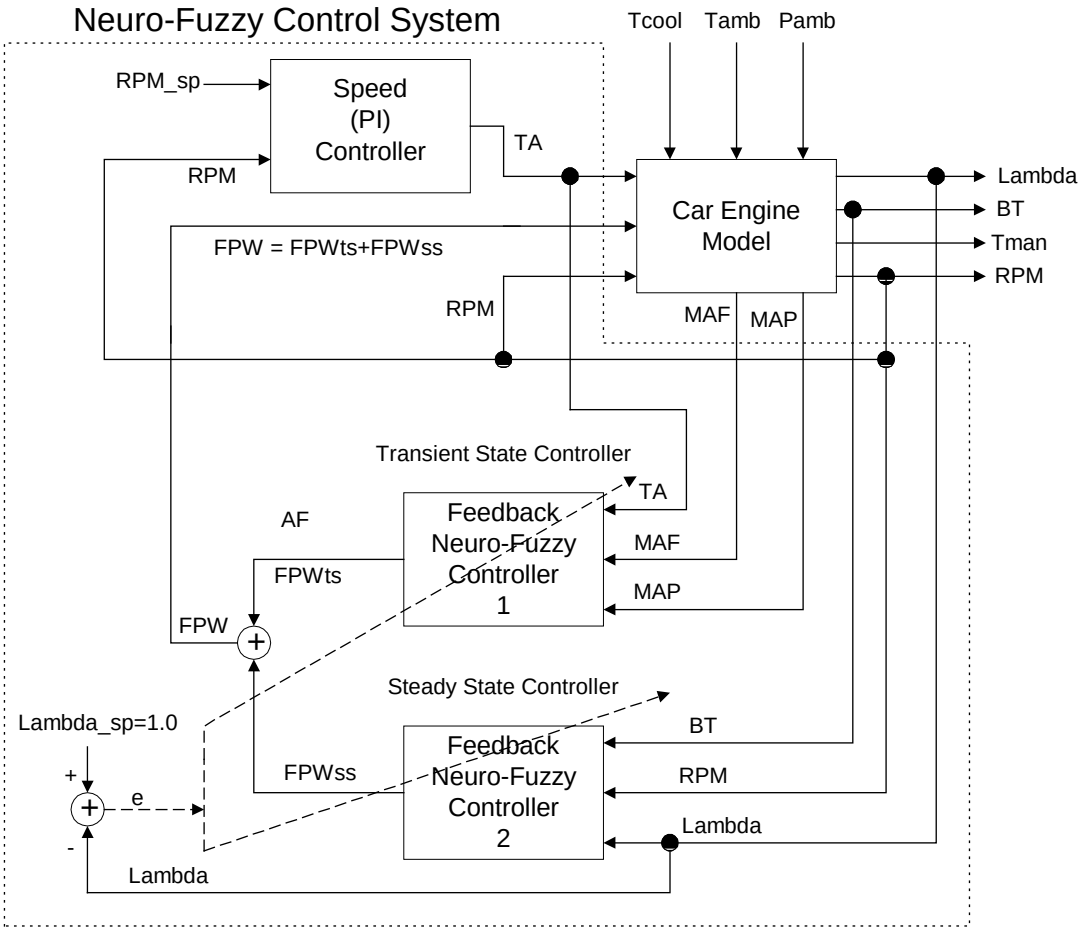

Figure 4.27 Block Diagram of the Car Engine Model with Neurofuzzy Control System No.6

The neurofuzzy control system has: an engine speed (PI) controller, a transient state and steady state neurofuzzy controllers. In order to define the transient state and steady state in the neurofuzzy controllers were selected the proper input variables for

each controller. Specifically, the variable which are not affected by the delays (TA, MAF and MAP) were selected as inputs of the transient state neurofuzzy controller and the variables affected by the delays (BT, RPM and Lambda) were selected as the input signals of the steady state neurofuzzy controller. Figure 4.27 shows the block diagram of the car engine model with a multivariable neurofuzzy Control System. The expression which defines the control signal $\boldsymbol{FPW}(\boldsymbol{k})$ is defined again by equation (4.3):

$$\boldsymbol{FPW}(\boldsymbol{k}) = \boldsymbol{FPW_{ts}}(\boldsymbol{k}) + \boldsymbol{FPW_{ss}}(\boldsymbol{k}) \qquad [10^{-3}\text{sec}] \qquad (4.5)$$

where $\boldsymbol{FPW_{ts}}(\boldsymbol{k})$ and $\boldsymbol{FPW_{ss}}(\boldsymbol{k})$ are the output signals for the transient state and steady state neurofuzzy controllers, respectively. Using equation (2.56), the output signal of the neurofuzzy controllers $\boldsymbol{FPW_{ts}}(\boldsymbol{k})$ and $\boldsymbol{FPW_{ss}}(\boldsymbol{k})$ are defined as follows:

$$\boldsymbol{FPW_{ts}}(\boldsymbol{k}) = \sum_{\boldsymbol{i}=1}^{\boldsymbol{N3}} \boldsymbol{\varsigma_i}(\mathbf{x}(\boldsymbol{k}))\, \boldsymbol{z_i}(\mathbf{x}(\boldsymbol{k})) \qquad [10^{-3}\text{sec}] \qquad (4.6)$$

$$\boldsymbol{FPW_{ss}}(\boldsymbol{k}) = \sum_{\boldsymbol{i}=1}^{\boldsymbol{N4}} \boldsymbol{\xi_i}(\mathbf{x}(\boldsymbol{k}))\, \boldsymbol{\omega_i}(\mathbf{x}(\boldsymbol{k})) \qquad [10^{-3}\text{sec}] \qquad (4.7)$$

where $\boldsymbol{\varsigma_i}(\mathbf{x}(\boldsymbol{k}))$ and $\boldsymbol{z_i}(\mathbf{x}(\boldsymbol{k}))$ the normalized degree of fulfilment and the local lineal model for the transient state neurofuzzy controller. $\boldsymbol{\xi_i}(\mathbf{x}(\boldsymbol{k}))$ and $\boldsymbol{\omega_i}(\mathbf{x}(\boldsymbol{k}))$ the normalized degree of fulfilment and the local lineal model for the steady state neurofuzzy controller. $\mathbf{x}(k)$ is the input (state) vector. *N3 and N4* are the amount of fuzzy rules for the transient state and steady state neurofuzzy controllers.

A complete definition of the structures of the neurofuzzy controller was explained in Section 2.3.

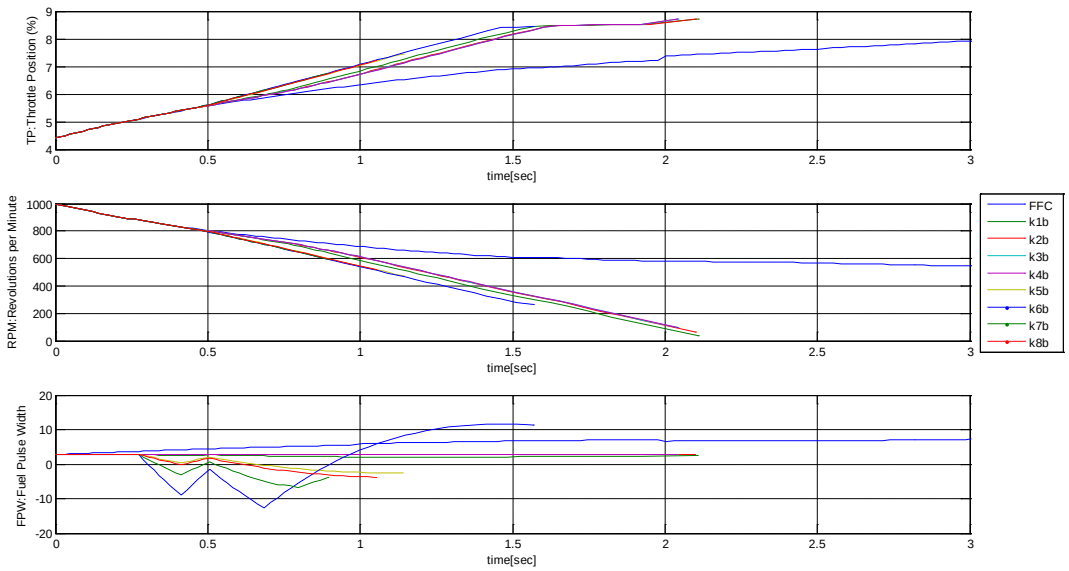

Figure 4.28 Input Signals of the Car Engine Model with Neurofuzzy Control System No.6

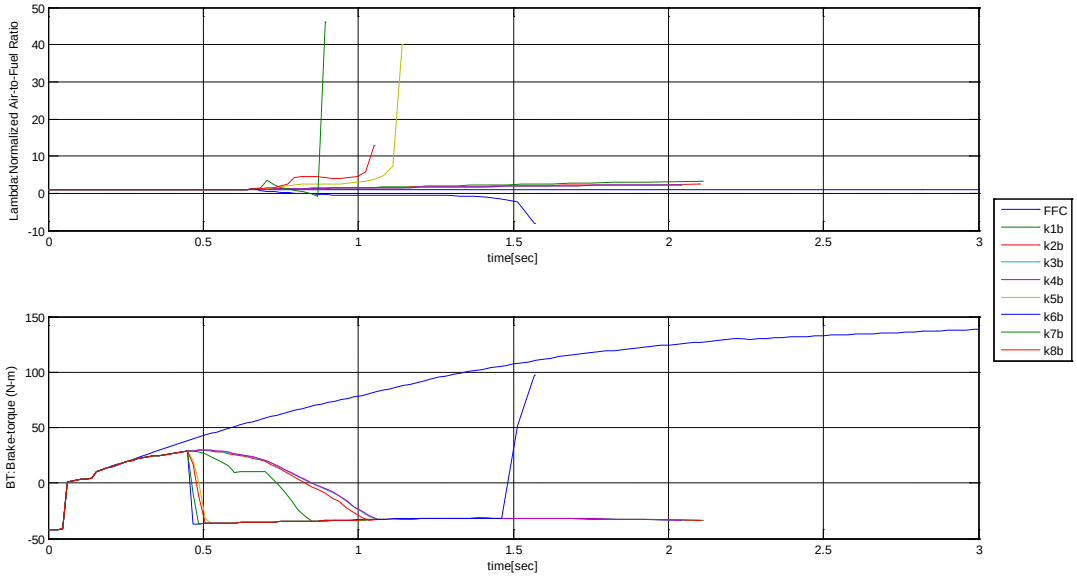

Figure 4.29 Output Signals of the Car Engine Model with Neurofuzzy Control System No.6

The input and output signals of the car engine model are shown in Figures 4.28 and 4.29. Figure 4.30 shows the output signals of the Car Engine Model with Neurofuzzy Control System. The blue line in Figures 4.28 and 4.29 show the car engine model applying the feedforward controller FFC alone and the rest of the lines belong to different values of the step size *k* which have the following values:

$k1b = 1.0 \times 10^{-3}$; $k2b = 5.0 \times 10^{-3}$; $k3b = 2.5 \times 10^{-3}$;$k4b = 1.25 \times 10^{-3}$;
$k5b = 1.25 \times 10^{-4}$; $k6b = 1.25 \times 10^{-5}$; $k7b = 1.25 \times 10^{-6}$; $k8b = 1.25 \times 10^{-7}$

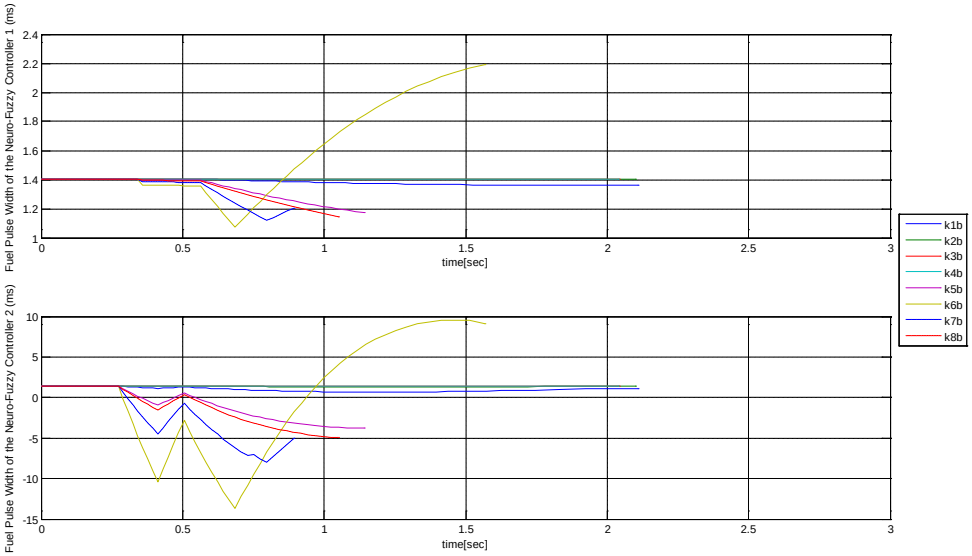

Figure 4.30 Output Signals of the Car Engine Model with Neurofuzzy Control System No.6

Finally, in the experiment was intended to synchronize both neurofuzzy controllers in order to produce an stable output signal but due to the low speed of convergence of the Gradient Descent and the delays between all the input variables then the neurofuzzy control system always shown a unstable behaviour.

4.4. Conclusions

In this section was used the Gradient Descent (or Backpropagation) optimization algorithm. The car engine is a very fast process with transient and steady state nonlinear dynamics with the following characteristics: high nonlinearity, delays between the sub-processes, multivariable process with strong interactions, complex dynamical nonlinear surface with several local minimum. The car engine is mainly treated as a transient state problem with a steady state component. The transient problem was dealing with the adaptive features of the neurofuzzy controllers

proposing several control systems structures as the neurofuzzy GMV, feedforward controller and Neurofuzzy Control with product an addition adaptive operation and the neurofuzzy control system. Also, trying to tune the neurofuzzy controllers, several step size k were used, several different fuzzy sets per inputs (or fuzzy rules per neurofuzzy system) and different sets of inputs were tested to capture more dynamic information about the car engine system. The adaptation of the neurofuzzy controllers requires to be on-line and hence the Gradient Descent was selected as a possible solution for the optimization problem.

The Gradient Descent (or Back propagation) is too slow to converge to the global minimum in order to solve the car engine problem because the nonlinear surface of the car engine has too many local minimum and also the car engine dynamics are too fast compared with the slow speed of convergence of the gradient descend algorithm. The control strategy can be improved by including local expert agents which learn previously the nonlinear behaviour of sections of all the operating range of the nonlinear car engine dynamic surface. After the local expert agents learned the dynamic behaviour which includes all local minimum then the searching for the global solution will be faster. Another suggestion for future research is to use a faster optimization algorithm than the Gradient Descent with the control system used in the experiments. On the other hand, using the neurofuzzy system with a different optimization algorithm and/or a different nonlinear control technique such as observer-based control or sliding mode control could be useful for the solution of the car engine problem.

Chapter 5 Power Electronics and Fuzzy Control System Applications

5.1. Introduction

The present chapter is concerned with the power electronics and fuzzy control systems applied to a ballast (with buck converter) and the igniter plus a lamp system. The experiments were developed with formal theoretical foundations followed by comparative analysis of simulation and experimental results.

This chapter starts with the Discrete-Sliding Mode Control followed by the Dimming Control using Adaptive Fuzzy Sliding Surface for Square-Waveform Ballast. The structure of the Dimming Control uses a Mamdani's Fuzzy model in order to define the Adaptive Fuzzy Sliding Surface. To design and tune the Dimming Control with the Adaptive Fuzzy Sliding Surface it is necessary to apply the techniques clearly explained in (Pinto, 2001). This is followed by the Thermal Dynamic Model for High Intensity Discharge (HID) Lamps with the Outer-Bulb Effects. Finally, the chapter includes a Simplified-Stability Analysis of Square-waveform Ballast Using a Nonlinear Lamp Model.

5.2. Analysis and Design of Discrete-Sliding-Mode Control for a Square-Waveform-Ballast

The acoustic resonance phenomenon in HID lamps is a consequence of pressure waves of the filled gas inside the lamp. This phenomenon is caused by the lamp power modulation. The arc discharge is deformed by these pressure waves. Heating spots are generated when the glass bladder is reached by the arc, and generally these spots break the lamp (Groot and Van Vliet, 1986).

One of the most reliable solutions for the elimination of the acoustic resonance phenomenon in HID lamps consists of feeding the lamp with square wave forms to reach a constant power. Most of the electronic ballasts that feed the lamps with square wave forms require a feedback control system to stabilize the lamp current (Deng, 1995; Deng and Cuk, 1997). Generally, the discharge arc in HID lamps is extinguished if the

power inferior limit is reached (approximately 50% of the nominal power) (Correa, 2002). Therefore, to avoid the arc extinction, it is important that the dimming control of the electronic ballast has a good reference tracking. Additionally, it is important to have a good dynamic response in illuminating systems where voltage variations or load changes are likely to occur. Good dynamic response, stability and regulation from voltage variations, are sought by the sliding mode control (Utkin, 1974; 1977). The HID lamp current is unstable when the lamp is feeding with a voltage source, an example is a variable structure dc-dc converter working in continuous conduction mode (CCM). The control will drive the system to the balance point.

An igniter is needed when the HID lamps are fed with square waves. A proposed igniter was based on a resonant network; this network works only for 40μs-60μs in a high resonant frequency. Also, there are semiconductor losses and the amount of the passive elements were reduced. An electronic ballast was introduced in (Ponce, et. al., 2001), feeding the HID lamp with low frequency square wave forms. The feedback control was designed with a non linear sliding control. The control stage was implemented in analog form, and then several electronic elements (1 operational amplifier, 1 high speed comparator, 2 logic circuits, 13 resistors, 1 microcontroller) were needed. The aim of this research is to use a Discrete Sliding Mode Control for a non resonant ballast. The following advantages were achieved against the Analog Sliding Mode Control (Orozco and Vazquez, 2000):

a) Reduction of the number of electronic components.
b) Possibility of applying adaptive controller to feed different lamps with the same electronic ballast.
c) Flexibility in the development of the sliding surface.
d) The same control strategy is useful to different converters with minimum adjustment.
e) Possibility for integration of advanced functions in the control algorithm, like digital compensators, etc.

The above advantages are in addition to those introduced by the sliding mode control. The simulations of the electronic ballast with the igniter plus the

nonlinear dynamic lamp model (Osorio, et. al., 2004a) were made in Simulink (SimPowerSystem and DSP libraries).

5.2.1. Power Stage

The block diagram of the selected ballast is shown in Figure 5.1. A buck converter was operating in Continuous Conduction Mode (CCM). This converter stabilizes the arc discharge and feeds the inverter. A dc bus is given by the dc-dc converter that integrates a power factor correction.

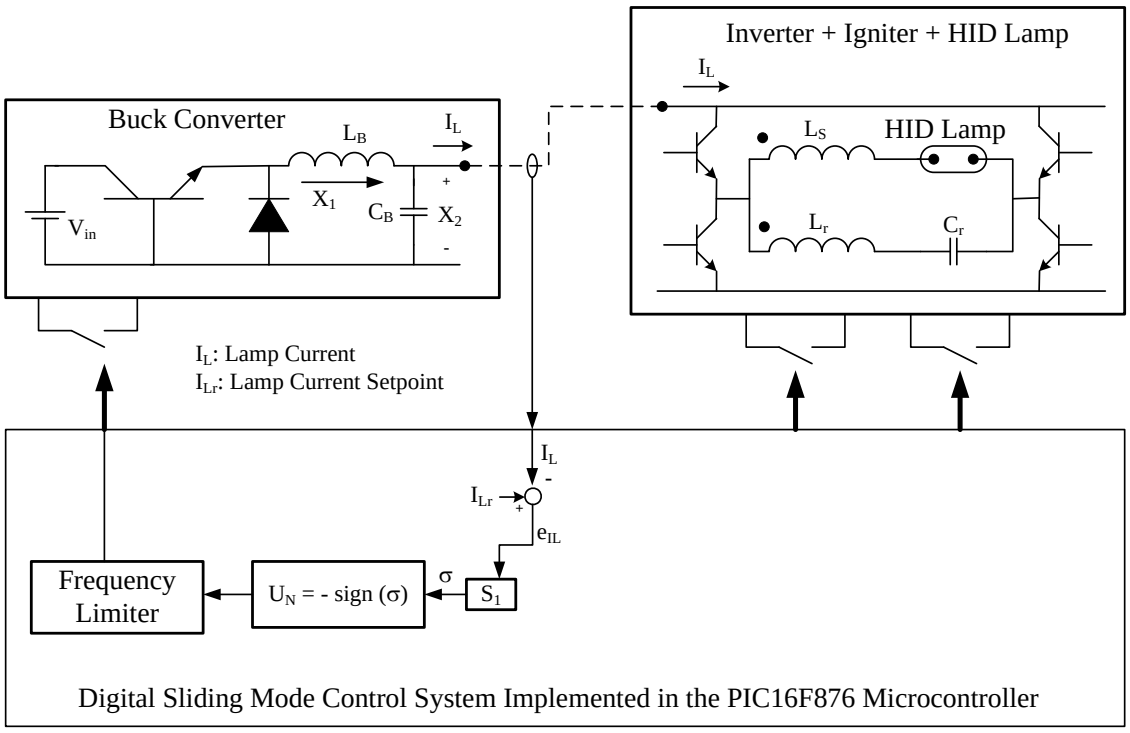

Figure 5.1 Block Diagram of Selected Topology with Nonlinear Control Stage

To avoid the acoustic resonance, the inverter feeds the HID lamp (70W metal Halide) with low frequency square waveforms (400Hz, avoiding the effects of parasitic elements). The igniter has the resonant network (*LrCr*) in series configuration. *Lr* is coupled to *Ls* (autotransformer configuration). High voltages (4.5kV peak) could be reached with this configuration assuring the lamp ignition.

The ignition sequence takes 40μs-60μs (4 or 6 pulses of 100 kHz). The inverter operation frequency changes to 400Hz when the lamp ignition is reached. Therefore, at this frequency, the inductor impedance is very low (short circuit) and the capacitor impedance is very high (open circuit) and both impedances can be ignored.

5.2.2. Control Stage

5.2.2.1. System Modeling

The power stage (Figure 5.2(a)) can be simplified as follows: The influence of the igniter in the ballast under stable state is worthless, (Figure 5.2(b)). The inverter current demanded from the Buck converter is constant and can be eliminated (Figure 5.2(c)). Finally, the semiconductors could be substituted by ideal switches and the lamp was considered unstable state as a constant resistance only for the control parameter estimations (Figure 5.2(d)). The lamp model proposed in (Orozco and Vazquez, 2000; Osorio, et. al., 2004c) was used in the simulations.

The resultant system in a matrix form considering the position of the switch u1 (1 and -1) is expressed as follows:

$$\begin{pmatrix}\dot{x}_1\\ \dot{x}_2\end{pmatrix} = \begin{pmatrix}0 & -\frac{1}{L_B}\\ \frac{1}{C_B} & -\frac{1}{C_B R}\end{pmatrix}\begin{pmatrix}x_1\\ x_2\end{pmatrix} + \begin{pmatrix}\frac{V_{in}}{2L_B}\\ 0\end{pmatrix}u + \begin{pmatrix}\frac{V_{in}}{2L_B}\\ 0\end{pmatrix} \quad (5.1)$$

Defined also as follows:

$$\dot{X} = AX + BU + B \quad (5.2)$$

where x_1 is the current of the inductor L_B, x_2 is the voltage of the capacitor C_B.

For L_B= 5mH, C_B= 1μF, R = 115Ω, V_{in} = 180V:

$$\begin{pmatrix}\dot{x}_1\\ \dot{x}_2\end{pmatrix} = 1\times 10^6 \begin{pmatrix}0 & -0.0002\\ 1 & -0.0087\end{pmatrix}\begin{pmatrix}x_1\\ x_2\end{pmatrix} + \begin{pmatrix}18\times 10^3\\ 0\end{pmatrix}u + \begin{pmatrix}18\times 10^3\\ 0\end{pmatrix} \quad (5.3)$$

The discrete system using a zero-order hold, with a sampling period of 16 μ s becomes as follows:

$$\begin{pmatrix} x_1(n+1) \\ x_2(n+1) \end{pmatrix} = \begin{pmatrix} 0.9757 & -0.002962 \\ 14.81 & 0.8469 \end{pmatrix} \begin{pmatrix} x_1(n) \\ x_2(n) \end{pmatrix} + \begin{pmatrix} 0.5713 \\ 2.1915 \end{pmatrix} u(n) + \begin{pmatrix} 0.5713 \\ 2.1915 \end{pmatrix} \quad (5.4)$$

The PIC16F876 microcontroller from the Microchip Company was used.

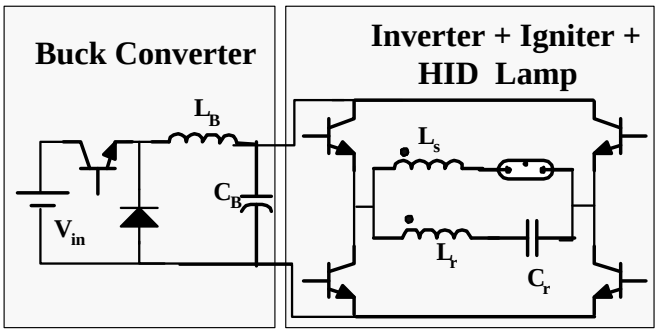

(a) Complete Power Stage

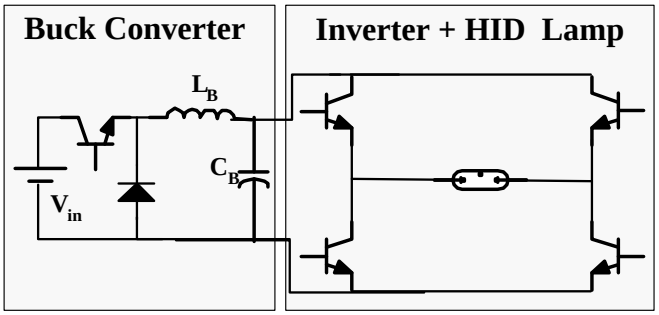

(b)Without Igniter

Buck Converter + HID Lamp

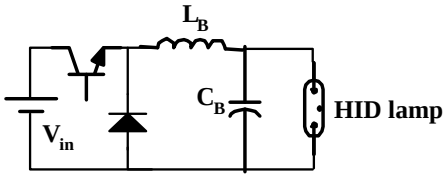

(c)Without Inverter

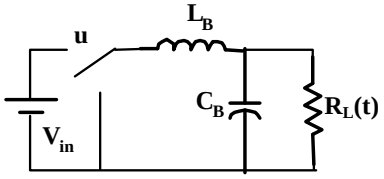

(c)Using Ideal Switch and Considering the Lamp as a Resistance

Figure 5.2 Ballast Simplifications

5.2.2.2. Sliding Surface

The continuous-sliding surface proposed in (Osorio, 2004c) is a linear combination of the lamp current I_L and the current reference I_{Lr} (see Figure 5.1):

$$\sigma = s_1(I_L - I_{Lr}) \tag{5.5}$$

where $s_1$is a parameter control.

Or

$$\sigma = [s_2 \quad s_3]\begin{bmatrix} x_1 - x_{1r} \\ \frac{dx_2}{dt} - x_{2r} \end{bmatrix} \tag{5.6}$$

and

$$s_2 = s_1 \tag{5.7}$$

$$s_3 = s_1 C_B \tag{5.8}$$

where x_{1r} and x_{2r} are the reference current signals.

From the previous equation, the discrete-sliding surface obtained was as follows (Utkin, 1977):

$$\sigma(n) = s_1\big(I_L(n) - I_{Lr}(n)\big) = [s_2 \quad s_3]\begin{bmatrix} x_1 - x_{1r} \\ \frac{x_2(n+1) - x_2(n)}{T} - x_{2r} \end{bmatrix} \tag{5.9}$$

Due to the operational amplifiers dc Bus limitations, the s_1 experimental value is practically chosen in the interval (1, 10), then the maxim value of s_3 was as follows:

$$s_3 = s_1 C_B = 10 \times 10^{-6} \ll s_2 \tag{5.10}$$

The previous equation implies the following:

$$\sigma(n) \cong s_1(x_1(n) - x_{1r}) \tag{5.11}$$

where s_1, s_2 and s_3 are the control parameters. I_L is current lamp, X are the state variables. I_{Lr} and X_r are the references signals or set-points.

The control law proposed was expressed as being: $u = u_{eq} + u_N$
Here: u_{eq} is the equivalent control and $u_N = -\text{sgn}(\sigma)$.

5.2.2.3. The Control Law

The discrete-time control law is expressed as follows (Sarpturk, 1987):

$$u(n) = u_{eq}(n) + u_N(n) \quad (5.12)$$

where $u_N(n) = -sgn(\sigma(n))$ is implemented control and $u_{eq}(n)$ is the equivalent control.

The equivalent control law $u_{eq}(n)$ is only for analysis purposes and this implies a guarantee of the existence condition only locally. The implemented control $u_N(n)$ does not include the equivalent control.

5.2.2.4. Existence and Convergence Conditions of Discrete Sliding Mode Control (DSMC)

Equations (5.13) and (5.14) describe the existence of DSMC (Sarpturk, 1987). The analysis starts with the convergence and sliding conditions expressed as follows:

$$(\sigma(n+1) + \sigma(n))sign(\sigma(n)) \geq 0, \text{ convergence condition} \quad (5.13)$$

$$(\sigma(n+1) - \sigma(n))sign(\sigma(n)) < 0, \text{ sliding condition} \quad (5.14)$$

From experimental results, the lamp always ignites from these values: $x_1(n)$=3A (maximum value), $x_2(n)$ = 20V, x_{1r} = 0.777A and $\sigma > 0$ when u_N = -1:

$4.31s_1 \geq 0$, convergence condition (5.15)

$-0.78s_1 < 0$, sliding condition (5.16)

$x_1(n)$ = 0.35A (minimum value), $x_2(n)$ = 115V, x_{1r} = 0.777A and $\sigma > 0$ when u_N = 1:

$0.06s_1 \geq 0$, convergence condition (5.17)

$-0.13s_1 < 0$, sliding condition (5.18)

In order to cover the convergence and sliding conditions, s_1 has to be positive in order to satisfy equations (5.15) to (5.18).

5.2.3. Simulation and Experimental Results

The electronic ballast was designed with the following parameters: Po = 70W, Vin =180Vdc, VC = 90Vdc, IL =0.777A, L = 5mH, C = 1μF, CDM70W830PH lamp, s1 = 1. The values of C and L were chosen according to current and voltage ripples. The simulated circuit (Buck converter, DSMC and lamp model) is shown in Figure 5.3. Simulation results of the electronic ballast with DSMC control are shown in Figures 5.4 and 5.5. The demanded current and the output voltage of the Buck converter are shown in Figure 5.4. Figure 5.5 shows a dimming test (from 100% to 50%), it is made with a change in the current reference. The demanded current and the output voltage to the Buck converter are shown. As it can be observed, a good dynamic response was obtained. The effect of death times are shown in Figures 5.4 and 5.5.

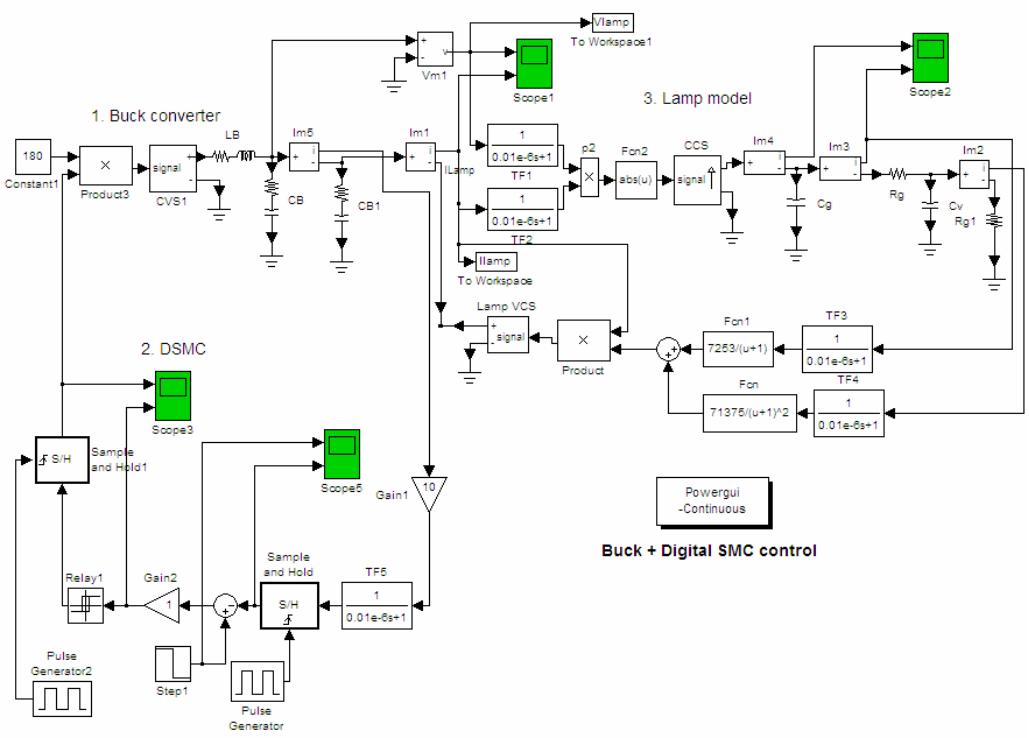

Figure 5.3 Simulation Scheme in Simulink

The DSMC program flow diagram is shown in Figure 5.6. Experimental results of the electronic ballast with DSMC control are shown in Figures 5.7 and 5.8. Figure 5.7 shows the experimental results of the electronic ballast with a Sliding Mode Control (SMC) under steady state condition. The current reference, lamp current and voltage are shown. Figure 8 shows the dimming test (from 100% to 50%); this dimming is made with a change in the current reference. The current demanded and the output voltage of the Buck Converter are shown, hence revealing a good dynamic response.

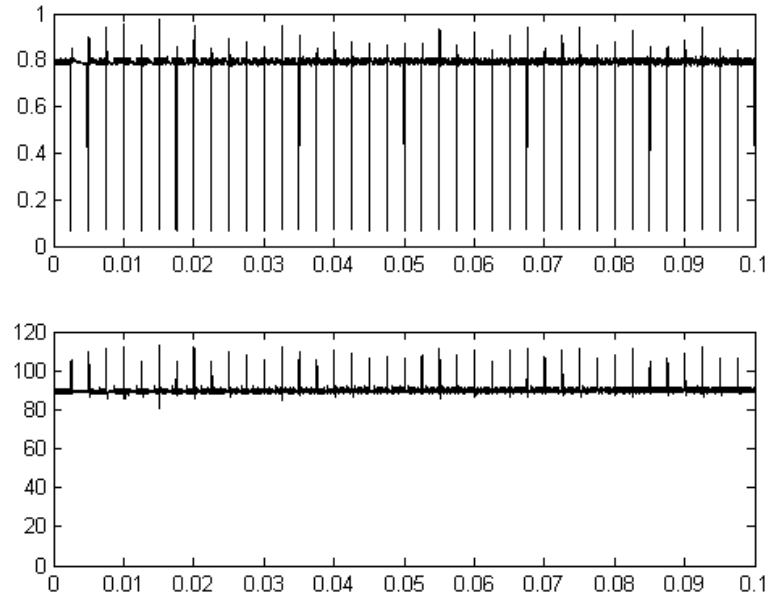

Figure 5.4 Wave Forms for Nominal Power (70W): (a) Typical Topology: Current Demanded (Top) and Output Voltage of Buck Converter. (b) Compact Topology: Lamp Current (Top) and Lamp Voltage (Bottom).

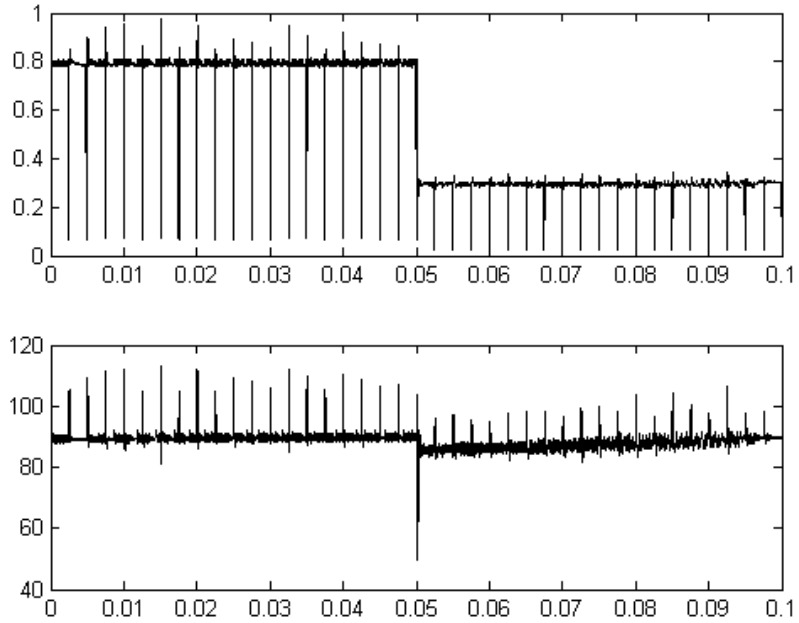

Figure 5.5 Dimming Test (from 100% to 50%), (a) Typical Topology: Current Demanded (Top) and Output Voltage of Buck Converter. (b) Compact Topology: Lamp Current (Top) and Lamp Voltage (Bottom)

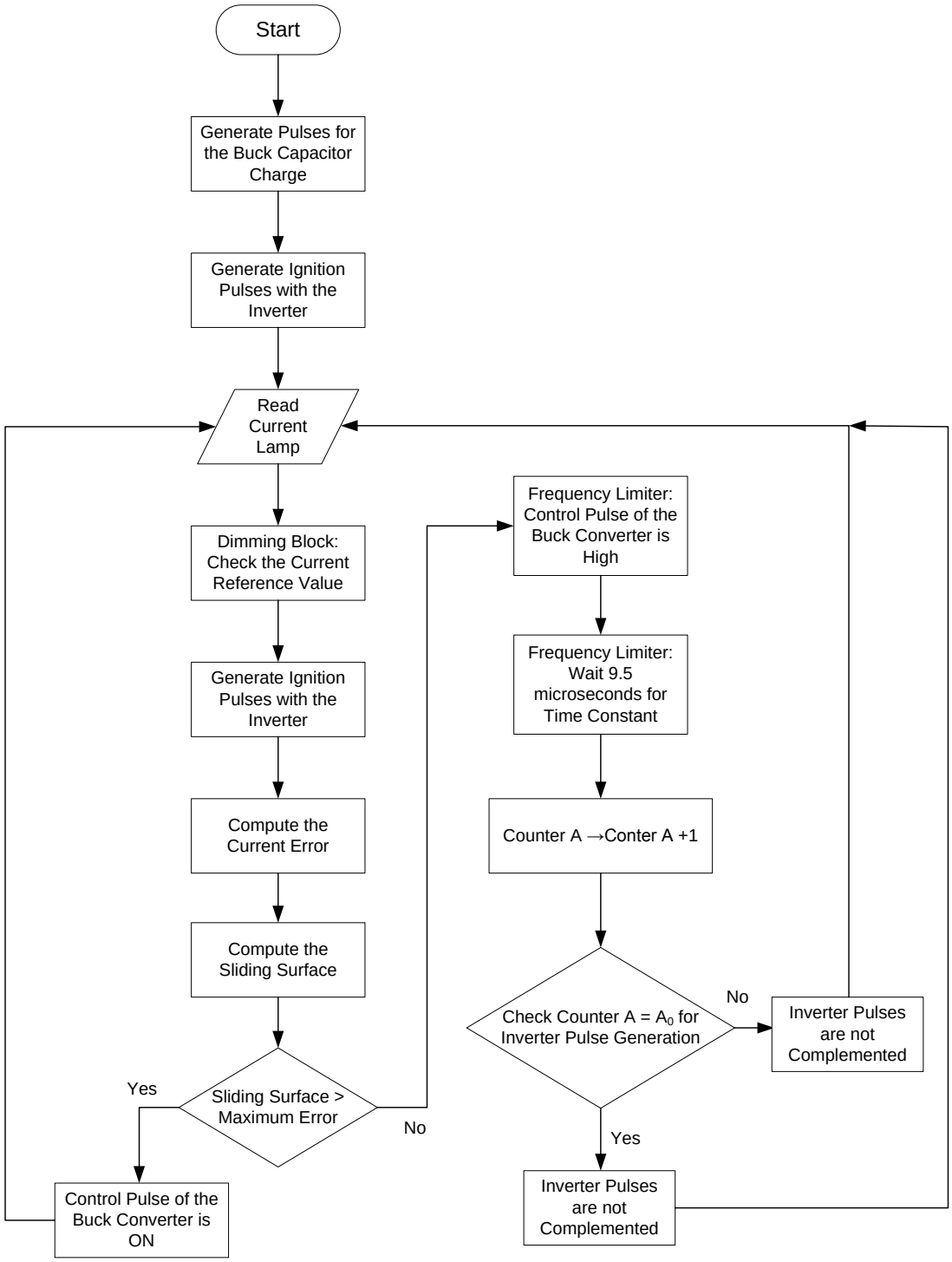

Figure 5.6 Program Flow Diagram for the Discrete Sliding Mode Control Implemented in PIC16F876 Microcontroller

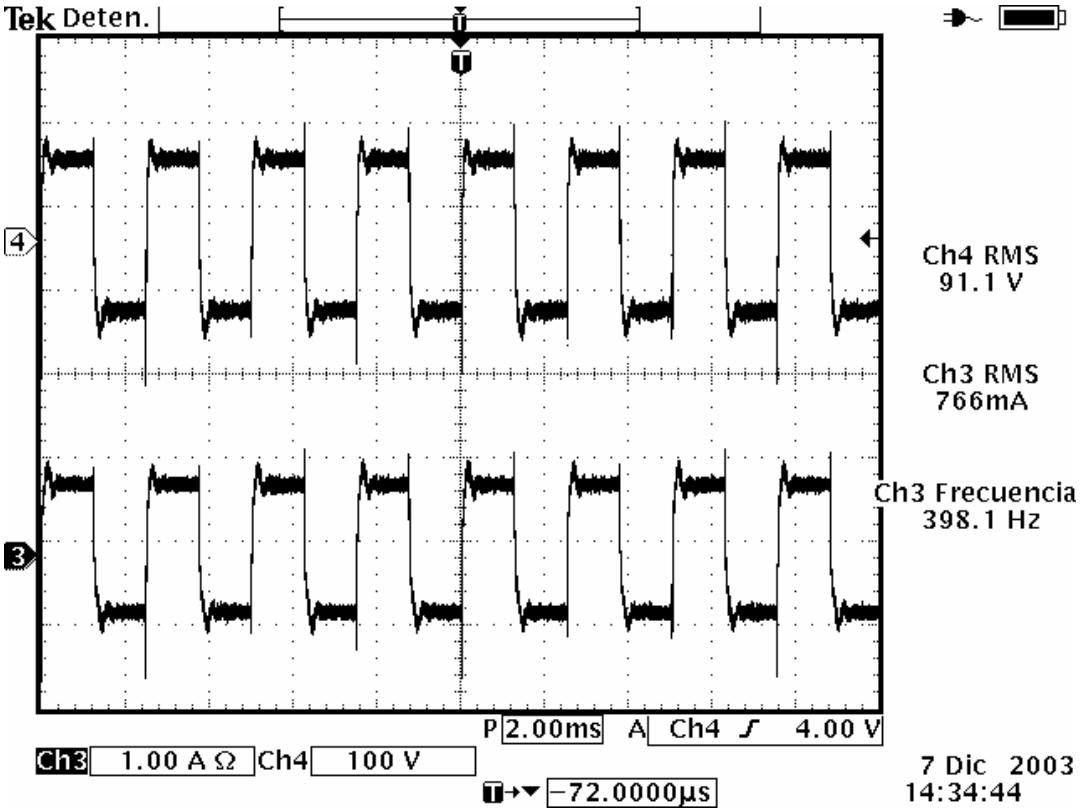

Figure 5.7 Experimental Results, Top to Bottom: Lamp Current and Lamp Voltage

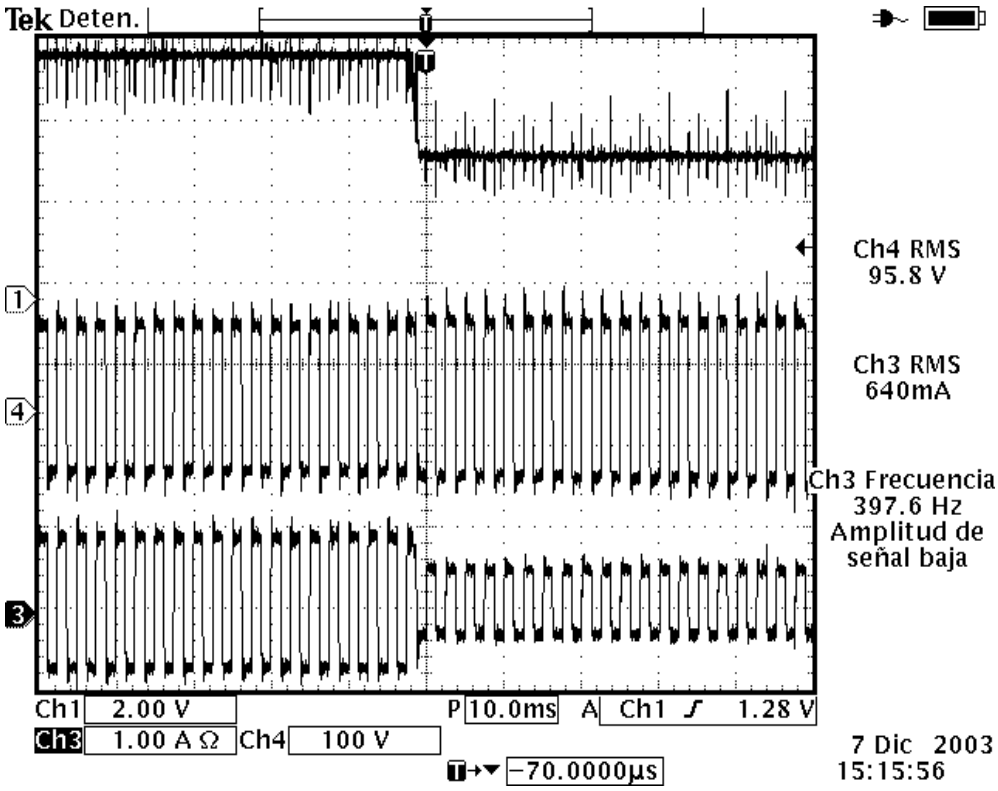

Figure 5.8 Experimental Results, Dimming Test (from 100% to 50%), Top to Bottom: Lamp Current and Lamp Voltage

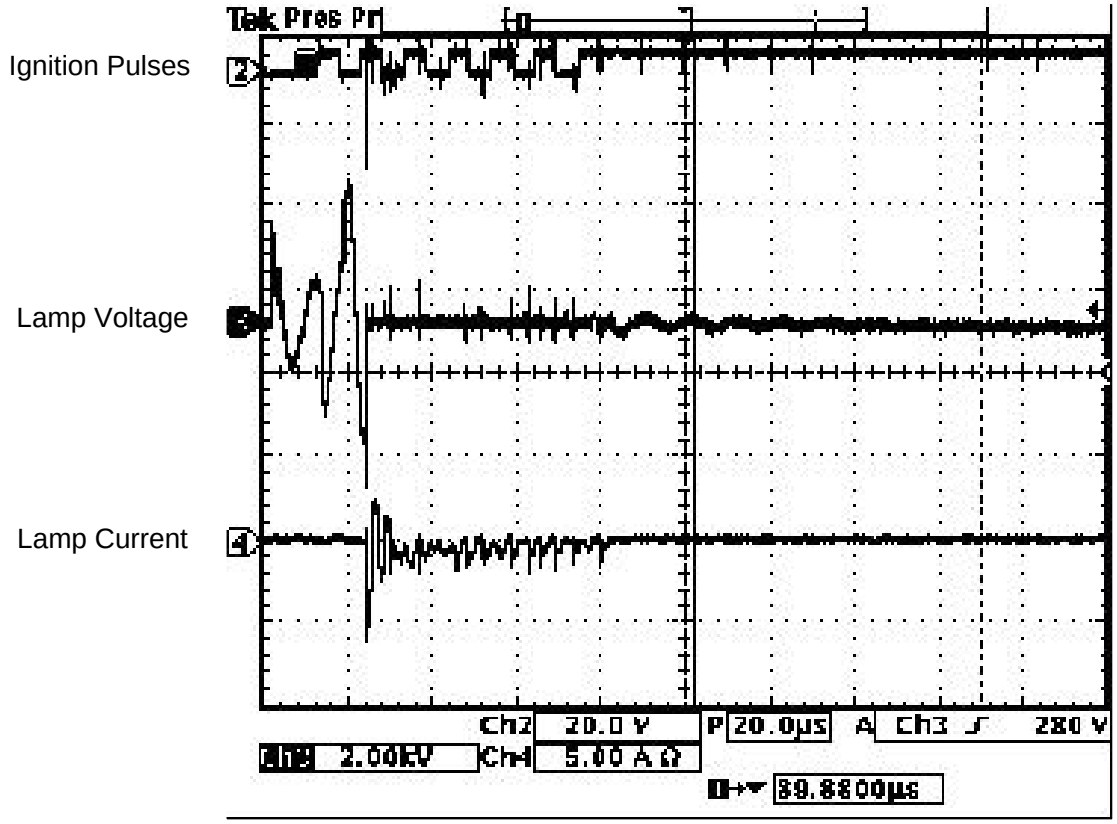

Figure 5.9 Experimental Results of the Igniter and Lamp: Igniter Pulses (Top), Lamp Voltage (Middle) and Lamp Current (Bottom)

The experimental results of the Igniter and Lamp are shown in Figure 5.9. The lamp ignites with two or five pulses due the high ignition capacity. The period covered by these pulses represent the transient state of the lamp. The settling time is approximately equal to 80.0 μs and after this started the steady state.

5.3. Dimming Control Using Adaptive Fuzzy Sliding Surface for Square-Waveform Ballast

The acoustic resonance phenomenon in Hight Intensity Discharge (HID) lamps is a consequence of pressure waves of the filled gas. This phenomenon is caused for the lamp power modulation. The arc discharge is deformed for these pressure waves. Heating fits are generated when the glass bladder was reached for the arc, and generally these fits are broken (Groot and Van Vliet, 1986).

One of the most reliable solutions for the elimination of the acoustic resonance phenomenon in HID lamps consists on feeding the lamp with square wave forms, since the lamp power is constant. Most of the electronic ballast that feed the lamps with square wave forms requires a closed loop control system to stabilize the lamp current (Deng, 1995; Deng and Cuk, 1997).

Generally, the discharge arc in HID lamps is extinguished if the power inferior limit is reached (approximately 50% of the nominal power) (Correa, et. al., 2002). Therefore, to avoid the arc extinction, it is important that the dimming control of the electronic ballast has a good reference pursuit. Because of that, to avoid the lamp turn off, the power inferior limit should not be surpassed. Additionally, it is important to have a good dynamic response in illuminating systems where existing main voltage variations or the load change.

A sliding mode control allows that the feedback system presents the following characteristics: robustness, good dynamic response and stability in load and main voltage variations and among others (Utkin, 1974; 1977). The HID lamp current is unstable when the lamp is feeding with a voltage source, an example is a dc-dc converter working in continuous conduction mode (CCM) with a variable structure. The system is stable using SMC although the system structures are unstable (if the system structures are unstable then the SMC can apply for stabilize the system). The output signal of the controller will be changing in order to drive the system to a balance point.

The lamp parameters have variations during its useful life period. This problem mainly affects the lamp impedance. It commonly decreases 20-30% of initial value of the lamp impedance (Groot and Van Vliet, 1986). This lamp characteristic affects the control system dynamic behaviour. Hence, an adaptive control is useful to reduce the lamp parameters variations.

An igniter is needed when the HID lamps are feeding with square waves. A proposed igniter is based on resonant network; this network works only 40μs-60μs. The resonant network works in high resonant frequency, the semiconductor losses and the size of the passive elements are then reduced.

Electronic ballast presented in (Ponce, et. al., 2001) feeds the HID lamp with high frequency cuasi-square waves. The feedback control law was designed with classic control strategy. However, a control analysis is valid for region near to operate point. Also, a dimming test was not included. Also, the wave shapes are deformed due to the high commutation frequency.

Electronic ballast developed by Ribas and partners (2003) fed the HID lamp with low frequency square waves. Also, the feedback control was designed with classic control strategy. Again, a control analysis was valid for region near to the operating point. Therefore, it does not ensure a good behavior during unitary impulse test of the lamp power. The arch discharge was stabilized with Buck-Boost dc-dc converter operating in discontinuous conduction mode (DCM). Therefore, semiconductor losses were high. Also, an extra circuit was needed to avoid the continuous conduction mode (CCM) converter operation.

Compact electronic ballast designed in (Shen, et. al., 2002a; 2002b; 2003) fed the HID lamp with low frequency square waves. This topology integrates a dc-dc converter and the full bridge inverter. Also, the current feedback control was designed using classic control strategy with the above mentioned drawbacks.

An analysis of the control system behaviour designed with a Sliding Mode (nonlinear) Control was presented in (Osorio, et. al., 2004a). To reduce the acoustic resonance the power stage feeds the HID lamp with low frequency square waves. A good dynamic response in dimming test was obtained because the control strategy was efficient. However, this control strategy did not integrate an adaptive process in the control law, and then it does not assure a good behaviour during the useful life period of the lamp. In this example, a control stage analysis was presented using sliding-mode-control (SMC) strategy with adaptive-fuzzy-sliding surface for electronic ballast that feed HID lamp with low-frequency-square waveforms was introduced. After that, the lamp current stabilized with a good dynamic response under the lamp parameters variation with this adaptive intelligent nonlinear control. Therefore, a satisfactory unitary impulse test of power lamp was obtained, avoiding the lamp turn off.

The simulations of electronic ballast were carried-out using Matlab (Simulink: SimPowerSystems) package. The selected lamp model was presented in (Osorio, et. al., 2004b). This mathematical model for HID lamps was based on electrical and thermal physical principles. This model could be used mainly in the design of nonlinear controllers. This model appropriately emulates the behaviour of negative resistance (it is deduced from an electric analysis of the HID lamps) and the dynamic response of the HID lamp (it was obtained from the thermal circuit of the lamp). The proposed model combines the advantages of simplicity and functionality. The parameters of the model could be adjusted precisely by means of electrical measurements of voltage and current in the lamp.

The electronic ballast can be implemented in two ways: The first (typical version) consist in three main components: a lamp current stabilizer based on Buck converter operating in CCM, an inverter and an igniter. The second (compact version) has two main elements: A buck converter integrated with full bridge inverter and an igniter (Shen, et. al., 2002a; 2002b; 2003). The CCM operation of Buck converter reduces the semiconductor losses more than the DCM operation. Also, this converter adjusts de CD bus to a required value. The example was structured as follow: An analysis of power stage of selected ballasts, an analysis of control stage and the introduction of the selected lamp model. Finally, the simulation results were presented with discussions and conclusions.

5.3.1. Power Stage

The block diagram of the selected ballast is shown in Figure 5.10. A buck converter is shown in Figure 5.10(a), which is operating in CCM. This converter stabilized the arc discharge and feed the inverter. A CD bus can be given by CD-CD converter that integrates a power factor correction.

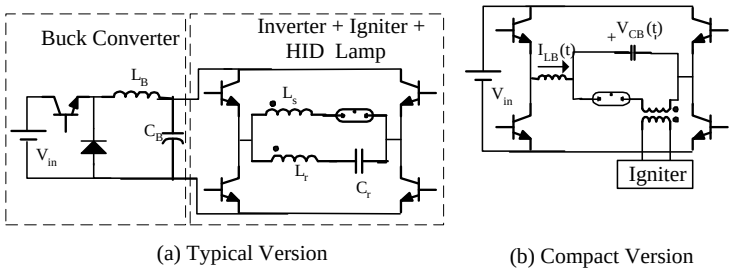

(a) Typical Version (b) Compact Version

Figure 5.10 Block Diagram of Selected Topologies.

To avoid the acoustic resonance, the inverter feeds the HID lamp (70W metal Halide) with low frequency square waveforms (400Hz, avoiding the effects of parasitic elements).

The igniter was conformed for resonant network (L_rC_r) in a series configuration. L_r is coupled to L_s (autotransformer configuration). High voltages (4.5kV peak) could be reached with this configuration assuring the lamp ignition. The ignition sequence took 60μs (6 pulses of 100 kHz). The operating frequency of 400Hz (in the inverter changes) was reached when there is a lamp ignition.

Therefore, at this frequency, inductor impedance was very low (short circuit) and the impedance capacitor was very high (open circuit) and both impedances could be ignored. A compact version of electronic ballast (Ponce, et. al., 2001) was shown in Figure 5.10(b). A Buck converter (operating in CCM) integrated with a full bridged inverter conform this ballast. A CD bus was needed in the input of the ballast.

5.3.2. Control Stage

Many papers have presented several steps for the sliding mode control design (Utkin, 1974; 1977; Decarlo, et. al., 1988; Hung, et. al., 1993; Matavelli, et. al., 1993; Vázquez, et. al., 1993; Hernández, et. al., 2001), these steps could be summarized as follows: to propose the sliding surface, to verify the existence of a sliding mode, and to analyze the stability of the sliding surface.

Typically, the sliding surface proposed is a linear combination of the state variables (Vázquez, et. al., 1993; Hernández, et. al., 2001). Because of that, the implementation

and theoretical analysis are very easy. The sliding mode controller (SMC) forces the system to be under this surface and the system is driven to the equilibrium point which must be included in the sliding surface. However, due to the lamp parameter variations and the system uncertainties an adaptive-fuzzy-sliding surface was used (Pinto, 2001).

5.3.3. System Modeling

Figure 5.11 can be described as follow: (a) Complete Power Stage, (b) Without Igniter, (c) Without Inverter, (d) Using Ideal Switch and Considering the Lamp as a Resistance. Compact Version: (e) Complete Power Stage, (f) Without Igniter, (g) Equivalent Circuit During Negative Wave Part, (h) Equivalent Circuit During Positive Wave Part, (i) Using Ideal Switch and Considering the Lamp as a Resistance. In other words, the typical version of power stage (Figure 5.11(a)) could be simplified as follows: The influence of the igniter on the ballast in stable state was diminished, (Figure 5.11(b)). The inverter current demanded to Buck converter is constant and it could be eliminated (Figure 5.11(c)). Finally, the semiconductors could be substituted for ideal switches and the lamp was considered in steady state as constant resistance only for controller parameters calculations (Figure 5.11(d)). In the simulations of the lamp model proposed in (Correa, et. al., 2002), it was considered with some modifications. A similar analysis can be applied to a compact version of the selected power stage (Figure 5.11(e)): The influence of the igniter on the ballast in stable state was diminished (Figure 5.11(f)). The inverter changes the polarity source (Figures 5.11(g) y (h)), this effect could be emulate with a bipolar source, $\left(\mathbf{V_{in} = V_{dc}\ sgn(sin\ 2\pi fl)}\right)$, Figure 5.11(i).

Finally, the semiconductors can be substituted for ideal switches and the lamp was considered in steady state as constant resistance only for controller parameters calculations (Figure 11(j)). Moreover, in the simulations of the lamp model proposed in (Correa, et. al., 2002) some modifications were considered.

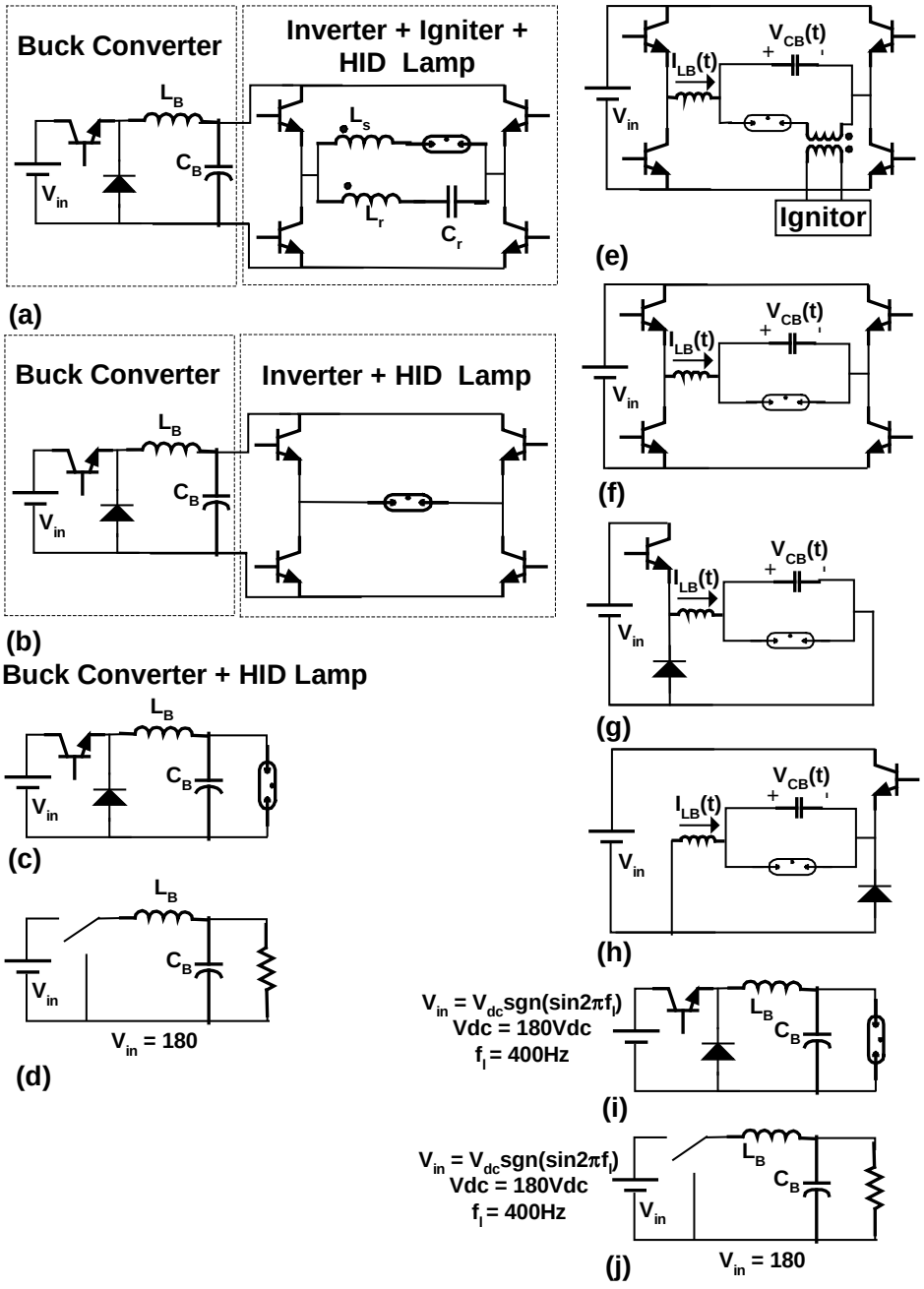

Figure 5.11 Ballast Simplification, Typical Version

The resultant system in state-matrix representation form considering the position of the switch u_1 (1 and -1) is as follows:

$$\begin{pmatrix} \dot{x}_1 \\ \dot{x}_2 \end{pmatrix} = \begin{pmatrix} 0 & -w_0 \\ w_0 & -w_1 \end{pmatrix} \begin{pmatrix} x_1 \\ x_2 \end{pmatrix} + \begin{pmatrix} b/2 \\ 0 \end{pmatrix} u \tag{5.19}$$

where:

$$w_0 = \frac{1}{\sqrt{L_B C_B}}, w_1 = \frac{1}{R\, C_B}, b = \frac{V_{in}}{\sqrt{L_B}} \quad (5.20)$$

$$x_1 = \sqrt{L} i_{LB} \quad (5.21)$$

$$x_2 = \sqrt{C}\, V_{CB} \quad (5.22)$$

or

$$\dot{X} = A\, X + BU + B \quad (5.23)$$

where:

R: the impedance of the lamp reduced to dynamic-nonlinear resistance.

L_B: inductance of the Buck inductor.

I_{LB}: current flow of the inductor L_B.

C_B: capacitance of the Buck capacitor.

V_{CB}: voltage across of the capacitor C_B.

x_1 and x_2 are the normalized state variables.

5.3.4. Architecture of the Adaptive Fuzzy Sliding Mode Controller

The current states of the controlled plant were used for adjusting the output scaling factors (gains of the controller). The Adaptive Fuzzy Sliding Mode Control law was divided into three blocks: the PI fuzzy, the Adaptive Fuzzy Mechanism and the block to compute the Adaptive Sliding Surface (see the Figure 5.12). The data for the design

and the tuning of the Adaptive PI Fuzzy Controller were shown in (Pinto, 2001). The tuning process starts with the tuning of the PI Fuzzy Controller setting the adaptive mechanism to 1 $(\alpha = 1)$. In other words, it is necessary to eliminate the effect of the adaptive mechanism by set α to 1. The scaling factor G_e has to be selected in order to cover the operating range belonging to the interval $[-1, 1]$. When the system has an slow response it is necessary to increment the value of G_e and G_u. The manipulation of the scaling factor G_u has to be done carefully because it affects the Proportional and Integral gains at the same time. If the system has a big overdamping then it is necessary increment the value of $G_{\Delta e}$. The selection of the input scaling factors $(G_e \text{ and } G_{\Delta e})$ and the output scaling factor (G_u) has to be done making the transient response of the target system acceptable.

5.3.4.1. Signals, Functions and Scaling Factors of the Adaptive PI Fuzzy Controller

So that to guarantee a convenient design of fuzzy logic controllers is crucial to make a good selection of the input and output scaling factors, in accordance with the fuzzy rules obtained from the expert and the definition of the fuzzy sets.

There exist many parameters possible to tune in the fuzzy controllers but the most important they are the scaling factors.

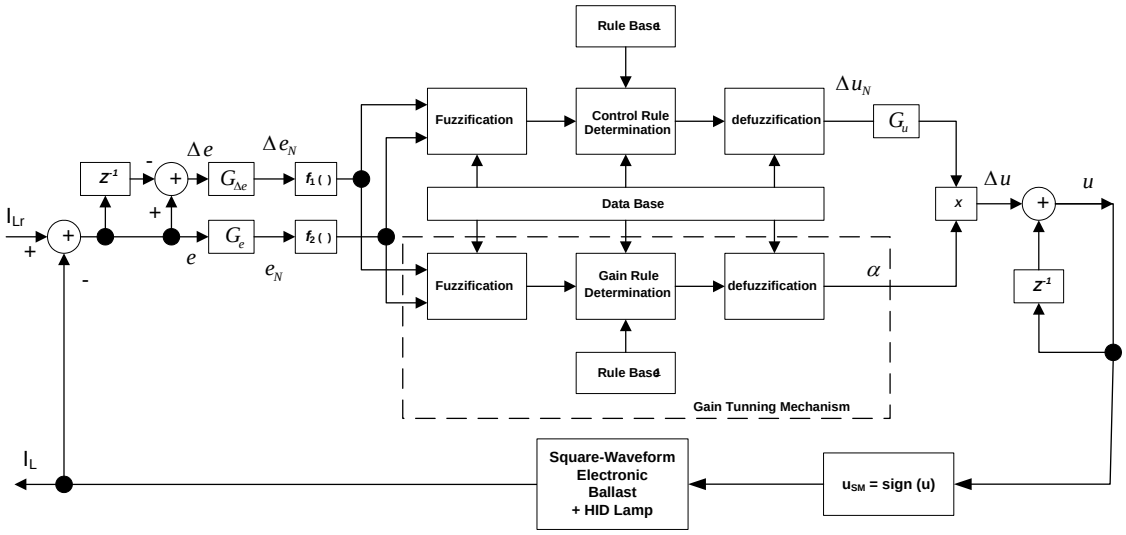

Figure 5.12 Block Diagram of Electronic Ballast with Sliding-Mode Control with Adaptive-Fuzzy-Sliding Surface.

The current error signal $\mathbf{e(k)}$ is expressed as follows:

$$\mathbf{e(k) = r(k) - y(k)} \tag{5.24}$$

where $\mathbf{r(k)}$ and $\mathbf{y(k)}$ are the current reference and plant output.

The current increment of the error signal $\mathbf{\Delta e(k)}$ is described by the following equation:

$$\mathbf{\Delta e(k) = e(k) - e(k-1)} \tag{5.25}$$

The normalized amounts for the current error $\mathbf{e_N(k)}$ and increment of the error $\mathbf{\Delta e_N(k)}$ are defined by:

$$\mathbf{e_N(k) = e(k) \cdot G_e} \tag{5.26}$$

$$\mathbf{\Delta e_N(k) = \Delta e(k) \cdot G_{\Delta e}} \tag{5.27}$$

where $\mathbf{G_e}$ and $\mathbf{G_{\Delta e}}$ are the input scaling factors of the error and increment of the error.

The Adaptive Proportional Integral (PI) Fuzzy Controller used here (Pinto, 2001) has different structure of the original control algorithm developed by Mudi and Pal (1999) (the proposed control law includes constraints over the inputs $\mathbf{e_N(k)}$ and $\mathbf{\Delta e_N(k)}$). These constraints were introduced in order to set up a limit in the inputs and guarantee faster convergence to the universe of discourse, which is defined by the interval $[\mathbf{-1, 1}]$.

The constrained values for the current error $\mathbf{e_c(k)}$ and increment of the error $\mathbf{\Delta e_c(k)}$ are defined as follows:

$$\mathbf{e_c(k) = f_1\left(e_N(k)\right)} \tag{5.28}$$

$$\mathbf{\Delta e_c(k) = f_2\left(\Delta e_N(k)\right)} \tag{5.29}$$

with

$$\mathbf{f_1\left(e_N(k)\right)} = \begin{cases} \mathbf{-1}, & \mathbf{\text{if } e_N(k) < -1} \\ \mathbf{e_N(k)}, & \mathbf{\text{if } -1 \leq e_N(k) \leq 1} \\ \mathbf{1}, & \mathbf{\text{if } e_N(k) > 1} \end{cases} \tag{5.30}$$

$$\mathbf{f_2\left(\Delta e_N(k)\right)} = \begin{cases} \mathbf{-1}, & \mathbf{\text{if } \Delta e_N(k) < -1} \\ \mathbf{\Delta e_N(k)}, & \mathbf{\text{if } -1 \leq \Delta e_N(k) \leq 1} \\ \mathbf{1}, & \mathbf{\text{if } \Delta e_N(k) > 1} \end{cases} \tag{5.31}$$

where $\mathbf{f_1(\cdot)}$ and $\mathbf{f_2(\cdot)}$ are the constrained (nonlinear) functions.

The output of the PI Fuzzy Controller $\Delta\mathbf{u_N}(\mathbf{k})$ and the output of the Adaptive Fuzzy Mechanism $\boldsymbol{\alpha}(\mathbf{k})$ which are defined by the following equations:

$$\Delta\mathbf{u_N}(\mathbf{k}) = \mathbf{f}\big(\mathbf{e_c}(\mathbf{k}), \Delta\mathbf{e_c}(\mathbf{k})\big) \tag{5.32}$$

$$\boldsymbol{\alpha}(\mathbf{k}) = \mathbf{g}\big(\mathbf{e_c}(\mathbf{k}), \Delta\mathbf{e_c}(\mathbf{k})\big) \tag{5.33}$$

where $\mathbf{f}(\cdot)$ and $\mathbf{g}(\cdot)$ are nonlinear fuzzy functions belonging to the fuzzy rules (5.37) and (5.39), respectively.

Moreover, the increment of the output signal is expressed by the following equation:

$$\Delta\mathbf{u}(\mathbf{k}) = \Delta\mathbf{u_N}(\mathbf{k}) \cdot \mathbf{G_u} \cdot \boldsymbol{\alpha}(\mathbf{k}) \tag{5.34}$$

where $\mathbf{G_u}$ is the output scaling factor.

The current value of the control output $\mathbf{u}(\mathbf{k})$ for the Adaptive PI Fuzzy Controller is equal to the addition between the delayed control output $\mathbf{u}(\mathbf{k}-\mathbf{1})$ and the current increment of the control signal $\boldsymbol{\Delta}\mathbf{u}(\mathbf{k})$. The control law is expressed by:

$$\mathbf{u}(\mathbf{k}) = \mathbf{u}(\mathbf{k}-\mathbf{1}) + \boldsymbol{\Delta}\mathbf{u}(\mathbf{k}) \tag{5.35}$$

where $\mathbf{k}$ is the sampling time for the integration of the output signal.

Nevertheless, after substituting the expressions for $\Delta\mathbf{u_N(k)}$ and $\boldsymbol{\alpha}\mathbf{(k)}$, the final expression for the control law (adaptive fuzzy sliding surface) will be defined as follows:

$$\mathbf{u(k)} = [\Delta\mathbf{u_N(k)} \cdot \mathbf{G_u} \cdot \boldsymbol{\alpha}\mathbf{(k)}]/[\mathbf{1} - \mathbf{z^{-1}}] \quad (5.36a)$$

or

$$\mathbf{u(k)} = \left[\mathbf{f}\left(\mathbf{e_c(k)}, \Delta\mathbf{e_c(k)}\right) \cdot \mathbf{G_u} \cdot \mathbf{g}\left(\mathbf{e_c(k)}, \Delta\mathbf{e_c(k)}\right)\right]/[\mathbf{1} - \mathbf{z^{-1}}] \quad (5.36b)$$

5.3.4.2. Proportional-Integral Fuzzy Controller

The Adaptive Proportional-Integral (PI) Fuzzy Controller may be classified as a Mamdani's Fuzzy Models (with max-min composition) and it was based on the original Control algorithm developed by Mudi-Rajani and Pal-Nikhil (1999).

The most important design data of the control law are the: membership functions, the rule base (i.e. fuzzy rules, shape of membership functions for the inputs and output) and the scaling factors for the inputs and output. The fuzzy rule base was developed using the phase plane.

The membership functions used were triangles and trapezoids. Also, a more efficient and simple methodologies for computing the degree of membership (fuzzification) and the centroid (defuzzification) were applied based on the rate and proportions of rectangular triangles, which is a geometric property of these (Pinto, 2001). The triangles and trapezoids are described by four points. The rate and proportions are obtained computing the distance between the specific input "x" and the four points for

each fuzzy set to compute the degree of membership (fuzzification). The procedure is developed taking advance of the triangle and trapezoid shapes. For the defuzzification the rate and proportion are computed using the degree of membership obtained (fuzzification) and the four points used in the description of the triangles and trapezoids. The fuzzification and defuzzification processes are developed more easily, faster and efficiently with this algorithm.

5.3.4.2.1. Membership Functions

The closed interval $[-\mathbf{1}, \mathbf{1}]$ represents the Universe of Discourse of the constrained inputs $\boldsymbol{e_c(k)}$ and $\Delta \boldsymbol{e_c(k)}$ and the output $\Delta \boldsymbol{u_N(k)}$ of the PI fuzzy control law. Figure 5.13 shows the membership functions used.

Triangles and trapezoids were the membership functions used having a symmetry between the triangles and having the set of supports of the membership functions with the same size (including the trapezoids in the extremes).

5.3.4.2.2. Fuzzy Rules Base

The fuzzy rules base are for the increment normalized output signal $\Delta \boldsymbol{u_N(k)}$ but the PI fuzzy controller produces the current output signal $\boldsymbol{u(k)}$, by means of the integrator included in the output of the fuzzy controller.

The type of fuzzy rules (Mamdani's Model) used in the PI Fuzzy controller are of the following form:

$$\mathbf{R_{PI}^{i}}\textbf{: IF } \mathbf{e_c(k)} \textbf{ is } \mathbf{E_i} \textbf{ AND } \mathbf{\Delta e_c(k)} \textbf{ is } \mathbf{\Delta E_i} \textbf{ THEN } \mathbf{\Delta u_N(k)} \textbf{ is } \mathbf{\Delta U_i} \textbf{ ;} \mathbf{i = 1, 2, \cdots, m} \quad (5.37)$$

where $\mathbf{R_{PI}^{i}}$ is the i[th] fuzzy rule for the PI fuzzy controller. $\mathbf{E_i}$ and $\mathbf{\Delta E_i}$ are the i[th] membership functions of the constrained error and increment of the error signals. $\mathbf{\Delta U_i}$ is the i-th membership function of the incremented output signal normalized $\mathbf{\Delta u_N(k)}$. $\mathbf{m}$ is the number of fuzzy rules. The fuzzy rules are shown in Table 5.1.

The fuzzy rules do not depend of the current increment of the control signal $\boldsymbol{\Delta u(k)}$ because this operation is carried out outside the fuzzy controller which has a Mamdani type Fuzzy structure.

$\mu(e_c(k))$, $\mu(\Delta e_c(k))$ and $\mu(\Delta u_N(k))$

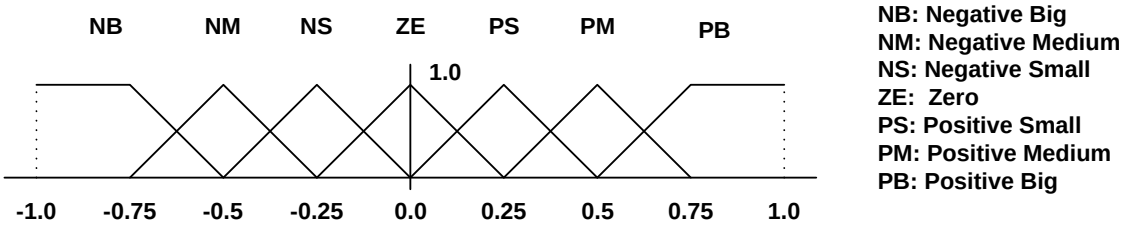

$e_c(k)$, $\Delta e_c(k)$

Figure 5.13 Membership functions $\mu(e_c(k))$, $\mu(\Delta e_c(k))$ and $\mu(\Delta u_N(k))$

5.3.4.3. Adaptive Fuzzy Mechanism

The Adaptive Fuzzy Mechanism (AFM) is a nonlinear model and a function of the states $e_c(k)$ and $\Delta e_c(k)$. Also, the AFM does not depend on the process to be controlled (Mudi and Pal, 1999; Pinto, 2001). The output signal of the AFM is called gain updating factor $\alpha(k)$.

The effective gain of the Adaptive PI fuzzy Controller is defined as follows:

$$\boldsymbol{\alpha(k)} \cdot \boldsymbol{G_u} \tag{5.38}$$

When the Adaptive PI Fuzzy Controller is working, the gain updating factor $\boldsymbol{\alpha(k)}$ does not keep constant because it varies in accordance with the tendency of the process output.

The design data of the Adaptive Fuzzy Mechanism are: the membership functions, and the fuzzy rules base.

Table 5.1 Fuzzy Rules Base used in the PI Fuzzy Controllers

$\Delta e_c / e_c$	NB	NM	NS	ZE	PS	PM	PB
NB	NB	NB	NB	NM	NS	NS	ZE
NM	NB	NM	NM	NM	NS	ZE	PS
NS	NB	NM	NS	NS	ZE	PS	PM
ZE	NB	NM	NS	ZE	PS	PM	PB
PS	NM	NS	ZE	PS	PS	PM	PB
PM	NS	ZE	PS	PM	PM	PM	PB
PB	ZE	PS	PS	PM	PB	PB	PB

5.3.4.3.1. Membership Functions

The gain updating factor $\boldsymbol{\alpha(k)}$ is a nonlinear (fuzzy) function depending on the constrained inputs $\mathbf{e_c(k)}$ and $\Delta\mathbf{e_c(k)}$ which are defined over the closed interval $[-\mathbf{1}, \mathbf{1}]$. The membership functions used were triangles and trapezoids and they are shown in Figure 5.14.

5.3.4.3.2. Fuzzy Rules Base

The fuzzy rules base applied for the gain updating factor are defined as a Mamdani type model and is expressed as follows:

$$\boldsymbol{R_{\alpha}^{j}}: \boldsymbol{IF}\ \boldsymbol{e_c(k)}\ \boldsymbol{is}\ \boldsymbol{E_i}\ \boldsymbol{AND}\ \Delta\boldsymbol{e_c(k)}\ \boldsymbol{is}\ \Delta\boldsymbol{E_i}\ \ \boldsymbol{THEN}\ \boldsymbol{\alpha(k)}\ \boldsymbol{is}\ \mathbf{A_i};\ \ \boldsymbol{j = 1, 2, \cdots, n} \qquad (5.39)$$

where $\boldsymbol{R_{\alpha}^{j}}$ is the i[th] fuzzy rule for Adaptive Fuzzy Mechanism. $\boldsymbol{E_i}$ and $\Delta\boldsymbol{E_i}$ are the i[th] membership functions of the constrained error and increment of the error signals. $\mathbf{A_i}$ is the i[th] membership function of the gain updating factor $\boldsymbol{\alpha(k)}$. The number of fuzzy rules is defined by $\boldsymbol{n}$.

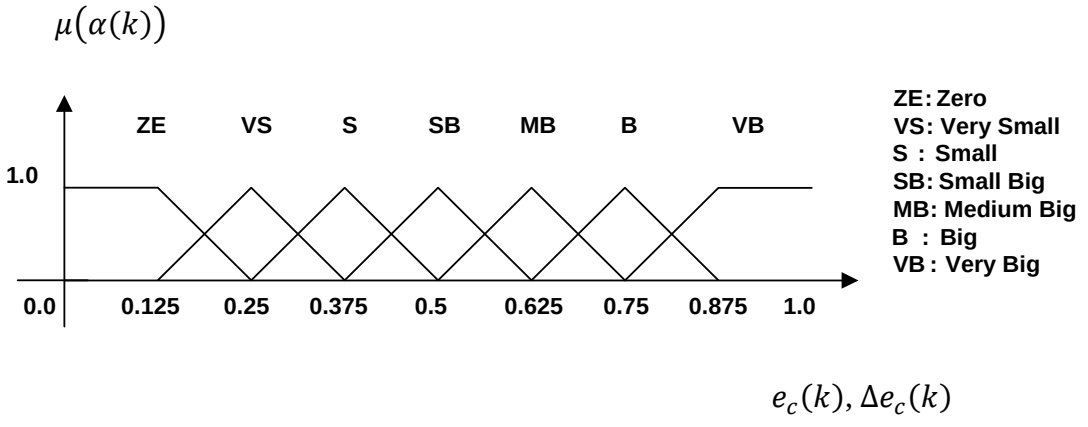

Figure 5.14 Membership function $\mu(\alpha(k))$

The fuzzy rules were obtained depending of the output signal of the target plant to be controlled. The fuzzy rules could be different which were developed in accordance with the fuzzy rules for the PI fuzzy controller. Table 5.2 shows the base of fuzzy rules.

5.3.4.4. Tuning the PI Fuzzy Controller

The adequate selection of the input and output scaling factors $\mathbf{G_e}, \mathbf{G_{\Delta e}}, \mathbf{and}\ \mathbf{G_u}$ is done taking into account the experience and expert knowledge about the dynamic behavior of the nonlinear process. This means that the scaling factors were chosen via trial and error based on the procedure described in the following paragraphs.

Table 5.2 Fuzzy Rules Base used in the Adaptive Fuzzy Mechanism

$\Delta e_c / e_c$	NB	NM	NS	ZE	PS	PM	PB
NB	VB	VB	VB	B	SB	S	ZE
NM	VB	VB	B	B	MB	S	VS
NS	VB	MB	B	VB	VS	S	VS
ZE	S	SB	MB	ZE	MB	SB	S
PS	VS	S	VS	VB	B	MB	VB
PM	VS	S	MB	B	B	VB	VB
PB	ZE	S	MB	B	VB	VB	VB

In order to tune the PI fuzzy controller basic it is necessary to eliminate the adaptive mechanism by setting the gain updating factor equal to 1 ($\boldsymbol{\alpha = 1}$).

It is convenient that the scaling factor $\boldsymbol{G_e}$ will be selected such as the error signal will cover all the Universe of Discourse $[\boldsymbol{-1, 1}]$.

When the system has a slow response it is necessary to increment the value of the $\boldsymbol{G_e}$ and $\boldsymbol{G_u}$ (Driankov, et. al., 1996; Reznik, 1997). The manipulation of the scaling factor $\boldsymbol{G_u}$ is very crucial in the tuning process because it has an effect over the proportional and integral gains of the PI Fuzzy control law in a similar manner as it occurs in a conventional interacting PI control algorithm (Pinto, 2001). If the system has a bigger overshoot then it is necessary to increment the amount of $\boldsymbol{G_{\Delta e}}$.

5.3.4.5. The Sliding Surface

The Sliding Surface (σ) belongs to the output signal of the Adaptive PI Fuzzy controller, it is also defined as an Adaptive Fuzzy Sliding Surface based on the idea of Pinto (2001) (refer to Figure 5.12). Recalling equation (5.36a) and equaling to the Sliding Surface as follow:

$$\boldsymbol{\sigma = u(k) = [\Delta u_N(k) \cdot G_u \cdot \alpha(k)]/[1 - z^{-1}]} \qquad (5.40)$$

where:

$u(k)$: Output signal of the Adaptive PI Fuzzy Controller.

$\Delta u_N(k)$: the increment of the normalized deffuzified output signal of the PI Fuzzy Controller.

G_u: the Output Scaling Factor of the PI Fuzzy Controller.

$\alpha(k)$: the normalized Gain Updating Factor.

Finally, the Adaptive Fuzzy Sliding Mode Control (AFSMC) law u_{SM} is defined as follows:

$$\boldsymbol{u_{SM} = sign(\sigma)} \tag{5.41}$$

The AFSMC bases its dynamical behavior on the nonlinear dynamics of the Adaptive PI Fuzzy controller.

5.3.4.6. Existence and stability of the sliding mode

The membership functions (Figures 5.13 and 5.14) plus the fuzzy-rule set (Tables 5.1 and 5.2) guarantee the existence and stability of the sliding mode under the universe of discourse (Miers and Sherif, 1985; Tanaka and Wang, 2001;Pinto, 2001; Ponce, et. al., 2001).

5.3.5. Lamp Modeling

A lamp model for dimming Pspice/Matlab/Simnon simulations was proposed in (Osorio, et. al., 2004b), see Figure 5.15. This model emulates two essential HID lamp characteristics for control design: (a) a lamp negative resistance and (b) its dynamic response using the thermal circuit of the HID lamps.

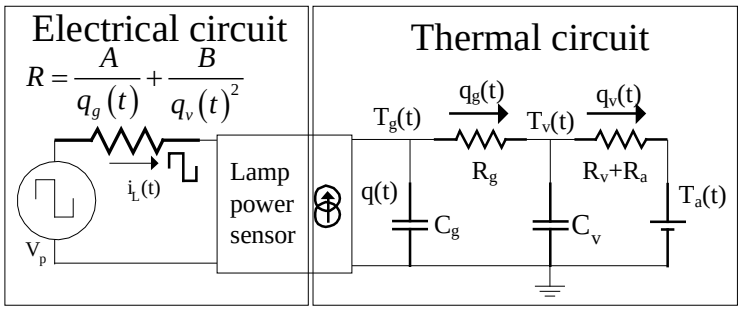

Figure 5.15 HID Lamp Model Reported

5.3.6. Simulation Results

The electronic ballast was designed with the following parameters: P_o = 70W, $V_{in} = 180Vdc$, V_C = 90Vdc, I_L = 0.777A, L = 5mH, C = 1μF, Lamp Model: CDM70W830PH. The C and L values were designed according to current and voltage ripples.

Several simulation results of the electronic ballast are shown in Figures 5.16 and 5.17. The current reference, lamp current and the lamp voltage when the lamp-resistance is R_L are shown in Figure 5.16. Figure 5.17 shows the same electrical variables when the lamp-resistance value is 130%R_L. In these figures the effect of death times is shown. A good dynamic response was obtained under lamp parameter variation ensuring that the lamp does not turn off. Figure 5.18 shows a voltage-variation test, as can be observed the lamp current and the lamp voltage are stable, and the proposed control is very efficient.

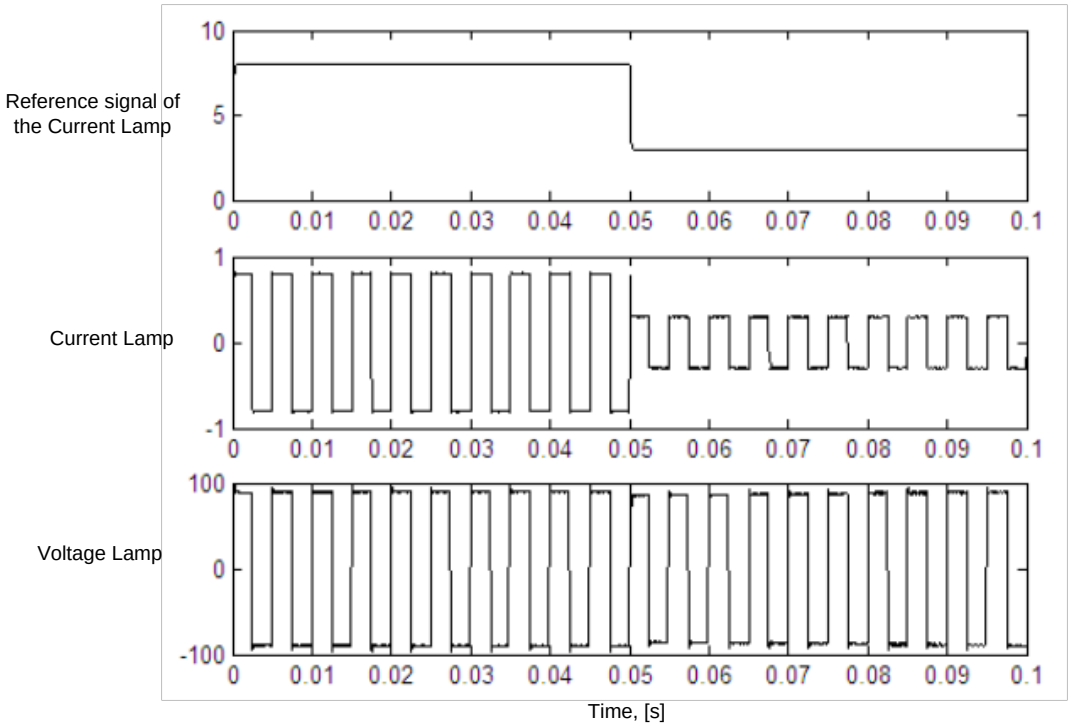

Figure 5.16 Dimming Test (100% through 60%), Lamp Resistance equal to R_L, Current Reference (Top), Lamp Current (Middle), Lamp Voltage (Down)

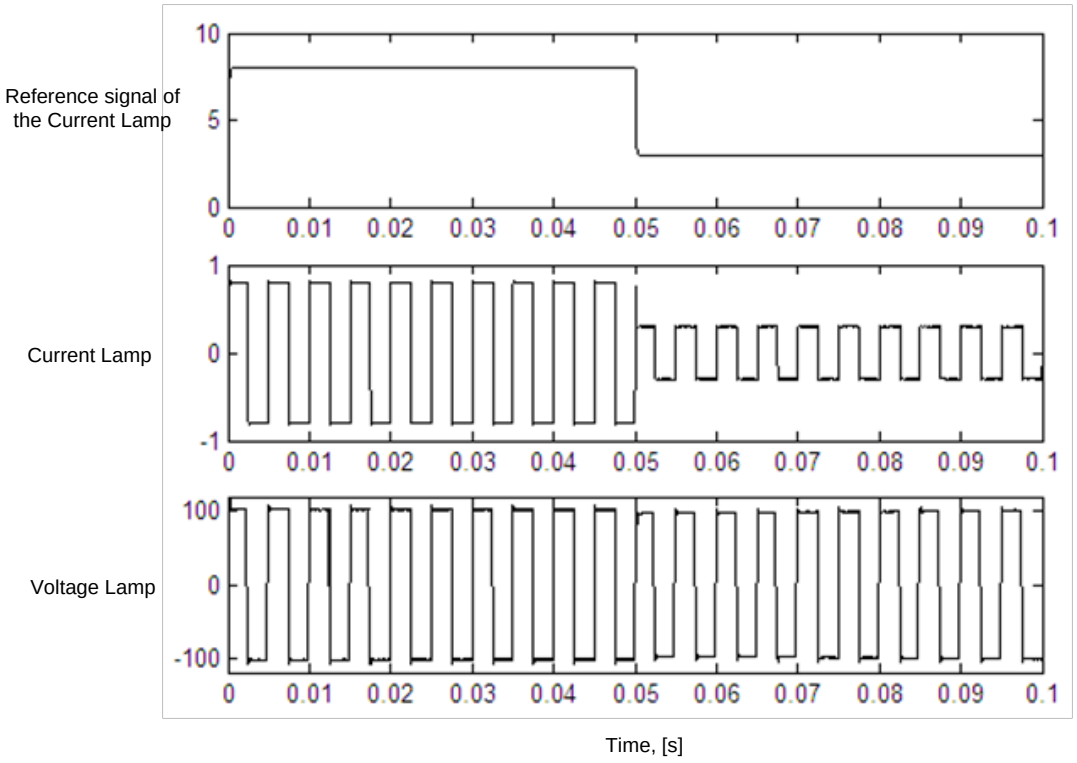

Figure 5.17 Dimming Test (100% through 50%), Lamp Resistance equal to 130%R_L, Current Reference (Top), Lamp Current (Middle), Lamp Voltage (Down)

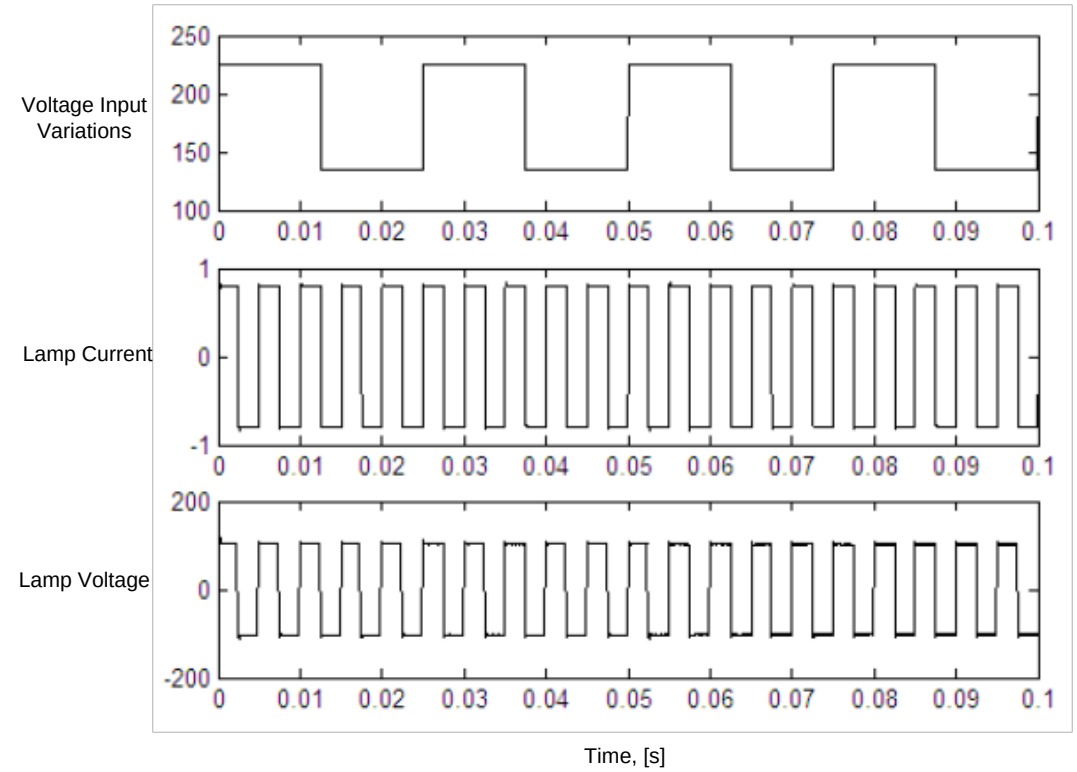

Figure 5.18 Voltage-Variation Test $\mathbf{V_{in} = 180 \pm 25\%}$[V], The Lamp Resistance = 130%R_L: $\mathbf{V_{in}}$ (Top), Lamp Current (Middle) and Lamp Voltage (Down)

5.4. Thermal Dynamic Model for HID Lamps with the Outer-Bulb Effects

There are several ways to stabilize the HID lamps, and one of them consists in the use of a close-loop controller which compares the lamp current with a reference (Deng, 1995; Deng and Cuk, 1997). This technique of stabilization was used mainly when the HID lamp is fed with square waveforms to reduce acoustic resonances in the lamp (Ponce, et. all, 2001; Ribas, et. al., 2003; Miaosen, et. al., 2003; Miaosen, et. al., 2002a; 2002b).

The acoustic resonance phenomenon in HID lamps is a consequence of pressure waves of the filling gas (see Figure 5.19). This phenomenon is caused by lamp power modulations. The arc discharge is deformed for these pressure waves and heating fits were generated when the glass bladder is reached for the arc (Groot and Van Vliet, 1986).

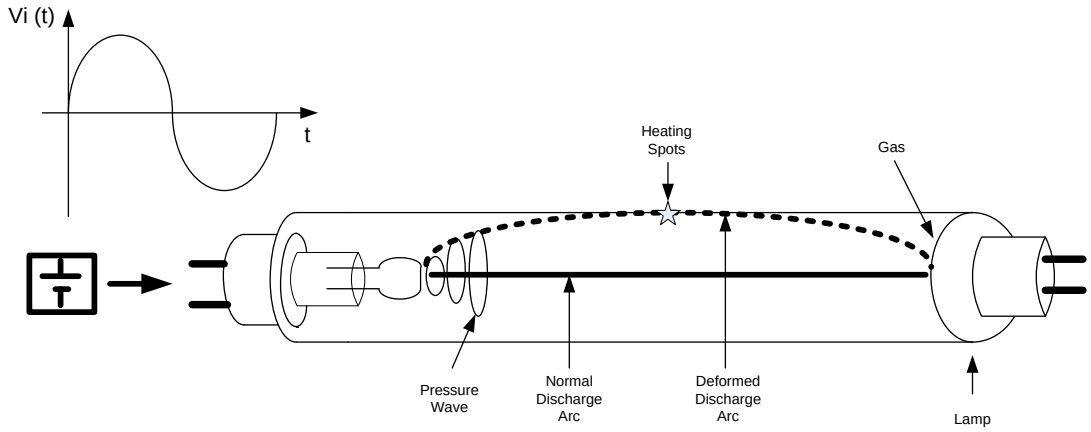

Figure 5.19 Heating Spots Produced by the Deformed Discharge Arc in a HID Lamp.

However, some specific applications require dimming (i.e. luminosity intensity control) for their operation and the ballast system is one of them. To dim and stabilize the lamp current simultaneously is necessary to use an efficient control strategy with good dynamic response and robustness. To obtain this efficiency with a control system it is necessary to use a nonlinear controller because the ballast and HID lamps have a nonlinear dynamic behavior. The sliding modes control strategy has been observed to be a very good solution for the ballast and HID lamps (Utkin, 1974; 1977; DeCarlo, et.

al., 1988; Hung, et. al., 1993; Mattavelli, et. al., 1993; Vázquez, et. al., 2000; Hernández, et. al., 2001).

To design a reliable control it was necessary to derive an accurate model of the target process (Skogestad and Postlethwaite, 1996). The main characteristics of the HID lamp models for good a design of nonlinear control system are: a) include the behaviour for the negative resistance of the lamp in the nonlinearities, b) modeling of the dynamic response. The behavior of the negative impedance determines the stability of the current flow in the lamp (Deng, 1995; Deng and Cuk, 1997) and with the dynamic response of the lamp was possible to infer the dynamic response of the control strategy. Furthermore, it is important that the dynamic response of the lamp was based on the physical parameters of the lamp.

Several models of HID lamps have been presented in the literature of power electronics for the analysis and design of electronic ballasts. The majority of the models were oriented towards the simulation analysis of electronic ballast operating at open loop, where the lamp current was stabilized with passive components. The speed of simulation for the dynamic behavior of a group ballast-lamp in close loop is slow.

The lamp models that have been presented in (Deng, 1995; Deng and Cuk, 1997) were linear models operating in closed loop and they were valid only in a small region near to the operation point (Skogestad and Postlethwaite, 1996). The simplified thermal-electric lamp model presented in (Osorio, et. al., 2004) emulates very well the lamp behaviour. However, the negative resistance was found by a polynomial approximation method, and it does not have any physical meaning. In (Shvartsas and Ben-Yaakov, 1999; Osorio, et. al., 2004; Yan, et. al., 2003) were presented physical models, but some values of variables were wrong like the power values (Yan, et. al., 2003), because the lamp parameter values were taken in an arbitrary way among a very wide value range. Also, this model only emulates the fast dynamic (transient) response, because the glass temperature was not taking into account.

In this example, a mathematical model for HID lamp based on electrical and thermal principles was introduced. This model can be used mainly in the design of nonlinear

control approaches. Also, it emulates with enough accuracy the behaviour of negative resistance with a physical function (Shvartsas and Ben-Yaakov, 1999; Osorio, et. al., 2004; Yan, et. al., 2003) and the dynamic response of the HID lamp obtained from the thermal circuit of the lamp (Osorio, et. al., 2004). The proposed model combines the advantages of good dynamic simulation of the lamp with simplified experimental method in order to find the lamp parameters. It can be used easily for design and simulation purposes of nonlinear controllers such as "Simnon" and "Matlab" and in software of electronic design such as "PSpice". The parameters of the model can be adjusted precisely by means of electrical measurements of voltage and current in the lamp. Experimental and simulation results of the proposed model are shown to verify the good performance of the proposed model.

5.4.1. New Proposed Model

5.4.1.1. Negative Resistance of the HID Lamps

The lamp dynamic resistance was expressed by a physical equation as follows (Shvartsas and Ben-Yaakov, 1999; Yan, et. al., 2003):

$$\mathbf{R_L}\left(\mathbf{T_g(t)}\right) = \mathbf{B_1}\mathbf{T_g(t)}^{-\frac{3}{4}}\,\mathbf{e}^{\frac{\mathbf{B_2}}{\mathbf{T_g(t)}}} \qquad (5.42)$$

where B_1 and B_2 are the adjustments. $T_g(t)$ is the gas temperature.

However the gas temperature varies from the inside to outside of the lamp, and the lamp resistance depends of this temperature. Also, the lamp resistance depends on the thermal resistances and capacitances of the filling gas and the glass that enclose the plasma (Shvartsas and Ben-Yaakov, 1999; Yan, et. al., 2003; Osorio, et. al., 2004). Also, the temperature is a function of lamp power, and then thermal equations have to be included in order to develop an accurate lamp model.

5.4.1.2. Modeling of the Thermal Equations

Most of the consumed energy at lamp discharges were transformed into heat; only a small percentage is transformed directly in radiated energy. Particularly, at metal halide lamps only approximately 10% of the energy delivered to the lamp is transformed into radiated energy, and the rest is transformed in heat (see Figure 5.20) (Osorio, et. al., 2004). Therefore, the dynamic response of the lamp (equation (5.42)) depends mainly on the heat transfer from inside the lamp to the outside (environment). The heat transfer from the inside to outside of the lamp depends of the thermal resistances and capacitances values of the filling gas (see Figure 5.21-a), arc tube (see Figure 5.21-b), the partial vacuum (see Figure 5.21-c) and the outer bulb (see Figure 5.21-d).

The heat transfer in gas and solids can be represented by an equivalent electrical circuit; this equivalent circuit is illustrated in Figures 5.22 and 5.23. With the analysis of the equivalent circuit is possible to obtain the dynamic response of the lamp in function of the thermal capacitances and resistances and the environmental temperature. The equations for the heat transfer circuit of Figure 5.23 are the following:

$$\frac{dT_g(t)}{dt} = \frac{q_L(t)}{C_g} - \frac{T_g(t) - T_{v1}(t)}{R_g C_g} \tag{5.43}$$

$$\frac{dT_{v1}(t)}{dt} = \frac{T_g(t) - T_{v1}(t)}{R_g C_{v1}} - \frac{T_{v1}(t) - T_{v2}(t)}{(R_{v1} + R_x) C_{v1}} \tag{5.44}$$

$$\frac{dT_{v2}(t)}{dt} = \frac{T_{v1}(t) - T_{v2}(t)}{(R_{v1} + R_x) C_{v2}} - \frac{T_{v2}(t) - T_a(t)}{(R_v + R_a) C_{v2}} \tag{5.45}$$

$$q_g(t) = \frac{T_g(t) - T_{v1}(t)}{R_g} \tag{5.46}$$

$$q_{v1}(t) = \frac{T_{v1}(t) - T_{v2}(t)}{R_{v1} + R_x} \tag{5.47}$$

$$q_{v2}(t) = \frac{T_{v2}(t) - T_a(t)}{R_v + R_a} \tag{5.48}$$

$$q_L(t) = \eta\, P_L(t) \tag{5.49}$$

$$\eta = B_3\, e^{-\frac{B_4}{Tg(t)}} \tag{5.50}$$

where C_g is the thermal capacitance of the filling gas, R_g is the thermal resistance of the filling gas, C_{v1} is the thermal capacitance of the arc tube, R_{v1} is the thermal resistance of the arc tube, R_x is the thermal resistance of the partial vacuum, C_{v2} is the thermal capacitance of the outer bulb, R_{v2} is the thermal resistance of the outer bulb, R_a is the thermal resistance of the ambient, $q_L(t)$ is the heat flow in the plasma, $q_g(t)$ is the heat flow in the filling gas, $q_{v1}(t)$ is the heat flow in the arc tube, $q_{v1}(t)$ is the heat flow in the outer bulb, k is the conversion efficient, $T_g(t)$ is the gas temperature, $T_{v1}(t)$ is the arc tube temperature, $T_{v2}(t)$ is the outer bulb temperature, $T_a(t)$ is the environment temperature, $P_r(t)$ is the radiate power, $P_L(t)$ is the lamp power.

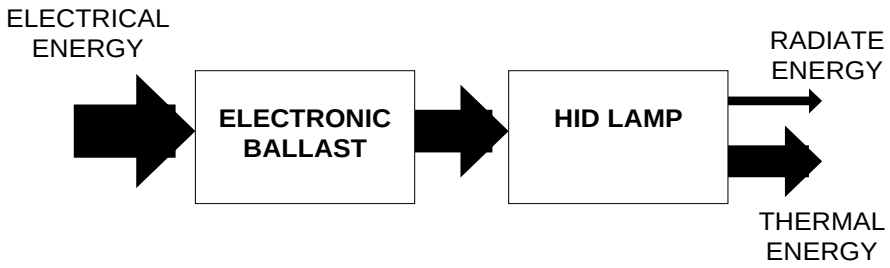

Figure 5.20 Energy Flow Diagram for an HID Lamp

The HID lamp has two glass recipients (see Figure 5.24). The internal glass recipient contains the filler gas, and the external-glass recipient that is good to protect the user when the internal-glass recipient exploits.

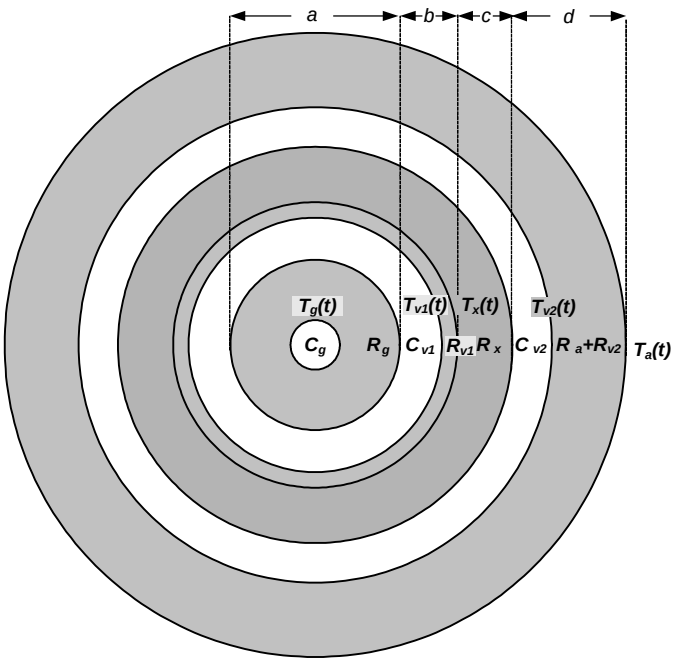

Figure 5.21. Thermal Parameters of the HID Lamp (Transversal Point of View)

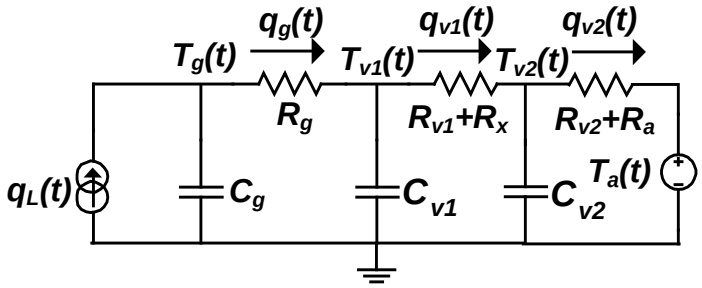

Figure 5.22 Equivalent Electrical Circuit of the Transfer Heat in the HID Lamps

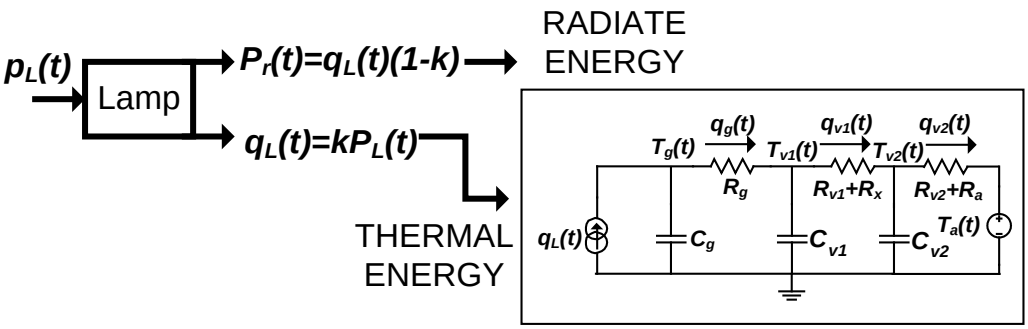

Figure 5.23 Power and Heat Diagram in HID Lamps

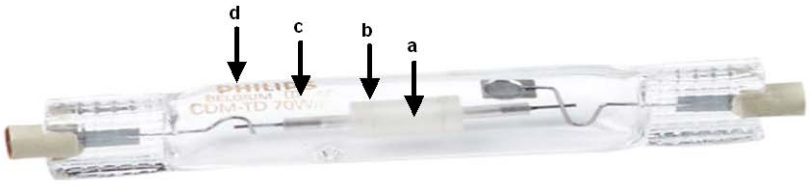

Figure 5.24 Glass Recipients of a HID Lamp

5.4.1.3. Relationships Between the Negative Resistance and the Dynamic Response

The heat flow produced by the plasma inside the lamp (see Figure 5.24), is related to lamp power by equation (5.51).

By substituting the equation (5.54) into (5.42) one obtains the following nonlinear dynamic of the lamp:

$$\mathbf{q_L(t) = p_L(t)\ k\ \left(T_g(t)\right)} \qquad (5.51)$$

Without loss generality, the value $\mathbf{k\ \left(T_g(t)\right)}$ in equation (5.51) was considered constant (equation (5.52)), because its small value (typical value is 11-14% $\mathbf{P_L(t)}$ for the HID halogen lamps. For exact calculations, it can be used the Boltzmann's formula (equation (5.53)), (Yan, et. al., 2003)) where the effects of its variations will be diminished.

.

$$\mathbf{q_L(t) = p_L(t)\ k} \qquad (5.52)$$

$$\mathbf{k\ \left(T_g(t)\right) = B_3\ e^{-\frac{B_4}{Tg(t)}}} \qquad (5.53)$$

where: B_3 and B_4 are constant.

Combining equations (5.43), (5.44), (5.45) and (5.51) leads to the following:

$$\mathbf{T_g(t) = -\left(R_g + R_{v1} + R_x + (R_{v2} + R_a)\right) C_g \frac{dT_g(t)}{dt} - \left(R_{v1} + R_x + (R_{v2} + R_a)\right) C_{v1} \frac{dT_{v1}(t)}{dt} - (R_{v2} + R_a) C_{v1} \frac{dT_{v1}(t)}{dt} + T_a \left(R_g + R_{v1} + R_x + (R_{v2} + R_a)\right) k \rho_L(t)} \quad (5.54)$$

$$\mathbf{R_L = B_1 \left(-\left(R_g + R_{v1} + R_x + (R_{v2} + R_a)\right) C_g \frac{dT_g(t)}{dt} - \left(R_{v1} + R_x + (R_{v2} + R_a)\right) C_{v1} \frac{dT_{v1}(t)}{dt} - (R_{v2} + R_a) C_{v1} \frac{dT_{v1}(t)}{dt} + T_a \left(R_g + R_{v1} + R_x + (R_{v2} + R_a)\right) k\, p_L(t) \right)^{-\frac{3}{4}} \times e^{\frac{B_2}{F(t)}}} \quad (5.55)$$

with

$$\boldsymbol{F(t) = -\left(R_g + R_{v1} + R_x + (R_{v2} + R_a)\right) C_g \frac{dT_g(t)}{dt} - \left(R_{v1} + R_x + (R_{v2} + R_a)\right) C_{v1} \frac{dT_{v1}(t)}{dt} - (R_{v2} + R_a) C_{v1} \frac{dT_{v1}(t)}{dt} + T_a \left(R_g + R_{v1} + R_x + (R_{v2} + R_a)\right) k\, p_L(t)} \quad (5.56)$$

5.4.2. Experimental Estimation of the Lamp Parameters

The $\mathbf{R(T_g(t))}$ stable state value is as follows:

$$\mathbf{R\left(T_g(t)\right) = B_1 \left(\left(R_g + R_{v1} + R_x + (R_{v2} + R_a)\right) k\, p_L(t) + T_a \right)^{-\frac{3}{4}} \times e^{\frac{B_2}{\left(R_g + R_{v1} + R_x + (R_{v2} + R_a)\right) k\, p_L(t) + T_a}}} \quad (5.57)$$

Equation (5.57) was simulated in Figure 5.25 and it was compared with the experimental results for a 70W metal halide HID lamp (CDM-R70W/830, Philips). In

this figure, it can be observed how equation (5.57) was adapted with high precision to the experimental results. The values of the thermal capacitances and resistances are not easy to calculate, because of that, it is necessary to know the chemical characteristics of the filling gas; also, the pressure inside the lamp and other parameters are not easy to obtain. Because of that, the lamp was considered as a black box, and their parameters were obtained by means of electrical measurements of the voltage and current signals of the lamp, when a unit step of power was applied to the lamp.

The lamp parameter can be deduced with an electrical analysis of circuit in Figure 5.23. A summary of the simplified equations are shown in Table 5.3 (Osorio, et. al., 2004).

Table 5.3 Equations for the Estimation of the Lamp Parameters

$R_g = \frac{T_g - T_{v1}}{q_{prom}}$	$R_{v1} + R_x = \frac{T_{v1} - T_{v2}}{q_{prom}}$	$R_{v2} + R_x = \frac{T_{v2} - T_a}{q_{prom}}$
$1 = 0.63\, e^{-\frac{1}{C_{v2}(R_{v2}+R_a)}t_{v2}}$	$1 = 0.63\, e^{-\frac{1}{C_{v2}(R_{v2}+R_a)}t_{v1}}$	$1 = 0.63\, e^{-\frac{1}{C_g R_g}t_g}$

where:

t_g is the time constant of the gas,

t_{v1} is the time constant of the arc tube,

t_{v2} is the time constant of the outer bulb.

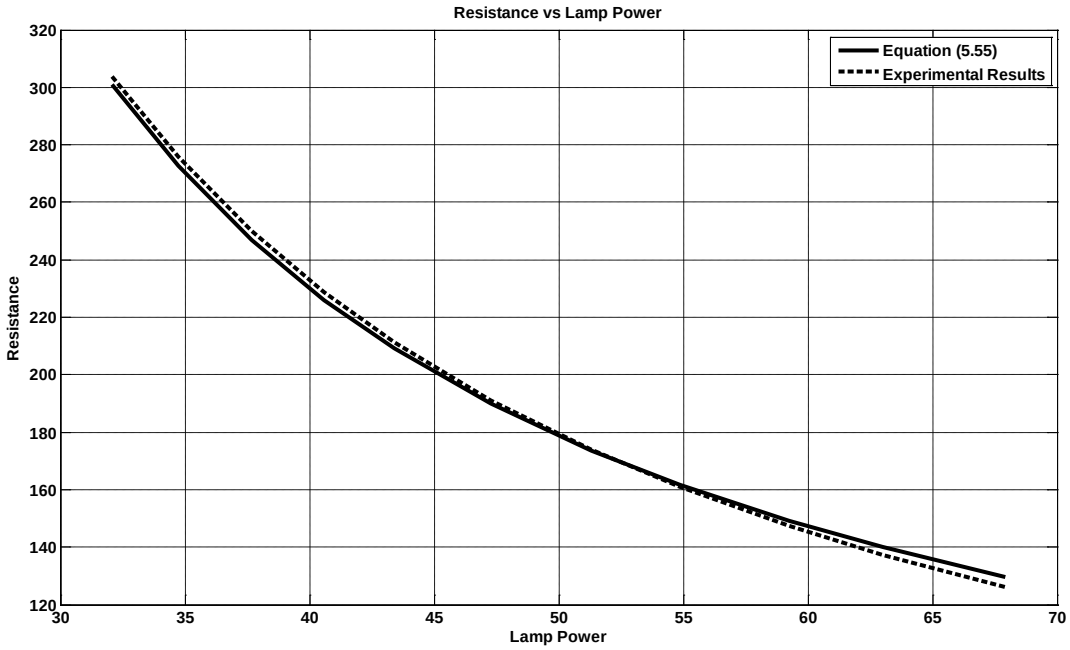

Figure 5.25 Equivalent Resistance of the Lamp in Function of the Lamp Power $R_L(T_g)$: Experimental Results (Dashed Line) and Equation (5.55) (Continuous Line)

The data obtained for 70W metal halide HID lamp (CDM-R70W/830, Philips) are :

$T_g \cong 4000\ ^oK = 3726\ ^oC$,

$T_{v2} = 679\ ^oC$,

$T_{v1} = 315\ ^oC$,

$T_a = 25\ ^oC$,

$q_{prom} = kP_L = 0.88(70\ W) = 62\ W$,

$t_g \cong 240\ \mu s$,

$t_{v1} \cong 47.5\ ms$,

$t_{v2} \cong 47\ s$.

Then de thermal parameters of the lamp are:

$R_g = 49.16\ ^oC/W$,

$R_{v1}+R_x = 5.9\ ^oC/W$,

$R_{v2}+R_a = 4.7\ ^oC/W$,

$C_g = 4.9\mu\ J/^oC$,

$C_{v1} = 8.1m\ J/^oC$,

$C_{v2} = 21.6\ J/^oC$,

The B and C parameters have only one combination, and they are found with a curve fitting method:

B_1 = 49772,

B_2 = 896.5.

5.4.3. Control stage

Many papers have presented several steps for designing purposes of the sliding mode controllers (Utkin, 1974; 1977; DeCarlo, et. al., 1988; Hung, et. al., 1993; Mattavelli, et. al., 1993) and those steps could be summarized as follows: 1. to propose the sliding surface, 2. to verify the existence of a sliding mode, and 3. to analyze the stability in the sliding surface. Typically, the sliding surface proposed is a linear combination of the state variables. This sliding surface made the implementation and theoretical analysis very easy. The SMC forces the system to be held in this surface and the system is driven to the equilibrium point which must be included in the sliding surface.

5.4.3.1. Control System Design

The complete power stage was previously described in Figure 5.2. In the simulations the proposed lamp model was considered.

The resultant system in matrix form considering the position of the switch *u* (1 and -1) is as follows:

$$\begin{pmatrix} \dot{x}_1 \\ \dot{x}_2 \end{pmatrix} = \begin{pmatrix} 0 & -w_0 \\ w_0 & -w_1 \end{pmatrix} \begin{pmatrix} x_1 \\ x_2 \end{pmatrix} + \begin{pmatrix} b/2 \\ 0 \end{pmatrix} u + \begin{pmatrix} b/2 \\ 0 \end{pmatrix} \quad (5.58)$$

where:

$$\mathbf{w_0} = \frac{1}{\sqrt{L_B C_B}}, \mathbf{w_1} = \frac{1}{R\, C_B}, \mathbf{b} = \frac{V_{in}}{\sqrt{L_B}}$$

$$\boldsymbol{x_1 = \sqrt{L} i_{LB}}$$

$$\boldsymbol{x_2 = \sqrt{C}\, V_{CB}}$$

Or: $\boldsymbol{\dot{X} = A\, X + BU + B}$

5.4.3.2. The Sliding Surface

The sliding surface proposed is a linear combination the x_1 variable:

$$\boldsymbol{\sigma = s(x_1 - x_r)} \qquad (5.59)$$

where: s is a control parameter,

x_1 is the state space related to L_B inductor current,

x_r is the current reference signal.

The proposed control law is: $\boldsymbol{u = u_{eq} + u_N}$

Here: $\boldsymbol{u_{eq}}$ = Equivalent control, $\boldsymbol{u_N = -sgn(\sigma)}$.

The equivalent-control law (u_{eq}) has been used only for analysis and this implies to guarantee the existence condition just locally. The actual control does not include the equivalent control.

5.4.3.3. Existence of the Sliding Mode

This implies that the condition $\sigma\dot{\sigma} < 0$ is fulfilled (Miaosen, et. al., 2002a; 2003). It can be easily shown that in order to guarantee the existence conditions of sliding mode the following inequality must be fulfilled:

$$\boldsymbol{-sw_0 x_2 < 0} \qquad (5.60)$$

$$-\boldsymbol{sw_0 x_2} + \boldsymbol{sb} > 0 \qquad (5.61)$$

In order to assure the existence conditions, "*s*" must be positive.

5.4.3.4. Stability Analysis of the Sliding Surface

The equivalent control was a tool developed in order to describe the movement in the sliding surface (Utkin, 1974; Miaosen, et. al., 2002b). The equivalent control is valid when the analysis of the system dynamics is made assuming that the system is on the sliding surface ($\sigma = 0$), hence $\dot{\sigma} = 0$. Therefore, the equivalent control (u_{eq}) is obtained from $\dot{\sigma} = 0$, resulting:

$$\boldsymbol{u_{eq} = -(SB)^{-1}(SAX + SB)} \qquad (5.62)$$

or

$$\boldsymbol{u_{eq} = \frac{2\,w_0}{b}\,x_2 - 1} \qquad (5.63)$$

The equivalent control was substituted in the model of the system, and the stability analysis must be made under this conditions.

5.4.4. Simulations and Experimental Results

The electronic ballast was designed with the following specifications: nominal lamp power P_o = 70W, main input voltage V_{in} =180Vdc, lamp voltage V_C = 90Vdc, RMS lamp current I_L = 0.777A, filtering inductor of the buck converter L = 5mH, filtering capacitor of the buck converter C = 2μF and a CDM70W830PH lamp. The C and L values were designed according to current and voltage ripples. The values of the model parameters obtained with the experimental characterization are: R_g = 49.16 $^oC/W$, $R_{v1}+R_x$ = 5.9 $^oC/W$, $R_{v2}+R_a$ = 4.7 $^oC/W$, C_g = 4.9μ J/^{o}C, C_{v1} = 8.1m J/^{o}C, C_{v2} = 21.6 J/^{o}C, B_1 = 49772, B_2 = 896.5.

To test the model the following methodology was used: first, the lamp was turned on until the lamp receives the nominal powe12r (70 W); after that, the current in the lamp was reduced until the 50% of the nominal value. This reduction was made with a current reference signal followed with the nonlinear controller of the ballast. The control strategy was that the sliding mode control assures a good dynamic response of the lamp current.

Figure 5.26 shows the simulation results using the proposed model in “Simnon”. The results illustrated the dynamic behavior of the lamp current and voltage signals. These waveforms were the result of application of a current step down of 50% to the lamp. The simulations (Figure 5.27) and the experimental results (Figure 5.28) were similar. Additionally, a good dynamic response and robustness were obtained ensuring that the lamp does not turn off, due to the nonlinear (sliding mode) controller used.

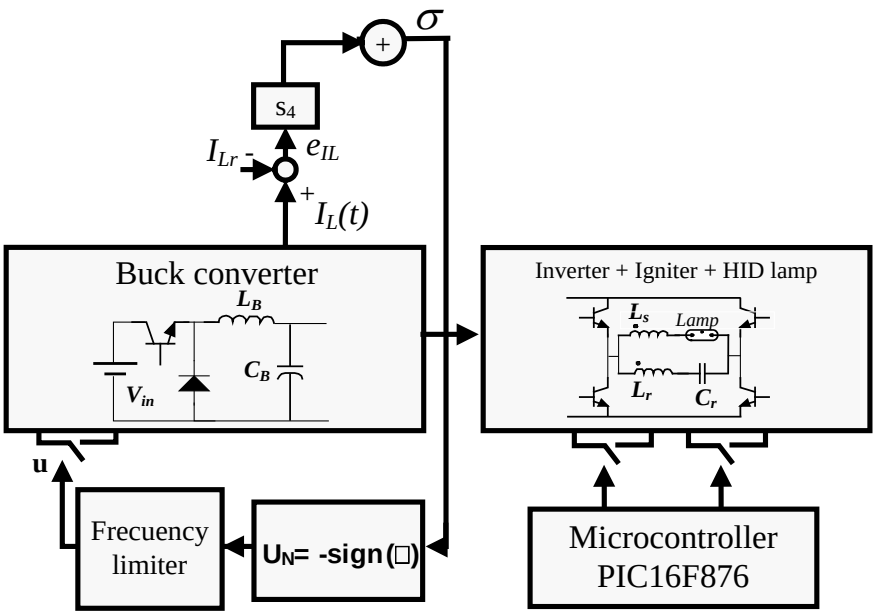

Figure 5.26 Test Circuit with Nonlinear Sliding Mode Controller

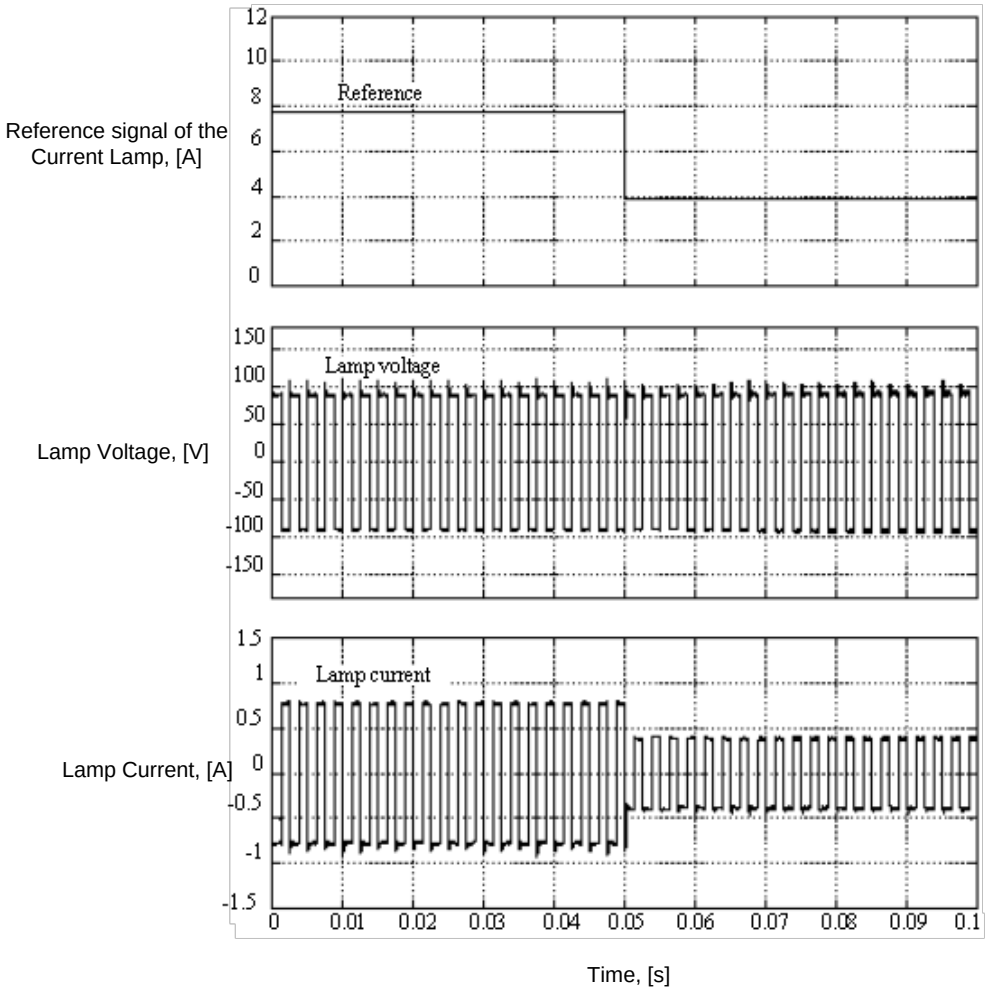

Figure 5.27 Simulation Results, Dimming Test (100% to 50%), Top to Down: Current Reference, Lamp Voltage and Lamp Current Signals

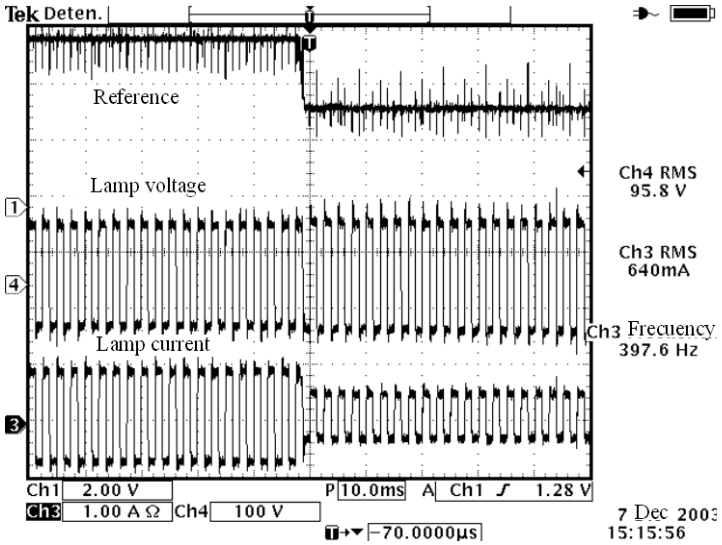

Figure 5.28 Experimental Results, Dimming Test (100% through 50%), Top to Down: Current Reference, Lamp Voltage and Lamp Current Signals

5.4.5. Conclusions

The example concerned an analysis of a HID lamp under the action of a discrete sliding mode nonlinear controller. To avoid the appearance of acoustic resonance, the power stage feeds the HID lamp with low frequency square waves. A good dynamic response in the dimming test was obtained because of the efficiency of the control strategy. Also, nonlinearities are considered in the buck model and the ignitier plus lamp model. This is the other advantage of the nonlinear control law over the classic control algorithm, because when a linearization model was obtained the analysis was limited only to a close region near to the operation point. Also, a dynamic nonlinear PSpice lamp model implementation in Simulink was developed. The experimental results have shown a good dynamic behaviour of the selected electronic ballast with a nonlinear control law (SMC). Square waves were obtained with this topology and hence, the acoustic resonance phenomenon was eliminated.

In the next example, an analysis of control stage behavior designed with a nonlinear controller (SMC) with adaptive-fuzzy-sliding surface was presented. To avoid the appearance of acoustic resonance the power stage feed the HID lamp with low frequency square waves.

Good dynamic responses in dimming test with lamp-parameter variation and in the input-voltage-variation test were obtained because the control strategy was efficient. Also, nonlinearities were considered in the buck model and the lamp model. This is the other advantage of the nonlinear control strategy over the classic control law, because when a linearization model is obtained the analysis is limited to the near region of the operation point.

The last example developed was a Thermal Dynamic Model for HID lamps, which was proposed. This new model was based on the thermal behavior of the lamp. With the proposed model it was possible to predict the dynamic response and the stability of the

lamp. In addition, the new model can be implemented in several simulation programs such as: “PSpice”, “Simnon” or “MATLAB”. The parameters of the proposed model are the thermal capacitances and resistances of the lamp and they were obtained by means of experimental measurements of the dynamic response of the lamp. The model was implemented in “Simnon” and the simulation results were compared with the experimental results. The results obtained were satisfactory.

The experimental results have shown a good behavior (fast dynamic response and robustness) of selected dimmable electronic ballast with a nonlinear controller (SMC). Square waves are obtained with this topology, and as a result the acoustic resonance phenomenon was eliminated.

Chapter 6 Fuzzy Nonlinear Predictive Controllers

6.1. Introduction

The fuzzy model based predictive controller is discussed in this chapter. A summary of the history of linear and nonlinear model predictive controllers have also been described as well as the state of the art for the model based predictive control technique.

The main characteristics or advantages of the model based predictive controller (MBPC) are the simplicity on its mathematics, richness on information of its components, easy controller tuning due to the intuitive definition of the cost function, easy extension to MIMO systems, delay intrinsically compensated, practicality in inputs/output constraints and demonstrability in real applications (Clarke, 1996; Gomez-Ortega and Camacho, 1996).

Complex processes have been successfully controlled by multivariable MBPC (Huang, et. al., 2000a). In advanced applications MBPC systems have become one of the promising control techniques. Altogether, the interacting inputs and output variables are used to compute the adjustment of the manipulated variables in the MBPC systems.

The main characteristics of the MBPC as a family of optimal controller are (Gomez-Ortega and Camacho, 1996): a) the future set-points are previously known; b) the future system output prediction are obtained using an explicit model; c) the control law is obtained from the minimization of a cost function; d) the use of receding-horizon approach.

MBPC technologies have been successfully applied to systems such as chemical, refinery, petrochemical, biotechnological and food products, process units and other process industries which are commonly defined as nonlinear, multivariable, cross coupling, interactive and time varying behaviours which are affected by unknown

disturbances (Gomm, et. al., 1997; Huang, et. al., 2000a; Zhao, et. al., 2001; Grimble and Ordys, 2001; Ibarrola, et. al., 2002). The great acceptance of the MBPC in the process industry is due to its ability to manage constraints implicitly with a MIMO control system (Onnen, et. al., 1997). The minimization of a cost function is carried out by using the process model computing the optimal sequences of the control actions by means of a MBPC. This accurate process model produces accurate process predictions and because of the interest to find a different model alternative has increased.

The optimization algorithm is one of the more important aspects of MBPC. Convex optimization problems have been solved by efficient optimization algorithms. Dynamic nonlinearities and constraints characteristics in the real processes often produce a non-convex optimization problem which is more complex than the convex optimization problem. Frequently, the main problem in the optimization is the selection of the optimization algorithm, because some of them are sensible to the initial condition in order to find the local minimum solution rather than the global minimum solution (i.e. the conventional iterative optimization method). To find the optimal operating point is a non trivial test if the process is affected by high disturbance (Zanin, et. al., 2002). Appendix C shows the basic development of the model based predictive controllers (MBPC). Another way of dealing with the nonlinear processes is to split the operating range into several local linear approximations to develop the control systems (Zayed, et. al., 2004b; 2004c),

6.1.1. State of the Art of Model Based Predictive Controllers

Camacho (1993), developed the generalized predictive controller with constraints establishing important theoretical background for the control law.

Clarke (1996), reviewed the evolution in the design and use of the model based predictive controllers. Also, he used a parameter estimator in order to design an adaptive predictive controller.

Fuzzy model-based predictive controller (FMBPC) was designed by Fischer and partners (1998) and applied to the temperature control of an industrial-scale cross-flow water/air heat exchanger. Measurement disturbances revealed time-variant behaviour in the process and because of this, on-line training of the process model was needed. Measurement data were used to train and identify the Takagi-Sugeno fuzzy model (1985). Local recursive least-square algorithm was proposed for the on-line adaptation of the fuzzy model.

A neuro-fuzzy model-based predictive controller (NFMBPC) was developed by Zhan and Kovacevic (1998) and applied to the welding process. The top-side and back-side bead widths of the weld pool specified the control of the weld fusion. An image processing algorithm and a neuro-fuzzy model were incorporated in order to made the measurement and estimation of the top-side and back-side bead widths founded on an advanced top-side vision sensor because many application only top-side sensor was allowed, which was attached and moves with the welding torch. The control variables selected are the welding current and speed. The value of another input defines the correlation between any input and output.

A modular neural network model of a three-effect, falling–film evaporator was developed by Russell and partners (2000). To train a network for prediction up to N steps ahead a data set which spans N time steps was used. This procedure is called long-range prediction. The modular neural network model is suitable for MBPC because it can predict over a horizon of arbitrary length. The modular neural network model uses a time-delay neural network, which captures the dynamics of the nonlinear plant. Mixing the modular neural network with prior knowledge of the plant to be modelled, the transparency and interpretability of the trained modular neural network model could be increased.

A fuzzy model predictive controller (FMPC) was designed by Huang, and partners (2000b), in order to deal with nonlinear processes. The fuzzy convolution model is the representation of the nonlinear process and consists of an amount of quasi-linear fuzzy implications. The FMPC is one type of nonlinear model predictive controller

(NMPC). The minimization of the prediction error and the control energy were made by means of a two-layered iterative optimization process in the control design. For each subsystem, the minimization of the prediction errors helps to identify the optimal local control policies at the lower layer. By coordinating the subsystems to obtain an overall minimum prediction error at the upper layer, a near optimum is identified. The design of the FMPC was based on linear control theory using the two-layered computing scheme to avoid with extensive on-line nonlinear optimization process.

A combination between a classical impedance controller with a fuzzy predictive algorithm was proposed by Baptista and partners (2001). The impedance controller obtains the optimal virtual trajectory from the calculation made by the fuzzy predictive algorithm. In the control design, the nonlinear model was included in a straightforward way, improving the global force control performance. A fuzzy scaling machine was included in the force control strategy reducing the oscillations of the optimized reference position. An experimental two-degree-of-freedom robot was the scenario to verify the performance of the force control scheme.

Supervisory predictive control law with fuzzy models were developed by Sáez and Cipriano (2001). The nonlinear process was represented by fuzzy models. The optimization problem at supervisory level was described by two different fuzzy predictors. The benchmarking problem was the application used for the proposed fuzzy predictive controller.

Mollov and partner (2002), developed a predictive controller based on Takagi-Sugeno fuzzy model applied on nonlinear process with a close-loop response. Open-loop bounded-input-bounded-output stable processes with an additive l_1-*norm* bounded model uncertainty were assumed in order to guarantee close-loop robust asymptotic stability with several conditions. The robust stability constraints obtained were less conservative because the previous idea was closely related with l_1-*control theory* because of the time-varying approach. The fuzzy model was expressed as a linear time-varying system rather than a nonlinear one. The

constraints were obtained in the control signal and the robust stability will be guarantee on its increment.

Mahfouf et al (2003), used the on-line administration of anaesthetic drugs during surgery evaluation with unconstrained and constrained Generalised Predictive Control (GPC). A patient simulator was designed with a physiological model of the patient and also via an extensive simulation studies was validated the required control software. The design engineers were involved in the trials in order to obtain a good regulation of the blood pressure with fixed-parameters and adaptative version of the algorithm.

Neural network model-based predictive control algorithm applied on a laboratory-scaled multivariable chemical reactor was developing by Yu and Gomm (2003). The reactor has common characteristics of industrial applications including structure, nonlinear behaviour, and internal couplings without a mathematical model. A neural network model with multiple-input single-output (MISO) with parallel process model for simulation, on-line identification and prediction were used.

Several MBPC with linear and nonlinear models were used by Sáez and Keremer (2003) in a laboratory tank in order to test and compare the algorithms. The dynamic nonlinear process was represented by the fuzzy models.

Zen and partners (2003), designed a neural network predictive controller applied to the coagulation process of wastewater treatment in a paper mill. The nonlinear relationships between the removal rates of pollutants and chemical dosages were expressed by a multi-layer back-propagation neural network to make adaptive the control system to the different operating condition with a flexible learning ability. A neural network model of the reaction process, a neural network controller and an optimization algorithm (gradient descend method) founded on the cost function were the subsystems included in the control system to identify desired control inputs.

A revision of the optimization in fuzzy model predictive control was made by Mollov and partners (2004). With no guarantee of finding an optimal solution the prediction model as fuzzy model, nonconvex and required time-consuming optimization were described. The linearization of the fuzzy model around the current operating point and the linear predictive controller (i.e., quadratic programming) were an alternative solution for the previous problem. The performance was reduced because the propagation of the linearization error for a long-range predictive control. The propagation of the linearization error was reduced by a linearization of the fuzzy model along the predicted input and output trajectories. Via an iterative application of the optimized control sequence to the fuzzy model and linearizing along of the so obtained simulated trajectories, the model prediction could be improved. Making the difference between a single linear method (or a set of linear model) were proposed for optimization algorithms. A desired tradeoff between the control performance and computational load, give the user the possibility to select the appropriated optimization technique. The applications used for testing the MPC were the pH control in a continuous stirred tank reactor and a high-purity distillation column.

Alayón and partners (2004), proposed a novel neural network predictive controller in order to reduce the computation effort of the NMPC. The proposed approach was compared with the nonlinear predictive controller and the approximated predictive control based on neural networks. The experiments were carried out in simulations and real time applications for a laboratory tank system.

6.2. Nonlinear Predictive Controllers

The definition of nonlinear model based predictive controller (NMBPC) was mainly based on using a nonlinear model to design the MBPC controller. Hence, there is a nonlinear predictor, which was used to compute the optimal sequences of future inputs using an optimization algorithm in order to regulate future outputs of the nonlinear plant.

The Block diagram of the NMBPC is shown in Figure 6.1. It includes several blocks as: optimization algorithm, discrete nonlinear model, a linearization block and a discrete linear model. The discrete nonlinear model is obtained using an artificial neural network, a neuro-fuzzy system or and Look-Up table. The linearization block is used to obtain the linear matrices to be used for the discrete linear model to be used by the optimization algorithm in order the find a local (or global) minimum, which will minimize a specific cost function. The fundamental concepts of the MBPC will be included in Section 6.2.1.

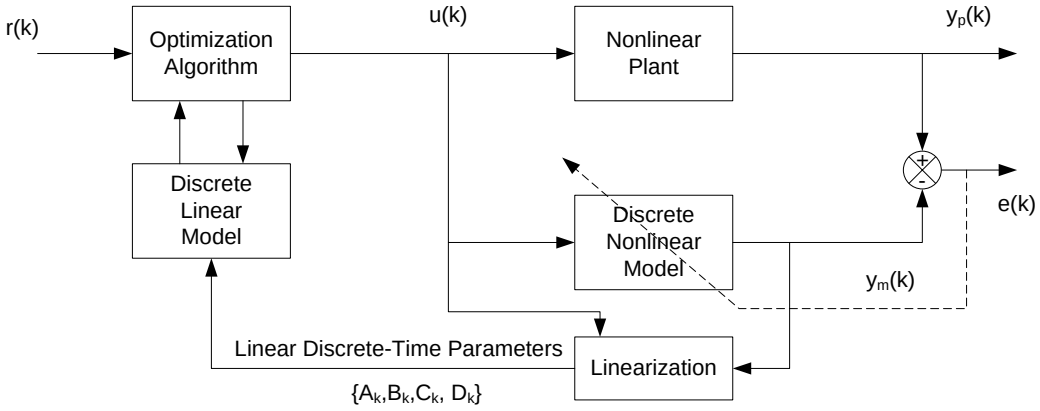

Figure 6.1 Block Diagram of the Nonlinear Model Based Predictive Controller

The most important problem with this controller is to find the local (or global) minimum, which is not easy to guarantee, especially when the internal model of the MBPC is nonlinear. The optimization problem for the NMBPC is a nonconvex problem because the model used is a nonlinear one, which increases the complexity of the solution (Mollov, 2002).

The difficulty of this nonconvex optimization solution is compounded by the fact that the plant is nonlinear and multivariable. The nonlinear models (predictors) more commonly used are the neural network and neuro-fuzzy and fuzzy models. Also, there is a possibility to use the on-line modelling and multiple models.

The way to solve the nonconvex optimization problem is to linearize the nonlinear model around the operating point and then apply the linear model predictive control technique. If a long prediction horizon is used, the MBPC suffers from error propagation of the linearization in the performance of the control system. By using neural model, neuro-fuzzy model and fuzzy model along the predicted inputs and outputs, the effect of the error propagation can be reduced.

6.2.1. The Fundamental Concepts of Model Based Predictive Controllers

Predictor, prediction horizon and control horizon. Figure 6.2 shows the fundamental concepts of the MBPC. A nonlinear model of the plant was used to predict the future process output over the *prediction horizon* H_p. Generally, a predictor with an ARX structure (inputs-outputs models are represented by a collection of delayed inputs and outputs) was used as model.

Step ahead outputs represent the predicted output values defined as $\hat{y}(k+i)$ for $i=1,\ldots,H_p$, as a function of the state of the process at current sampling time k and also in function of the future control signals $u(k+i)$ for $i=0,\ldots,H_c-1$, where H_c is the *control horizon*. The control signal is manipulated with the control horizon if the condition $H_c \le H_p$ is selected and after that the input remain constants as $u(k+i)=u(k+H_c-1)$ for $i=H_c,\ldots,H_p-1$.

Cost function. The optimization of the cost (objective) function is used to compute the sequence of the future control signals $u(k+i)$ *for* $i=0,\ldots,H_c-1$, in order to keep close the output signal to the reference signal. Several modifications of the following cost function are used (Clarke, et. al.,1987b):

$$J=\sum_{i=1}^{H_p}\alpha_i\left(r(k+i)-\hat{y}(k+i)\right)^2+\sum_{i=1}^{H_c}\beta_i\,\Delta u(k+i-1)^2 \qquad (6.1)$$

The first term computes the minimum variance of the output signal by the control error signal produced by the difference between the reference signals $r(k+i)$ and the predicted process outputs $\hat{y}(k+i)$ (Fischer, et. al., 1998).

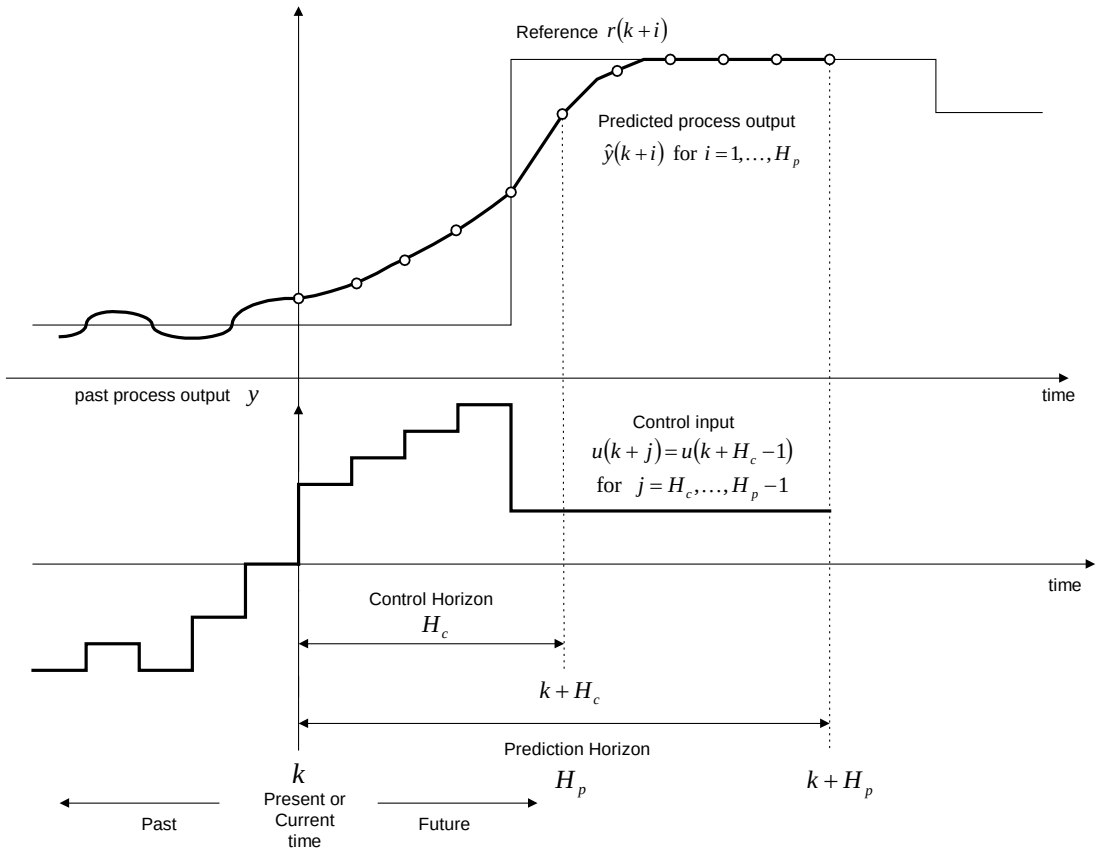

Figure 6.2 Fundamental Concepts of the Model Based Predictive Controller

The second term established the penalization over the increment of the control signal $\Delta u(k+i-1)=u(k+i)-u(k+i-1)$ produced in the control horizon H_c (Souza, et. al., 1997). In accordance with the control problem, the second term can be expressed by the control signal $u(k+i-1)$ rather than its increment or any different filter structure (Soeterboek, 1992). The output error weighting α and control effort weighting β vectors with respect to each other and the prediction step.

Only the outputs were considered in the cost function from time $k+n_d$ when the system has a dead time of n_d samples because the output signal does not have

influence on the control signal $u(k)$ before this time (Babuška, 1996). Similarly, a delay is introduced in a non-minimum phase system in order to avoid the non-minimum phase part of the response. Moreover, constraints over other variables such as the manipulated variables and other process variables could be included in the cost function as additional terms in accordance to the control problem. The process outputs $\hat{y}(k+i)$ are obtained from the process model for a set of future control increments $\Delta u(k+j-1)$ (Fischer, et. al., 1998).

Receding horizon principle. The first control output signal applied to the nonlinear plant is defined by:

$$u(k) = u(k-1) + \Delta u(k) \tag{6.2}$$

At the next sampling-time $k+1$, the time-dependent variables included in the cost function are shifted one-step ahead and the optimization of the cost function starts again. This strategy is called receding horizon. In other words, only the control signal $u(k)$ is available and applied to the process at the beginning and after that in the next sampling time the output signal $y(t+1)$ is available, computing again the optimal values and making possible to obtain the updated prediction values.

6.3. Nonlinear Model Predictive Controller Based on Takagi-Sugeno Fuzzy Structures for Wastewater Application

The fuzzy structure of the nonlinear model based predictive controller (NMBPC) was based on the Takagi-Sugeno fuzzy models, which have local linear models in order to cover the whole operating region for a nonlinear plant. The block diagram of the NMBPC was founded on a fuzzy structure shown in Figure 6.3 and this structure was

inspired in the previous work developed by Pinto, Grimble and Katebi (2004) using Takagi-Sugeno fuzzy models (Takagi and Sugeno, 1985). The control algorithm structure was designed by Pinto, producing an example published by O'Brien, Pinto and Katebi (2005).

The application of MBPC methods in two systems: the linear control of a wastewater treatment plant, and fuzzy-nonlinear control of an integrated wastewater system (consisting of a sewer network, a treatment plant, and the receiving waters). There has been little work on control of the latter systems; the majority of research has concentrated on the treatment plant alone. A similar approach to that described here was developed by Marsili-Libelli and Giunti (2002) and by Brdys and Diaz-Maiquez- (2002) where fuzzy predictive control was applied to the case of treatment plant system, without modelling the effect on the receiving waters.

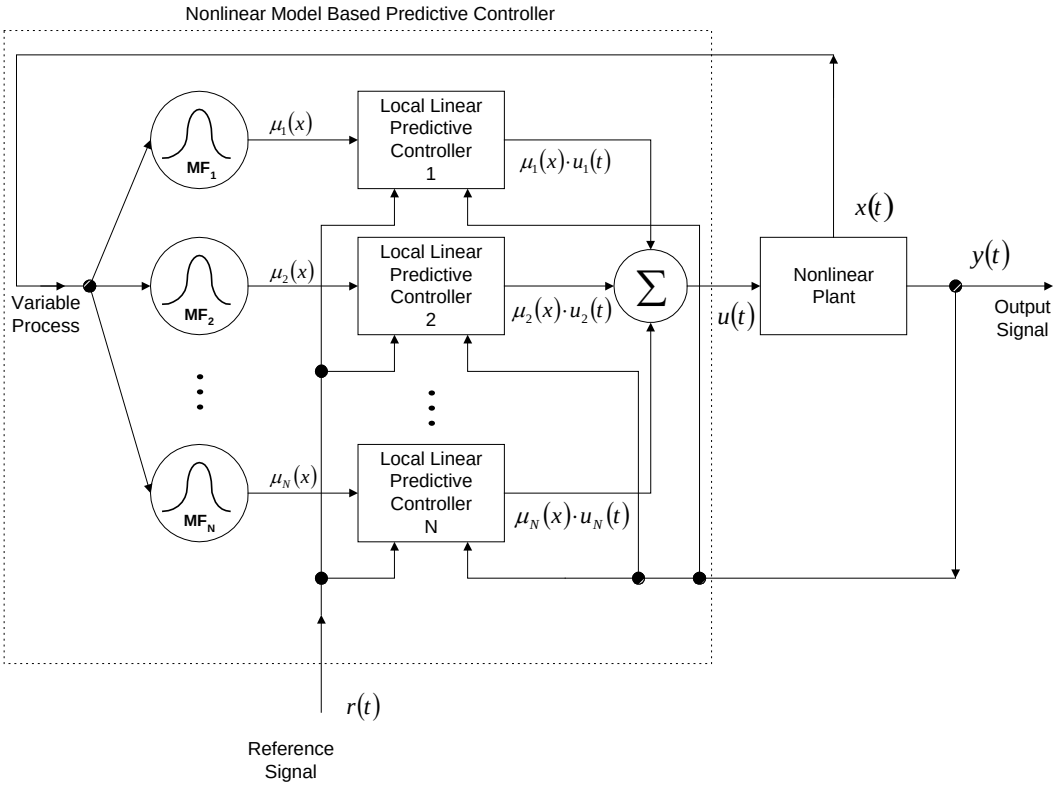

Figure 6.3 Block Diagram of the Nonlinear Model Based Predictive Controller Founded on Fuzzy Structure

6.3.1. Nonlinear Model Based Predictive Control with Takagi-Sugeno Fuzzy Structure

The NMBPC of Figure 6.3 can be represented by the following fuzzy rules:

$$\text{Rule } i\text{: IF } x(t) \text{ is } MF_i \text{ THEN } u(t) = u_i(t);\ i = 1, 2, \ldots, N \tag{6.2}$$

where $x(t)$, MF_i , $u_i(t)$, $u(t)$ and N are the process variable used to define the universe of discourse or the complete operating range, the i[th] membership function or fuzzy set (see Chapter 2 of this document for more details), the i[th] control signal of the i[th] local linear model based predictive controller (LLMBPC), the control signal of the NMBPC and the number of LLMBPC (or fuzzy sets or sub-operating region with linear behaviour).

The i[th] membership function $\mu_i(x)$ previous fuzzy rules have to cover the following relationship:

$$\sum_{i=1}^{N} \mu_i(x) = \mu_1(x) + \mu_2(x) + \ldots + \mu_N(x) = 1.0 \tag{6.3}$$

where $\mu_i(x)$ is the i[th] membership value corresponding to the i-th LLMBPC. The equation guarantees that all the universe of discourse (or nonlinear operating range) is covered by the membership functions (see Chapter 2 of the thesis). Figure 6.4 show how the universe of discourse (or the complete operating range) of the nonlinear plant was divided in *N* sub-linear regions by N membership functions or (or fuzzy sets) (Pinto, 2001).

Also, from Figure 6.3 the NMBPC obeys to the following control law:

$$u(t) = \sum_{i=1}^{N} \mu_i(x) \cdot u_i(t) = \mu_1(x) \cdot u_1(t) + \mu_2(x) \cdot u_2(t) + \ldots + \mu_N(x) \cdot u_N(t) \tag{6.4}$$

where $u(t)$, $\mu_i(x)$ and $u_i(t)$ are the control signal, i[th] membership function and the i[th] control signal of the i[th] LLMBPC.

The previous equation shows how each control signal of the LLMBPC is equalized by the weighting of membership value.

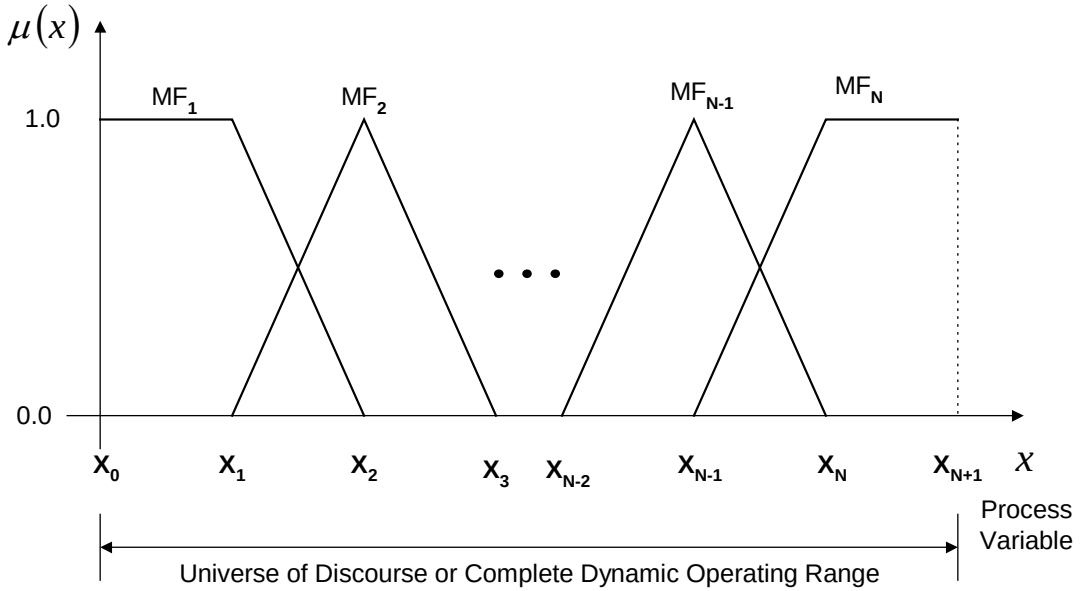

Figure 6.4 Fuzzy Membership Functions Dividing the Universe of Discourse in N Membership Functions

The NMBPC was designed using the linearization concept in local regions for the nonlinear dynamic system. The main principle used was "divide and conquer", which is the philosophy of the multiple linear approaches (i.e. Takagi-Sugeno fuzzy models). In essence, the universe of discourse (the whole dynamic operating range) of a process variable (i.e. state variable) in a nonlinear plant is divided into pieces in order to obtain sub-regions with linear dynamic behaviour. Each sub-region is mapping to the fuzzy space by membership functions (i.e. Triangle, Trapezoid and Gaussian membership functions.) and its linear dynamic behaviour is described by a local linear model in the same way of the Takagi-Sugeno fuzzy models.

Figure 6.5 shows the fuzzy membership function dividing the universe of discourse in *N* linear sub-regions using at each sub-region of a membership function. The previous concept was founded in the overlapping concept of the local linear models to reproduce a nonlinear plant. The local linear subsystems were defined in the Table 6.1 with their corresponding sub-operating range and the membership functions.

Table 6.1 Local linear subsystems, Sub-Operating Range and Membership Function

Local Linear Subsystem	Sub-Operating Range	Membership Functions
1	$x_0 \le x \le x_2$	MF_1
2	$x_1 \le x \le x_3$	MF_2
⋮	⋮	⋮
N-1	$x_{N-2} \le x \le x_N$	MF_{N-1}
N	$x_{N-1} \le x \le x_{N+1}$	MF_N

Algorithms of the NMBPC

The NMBPC based on Takagi-Sugeno structure was developed by the following algorithm:

Step 1: Divide the whole nonlinear dynamic operating range in N sub-ranges with linear behaviours.

Step2: Linearize the nonlinear plant for each sub-range in order to guarantee that the j^{th} sub region is governed by the dynamic behaviour of the j^{th} local linear model based predictive controller. Selection of the implementation details of the local

linear model based predictive controller such as: control horizon, prediction horizon, inputs/outputs constraints in the waste water system.

Step 3: Assign the membership functions (i.e triangle shape) and/or fuzzy sets for each sub-range in an explicit manner, as Figure 6.5 shows with the intersection points between them.

Step 4: Design the local linear model based predictive controllers with constraints using equations (6.3 – 6.4).

Step 5: Build the final structure for the NMBPC as the Figure 6.4. The nonlinear operating region includes all dynamic behaviours necessary to cover for the nonlinear dynamic plant. Also, the whole operation region (i.e. Universe of discourse) defined by a process variable has to be divided in portions called dynamic local regions. Each dynamic local region is represented by a local linear model of the plant. The nonlinear plant was testing in a portion (dynamic local region) of the whole operating region, finding the linearization of the plant and after that was designed the local linear model based predictive controller (LLMBPC).

6.4. Nonlinear Model Based Predictive Control with Takagi-Sugeno Fuzzy Structure Applied to Waste Water Treatment

The problem of controlling both oxygen and nitrate levels in a wastewater treatment system is considered in this application. The initial system to be controlled is that presented in the COST 624 benchmark for the Activated Sludge Model (ASM) 1 model. This demonstrates that MBPC linear predictive control is possible for a treatment system, which consists of only the water treatment plant. However, it is also necessary to demonstrate predictive control on the integrated system, that is, including the sewer and the receiving waters, as well as the treatment plant. The majority of control research in the area of wastewater treatment has concentrated on

the effluent from the plant, and meeting regulatory requirements at this point. The research now has begun to concentrate on the effect this effluent has on the receiving waters. To this end, a simple model of an urban wastewater system (UWS) was used for the control implementation, for the latter case study. The aim therefore of first study was to control the nitrate and the oxygen to a specified setpoint. The control of these concentrations was investigated using multivariable predictive control. The control of the integrated wastewater system includes the Takagi-Sugeno structure implicitly, in controlling the dissolved oxygen.

6.4.1. Cost 624 Benchmark Control

The COST 624 research group developed a benchmark model of wastewater treatment, using the ASM1 model developed by Mogens, et. al., (2000), in order to effectively compare several control strategies. Unless a general model was used for control design purposes, then the effectiveness of different controllers cannot be determined. The COST benchmark system is shown in the Figure 6.5.

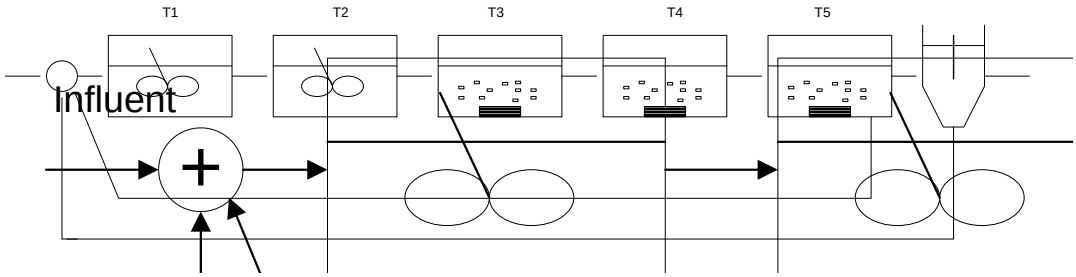

Figure 6.5 COST Benchmark System: Tanks 1 and 2 Fully Mixed, Tanks 3, 4 and 5 Aerated, Followed by a Non Reactive Secondary Settler

The plant model shown in Figure 6.5 is comprised of:

- five biological tanks in series, each using the ASM1 model, first two tanks unaerated, the other three aerated.

- one non reactive secondary settler based on the settling function by Takacs et al.
- two internal recycles, nitrate from 5th tank to 1st, and sludge from settler to front end of plant.

This system considers only the treatment plant dynamics, that is the influent into the plant is that of the average statistics for given rain events, but does not take into account any sewer dynamics. Similarly, the control implemented only considers the effluent, and not the affect downriver.

The system presented by Copp (2002) used low level control in the form of PID control, on the Dissolved Oxygen (DO) levels of the 5th tank, and nitrate levels in the 2nd tank. The control aim therefore is to improve on this, by implementing predictive control around these PID loops, thereby feeding a variable setpoint to them (See Figure 6.6). The variables Sno, So, Kla and Qin are the nitrate and nitrite nitrogen, oxygen, oxygen transfer coefficient and the correction flow for the internal nitrate recycle, respectively.

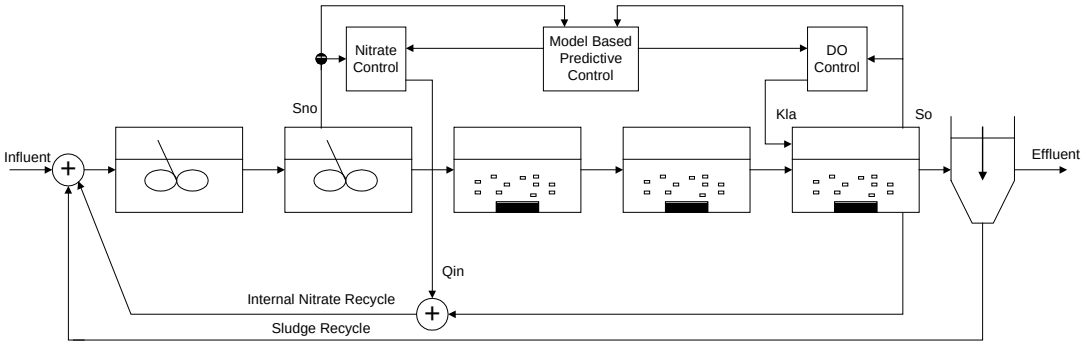

Figure 6.6 Model Based Predictive Controller Applied in the COST Benchmark System: Dissolved Oxygen and Nitrate/Nitrite Control

For this MBPC format used here a linear state space model is required, which is found by implementation of Subspace Identification, developed by Van Overschee and De Moor (1996). For implementing the linear MBPC methods, the system is

run to control a DO setpoint of 2gm^{-3}, and the nitrate level is controlled to a setpoint of 1gm-3 as is show in Figure 6.7.

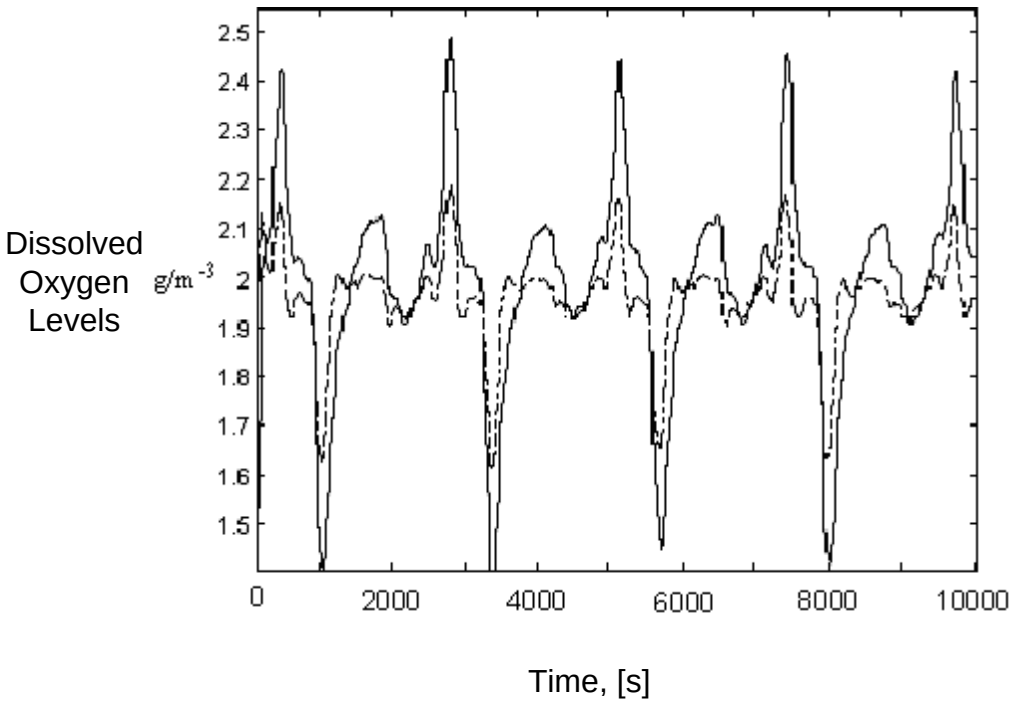

Figure 6.7 Dissolved Oxygen Control (dotted line) vs. PID Control

It can be seen that for the Dissolved Oxygen levels, the predictive control (dotted line) response was considerably better than that of the original PID control (full line) as it is shown in Figure 6.7. For the Nitrate, the improvement is even more obvious (see Figure 6.8). The reason for this is the fact that the predictive controller is a cascaded controller, around the inner PID loop, and therefore can vary the setpoint of the inner loop, avoiding the error due to tuning.

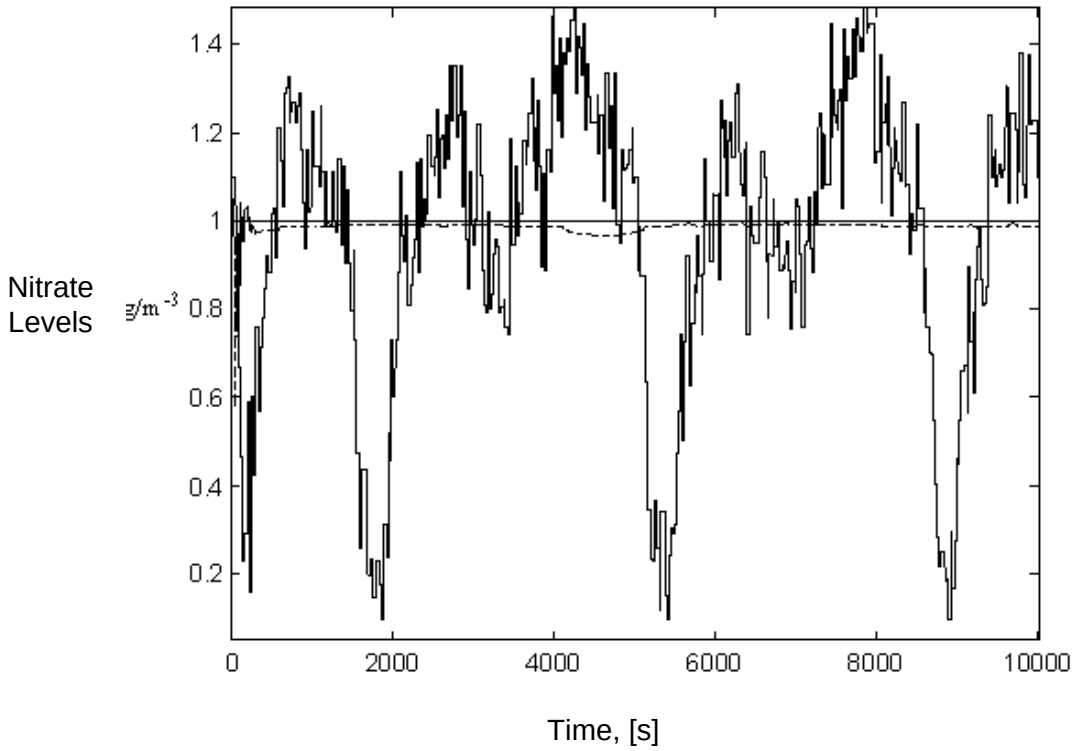

Figure 6.8 Nitrate Control (dotted line) vs. PID Control

In constraint handling, the system demonstrates the following response for the output constraint of 2.5gm-3, Figure 6.9 shows the unconstrained and constrained case respectively for a setpoint step of 0.75gm-3 to 2.5gm-3 for Dissolved Oxygen. It can be seen in Figure 6.9 that the constraints are implemented on the output functions, though they operate strictly.

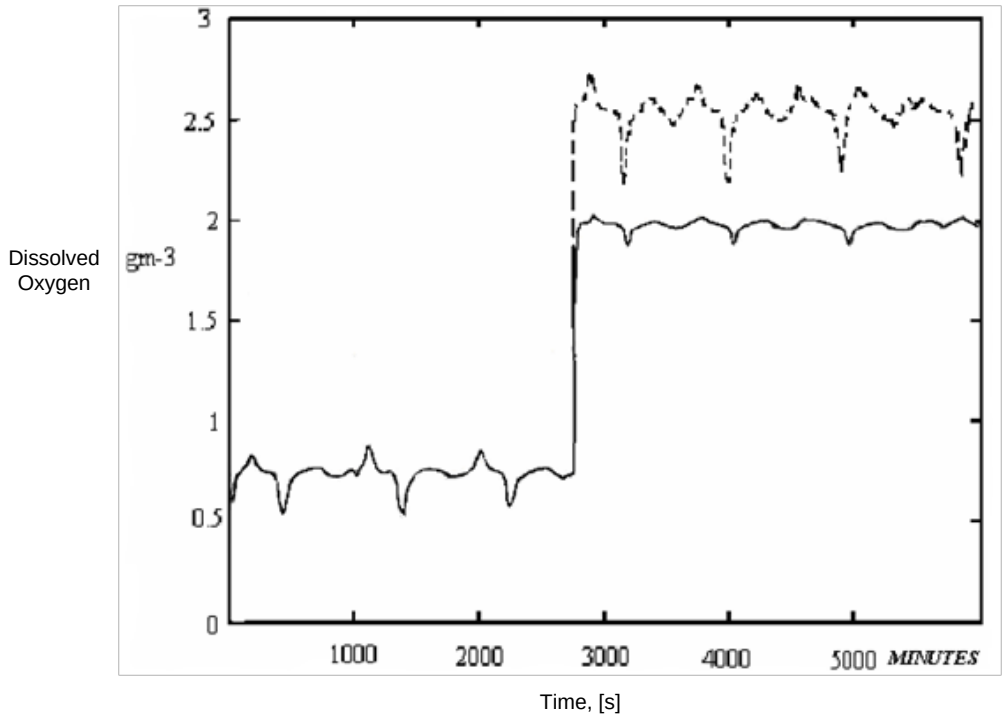

Figure 6.9 Dotted line: Unconstrained Case, Full line: Constrained Case

Gain Scheduling for Integrated UWS

The system considered as an integrated urban waste water system consists of a sewer network model, a treatment plant model, and the model of the receiving waters (which in this case is a river model). The input to the sewer network is that of the influent from the catchment areas, which consists of human urban wastewater, and other influents from runoff.

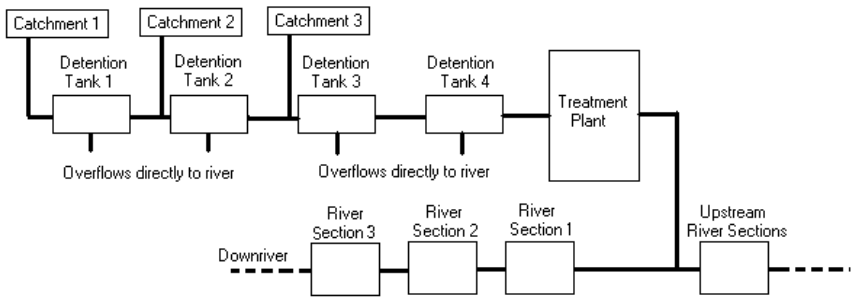

Figure 6.10 Integrated Urban Wastewater System

It can be seen from Figure 6.10, that the sewer network affects the receiving waters in two ways, the first being the effects of the effluent of the sewer network, which is in turn the influent to the treatment plant. It also affects the receiving waters through overflows. In storm conditions, overflows occur in the sewer network, causing fluctuations of the fractions (such as Dissolved Oxygen) in the river.

The control objective here is to show the possibility of control of the quality of the receiving water using the treatment plant effluent dynamics. Research has been done by Cembrano, et al (2004) in the use of MBPC in reducing overflows, so this paper does not consider this area.

The NMPC was designed using the Takagi-Sugeno structures. This was implemented for the integrated model shown in Figure 6.10.

The subspace identification algorithm used previously in identification of the treatment plant model was used again in this case to also obtain a multivariable model. This model however is of the form of a measured disturbance, as the model input of upstream river dynamics was not controllable here. There was also the difference here that the predictive controller, whilst still applying a variable setpoint to a PID, does not cascade around this PID loop, but around the entire system. There exists only one controlled input, the set point of the Dissolved Oxygen levels in the Treatment Plant. Due to this fact, that there are three models, for low flow, medium flow and high flow, there are three fuzzy rules for the model of the Nonlinear Predictive Controller using a Takagi-Sugeno structure. The structure of the Nonlinear Predictive Controller is shown in Figure 6.9. The formula that describes the Nonlinear Predictive Controller output *u* is expressed as follows:

$$u(t) = \mu_1(Q) \cdot u_1(t) + \mu_2(Q) \cdot u_2(t) + \mu_3(Q) \cdot u_3(t) \tag{6.5}$$

where $\mu_1(Q)$, $\mu_2(Q)$ and $\mu_3(Q)$ are the membership values (weightings) for the low flow, medium flow and the high flow. Q is the flow (process variable). $u_1(t)$, $u_2(t)$ and $u_3(t)$ are the local linear model based predictive controllers corresponding for the low flow, medium flow and the high flow. The membership values satisfied the following equation:

$$\mu_1(Q)+\mu_2(Q)+\mu_3(Q)=1.0 \tag{6.6}$$

The process variable, that is the variable upon which the ranges are based, is the input flow to the treatment plant, *Q*. By choosing three models that cover a range from 0 to 12,000m3 of flow, then the nonlinear control should take into account both the normal flow (in the region of 1000m3) and the storm weather flow (the maximum 12,000m3). The membership functions were therefore defined as shown here in equation (6.7), and subject to the constraints defined as follows:

$$\mu(Q)=\begin{cases}\mu_1(Q)+\mu_2(Q)=1.0, & for\ \ 0\le Q\le 6000\,m^3\\ \mu_2(Q)=1.0, & for\ \ 6000\,m^3\le Q\le 6500\,m^3\\ \mu_2(Q)+\mu_3(Q)=1.0, & for\ \ 6500\,m^3\le Q\le 9000\,m^3\end{cases} \tag{6.7}$$

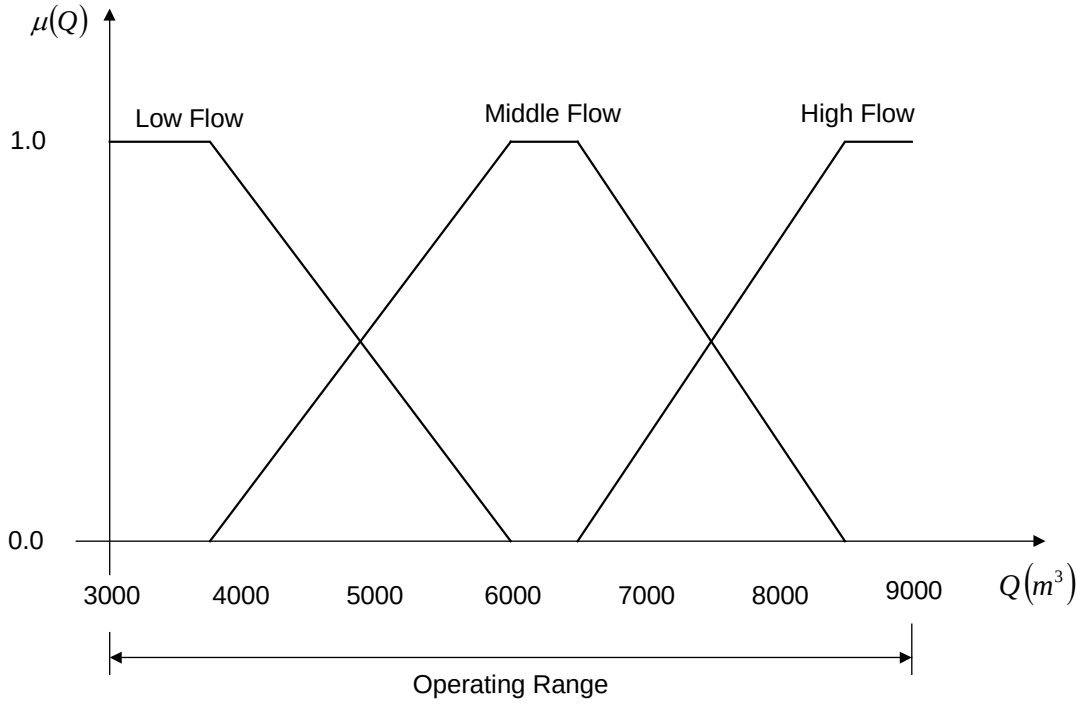

Figure 6.11 Fuzzy Membership Function for the Flow Q

The fuzzy sets low flow, middle flow and high flow cover the whole operating range to be defined for each LLMBPC in order to satisfy the nonlinear operating range of the system. The internal structure of the NMBPC was exactly the same as that of Figure 6.3 with the amount N equal to 3 (i.e. three LLMBPCs). The operating range was divided into the form shown in Figure 6.10, using triangular and trapezoidal membership functions, chosen due to their characteristic of having a unity-weighting sum. To demonstrate the improvement resulting from the use of a NMBPC, the following tests were run on the system.

Firstly, as in Figure 6.12, the NMBPC was tested at a step flow from 4000m3 to a flow of 9000m3, for which the set point to be reached in the river was a value of 8.2gm-3. Both systems were tuned in order that their maximum values would reach the set point. The linear controller was tuned for the flow range of 5000m3 to 7000m3.

The NMBPC was tuned to reach a given set point for all flow ranges, and any flow change results only in a minor transient dip in Dissolved Oxygen levels. In comparison, it can be seen that the response for a single linear predictive controller, it is erroneous at both flows and has a considerably larger transient dip during the flow change.

There is, therefore, an improvement in the response of an integrated wastewater system when a sudden flow change was applied. This is significant, as the most likely significant change in the system would be an increase in flow, due to storm weather. Using a nonlinear controller, such as a gain scheduler, allows for the system to react to such a transient.

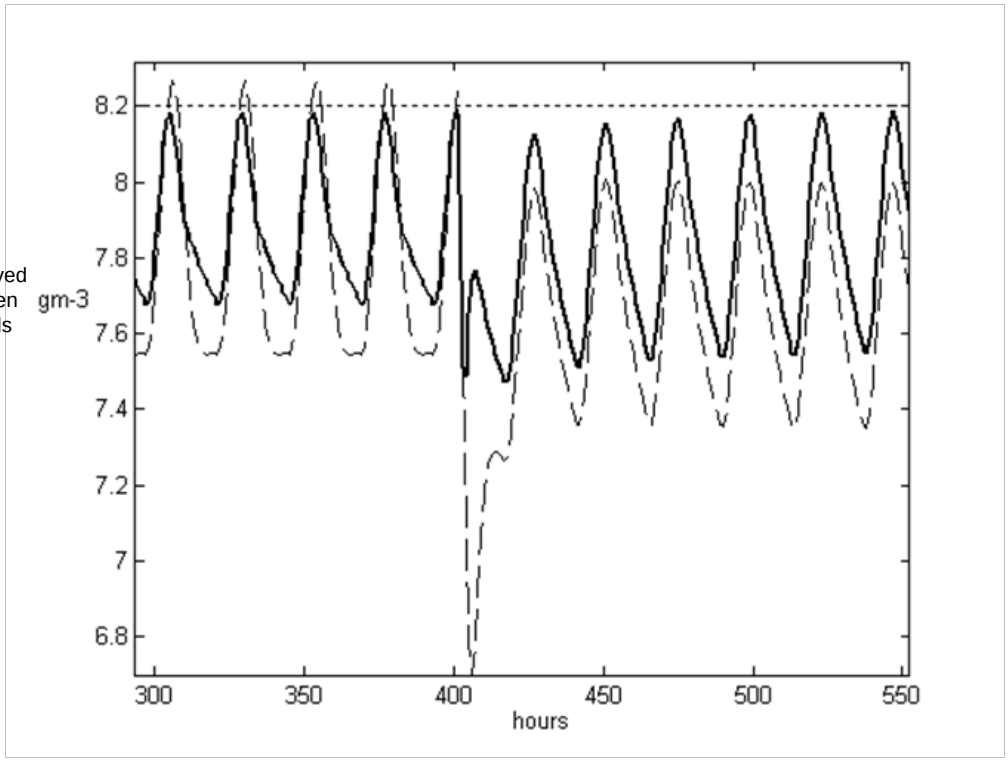

Figure 6.12 Nonlinear Model Based Predictive Controller (full line) vs. Linear Model Based Predictive Controller (large dotted line), with Respect to Setpoint (small dotted line)

In summary, the output constraints demonstrated in Figure 6.8 show the significant advantage of using MBPC. Lower control methods, such as PID control, do not allow for constraint handling. The responses in Figures 6.6 and 6.7 also show the distinct improvement of MBPC over PID in terms of set point tracking. This is because the PID controller does not allow for intuitive tuning of multivariable controllers. Figure 6.11 demonstrates the advantage of using a NMBPC controller for the more nonlinear integrated system.

To demonstrate the improvement resulting from the use of a Takagi-Sugeno MBPC (Nonlinear MBPC), the following tests were run on the system. Firstly, as in Figure 6.12, the fuzzy controller was tested at a step flow from $4000m^3$ to a flow of $9000m^3$, for which the set point to be reached in the river was a value of $8.2gm^{-3}$. Both systems were tuned in order that their maximum values would reach the set point. The linear controller was tuned for the flow range of $5000m^3$ to $7000m^3$.

The fuzzy predictive controller was tuned to reach a given set point for all flow ranges, and any flow change results only in a minor transient dip in dissolved oxygen levels. In comparison, it could be seen that the response for a single linear predictive controller, without gain scheduling, was erroneous at both flows and has a considerably larger transient dip during the flow change

6.5. Conclusions

The majority of control approaches have been focussed on control of the treatment plant. However, the more realistic approach was focussed instead on the effect of the effluent on the river, and to use this knowledge to attempt to control the river dynamics. Thus, the effect of overflows on Dissolved Oxygen, and nutrients could be negated by the control of the WWTP effluent with respect to river dynamics. The Activated Sludge Model (ASM) 1 was the used model and it was developed by Mogens, et. al., (2000).

The predictive control method used in this application was outlined in (Krauss, et. al., 1994; Maciejowski , 2002). It was seen that it is possible to develop nonlinear predictive control using linear methods with Takagi-Sugeno structure. The NMBPC demonstrates the ability to control a waste water treatment plant for dissolved oxygen and nitrate levels, and also the control of an integrated urban wastewater system by the use of NMBPC. The latter was implemented for Dissolved Oxygen. The research in this application presents the control of wastewater systems with the use of MBPC, and demonstrates how even nonlinear wastewater systems are controllable with linear techniques, with the use of multiple model predictive controller based on Takagi-Sugeno structure which is a NMBPC. Further work could be carried-out to implement this control for nutrients such as Nitrates or Phosphates, therefore requiring more complex nonlinear predictive control methods, as well as progression to the use of a more complicated integrated system model.

There is, therefore, an improvement in the response of an integrated wastewater system when a sudden flow change is applied. This is significant, as the most likely significant change in the system would be an increase in flow, due to storm weather. Using a nonlinear controller, such as a gain scheduler, allows for the system to react to such a transient.

Chapter 7 Conclusions and Future Work

7.1. Summary and Conclusions

This thesis was concerned with the application of the Neuro-Fuzzy control systems to industrial and power electronics applications. The justification and motivation were to use adaptive characteristics of the Neuro-Fuzzy systems conjugated with the capability of implementation to nonlinear control systems without an exact model and possible uncertainties in the target nonlinear model. In addition, the Neuro-Fuzzy control systems are a promising multidisciplinary field of the control engineering.

The control engineer should have the following expertise to be able to use these technologies: a) know the physical laws or expert rules that govern the target process in order to understand and analyze the control system, b) be able to develop a quantitative (mathematical model) or qualitative model (fuzzy model) of the nonlinear process, c) select and design the proper control algorithm in accordance to the dynamic behaviour of the target process, d) to have enough knowledge and experience of microcomputers (microcontrollers) to implement the algorithms.

The Artificial Neural Networks (ANNs), the Fuzzy Systems and the Neuro-Fuzzy Systems were introduced in Chapter 2, from their basic knowledge in order to obtain the model and control law applied to the target nonlinear plant. The Chapter introduced the basic concepts of the Multilayer Perceptron, Adaptable Neural Networks (i.e. Feedforward Neural Network and Recurrent Neural Network), the training methods (i.e. Backpropagation or Gradient Descend) of the ANNs.

In addition, the Chapter included a historical development of Fuzzy Systems describing the origin of these. After that, the Neuro-Fuzzy systems were presented as a combination between the ANNs and the Fuzzy Systems. Also, the Neuro-Fuzzy models were described as a linguistic model in detail based on the Takagi-Sugeno-Kang models. Nevertheless, the OFF-Line and ON-Line training methods were

widely explained. The training methods used the Backpropagation or Gradient Descent and the Hybrid (i.e. Backpropagation and Least Square) Algorithms.

Finally, a novel Fuzzy Difference Equation (FDE) was introduced as a formal mathematical structure of the Neuro-Fuzzy Systems (Artificial Intelligence). Initially, the Neuro-Fuzzy models were obtained. After that, a SISO and MIMO examples were used in order to develop the examples of the FDE´s. The FDE was developed based on the dynamic information obtained from the Fuzzy rules (model) and it represents the formal link between the Artificial Intelligence (AI) and the formal mathematics.

In Chapter 3, the basic theory of the novel Neuro-Fuzzy Generalised Minimum Variance (NFGMV) Controller and the Self-Tuning Generalised Minimum Variance (STNFGMV) Controller were introduced. The stochastic control system was developed using the polynomial approach based on the original idea of Grimble (2003) for the Nonlinear Generalised Minimum Variance Controller.

The novel NFGMV control algorithm was presented in Chapter 3 by combining the Nonlinear Generalised Minimum Variance (Stochastic) Control law and the Neuro-Fuzzy Modelling. The Chapter also include state of the art for several structures of the Nonlinear GMV controller by using ANNs and Neuro-Fuzzy Systems to find out the benefits in the implementation procedure of the novel NFGMV and the STNFGMV. The expert knowledge for controller tuning were also presented for the STNFGMV which include a Fuzzy tuning mechanism as an additional sub-structure.

In Chapter 4 a completed analysis of the car engine system was developed including the control targets, the most common problem applying the control systems and the problems to solve. The analysis of the car engine system was done by decomposing the engine into three subsystems (see Figure 4.1). After the analysis, the car engine problem was classified as a dynamic transient control problem (most of the time combined with a steady control problem). In other words, such a problem was defined as a transient control problem due to the delays in the measurements and the

propagation from the intake manifold to the combustion chamber. The Chapter also includes the state of the art for the nonlinear controller applied to the powertrain control problem of the car engine. The Chapter also includes the revisited explanation for the development of the car engine model developed by Dutka (2005), motivated by the necessity to know more about nonlinear process.

After that, a free delay Neuro-Fuzzy model was developed for the car engine in order to apply a MIMO NFGMV controller which showed great weakness. Also, several Neuro-Fuzzy structures based on the total solution (i.e. transient and steady solutions) of the nonlinear differential equation of the system were developed and applied to the car engine model. The Neuro-Fuzzy control algorithms developed (varying the selected inputs, the number of inputs, fuzzy rules and the sampling time) in Chapter 4 did not stablise the system because of the low speed of convergence for the global minimum of the Backpropagation or Gradient Descend optimization algorithm.

In Chapter 5, Analysis, estimation and modeling of the power electronic ballast with buck converter plus the igniter and the lamp (Power Electronic System) were studied. Also a discrete-time Sliding Mode Control law and a Dimming Control were designed using Adaptive Fuzzy Sliding Surface for a Square-Waveform Ballast (power electronic process). In addition, a stability analysis was developed for a Square-Waveform Ballast using a nonlinear lamp model with sensing average output voltage and current tests. All the developments and examples were simulated and compared with the real implementations in order to have well founded conclusions.

Chapter 6 started with the summary of the introduction of linear and nonlinear predictive controllers followed by the state of the art of the model based predictive controllers. The nonlinear predictive controllers were described starting with the fundamental concepts (i.e. predictor, predictor and control horizon, etc). Finally, a novel nonlinear model predictive controller was designed based on Takagi-Sugeno-Kang fuzzy structures. The key to the nonlinear predictive controller is the overlapping of local linear predictive controllers. The dynamic operation range of

the nonlinear plant is divided into ”n” sub-operation ranges where “n” local linear (model based) predictive controllers were designed to overlap with Takagi-Sugeno-Kang fuzzy structures. In order to demonstrate the performance of the nonlinear model predictive control algorithm, a SISO and MIMO wastewater system plant were studied.

7.2. Future Work

In this thesis the theoretical and application research results introduced may further be developed. In the analysis and justification of the Neuro-Fuzzy Systems there exist a great amount of issues that have to be researched in a deeper manner. In addition, the car engine problem such as a transient control problem represents a great challenge for the control engineers and because of that there are significant numbers of topics that may be developed. Moreover, a faster optimisation algorithm represents a very promising research topic because most of the weaknesses for the control systems caused by the slow speed of searching a global (or local) minimum. The future researches to be developed will be:

1. A further analysis of convergence and stability of the Neuro-Fuzzy Systems (NFSs) using the Fuzzy Difference Equations (FDEs). It will be a formal mathematical analysis and justification for using NFSs for control and modelling purposes.

2. A MIMO Neuro-Fuzzy Generalised Minimum Variance (GMV) controller for an industrial application using the polynomial approach. The application could be applied to a nonlinear MIMO process with the same delays in each input or output channel. Also, the nonlinear MIMO system could have different delays in each path. The free delay Neuro-Fuzzy model may be obtained using on-line or off-line training method. Another alternative to obtain the free delay model is to use Artificial Neural Networks (ANNs).

3. A Neuro-Fuzzy GMV control law using the state representation solved using the Bernoulli's equation applied for SISO and MIMO cases of nonlinear processes.

4. The parameter estimation of the Lamp system using the methods of the Least-Square Estimator and the Extended Kalman Filter.

5. A nonlinear control law with power factor correction applied to a Ballast (Buck Converter) with the Igniter plus the Lamp. The main objective will be to quantify the performance index in function of the power factor improvement (amount of energy and money saved).

6. A faster optimisation algorithm in order to find a global (or local) minimum for the Neuro-Fuzzy control systems. The improvement in the speed of searching a cost function solution increases the success in modelling, identification, estimation and control applications.

7. A Multiple Model Based Predictive controller with a Takagi-Sugeno-Kang structure including an on-line estimation of the nonlinear parameters for the membership functions.

APPENDIXES

APPENDIX A

A.1. Adaptable Neural Networks

In the Adaptable Neural Network, the outputs of the nodes are function of the modifiable parameters (Pinto, 2006). The parameters are updated by means of a learning rule. The difference between the network's current output and a desired output is the error measured, which is used to update the parameters in the nodes. Choosing the appropriated network architecture, a set of parameters should be found such that the ANN outputs fit the real data. All node functions are assumed to be differentiable except at a finite number of points in order to have the possibility to apply the learning algorithms. Each node has its own function different from the other nodes with a local parameter set. The weights in each node do not have any relation with the links between the nodes.

A.1.1. Decomposition of Adaptable Nodes

The decomposition of adaptable nodes is one of the most important concepts to develop an ANN. The concept of the decomposition of nodes in a ANN is shown in Figure A.1.

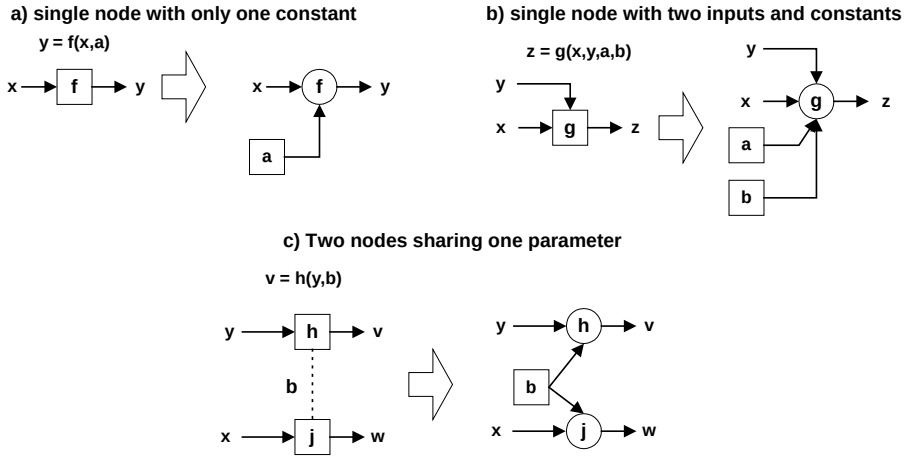

Figure A.1. Most Common Decomposition of Adaptable Nodes in an ANN

Figure A.1-a shows a single adaptive node with one constant ("a"), an input x and an output y with an activation function $f(\cdot)$ expressed in equivalent manner as a fixed node (constant) with input x and output y.

Figure A.1-b shows a single node with two constants ("a and b") and two inputs ("*x* and *y*"). The node has the activation function $g(\cdot)$. The equivalent structure using four inputs and two constants ("a and b"), is also shown.

Figure A.1-c shows two nodes sharing one parameter, where the constant parameter ("a") feeds both activation functions $h(\cdot)$ and $j(\cdot)$. These nodes have each one independent inputs ("*x* and *y*") and the outputs *v* and *w*, respectively.

A.1.2. Training Process of the Artificial Neural Networks

The training data set are the input-output data of the target system. They are used to modify the values of the parameters to improve the network's performance by means of the optimization algorithms or learning rules (Pinto, 2006). The difference between the desired output and the network's output is called error measured, which is used to improve the network's performance. The Steepest Descendent Method (SDM) is the basic learning rule of the Adaptable Artificial Neural Network (AANN), which uses the gradient vector with successive use of the chain rule. The learning rule computes the gradient vector in the opposite direction of the output flow of each node. The SDM is often called backpropagation algorithm.

The training processes can be either OFF-LINE or ON-LINE. The OFF-LINE training process is often applied to stable open-loop plants (linear and nonlinear). This training process is developed by applying step inputs plus a random signal (White noise zero-mean signal) covering the operation range of each input. Finally, a register of the pair input-output data has to be generated. All the parameters could be expressed by lumped constants obtained after the training process is applied. The OFF-LINE Training Process is the most applied and reported method for modelling

and control processes. The optimization algorithm for this approach could be developed with local minimum or global minimum. Another option of optimization algorithms are the Genetic Algorithms and Fuzzy Cluster Optimization.

The ON-LINE Training Process is usually applied when the plant is linear or nonlinear with time-varying dynamics (Pinto, et. al., 2004). In other words, there is a different plant every sample time with a specific dynamic. This training method was used to catch the variation in the dynamics due to the nonlinearities, time-delays and uncertainties using local minimum optimizations techniques.

A.2. Fundaments of Takagi-Sugeno-Kang (TSK) Models

There are three types of TSK fuzzy models called:

a) TSK Homogeneous Fuzzy Models

b) TSK Zero-Order (Singleton) Fuzzy Models

c) TSK First-Order (Piece Wise or Affine) Fuzzy Models

All these models have in common the same normalized degree of fulfilment $\gamma_i(\mathbf{x}(k))$, which is possible to use several types of membership functions (i.e, triangular, trapezoidal, Gaussian membership functions). All of the models represent hyperplanes defined in the space $(R^p \times R)$ with $(Ny + Nu + 1 = p)$ linear dimensions (Babuška, 1996). The local models are interpolated in order to obtain the global model (Mourot, et. al., 1999). When a NARX model is used in a TSK fuzzy model, it becomes a Dynamic Fuzzy Model because it takes information about the states of the systems by means of the delayed inputs and outputs (Pinto, et. al., 2006). The full operating space of the nonlinear plant is covering by the operating regimes,

which is described qualitatively by the corresponding local linear model (Angelis, 2001).

The TSK fuzzy models are easily identifiable from numerical data but they do not have an easily linguistic interpretation (Su, 1997). When the fuzzy sets are defined by trapezoidal membership functions the approximation capacity of the TSK fuzzy models are affected considerably.

A.2.1. TSK Homogeneous Fuzzy Models

The structure of these models is described for homogeneous linear models in the consequent part of the fuzzy rules. The linguistic model of the TSK Homogeneous Fuzzy Models using IF-THEN rules is defined as follows:

$$R_i : \text{If } \mathbf{x}(k) \text{ is } A_i \text{ then } y_i = \mathbf{a}_i^T \mathbf{x}(k) \qquad i = 1, 2, \ldots, N \tag{A.1}$$

where R_i, $\mathbf{x}(k)$, A_i are the i-th fuzzy rule, the regressor vector and the ith antecedent of the ith fuzzy rule. y_i and $\mathbf{a}_i$ are ith crisp output signal and the ith parameter vector. N is the total amount of the fuzzy rules. Substituting equations (2.15) in the equation (2.11) is obtained the Homogeneous TKS fuzzy models are expressed as follows:

$$y(k) = \sum_{i=1}^{N} \gamma_i(\mathbf{x}(k)) \left(\mathbf{a}_i^T \mathbf{x}(k)\right) \tag{A.2}$$

where $y(k)$, $\gamma_i(\mathbf{x}(k))$, $\mathbf{a}_i$ and $\mathbf{x}(k)$ are the output signal, normalized degree of fulfilment, ith parameter vector and the regressor vector.

These models have been considering quasi linear (or sometimes called linear) TSK models because they do not have a off-set term. Because of that is possible to apply

the majority linear techniques for the stability analysis and control design using its quasi-linear structure. The model can be expressed in a quasi-linear form as follows:

$$y(t)=\left(\sum_{i=1}^{N}\gamma_i(\mathbf{x}(t))\mathbf{a}_i^T\right)\mathbf{x}(t) \qquad \text{(A.3)}$$

and

$$\mathbf{a}(x(t))=\left(\sum_{i=1}^{N}\gamma_i(\mathbf{x}(t))\mathbf{a}\right) \qquad \text{(A.4)}$$

where $\mathbf{a}(x(t))$ is the matrix convex linear combination of the consequent parameters.

Fantuzzi and Rovatti (1996) shown the Homogeneous TSK fuzzy models have limitations on its approximation properties in comparison with Piece-wise TSK fuzzy models (with $b_i \neq 0$).

An study of the stability issues of linear TSK fuzzy models based on Tanaka's Theorem and also developed an iterative algorithm for the choice of the common matrix (Joh, et. al., 1998). Lyapunov's functions and stability analysis have been developed founded in the solution of Riccati's Equation and Tanaka's Theorem in (Yu and Fei, 2005).

A.2.1.1. TSK Zero-Order Fuzzy Models

The TSK Zero-order fuzzy models are commonly called Singleton fuzzy models (Babuška, 1996; Hellerdoorn and Driankov, 1997; Babuška and Verbruggen, 2003). Also, the constant or singleton values in the consequent part of the fuzzy rules make it similar to a Mamdani Fuzzy Model and because that they are called Singleton fuzzy models (Hellerdoorn and Driankov, 1997). The linguistic model of the TSK Zero-Order Fuzzy Models using IF-THEN rules is expressed as follows:

$$R_i: \text{If } \mathbf{x}(t) \text{ is } A_i \text{ then } y_i = b_i \qquad i = 1, 2, \ldots, N \qquad \text{(A.5)}$$

where R_i, $\mathbf{x}(t)$, A_i are the i[th] fuzzy rule, the regressor vector and the i[th] antecedent of the i[th] fuzzy rule. y_i and b_i are i[th] crisp output signal and the i[th] singleton (weighting). N is the total amount of the fuzzy rules.

Babuška (1996) developed an algorithm in order to find the invert model of the Singleton fuzzy model, which is used in several control techniques (i.e. invert controller). Substituting equation (2.16) in equation (2.11) is obtained the Zero-order TSK fuzzy model is defined by the following equation:

$$y(t) = \sum_{i=1}^{N} \gamma_i(\mathbf{x}(t))\, b_i \qquad \text{(A.6)}$$

Where $y(t)$, $\gamma_i(\mathbf{x}(t))$, b_i and $\mathbf{x}(t)$ are the output signal, i[th] normalized degree of fulfilment, i[th] off-set weighting and the regressor vector.

Jang and Sun (1993) shown these fuzzy models have a similar structure to the Radial Basis Function Networks (RBFN). They have been classified as part of the basis function expansion, which are a general class of function approximators.

A.2.1.2. TSK First-Order Fuzzy Models

The TSK First-Order Fuzzy Models were developed initially in (Takagi and Sugeno, 1985; Sugeno and Kang, 1988). They often are called Affine (or Piece-Wise) Fuzzy Model (Babuška, 1996). They have a linear model plus an offset term in the consequent part (local models). In other words, they are the combination between the TSK homogeneous and Zero-Order Fuzzy Models. The linguistic model of the TSK First-Order Fuzzy Models using IF-THEN rules is defined as follows:

$$R_i: \text{If } \mathbf{x}(t) \textit{ is } A_i \text{ then } y_i = \mathbf{a}_i^T\, \mathbf{x}(t) + b_i \qquad i = 1, 2, \ldots, N \qquad \text{(A.7)}$$

where R_i, $\mathbf{x}(t)$, A_i are the i[th] fuzzy rule, the regressor vector and the i[th] antecedent of the i[th] fuzzy rule. y_i, $\mathbf{a}_i$ and b_i are i[th] crisp output signal, the i[th] parameter vector and the i[th] scalar off-set. N is the total amount of the fuzzy rules. Substituting equations (2.16) in the equation (2.11) is obtained the First-order TKS fuzzy models defined as follows:

$$y(t) = \sum_{i=1}^{N} \gamma_i(\mathbf{x}(t)) \left(\mathbf{a}_i^T \mathbf{x}(t) + b_i\right) \tag{A.8}$$

where $y(t)$, $\gamma_i(\mathbf{x}(t))$ and $y_i(\mathbf{x}(t))$ are the output signal, i[th] the normalized degree of fulfilment and the i[th] local lineal model. The parameter vector and the offset constant are defined by $\mathbf{a}_i$ and b_i. Also the global nonlinear hyperplane (model) can be approximated as follows:

$$y(t) = \sum_{i=1}^{N} \gamma_i(\mathbf{x}(t))\, \mathbf{a}_i^T \mathbf{x}(t) + \sum_{i=1}^{N} \gamma_i(\mathbf{x}(t))\, b_i = \mathbf{a}^T(\mathbf{x}(t))\, \mathbf{x}(t) + b(\mathbf{x}(t)) \tag{A.9}$$

The TSK First-Order Fuzzy Models is one the most used TSK structure because they have the better approximation capacity than the TSK Homogeneous and Zero-Order Fuzzy Models as universal approximator (Rovatti, 1996). In other words, these models eliminate the individual disadvantages that have the others two models. The first-order TKS fuzzy model can be divided in an homogeneous and a zero-order TSK fuzzy models. The affine linear models in the consequent part of the fuzzy rules have a validity region determined by the antecedent part of the fuzzy rules (Takagi and Sugeno, 1985; Babuška, 1996). The interpolation of the local hyperplanes (affine local lineal models) with dimension $\left(R^{Ny+Nu+1} + \times R\right)$ with is done in order to approximate the global nonlinear surface (or model).

A.2.2. Signal Processing and Analysis of the Layers in a NFS (Figure 2.3)

Layer 1

All the nodes in this layer are adaptive node with a node functions defined by Gaussian membership functions (activation functions) and expressed as follows:

$$\mu_{A_1}(x_1) = \exp\left(-\frac{(x_1 - c_1)^2}{2\,\sigma_1^2}\right) \tag{A.10}$$

$$\mu_{A_2}(x_1) = \exp\left(-\frac{(x_1 - c_2)^2}{2\,\sigma_2^2}\right) \tag{A.11}$$

$$\mu_{B_1}(x_2) = \exp\left(-\frac{(x_2 - c_3)^2}{2\,\sigma_3^2}\right) \tag{A.12}$$

$$\mu_{B_2}(x_2) = \exp\left(-\frac{(x_2 - c_4)^2}{2\,\sigma_4^2}\right) \tag{A.13}$$

where the c_1, σ_1, $c_2, \sigma_2, c_3, \sigma_3, c_4$ and σ_4 are the nonlinear parameters or premise parameters. x_1 and x_2 are inputs. $\mu_{A_1}(x_1), \mu_{A_2}(x_1), \mu_{B_1}(x_2)$ and $\mu_{B_2}(x_2)$ are the degree of membership of x_1 and x_2 belongs to the fuzzy sets (linguistic labels) A_1, A_2, B_1 and B_2. Equations (A.10-A.13) can be replaced by whatever membership function (i.e. triangle membership function, trapezoid membership function, etc.).

The outputs of the membership functions represent the degree of membership of the inputs x_1 and x_2 to each membership function, which represent a fuzzy set or antecedent of the fuzzy rule (Pinto, 2001; Pinto, et. al., 2004). The outputs of the Layer 1 are such as Fuzzy mapping.

Layer 2

The nodes in this layer are fixed, label with the Π symbol, which represent the product of the degree of membership (fulfilment) obtained with equations (A.10-A.13).

The outputs of the layer 2 are expressed as the product between the income signals, which are defined as follows:

$$\omega_i(x_1, x_2) = \mu_{A_j}(x_1)\,\mu_{B_k}(x_2)$$
$$i = 1,2,3,4\ ;\quad j = 1,2;\ k = 1,2 \tag{A.14}$$

The firing strength of each rule is defined by the node output. The fuzzy AND is developed by the product and also can be developed by other T-norm operators in the node function in this layer (Jang, et. al., 1997).

Layer 3

The outlet signals are the normalized signals of the income signals (i.e. the output signals of the layer 2). All the nodes in this layer are fixed and labelled with the letter "**N**", which means normalization of the income signals.

The outlet signals are defined as follows:

$$\overline{\omega}_i(x_1, x_2) = \frac{\omega_i(x_1, x_2)}{\omega_T(x_1, x_2)}\ ;\ i = 1,\ldots,4. \tag{A.15}$$

$$\omega_T(x_1, x_2) = \sum_{i=1}^{N=4} \omega_i(x_1, x_2) \tag{A.16}$$

where $\overline{\omega}_i(x_1, x_2)$ is the ith normalized degree of fulfilment (or membership).

Layer 4

All the nodes in this layer are adaptive node. The layer 4 has as activation functions, the local piece-wise linear models, which are expressed as follows:

$$y_i = f_i(x_1, x_2) = p_i\ x_1 + q_i\ x_2 + b_i\ ;\quad i = 1,\ldots,4\,. \tag{A.17}$$

where p_i, q_i, and b_i are the i[th] linear parameters or consequent parameters. y_i is the i[th] piece-wise local linear models, which are expressed also as $f_i(x_1, x_2)$.

The output signals of the layer 4 are defined by the product between the normalized degree of fulfilments (membership) with the piece-wise local linear model. These products are expressed by the following equation:

$$\hat{\omega}_i(x_1, x_2) = \overline{\omega}_i(x_1, x_2)\, y_i = \overline{\omega}_i(x_1, x_2)\,(p_i\, x_1 + q_i\, x_2 + b_i) \quad \text{with} \quad i = 1,\ldots,4. \tag{A.18}$$

where $\hat{\omega}_i(x_1, x_2)$ is the i[th] output signal of the layer 4, which is in essence nonlinear function.

Layer 5

This layer is formed by a single fixed node with symbol of Σ, which is an addition point of the all income signals and expressed as follows:

$$y = \sum_{i=1}^{N=4} \hat{\omega}_i(x_1, x_2) \tag{A.19}$$

Substituting equation (2.39) in equation (2.40) is obtained the final expression of the output signal computed using the *weighted average*, which is expressed as follows:

$$y = \sum_{i=1}^{N=4} \overline{\omega}_i(x_1, x_2)\; y_i = \sum_{i=1}^{N=4} \overline{\omega}_i(x_1, x_2)\; (p_i\; x_1 + q_i\; x_2 + b_i) \tag{A.20}$$

where y is the final output signal (nonlinear function) of the NFS. Equation (A.20) is equivalent to equations (2.27) or (2.28). The output of the Layer 5 is the Inverse Fuzzy mapping.

A.3. Training Algorithms used in ANNs and Neuro-Fuzzy Systems

The training algorithms represent an important part of the ANNs and the NFSs because the expert knowledge obtained need to be acquired in as faster as possible in order to reach the global (or local) minimum. The most common optimization algorithms used are the Backpropagations (BP) (either also called the Gradient Descent (GD) or Steepest Descent (SD)) and the Least Square Estimator (LSE) algorithms. A combination between the GD and the LSE is commonly called Hybrid Learning algorithm. Another important factor is the learning rate (or sampling time) of the optimization algorithm, which could improve of the speed of searching for the optimal solution. There exist adaptive learning rates, which can possibly improve the speed of the convergence for the optimization algorithm.

A.3.1. Definition of the Input and Output Variables for All the Layer

The BP or GD algorithm is the commonly approach used in on-line training process of the ANN and NFS.

In order to illustrate how the BP algorithm work was selected the previous NFS of Figure 2.3. The names of the variables in the example have been changing in order to apply the GD approach using the formulas exposed in the Section 2.2. Figure A.2 shows the new variables of the NFS. The equivalence between the variables in the Figures 2.3 and A.2 are:

Layer 1

$l = 1$

$$x_{1,1} = \mu_{A_1}(x_1) \qquad \text{(A.21)} \qquad x_{1,2} = \mu_{A_2}(x_1) \qquad \text{(A.22)}$$

$$x_{1,3} = \mu_{B_1}(x_2) \qquad \text{(A.23)} \qquad x_{1,4} = \mu_{B_2}(x_2) \qquad \text{(A.24)}$$

Layer 2

$l = 2$

$$x_{l,i} = \omega_i(x_1, x_2) \qquad i = 1,\ldots,4. \qquad \text{(A.25)}$$

Layer 3

$l = 3$

$$x_{l,i} = \overline{\omega}_i(x_1, x_2) \qquad i = 1,\ldots,4. \tag{A.26}$$

Layer 4

$l = 4$

$$x_{l,i} = \hat{\omega}_i(x_1, x_2) \qquad i = 1,\ldots,4. \tag{A.27}$$

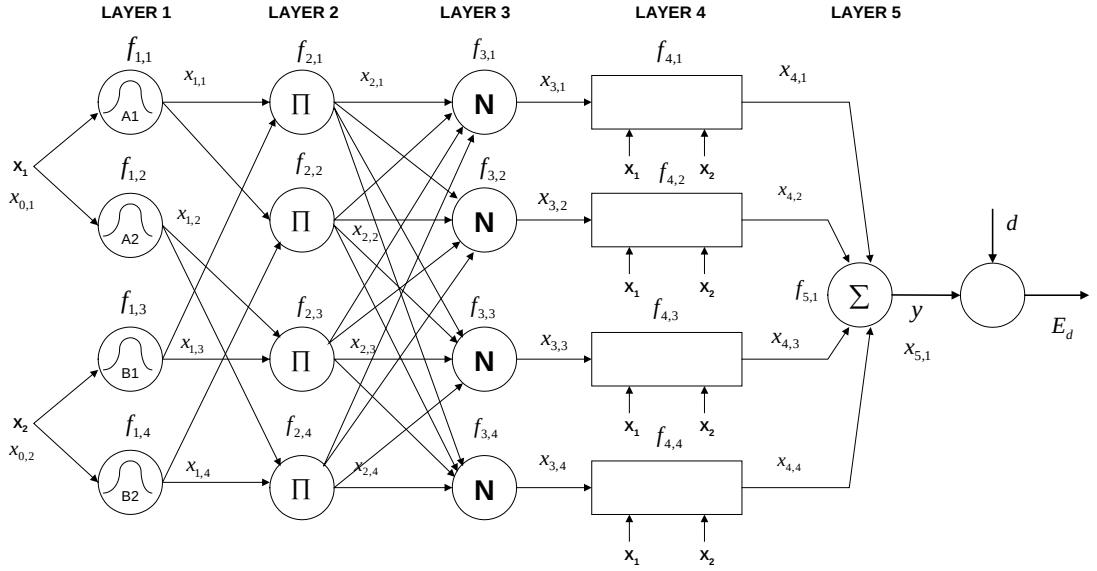

Figure A.2. Two-inputs one-output Neuro-Fuzzy System used to apply the Gradient Descent or Backpropagation Algorithm

Layer 5

$l = 5$

$$x_{5,1} = y \tag{A.28}$$

A.3.2. Application of the Gradient Descend (GD) Algorithm

In order to apply the GD algorithm, using equation (2.11), the error signal is defined as follows:

$$E_p = \left(d - x_{5,1}\right)^2 \tag{A.29}$$

This error is propagated from the output layer to the hidden layer of the NFS. Applying back-propagation error to the layer 5 gives the BP error from the output to the layer 5 and node 1 and expressed as follows:

Layer 5

$l = 5$

$$\in_{5,1} = \frac{\partial E_d}{\partial x_{5,1}} = -2\left(d - x_{5,1}\right) \tag{A.30}$$

The back-propagation error (or gradient descent error) is also applied for the rest of the layers 4, 3, 2, and 1. For the layer 4 are obtained the BP error as follows:

Layer 4

$l = 4$

$$\in_{l,i} = \in_{l+1,i} \frac{\partial f_{l+1,1}}{\partial x_{l+1,i}} \qquad i = 1,\ldots,4. \tag{A.31}$$

The activation function of the node 1 of the layer 5 is expressed as follows:

$$f_{5,1} = \sum_{i=1}^{4} x_{l,i} \qquad l = 4 \tag{A.32}$$

The partial derivatives of $f_{5,1}$ with respect to $x_{4,1}$, $x_{4,2}$, $x_{4,3}$ and $x_{4,4}$ are obtained by the following formula:

$$\frac{\partial f_{l+1,1}}{\partial x_{l,i}} = 1 \qquad i = 1,\ldots,4. \quad l = 4 \tag{A.33}$$

Substituting equation (A.33) in equation (A.31) is obtained the following equation:

$$\in_{l,i} = \in_{l+1,i} \qquad i = 1,\ldots,4. \quad l = 4 \tag{A.34}$$

where $\in_{l,i}$ is the propagating error in the l[th] layer for the i[th] node was expressed as a function of the propagating error in the (l+1)[th] layer for the i[th] node.

The activation functions of the layer 4 are defined as follows:

$$f_{l,i} = x_{l-1,\,i}\left(p_i\, x_1 + q_i\, x_2 + b_i\right) \qquad i = 1,\ldots,4. \quad l = 4 \tag{A.35}$$

Finally, the *backpropagation error without line minimization* is applied to the layer where there are parameters, computing the parameter increments $\Delta\rho_k$ as follows (Jang, et. al., 1997):

$$\Delta\rho_k = -\mu\frac{\partial E_{l,j}}{\partial\rho_k} \tag{A.36}$$

$k=1, ..., Np$

where Np is the total amount of parameter present in the l[th] layer and the j[th] node. "μ" is the leaning rate and it is defined as follows:

$$\mu = \frac{\tau}{\sqrt{\sum_{k=1}^{Np}\left[\frac{\partial E_{l,j}}{\partial\rho_k}\right]^2}} \tag{A.37}$$

The length of each transition in the parameter space along the gradient direction is called the step size "τ". This parameter has a strong influence over the speed of convergence and the stability of the Neural Network. If the step size is too small the system becomes unstable.

The parameters ρ_{k+1} are updated using the following formula:

$$\rho_{k+1} = \rho_k + \Delta\rho_k \tag{A.38}$$

Until now, the process of BP algorithm shows if the number of inputs or membership functions increase then the computation load will increase. The process of tuning for a NFS training on-line is not an easy or straightforward process because the control engineer needs to know very well the dynamic behaviour of the nonlinear plant.

A.3.3. Application of the Hybrid Learning Algorithm

The HL algorithm is used normally in two steps in the NFS. The HL is applied in off-line or on-line training modes. The off-line training method is frequently called Batch learning method. The process of application of the HL algorithm is shown in the Figure A.3. The application process of the HL algorithm is defined as follows:

1. In the first step, the linear (consequent) parameters c_1, σ_1, $c_2, \sigma_2, c_3, \sigma_3, c_4$ and σ_4 are fixed and the nonlinear parameters are computed by using the GD method (see equations A.28-A.38).

2. In the second step, the nonlinear (antecedent) parameters p_1, q_1, b_1, p_2, q_2, $b_2, p_3, q_3, b_3, p_4, q_4$ and b_4 are fixed and the linear parameters are computed by using the LSE method (see equations A.40-A.42) .

Taking into account equations (2.22-2.25) the output of the NFS obtained is expressed as follows:

$$\begin{aligned} y &= \sum_{\substack{i=1 \\ (l=4)}}^{N=4} x_{l,i} = \sum_{\substack{i=1 \\ (l=4)}}^{N=4} f_{l,i} = \sum_{\substack{i=1 \\ (l=3)}}^{N=4} x_{l,i}\left(p_i\ x_1 + q_i\ x_2 + b_i\right) \\ &= \sum_{\substack{i=1 \\ (l=3)}}^{N=4} \left[\left(x_{l,i}\ x_1\right) p_i + \left(x_{l,i}\ x_2\right) q_i + \left(x_{l,i}\right) b_i\right] \end{aligned} \tag{A.39}$$

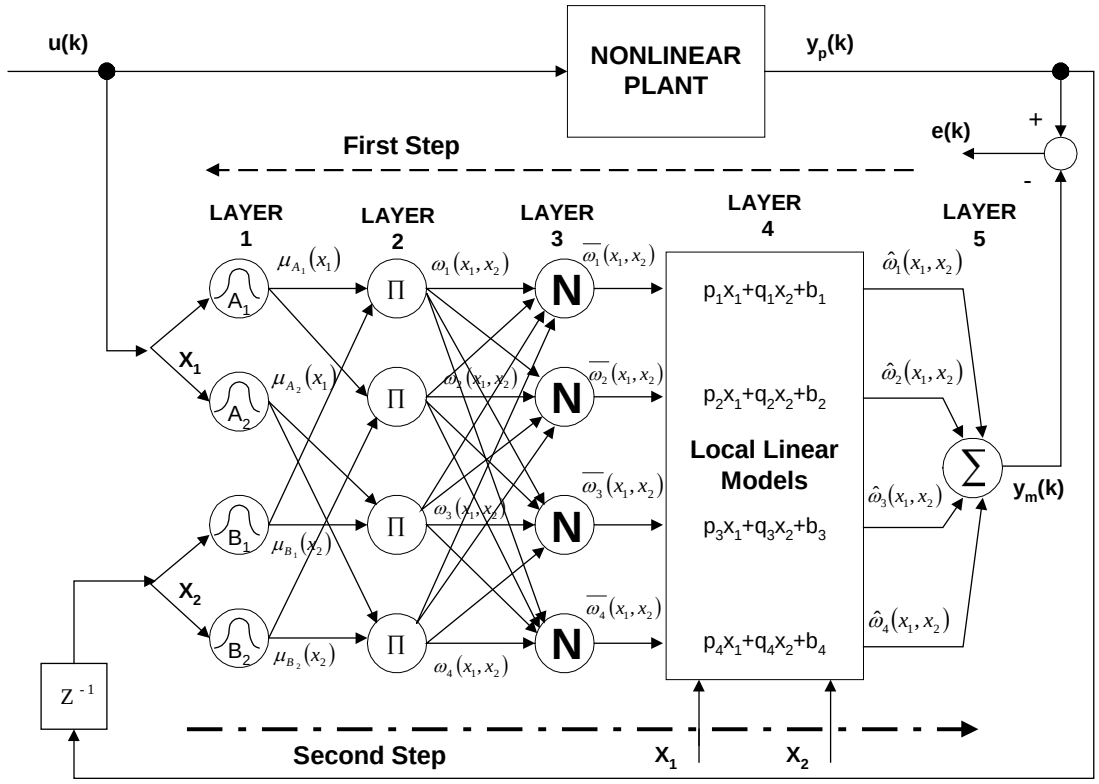

Figure A.3. Application of the First and Second Steps of the Hybrid Learning Algorithm in a Neuro-Fuzzy System

Expressing equation (A.39) in the same way as equation (A.38), the constant matrix A and the unknown parameter vector θ are defined as follows:

$$A = \begin{pmatrix} x_{3,1}x_1 & x_{3,1}x_2 & x_{3,1} & x_{3,2}x_1 & x_{3,2}x_2 & x_{3,2} & x_{3,3}x_1 & x_{3,3}x_2 & x_{3,3} & x_{3,4}x_1 & x_{3,4}x_2 & x_{3,4} \end{pmatrix}$$

(A.40)

$$\theta = \begin{pmatrix} p_1 & q_1 & b_1 & p_2 & q_2 & b_2 & p_3 & q_3 & b_3 & p_4 & q_4 & b_4 \end{pmatrix}^T \quad \text{(A.41)}$$

The LSE method is applied using the following equation:

$$\theta^* = \left(A^T\, A\right)^{-1} A^T\, y \tag{A.42}$$

where $\left(A^T\, A\right)^{-1} A^T$ and A^T are the pseudoinverse and the transpose of the constant matrix A if the matrix product $A^T A$ is a nonsingular matrix.

Another option in order to use the LSE is using the recursive LSE equation described in (Lin and Lee, 1996; Jang et. al., 1997; Nauck, et al., 1997; Pinto, et. al., 2006). The HL is often used in off-line training process. The speed of convergence of the HL is higher than the speed of convergence of the BP (or GD) algorithm (Jang, et. al., 1997).

A.4. TSK fuzzy models as Universal Approximator

The proof of the Theorem 1 is done by mean of the **Theorem 2 (Stone-Weierstrass).**

Remembering equations (A.8) and (2.12) of the Affine TSK fuzzy model

$$y(t) = \sum_{i=1}^{N} \gamma_i(\mathbf{x}(t)) \left(\mathbf{a}_i^T\, \mathbf{x}(t) + b_i\right) \tag{A.8}$$

and

$$\gamma_i(\mathbf{x}(t)) = \frac{\prod_{j=1}^{p} \exp\left[-\frac{1}{2}\left(\frac{x_j - c_{ij}}{\sigma_{ij}}\right)^2\right]}{\sum_{i=1}^{N} \prod_{j=1}^{p} \exp\left[-\frac{1}{2}\left(\frac{x_j - c_{ij}}{\sigma_{ij}}\right)^2\right]} \tag{A.43}$$

Substituting equation (A.43) in equation (A.8) is obtained the following equation:

$$y(t) = f(x) = \frac{\sum_{i=1}^{N} y_i(\mathbf{x}(t)) \prod_{j=1}^{p} \exp\left[-\frac{1}{2}\left(\frac{x_j - c_{ij}}{\sigma_{ij}}\right)^2\right]}{\sum_{i=1}^{N} \prod_{j=1}^{p} \exp\left[-\frac{1}{2}\left(\frac{x_j - c_{ij}}{\sigma_{ij}}\right)^2\right]} \tag{A.44}$$

Computing $f_1(x)$ and $f_2(x)$ as follows:

$$f_1(x) = \frac{\sum_{i1=1}^{N} y_{i1}(\mathbf{x}(t)) \prod_{j=1}^{p} \exp\left[-\frac{1}{2}\left(\frac{x_j - c_{ij}}{\sigma_{ij}}\right)^2\right]}{\sum_{i1=1}^{N} \prod_{j=1}^{p} \exp\left[-\frac{1}{2}\left(\frac{x_j - c_{ij}}{\sigma_{ij}}\right)^2\right]} \tag{A.45}$$

$$f_2(x) = \frac{\sum_{i2=1}^{N} y_{i2}(\mathbf{x}(t)) \prod_{j=1}^{p} \exp\left[-\frac{1}{2}\left(\frac{x_j - c_{ij}}{\sigma_{ij}}\right)^2\right]}{\sum_{i2=1}^{N} \prod_{j=1}^{p} \exp\left[-\frac{1}{2}\left(\frac{x_j - c_{ij}}{\sigma_{ij}}\right)^2\right]} \tag{A.46}$$

with

$$y_{i1}(\mathbf{x}(t)) = \mathbf{a}_{i1}^T \mathbf{x}(t) + b_{i1} \tag{A.47}$$

$$y_{i2}(\mathbf{x}(t)) = \mathbf{a}_{i2}^T \mathbf{x}(t) + b_{i2} \tag{A.48}$$

First, proceeding to compute $k_1 f_1(x) + k_2 f_2(x)$ is obtained as follows:

$$k_1 f_1(x) + k_2 f_2(x) =$$
$$= \frac{\sum_{i1=1}^{N}\sum_{i2=1}^{N} \left[k_1 y_{i1}(\mathbf{x}(t)) + k_2 y_{i2}(\mathbf{x}(t))\right] \prod_{j=1}^{p} \exp\left[-\frac{1}{2}\left(\frac{x_j - c_{i1j}}{\sigma_{i1j}}\right)^2 - \frac{1}{2}\left(\frac{x_j - c_{i2j}}{\sigma_{i2j}}\right)^2\right]}{\sum_{i1=1}^{N}\sum_{i2=1}^{N} \prod_{j=1}^{p} \exp\left[-\frac{1}{2}\left(\frac{x_j - c_{ij}}{\sigma_{ij}}\right)^2 - \frac{1}{2}\left(\frac{x_j - c_{i2j}}{\sigma_{i2j}}\right)^2\right]} \tag{A.49}$$

with

$$k_1\ y_{i1}(\mathbf{x}(t))+k_2\ y_{i2}(\mathbf{x}(t))=k_1\ \mathbf{a}_{i1}^T\ \mathbf{x}(t)+k_1 b_{i1}+k_2\ \mathbf{a}_{i2}^T\ \mathbf{x}(t)+k_2\ b_{i2}$$
$$=\left(k_1\ \mathbf{a}_{i1}^T+k_2\ \mathbf{a}_{i2}^T\right)\mathbf{x}(t)+\left(k_1\ b_{i1}+k_2\ b_{i2}\right) \quad \text{(A.50)}$$

Simplifying $k_1\ f_1(x)+k_2\ f_2(x)$ is obtained as follows:

$$k_1\ f_1(x)+k_2\ f_2(x)=$$
$$\frac{\sum_{i1=1}^{N}\sum_{i2=1}^{N}\left[\left(k_1\ \mathbf{a}_{i1}^T+k_2\ \mathbf{a}_{i2}^T\right)\mathbf{x}(t)+\left(k_1 b_{i1}+k_2 b_{i2}\right)\right]\prod_{j=1}^{p}\exp\left[-\frac{1}{2}\left(\frac{x_j-\frac{\sigma_{i2j}^2 C_{i1,j}+\sigma_{i1j}^2 C_{i2,j}}{\sigma_{i1j}^2+\sigma_{i2j}^2}}{\frac{\sigma_{i1j}\ \sigma_{i2j}}{\sqrt{\sigma_{i1j}^2+\sigma_{i2j}^2}}}\right)^2\right]}{\sum_{i1=1}^{N}\sum_{i2=1}^{N}\prod_{j=1}^{p}\exp\left[-\frac{1}{2}\left(\frac{x_j-\frac{\sigma_{i2j}^2 C_{i1,j}+\sigma_{i1j}^2 C_{i2,j}}{\sigma_{i1j}^2+\sigma_{i2j}^2}}{\frac{\sigma_{i1j}\ \sigma_{i2j}}{\sqrt{\sigma_{i1j}^2+\sigma_{i2j}^2}}}\right)^2\right]} \quad \text{(A.51)}$$

Then $k_1\ f_1(x)+k_2\ f_2(x)\in Y$

Second, proceeding to compute $f_1(x)\times f_2(x)$ is obtained as follows:

$$f_1(x)\times f_2(x)=$$
$$=\frac{\sum_{i1=1}^{N}\sum_{i2=1}^{N}\left[y_{i1}(\mathbf{x}(t))\times y_{i2}(\mathbf{x}(t))\right]\ \prod_{j=1}^{p}\exp\left[-\frac{1}{2}\left(\frac{x_j-c_{i1j}}{\sigma_{i1j}}\right)^2-\frac{1}{2}\left(\frac{x_j-c_{i2j}}{\sigma_{i2j}}\right)^2\right]}{\sum_{i1=1}^{N}\sum_{i2=1}^{N}\prod_{j=1}^{p}\exp\left[-\frac{1}{2}\left(\frac{x_j-c_{ij}}{\sigma_{ij}}\right)^2-\frac{1}{2}\left(\frac{x_j-c_{i2j}}{\sigma_{i2j}}\right)^2\right]} \quad \text{(A.52)}$$

Simplifying $f_1(x)\times f_2(x)$ was obtained the following equation:

$$f_1(x)\times f_2(x)=$$

$$\frac{\sum_{i1=1}^{N}\sum_{i2=1}^{N}\left[\mathbf{a}_{i1}^{T}\,\mathbf{x}(t)+b_{i1}\right]\left[\mathbf{a}_{i2}^{T}\,\mathbf{x}(t)+b_{i2}\right]\;\prod_{j=1}^{p}\exp\left[-\frac{1}{2}\left(\frac{x_j-\frac{\sigma_{i2\,j}^{2}\,C_{i1,\,j}+\sigma_{i1\,j}^{2}\,C_{i2,\,j}}{\sigma_{i1\,j}^{2}+\sigma_{i2\,j}^{2}}}{\frac{\sigma_{i1\,j}\;\sigma_{i2\,j}}{\sqrt{\sigma_{i1\,j}^{2}+\sigma_{i2\,j}^{2}}}}\right)^{2}\right]}{\sum_{i1=1}^{N}\sum_{i2=1}^{N}\;\prod_{j=1}^{p}\exp\left[-\frac{1}{2}\left(\frac{x_j-\frac{\sigma_{i2\,j}^{2}\,C_{i1,\,j}+\sigma_{i1\,j}^{2}\,C_{i2,\,j}}{\sigma_{i1\,j}^{2}+\sigma_{i2\,j}^{2}}}{\frac{\sigma_{i1\,j}\;\sigma_{i2\,j}}{\sqrt{\sigma_{i1\,j}^{2}+\sigma_{i2\,j}^{2}}}}\right)^{2}\right]} \qquad \text{(A.53)}$$

Then $f_1(x)\times f_2(x)\in Y$

Third, proceeding to compute $k\;f_1(x)$ is obtained as follows:

$$k\;f_1(x)=\frac{\sum_{i1=1}^{N}\;k\;y_{i1}(\mathbf{x}(t))\;\prod_{j=1}^{p}\exp\left[-\frac{1}{2}\left(\frac{x_j-c_{i\,j}}{\sigma_{i\,j}}\right)^{2}\right]}{\sum_{i1=1}^{N}\prod_{j=1}^{p}\exp\left[-\frac{1}{2}\left(\frac{x_j-c_{i\,j}}{\sigma_{i\,j}}\right)^{2}\right]}$$

$$=\frac{\sum_{i1=1}^{N}\left(k\,a_{i1}^{T}\,\mathbf{x}(t)+k\,b_{i1}\right)\prod_{j=1}^{p}\exp\left[-\frac{1}{2}\left(\frac{x_j-c_{i\,j}}{\sigma_{i\,j}}\right)^{2}\right]}{\sum_{i1=1}^{N}\prod_{j=1}^{p}\exp\left[-\frac{1}{2}\left(\frac{x_j-c_{i\,j}}{\sigma_{i\,j}}\right)^{2}\right]} \qquad \text{(A.54)}$$

Then $k\;f_1(x)\in Y$

Assuming that $x_1^0,\,x_2^0\in X$, $x_1^0\neq x_2^0$, $N=2$; $j=1,\,2,\,\ldots,\,p$; $y_1(\mathbf{x}(t))=1, y_2(\mathbf{x}(t))=0$, $\sigma_{i\,j}=1$, $c_{1\,j}=x_1^0$ and $c_{2\,j}=x_2^0$, we can proceed now to compute $f(x)$, $f(x_1^0)$ and $f(x_2^0)$ as follows:

$$f(x)=\frac{\sum_{i=1}^{2} y_i(\mathbf{x}(t))\ \prod_{j=1}^{p}\exp\left[-\frac{1}{2}\left(x_j-c_{ij}\right)^2\right]}{\sum_{i=1}^{N}\prod_{j=1}^{p}\exp\left[-\frac{1}{2}\left(x_j-c_{ij}\right)^2\right]}$$

$$=\frac{y_1(\mathbf{x}(t))\exp\left[-\frac{1}{2}\left[\left(x_1-c_{11}\right)^2+\left(x_2-c_{12}\right)^2+\ldots+\left(x_p-c_{1p}\right)^2\right]\right]}{den}+ \qquad \text{(A.55)}$$

$$+\frac{y_2(\mathbf{x}(t))\exp\left[-\frac{1}{2}\left[\left(x_1-c_{21}\right)^2+\left(x_2-c_{22}\right)^2+\ldots+\left(x_p-c_{2p}\right)^2\right]\right]}{den}$$

$$=\frac{y_1(\mathbf{x}(t))\exp\left[-\frac{1}{2}\left\|x-x_1^0\right\|_2^2\right]+y_2(\mathbf{x}(t))\exp\left[-\frac{1}{2}\left\|x-x_2^0\right\|_2^2\right]}{den}$$

$$den=\exp\left[-\frac{1}{2}\left[\left(x_1-c_{11}\right)^2+\left(x_2-c_{12}\right)^2+\ldots+\left(x_p-c_{1p}\right)^2\right]\right]+$$

$$\exp\left[-\frac{1}{2}\left[\left(x_1-c_{21}\right)^2+\left(x_2-c_{22}\right)^2+\ldots+\left(x_p-c_{2p}\right)^2\right]\right] \qquad \text{(A.56)}$$

$$=\exp\left[-\frac{1}{2}\left\|x-x_1^0\right\|_2^2\right]+\exp\left[-\frac{1}{2}\left\|x-x_2^0\right\|_2^2\right]$$

Substituting the values as follows:

$$f(x)=\frac{\exp\left[-\frac{1}{2}\left\|x-x_1^0\right\|_2^2\right]}{\exp\left[-\frac{1}{2}\left\|x-x_1^0\right\|_2^2\right]+\exp\left[-\frac{1}{2}\left\|x-x_2^0\right\|_2^2\right]} \qquad \text{(A.57)}$$

$$f\left(x_1^0\right)=\frac{1}{1+\exp\left[-\frac{1}{2}\left\|x_1^0-x_2^0\right\|_2^2\right]} \qquad \text{(A.58)}$$

$$f\left(x_2^0\right)=\frac{\exp\left[-\frac{1}{2}\left\|x_2^0-x_1^0\right\|_2^2\right]}{1+\exp\left[-\frac{1}{2}\left\|x_2^0-x_1^0\right\|_2^2\right]} \qquad \text{(A.59)}$$

Therefore:

$$f\left(x_1^0\right) \neq f\left(x_2^0\right) \quad \text{and} \quad x_1^0 \neq x_2^0 \tag{A.60}$$

Using this test of the Stone-Weierstrass Theorem, was proved that TSK fuzzy models are Universal Approximators.

A.5. Proof of Theorem 3

From the linear systems identification (Spooner, et. al., 2002) is well known that the output signal for a system is defined by a NARX model expressed as follows:

$$y(t) = \sum_{i=1}^{Ny} A_i \; y(t-i) + \sum_{j=0}^{Nu} B_j \; u(t-j) \tag{A.61}$$

where A_i and B_j are the delayed input and output parameters. Ny and Nu are the degree of the output and input .

Founded in the previous equation we can express a nonlinear system as follows:

$$y(t) = \sum_{i=1}^{Ny} h_i(\mathbf{x}(t)) \; y(t-i) + \sum_{j=0}^{Nu} g_j(\mathbf{x}(t)) \; u(t-j) \tag{A.62}$$

where $\mathbf{x}(t)$ is the regressor vector used in the equation (2.34). The system describes a single-input single-output (SISO) nonlinear system as a multiple-input single-output (MISO) system.

Computing the previous system with the terms, we obtained the following equation:

$$\begin{aligned} y(t+1) = {} & h_0(\mathbf{x}(t))y(t) + h_1(\mathbf{x}(t))y(t-1) + \ldots + h_{Ny}(\mathbf{x}(t))y(t-Ny) + \\ & g_0(\mathbf{x}(t))u(t) + g_1(\mathbf{x}(t))u(t-1) + \ldots + g_{Nu+1}(\mathbf{x}(t))u(t-Nu-1) \end{aligned} \tag{A.63}$$

This system is a nonlinear causal system.

The next step is use the states variables representation as follows:

$$\left.\begin{aligned} x_1(t) &= y(t) \\ x_2(t) &= y(t-1) \\ &\vdots \\ x_{Ny}(t) &= y(t-Ny) \end{aligned}\right\} \tag{A.64}$$

$$\left.\begin{aligned} u_1(t) &= u(t) \\ u_2(t) &= u(t-1) \\ &\vdots \\ u_{Nu+1}(t) &= u(t-Nu-1) \end{aligned}\right\} \tag{A.65}$$

Representing the nonlinear system in a matrix form is obtained as follows:

$$\begin{pmatrix} x_1(t+1) \\ x_2(t+1) \\ \vdots \\ x_{Ny}(t+1) \end{pmatrix} = \begin{pmatrix} h_o(\mathbf{x}(t)) & h_1(\mathbf{x}(t)) & \cdots & h_{Ny-1}(\mathbf{x}(t)) \\ 1 & 0 & \cdots & 0 \\ \vdots & \vdots & \ddots & 0 \\ 0 & 0 & \cdots & 1 \end{pmatrix} \begin{pmatrix} x_1(t) \\ x_2(t) \\ \vdots \\ x_{Ny}(t) \end{pmatrix} + \begin{pmatrix} g_0(\mathbf{x}(t)) & g_1(\mathbf{x}(t)) & \cdots & g_{Nu-1}(\mathbf{x}(t)) \\ 1 & 0 & \cdots & 0 \\ \vdots & \vdots & \ddots & 0 \\ 0 & 0 & \cdots & 1 \end{pmatrix} \begin{pmatrix} u_1(t) \\ u_2(t) \\ \vdots \\ u_{Nu+1}(t) \end{pmatrix} \tag{A.66}$$

The previous system can be generally represented as follows:

$$\mathbf{x}^1(t+1) = \mathbf{F}(\mathbf{x}(t))\,\mathbf{x}^1(t) + \mathbf{G}(\mathbf{x}(t))\,\mathbf{u}(t) \tag{A.67}$$

Taking into account $\mathbf{x}^1(t) \in R^{Ny}$, $\mathbf{u}(t) \in R^{Nu+1}$, and $\mathbf{x}^1(t), \mathbf{u}(t) \subset \mathbf{x}(t) \in R^{Ny+Nu+1}$ we can express the nonlinear system as follows:

$$\mathbf{x}^1(t+1) = \mathbf{F}(\mathbf{x}(t)) + \mathbf{G}(\mathbf{x}(t))\,\mathbf{u}(t) \tag{A.68}$$

or

$$\mathbf{x}^1(t+1) = \mathbf{F}_1(\mathbf{x}^1(t), \mathbf{u}(t)) = \mathbf{F}_1(\mathbf{x}(t)) \tag{A.69}$$

with

$$\mathbf{x}(t) = \left[\mathbf{x}^1(t)\ \ \mathbf{u}(t)\right]^T \quad \text{(regressor vector)} \tag{A.70}$$

and

$$\mathbf{x}^1(t) = \left[y(t), \ldots, y(t - Ny)\right] \quad \text{(input lagged vector)} \tag{A.71}$$

and

$$\mathbf{u}(t) = \left[u(t), \ldots, y(t - Nu - 1)\right] \quad \text{(output lagged vector)} \tag{A.72}$$

with $\mathbf{x}^1(t), \mathbf{u}(t) \subset \mathbf{x}(t) \in R^{Ny+Nu+1}$, where $\mathbf{F}_1(\cdot)$ represent a nonlinear system. The degree of $\mathbf{x}(t)$ is defined by $(Ny + Nu + 1)$. The **definition 5** has been proved with the previous result.

The nonlinear function $\mathbf{F}_1(\cdot)$ is a causal system with the degree of $(Ny + Nu + 1)$. The conditions for the causal systems imply:

$$Nu \leq Ny \tag{A.73}$$

Substituting the condition of the causal systems in the degree of the system is obtained as follows:

$$Ny \leq 2\,Nu + 1 \tag{A.74}$$

Finally the complete condition for the Causal Nonlinear system with the NARX model is expressed as follows:

$$Nu \leq Ny \leq 2\,Nu + 1 \tag{A.75}$$

The alone equation proves **Theorem 3**.

A.6. Proof of the Theorem 4

Remembering the equation (A.8) a Neuro-Fuzzy system for SISO systems could be expressed as follows:

$$y(t) = \sum_{i=1}^{N} \gamma_i \left(\mathbf{a}_i^T \, \mathbf{x}(t) + b_i \right) \tag{A.76}$$

with $\mathbf{a}_i^T = \left[a_i^1, \cdots, a_i^{Ny}, c_i^0, \cdots, c_i^{Nu} \right]$

and $\mathbf{x}(t) = \left[y(t-1), \cdots, y(t-Ny), u(k), \cdots, u(t-Nu) \right]^T$

By definition the product $\mathbf{a}_i^T \, \mathbf{x}(t)$ can be expressed as follows:

$$\begin{aligned} \mathbf{a}_i^T \, \mathbf{x}(t) &= \left[a_i^1, \cdots, a_i^{Ny}, c_i^0, \cdots, c_i^{Nu} \right] \left[y(t-1), \cdots, y(t-Ny), u(k), \cdots, u(t-Nu) \right]^T \\ &= \sum_{j=1}^{Ny} a_i^j \; y(t-j) + \sum_{j=0}^{Nu} c_i^j \; u(t-j) \end{aligned} \tag{A.77}$$

Combining the equations (A.76) and (A.77) is obtained as follows:

$$y(t) = \sum_{i=1}^{N} \gamma_i \sum_{j=1}^{Ny} a_i^j \; y(t-j) + \sum_{i=1}^{N} \gamma_i \sum_{j=0}^{Nu} c_i^j \; u(t-j) + \sum_{i=1}^{N} \gamma_i \; b_i \tag{A.78}$$

Expanding the previous formula is obtained the following equation:

$$\begin{aligned} y(k) = {} & \gamma_1 \left[a_1^1 \; y(t-1) + a_1^2 \; y(t-2) + \ldots + a_1^{Ny} \; y(t-Ny) \right] + \\ & \gamma_2 \left[a_2^1 \; y(t-1) + a_2^2 \; y(t-2) + \ldots + a_2^{Ny} \; y(t-Ny) \right] + \ldots + \\ & \gamma_N \left[a_N^1 \; y(t-1) + a_N^2 \; y(t-2) + \ldots + a_N^{Ny} \; y(t-Ny) \right] + \\ & \gamma_1 \left[c_1^0 \; u(t) + c_1^1 \; u(t-1) + \ldots + c_1^{Nu} \; u(t-Nu) \right] + \\ & \gamma_2 \left[c_2^0 \; u(t) + c_2^1 \; u(t-1) + \ldots + c_2^{Nu} \; u(t-Nu) \right] + \ldots + \\ & \gamma_N \left[c_N^0 \; u(t) + c_N^1 \; u(t-1) + \ldots + c_N^{Nu} \; u(t-Nu) \right] + \\ & \gamma_1 b_1 + \gamma_2 b_2 + \ldots + \gamma_N b_N \end{aligned} \tag{A.79}$$

Factorizing the lagged inputs and outputs in the formula (A.79) can be obtained in a extended form the Fuzzy Difference Equation as follows:

$$\begin{aligned} y(t) = {} & \left[\gamma_1 \; a_1^1 + \gamma_2 \; a_2^1 + \ldots + \gamma_N \; a_N^1 \right] y(t-1) + \left[\gamma_1 \; a_1^2 + \gamma_2 \; a_2^2 + \ldots + \gamma_N \; a_N^2 \right] y(t-2) \\ & + \ldots + \left[\gamma_1 \; a_1^{Ny} + \gamma_2 \; a_2^{Ny} + \ldots + \gamma_N \; a_N^{Ny} \right] y(t-Ny) + \\ & \left[\gamma_1 \; c_1^0 + \gamma_2 \; c_2^0 + \ldots + \gamma_N \; c_N^0 \right] u(t) + \left[\gamma_1 \; c_1^1 + \gamma_2 \; c_2^1 + \ldots + \gamma_N \; c_N^1 \right] u(t-1) \\ & + \ldots + \left[\gamma_1 \; c_1^{Nu} + \gamma_2 \; c_2^{Nu} + \ldots + \gamma_N \; c_N^{Nu} \right] u(t-Nu) + \gamma_1 b_1 + \gamma_2 b_2 + \ldots + \gamma_N b_N \end{aligned} \tag{A.80}$$

Expressing the Fuzzy Difference Equation using a general formula is obtained the proof for the **Theorem 4** for SISO Systems as follows:

$$y(t) = \sum_{j=1}^{Ny} \sum_{i=1}^{N} \gamma_i \; a_i^j \, y(t-j) + \sum_{j=0}^{Nu} \sum_{i=1}^{N} \gamma_i \; c_i^j \, u(t-j) + \sum_{i=1}^{N} \gamma_i \; b_i \tag{A.81}$$

For the MIMO Neuro-Fuzzy Systems:

$$y_M(t) = \sum_{i=1}^{N} \gamma_{i,M} \; \left(\mathbf{a}_{i,M}^T \; \mathbf{x}(t) + b_{i,M} \right) \tag{A.82}$$

with

$$\begin{aligned} \mathbf{a}_{i,M}^T = \big[& a_{i,1,M}^1, a_{i,2,M}^1, \cdots, a_{i,m,M}^1, \cdots, a_{i,1,M}^{Ny}, a_{i,2,M}^{Ny}, \cdots, a_{i,m,M}^{Ny}, \; c_{i,1,M}^0, c_{i,2,M}^0, \cdots, c_{i,n,M}^0, \cdots \\ & c_{i,1,M}^1, c_{i,2,M}^1, \cdots, c_{i,n,M}^1, \cdots, c_{i,1,M}^{Nu}, c_{i,2,M}^{Nu}, \cdots, c_{i,n,M}^{Nu} \big] \end{aligned}$$

and

$$\mathbf{x}(t)=[y_1(t-1),y_2(t-1),\cdots,y_m(t-1),\cdots,y_1(t-Ny),y_2(t-Ny),\cdots,y_m(t-Ny),u_1(t),u_2(t),\cdots,u_n(t),u_1(t-1),u_2(t-1),\cdots,u_n(t-1),\cdots,u_1(t-Nu),u_2(t-Nu),\cdots,u_n(t-Nu)]^T$$

Developing $\mathbf{a}_{i,M}^T\ \mathbf{x}(t)$ as follows:

$$\mathbf{a}_{i,M}^T\ \mathbf{x}(t)=$$

$$\mathbf{a}_{i,M}^T\ \mathbf{x}(t)=[a_{i,1,M}^1,a_{i,2,M}^1,\cdots,a_{i,m,M}^1,\cdots,a_{i,1,M}^{Ny},a_{i,2,M}^{Ny},\cdots,a_{i,m,M}^{Ny},\ c_{i,1,M}^0,c_{i,2,M}^0,\cdots,c_{i,n,M}^0,\cdots c_{i,1,M}^1,c_{i,2,M}^1,\cdots,c_{i,n,M}^1,\cdots,c_{i,1,M}^{Nu},c_{i,2,M}^{Nu},\cdots,c_{i,n,M}^{Nu}]\ [y_1(t-1),y_2(t-1),\cdots,y_m(t-1),,\cdots,y_1(t-Ny),y_2(t-Ny),\cdots,y_m(t-Ny),u_1(t),u_2(t),\cdots,u_n(t),u_1(t-1),u_2(t-1),u_n(t-1),\cdots,u_1(t-Nu),u_2(t-Nu),\cdots,u_n(t-Nu)]^T$$

Developing the product as follows:

$$\mathbf{a}_{i,M}^T\ \mathbf{x}(t)=a_{i,1,M}^1y_1(t-1)+a_{i,2,M}^1y_2(t-1)+\cdots+a_{i,m,M}^1y_m(t-1)+\cdots+a_{i,1,M}^{Ny}y_1(t-Ny)+a_{i,2,M}^{Ny}y_2(t-Ny)+\cdots+a_{i,m,M}^{Ny}y_m(t-Ny)+c_{i,1,M}^0u_1(t)+c_{i,2,M}^0u_2(t)+\cdots+c_{i,n,M}^0u_n(t)+c_{i,1,M}^1u_1(t-1)+c_{i,2,M}^1u_2(t-1)+\cdots+c_{i,n,M}^1u_n(t-1)+\cdots+c_{i,1,M}^{Nu}u_1(t-Nu)+c_{i,2,M}^{Nu}u_2(t-Nu)+\cdots+c_{i,n,M}^{Nu}u_n(t-Nu)$$

Rearrange the terms as follows:

$$\mathbf{a}_{i,M}^T\ \mathbf{x}(t)=a_{i,1,M}^1y_1(t-1)+\cdots+a_{i,m,M}^1y_m(t-1)+a_{i,2,M}^1y_2(t-1)+\cdots+a_{i,2,M}^{Ny}y_2(t-Ny)+a_{i,m,M}^1y_m(t-1)+\cdots+a_{i,m,M}^{Ny}y_m(t-Ny)+c_{i,1,M}^0u_1(t)+c_{i,1,M}^1u_1(t-1)+\cdots+c_{i,1,M}^{Nu}u_1(t-Nu)+c_{i,2,M}^0u_2(t)+c_{i,2,M}^1u_2(t-1)+\cdots+c_{i,2,M}^{Nu}u_2(t-Nu)+c_{i,n,M}^0u_n(t)\ c_{i,n,M}^1u_n(t-1)+\cdots+c_{i,n,M}^{Nu}u_n(t-Nu)$$

Representing the terms as series as follows:

$$\mathbf{a}_{i,M}^T\ \mathbf{x}(t)=\sum_{j=1}^{Ny}a_{i,1,M}^j\ y_1(t-j)+\sum_{j=1}^{Ny}a_{i,2,M}^j\ y_2(t-j)+\ldots+\sum_{j=1}^{Ny}a_{i,m,M}^j\ y_m(t-j)+\sum_{k=0}^{Nu}c_{i,1,M}^j\ u_1(t-k)+\sum_{k=0}^{Nu}c_{i,2,M}^j\ u_2(t-k)+\ldots+\sum_{j=1}^{Nu}c_{i,n,M}^j\ u_n(t-k)$$

Developing the equation (A.82) and expressing the Fuzzy Difference Equation using a general formula is obtained the proof for the **Theorem 4** for MIMO Systems as follows:

$$y_M(t) = \sum_{l=1}^{m}\sum_{j=1}^{Ny}\sum_{i=1}^{N}\gamma_{i,M}\, a_{i,l,M}^{j}\, y_l(t-j) + \sum_{z=1}^{n}\sum_{k=0}^{Nu}\sum_{i=1}^{N}\gamma_{i,M}\, c_{i,l,M}^{k}\, u_z(t-k) + \sum_{i=1}^{N}\gamma_{i,M}\, b_{i,M} \quad \text{(A.83)}$$

APPENDIX B

B.1. Nonlinear Generalised Minimum Variance Control Law

Figure B.1 shows the basic structure of the Nonlinear Generalised Minimum Varianc**e** Controller Dynamically Weighted (Grimble, 2003). The process W is a nonlinear process. It is assumed that the reference and disturbance models are linear. The input signals $\{\varsigma(t)\}$ and $\{\xi(t)\}$ are considered as zero-mean white noises with identity covariance matrices. One of the more important assumptions is there exist a PID controller, which stabilize the nonlinear process.

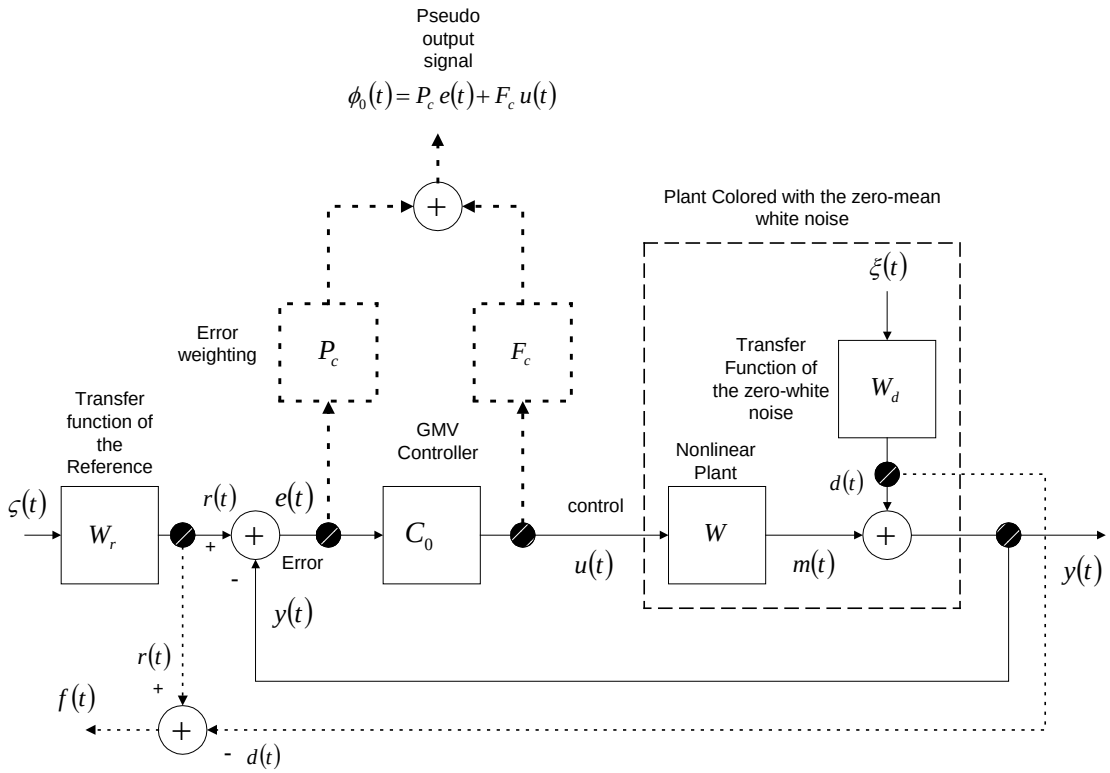

Figure B.1 Basic Structure of the Nonlinear Generalised Minimum Variance Controller Dynamically Weighted

B.1.1. Signals of the NGMV Controller Dynamically Weighted

Figure B.1 shows the complete set of signals present in the NGMV controller dynamically weighted. There are two "*pseudo signals*" in the block diagram of the Figure B.1, the combined signal $f(t)$ and the pseudo output signal $\phi(t)$. The signals are defined as follows:

Error signal: $e(t) = r(t) - y(t)$ (B.1)

Reference: $r(t) = W_r\, \varsigma(t)$ (B.2)

Nonlinear plant: $y(t) = (W\,u)(t) + d(t)$ (B.3)

Disturbance model: $d(t) = W_d\ \xi(t)$ (B.4)

Combined signal: $f(t) = r(t) - d(t)$ (B.5)

The power spectrum of the combined signal Φ_{ff} and the generalised spectral factor Y_f (assumed to be strictly minimum phase) are defined as:

$$\Phi_{ff} = \Phi_{rr} + \Phi_{dd} = W_r W_r^* + W_d W_d^* \quad \text{(B.6)}$$

$$Y_f\, Y_f^* = \Phi_{ff} \quad \text{(B.7)}$$

B.1.2. Subsystem Models of the NGMV

The subsystems model can be represented by left-coprime polynomial matrices. They are expressed by the following formulas:

Disturbance model: $W_d(z^{-1}) = A^{-1}(z^{-1})C_d(z^{-1})$ (B.8)

Reference model: $W_r\left(z^{-1}\right) = A^{-1}\left(z^{-1}\right)E_r\left(z^{-1}\right)$ (B.9)

Linear plant subsystem: $W_{0k}\left(z^{-1}\right) = A^{-1}\left(z^{-1}\right)B_{0k}\left(z^{-1}\right)$ (B.10)

The common denominator polynomial matrix of the previous models is defined as $A^{-1}\left(z^{-1}\right)$. In order to make easier the formulas the arguments of the polynomial matrices is omitted $\left(i.e.\ A^{-1} = A^{-1}\left(z^{-1}\right)\right)$.

Nonlinear time-varying plant model:

The nonlinear time-varying plant model is defined as the product between the function of the model of nonlinear time-varying plant $W(t)$ and its input signal $u(t)$. $W(t)$ is assumed to be expressed as the product between the delay matrix D_k and the free delay nonlinear plant W_k .

$$W(t)\,u(t) = (W\ u)(t) = D_k\,(W_k\ u)(t) \tag{B.11}$$

where the delay matrix D_k is a diagonal matrix, which contains the common delay elements with respect to the output signal paths and it is expressed by:

$$D_k = diag\ \left\{z^{-k_1},\ z^{-k_2},\ldots,z^{-k_r}\right\} \tag{B.12}$$

or

$$D_k = \begin{bmatrix} z^{-k_1} & 0 & 0 & 0 \\ 0 & z^{-k_2} & 0 & 0 \\ 0 & 0 & \ddots & 0 \\ 0 & 0 & 0 & z^{-k_r} \end{bmatrix} \tag{B.13}$$

The choice of the previous matrix as a diagonal matrix is because the nonlinearities and the internal interactions between loops are included in the free delay nonlinear plant model $W_k(t)$. The linear plant subsystem of the equation (B.10) is stable/unstable linear time invariant block, which has all unstable modes of the nonlinear plant W. The free delay nonlinear plant is expressed as follows:

$$W_k(t)\,u(t) = (W_k\ u)(t) = W_{0k}(W_{1k}\ u)(t) \tag{B.14}$$

where $W_{0k}(t)$ and $W_{1k}(t)$ are the linear time invariant block and the nonlinear invariant block.

The complete nonlinear plant model is obtained by substituting the equation (B.14) in the equation (B.11) as follows:

$$W(t)\,u(t) = (W\ u)(t) = D_k(W_k\ u)(t) = D_k\,W_{0k}(t)\,W_{1k}(t)\,u(t) = D_k\,W_{0k}(W_{1k}\ u)(t) \tag{B.15}$$

B.1.2.1. Optimization Problem

The optimization problem is based on the minimization of the variance pseudo output signal $\phi_0(t)$ as follows:

$$\phi_0(t) = P_c\,e(t) + F_c\ u(t) \tag{B.16}$$

where P_c and F_c are the dynamic error and control weightings. Sometimes, this pseudo output signal $\phi_0(t)$ can be a signal which can not be measured in a direct manner. The cost function to be minimized is defined as follows:

$$J = E\left\{\phi_0^T(t)\phi_0(t)\right\} = E\left\{trace\left\{\phi_0^T(t)\phi_0(t)\right\}\right\} \tag{B.17}$$

where the expectation operator is defined as $E\{\cdot\}$.

The philosophy for the selection of the dynamic weightings is made selecting the dynamic error weighting P_c as a low-pass filter and dynamic control weightings as a high-pass filter. In other words, the intention is to build a band-pass filter through the individual contributions of the dynamic weightings in the frequency domain. The dynamic error weighting implies a $(r \times m)$ matrix defined as follows:

$$P_c\left(z^{-1}\right) = P_{cd}^{-1}\left(z^{-1}\right)\ P_{cn}\left(z^{-1}\right) \tag{B.18}$$

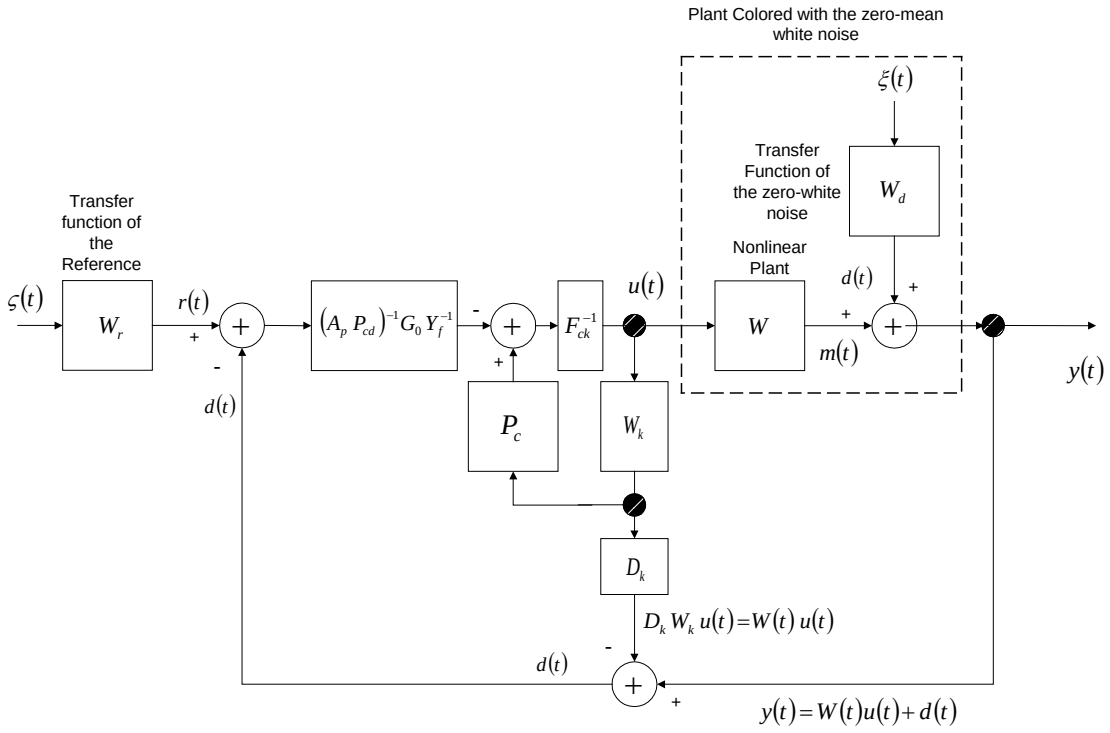

Figure B.2 First Structure of the Nonlinear Generalised Minimum Variance Controller

The product between the control weighting F_c and the control signal $u(t)$ is well known as *nonlinear dynamic control signal costing operator term* $F_c(t)\,u(t) = (F_c\,u)(t)$ (with dimension m-square). From the equations (B.12) and (B.13), $\{k_1, k_2, \ldots, k_r\}$ are the smallest of the delays present in each output path, respectively. In other words, the j^{th} output is affected k_j steps later by the control

signal at time t. The *nonlinear dynamic control signal costing operator term* can be defined as follows:

$$F_c(t)\,u(t) = (F_c\,u)(t) = D_k\,(F_{ck}\,u)(t) \tag{B.19a}$$

where the control weighting operator F_{ck} is assumed to be invertible with full rank in the linear case or a diffeomorphism in the nonlinear case (Isidori, 1995) in order to cancel the nonlinearities of the plant. The control weighting can be expressed by the following equation:

$$F_c\left(z^{-1}\right) = D_k F_{ck}\left(z^{-1}\right) = D_k F_{cd}^{-1}\left(z^{-1}\right) F_{cn}\left(z^{-1}\right) \tag{B.19b}$$

After substitute the equation (3.2) in the equation (3.27) is obtained the following result:

$$u(t) = F_{ck}^{-1}\left(\left(A_p\,P_{cd}\right)^{-1} P_{cf}\,D_f\,Y_f^{-1} W_k(t) u(t) - \left(A_p\,P_{cd}\right)^{-1} G_0\,Y_f^{-1}\left(r(t) - d(t)\right)\right) \tag{B.20}$$

Dynamically Weighted as a Nonlinear Smith Predictor with Internal Model. The Figure B.2 belongs to the block diagram of the equation B.20.

Appendix C

C.1. Linear Model Based Predictive Control

Predictive control is one of the most widely used advanced forms of control used in industry. The reason for this is due to the fact that predictive control algorithms can easily be adjusted to allow constraint handling, that it allows for multivariable control without any extra complexity and that it can be intuitively tuned. Implicitly, a linear MBPC with constraint is a NMBPC approach (Maciejowski, 2002). Feedforward control was also easily accommodated, by using the model-based aspect of the control.

The control method used was that presented by Krauss and partners (1994), a predictive controller based on a system model as follows, requiring the standard state vector $x(k)$, found by identification, to be augmented to include $u(k)$:

$$\begin{aligned} x(k+1) &= A\,x(k) + B\,\Delta u(k) + B_d\,d(k) \\ y(k) &= C\,x(k) + D\,\Delta u(k) + D_d\,d(k) \end{aligned} \qquad \text{(C.1)}$$

This form allows for the inclusion of measured disturbance $d(k)$, allowing the controller to take into account system inputs that are uncontrolled.

Further disturbance modelling by the inclusion of a constant disturbance state allows the controller to compensate for the plant-model mismatch and reject disturbances in the system, for example, changes in influent or river characteristics due to storm conditions, as shown in Maciejowski (2002). In Krauss et al (1994), the equation for the predicted output was shown to be

$$\hat{y}(k) = F\hat{x}(k) + H\,\Delta u(k) \qquad \text{(C.2)}$$

The matrices *F* and *H* in the above prediction equation were found by iteration of the linear model over the controller prediction horizon, H_p, and are of the following form, where H_u is the control horizon:

$$F = C\begin{bmatrix} A \\ \vdots \\ A^{H_p} \end{bmatrix} \qquad \text{(C.3)}$$

$$H = C\begin{bmatrix} B & \cdots & 0 \\ \vdots & \ddots & \\ \sum_{i=0}^{H_p-1} A^i B & \cdots & \sum_{i=0}^{H_p-H_u} A^i B \end{bmatrix} \qquad \text{(C.4)}$$

The error, upon which the controller must act, was calculated using the estimated augmented states, the setpoint $R(k)$, and the input and measured disturbance $d(k)$ values:

$$E(k) = R(k) - F\,\hat{x}(k) - \Xi\, d(k) \tag{C.5}$$

It can be seen therefore that state estimation was required, and so a simple pole-placement estimator calculates the states. By optimisation of the process cost function is expressed as follows:

$$J = \left\| H\,\Delta u(k) - E(k) \right\|_Q^2 + \left\| \Delta u(k) \right\|_\lambda^2 \tag{C.6}$$

with respect to $Du(k)$, where Q and λ are the error and control change weights respectively, the optimal control input $Du(k)$ was found. In constraint handling, Maciejowski (2002) shows the method of implementing constraints defined by inequalities (on the input changes, the input range, and the output range, respectively):

$$E\begin{bmatrix} \Delta u(k) \\ 1 \end{bmatrix} \le 0 \qquad F\begin{bmatrix} \Delta u(k) \\ 1 \end{bmatrix} \le 0 \qquad G\begin{bmatrix} Z(k) \\ 1 \end{bmatrix} \le 0 \tag{C.7}$$

These constraints were implemented during the cost function minimisation, as constraints on the optimisation problem. The control of parameters in the wastewater treatment plant requires only linear predictive control methods. However, with the addition of the river dynamics to the control objective, significant nonlinearity was introduced, requiring nonlinear control methodology.

APPENDIX D

D.1. The Car Engine Model

The car engine model was obtained via system identification using a grey-box model with driving cycle data collected for the Federal Test Procedure (FTP) from the Chevrolet Corvette with V8 5.7L engine. During the driving cycle all the data were collected. The complete model was split into several subsystems and after that, the subsystems were identified with the driving cycle data (Dutka, 2005):

1) Using the upstream engine sensor information for the identification of the intake manifold model.

2) Using the measured air-fuel ratio to identify the fuel path model

3) Assuming the air-fuel ratio is near to complete stoichiometry combustion with a particular engine torque.

Also, in order to validate the air-fuel model several criteria were used such as the integral absolute, integral squared error and a correlation between the measured and estimated variable. During the FTP, the transient and steady state error in the air-fuel ratio were included. The current air-fuel ratio was measured after a long time period when the fuel injection was completed because of the engine operating cycle and a considerable transport delay in the exhaust manifold. An accurate air-fuel ratio control can be obtained founded in an accurate modelling of the engine forward path. Conventional control systems have poor performance because of the delayed measurement of the air-fuel ratio.

D.1.1. Development of the Car Engine Model

The physical laws and black box were used to develop the car engine model, which means the use of it to reproduce several dynamic behaviours. On the other hand, the

physical model for parameter estimation was developed using physical laws that govern the process.

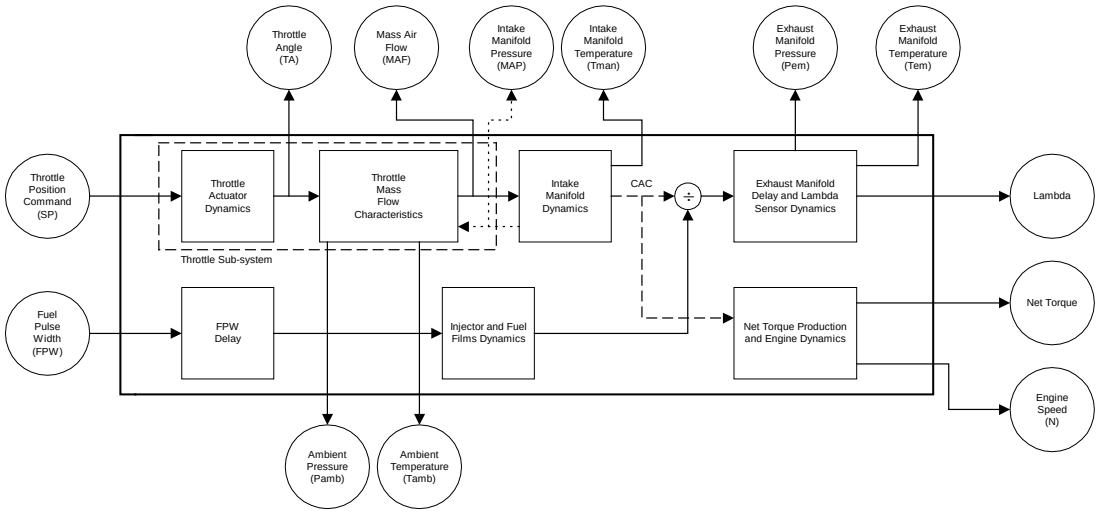

Figure D.1. Block Diagram of the Spark Engine Model

The important measurements and input/output variables of the spark engine model are described in the Figure D.1. The input variables are the throttle position command (SP) and the fuel pulse width (FPW). The output variables are the Lambda (normalised air-fuel ratio), net torque and the engine speed (N). The indicated throttle angle (TA), mass airflow rate (MAF), ambient pressure $\left(P_{amb}\right)$ and ambient temperature $\left(T_{amb}\right)$ are measured in the throttle sub-system.

Intake manifold pressure (MAP) and intake manifold gas temperature (T_{man}) are measured in the intake manifold sub-system. The sub-systems (sub-models) were developed by Dutka (2005). Measurements of Gas pressure (P_{em}), gas temperature (T_{em}) and the exhaust air-fuel ratio (called as lambda or AFR) are available in the exhaust manifold sub-system. In addition, the measurement of the engine torque is straightforward taken from the crankshaft. Nevertheless, the coolant temperature and engine speed (N) measurements are available as well.

The blocks belonging to the throttle mass flow characteristic, intake manifold dynamics, the injector and the fuel film dynamics have to be identified separately by selecting the adequate structure of the model as a black or a grey box. The throttle position indirectly controls the torque by means of the pedal position. The control strategy used in the car engine model was the feedforward control system which is a nonlinear function of the throttle position (TA) and several upstream engine parameters (i.e. MAF, MAP).

The output of the intake manifold dynamics is the cylinder air charge (CAC) identified using measurements. However, take the measurement of the CAC is not possible and because of that, it is necessary to obtain a physical model of the intake manifold in order to identify the CAC model through a grey-box approach. The laws of mass and energy balance were applied to the intake manifold to establish the physical model and several measured parameters (i.e. MAP, T_{man}, MAF) were the base for the identification. The fuel delivery model was identified using only the lambda measurement. In order to identity the model of the fuel delivery and lambda λ measurement path may be used CAC as identification parameter. For an effective identification it is necessary to consider together the intake manifold and the fuel dynamics models.

The multivariable control structure for the automotive powertrain has mainly two inputs or manipulated variables (i.e. throttle position and the fuel pulse width) and two outputs (i.e. air-fuel ratio and the torque). The most challenging problems in the identification were the time-varying delay and the fast transients added to the high nonlinearities included in the car engine system.

D.1.2. Dynamic Model of the Throttle Actuator

The driver or the engine controller (PCM) defines the input signal to the throttle actuator (or electronic throttle). The driving cycle dataset was used to identify the actuator model. The nonlinear model of the throttle was linearised and discretized

(using the sampling rate which is inversely proportional to the engine speed) with enough accuracy.

Every 90^o crank angles, the throttle position set point and the throttle angle were sampled. After that, both signals were re-sampled, keeping constant the sampling time using the interpolation of the previous sampled signals. The discrete model was obtained using the re-sampled signals. The least square method was used in the identification. A second order discrete model was selected for identification, which is as follows:

$$TPS_{n+1} = -p_1(N_n)\,TPS_n - p_2(N_n)\,TPS_{n-1} + p_3(N_n)\,SP_n + p_4(N_n)\,SP_{n-1} \quad \text{(D.1)}$$

where TPS_n ,SP_n and N_n are the indicated throttle position [V], the throttle setpoint (input to the ET) [V] and the engine speed [rpm]. The discrete model parameters were defined as $p_i(N_n), i = 1,2,3,4.$ A second order discrete model was selected by Dutka (2005) because it produce a more accurate model with all its poles inside of the unit circle (stable system).

Each 90 degrees sampling event, the sampling time used was expressed as $T_{s,i} = 15/N_i$ (using the least square parameters regression for the identification).

The dynamics of the poles and zeros of the models were located between 200 and 3100 rpm. The engine speed defines the variation of the discrete time dynamics. These are the discrete values of the vector; N_{thr}= [200, 250, …, 1200, 1300, …,3100] using the nearest values computed by interpolation in order to identify the parameters $p_i(N_n), i = 1,2,3,4$.

D.1.2.1. Throttle Flow Rate Model

A relationship between the throttle position and the mass airflow through the throttle was described by the throttle flow rate model. An angle α between the closed

throttle plate position and the current position was developed as a linear function of TPS_n. The expression for α was defined as follows:

$$\alpha = k_{Thr}\, TPS_n + O_{Thr} \tag{D.2}$$

where k_{Thr} and O_{Thr} are constant parameters.

As a one-dimensional isentropic compressible flow equation for flow through the orifice (without choked flow) was assumed the throttle body model structure is as follows (Dutka, 2005):

$$\dot{m}_{at} = C_d\, A_{th}(\alpha)\, \frac{P_a}{[R_{air}\, T_a]^{1/2}} \left[\frac{P_{im}}{P_a}\right]^{1/k} \sqrt{\frac{2\,k}{k-1}\left(1 - \left[\frac{P_{im}}{P_a}\right]^{\frac{k-1}{k}}\right)} \tag{D.3}$$

with $C_d = f\left(\frac{P_{im}}{P_a}, \alpha\right)$

where $\dot{m}_{at}$, C_d , $A_{th}(\alpha)$, P_{im}, P_a and T_a are the throttle mass flow rate, the discharge coefficient, the throttle cross-sectional area, downstream pressure (intake manifold), the upstream pressure (ambient) and the upstream temperature (ambient). k and R_{air} are the ratio of specific heats and the ideal gas constant for dry air.

On the other hand, for chocked flow (Dutka, 2005):

$$\frac{P_{im}}{P_a} \leq \left[\frac{2}{k+1}\right]^{\frac{k}{k-1}} \tag{D.4}$$

and

$$\dot{m}_{at} = C_d\, A_{th}(\alpha)\, \frac{P_a}{[R\, T_a]^{1/2}}\, \sqrt{k}\left[\frac{2}{k-1}\right]^{\frac{k+1}{2[k-1]}} \tag{D.5}$$

and the cross-sectional area $A_{th}(\alpha)$ was defined as follows:

$$A_{th}(\alpha) = \pi\, R_{th}^2 \left[1 - \frac{cos(\alpha+\alpha_0)}{cos(\alpha_0)}\right] \tag{D.6}$$

where R_{th}, α_0 and α are the radius of the throttle, the throttle offset angle (minimum throttle angle) and the throttle angle.

D.1.2.2. Model of the airflow sensor

Airflow sensor (MAF) was modelled with a first order system as follows (Dutka, 2005):

$$MAF = \frac{1}{s T_{MAF}+1} \dot{m}_{at} \tag{D.7}$$

where MAF, T_{MAF} and $\dot{m}_{at}$ are the throttle mass flow measurement, the MAF sensor time constant and the throttle mass flow rate.

The main sampling rate is lower than the internal sampling time of the sensor. The time constant of the MAF sensor was $T_{MAF} = 5\ [ms]$ but in order to be able to identify the sensor dynamic model the data were sampled five times than the shorter sampled period (i.e. 1 [ms]). The model in (D.7) was inverted in order to reconstruct the current flow rate with the time constant available from another experiment. With the assumption that $m_{at} \cong MAF$, the parameters of equation (D.3) were identified.

D.1.2.2.1. Estimation of the airflow parameters

The radius of the throttle and throttle offset angle were known by measurements previously to the identification. The structure of the identified discharge coefficient map $C_d = f\left(\frac{p_{im}}{p_a}, \alpha\right)$ is a complex function, and because of that a two dimensional resource of look-up table (black-box approach) was used. Uncertainties in the model due to the cross-sectional area $A_{th}(\alpha)$ were compensated by the C_d coefficient.

A nonlinear static model of the mass airflow through the throttle (equation (D.3) or (D.5)) was described as a function of the P_a, T_a, MAP and TA (excluding the dynamics of MAF sensor) for the estimation. All the variables are available in the measurements of the car engine. Originating from in measurements, the flow equations (D.3) or (D.5) may be used in order to compute the discharge coefficient in an easy manner.

D.2. Intake Manifold Dynamic Model

The dynamic models actually used for the intake manifold were developed based on physical laws. They were described for only the mass conservation law (first model) and the combination of the mass and energy conservation laws (second model). Nevertheless, the better representation of the intake manifold was the second model because of its high nonlinearities and accuracy. In addition, a function of the number of engine variables with an unknown nonlinear structure for the volumetric efficiency (parameter of the model) was used. A look-up table (black-box) was used in this model together with the physical laws because of the previous comments.

D.2.1. Dynamic Model based on Mass Conservation Law

The dynamic model based on mass conservation law has only one state. The model was identified based on the assumption that the temperature was slowly varying and using the ideal gas law, defining the differential of intake manifold pressure with respect to time as follows (Dutka, 2005):

$$\dot{P}_{im}(t) = \frac{R_{air}\, T_{im}(t)}{V_{im}} [\dot{m}_{at}(t) - \dot{m}_{ac}(t)] \qquad \text{(D.8)}$$

where P_{im}, $T_{im}(t)$, $\dot{m}_{at}(t)$, $\dot{m}_{ac}(t)$, R_{air} and V_{im} are the intake manifold pressure [KPa or KN/m^2], intake manifold temperature with perfect mixing $[°K]$, mass airflow rate through the throttle $[g/s]$, airflow rate into the cylinder $[g/s]$, gas constant $[J/g\ °K]$ and the intake manifold volume $[m^3]$.

Using the speed density approach the cylinder (valve) flow rate was modelled as follows:

$$\dot{m}_{ac}(t) = \frac{V_d}{120\ R_{air}\ T_{im}(t)}\ \eta\big(P_{im}(t), N(t)\big)\ P_{im}(t)\ N(t) \tag{D.9}$$

where V_d, $\eta\big(P_{im}(t), N(t)\big)$, and $N(t)$ are the engine displacement $[dm^3]$, volumetric efficiency and the engine speed $[rpm]$.

Combining equations (D.8) and (D.9) was obtained a continuous time model of the intake manifold expressed as follows:

$$\dot{P}_{im}(t) = -\frac{V_d\ N(t)\ \eta\big(P_{im}(t),N(t)\big)}{120\ V_{im}}\ P_{im}(t) + \frac{R_{air}\ T_{im}(t)}{V_{im}}\ \dot{m}_{at} \tag{D.10}$$

The engine speed $N(t)$ was the main variable which defines strongly the dynamics of the model. The discrete model of equation (D.10) was expressed as follows:

$$P_{im,n+1} = \left[1 - \frac{V_{cyl}}{V_{im}}\ \eta_n\right] P_{im,n} + \frac{R_{air}\ T_{im,n}\ T_{s,n}}{V_{im}} \dot{m}_{at,n} \tag{D.11}$$

where

$V_{cyl} = \frac{V_d}{8}$: cylinder displacement $[dm^3]$

$T_{s,n} = \frac{0.25\ [rot]\ \ 60[s/min]}{N_n[rot/min]}$: sampling period

The previous model (D.11) depends indirectly on the engine speed through the function of the volumetric efficiency. The sub-index "*n*" imply a discrete evaluation of the model. In the identification of the model parameters for equation (D.11) the parameters V_{cyl} and V_{im} were typically known and the system input intake manifold air charge per event T_s . $\dot{m}_{at}$ was also measured. The pressure P_{im} (output of the system) and temperature T_{im} of the intake manifold were also measured. T_{im} is a constant for the one-state model. A look-up table was used to model the volumetric efficiency, which can be also computed for each discrete event *n* assuming all constant parameters are known in (D.11).

Equation (D.11) was also expressed as a function of a new variable η_0 by the following equation:

$$P_{im,n+1} = \left[1 - \frac{\eta_{0,n}}{V_{im}}\right] P_{im,n} + \frac{R_{air}\, T_{im,n}\, T_{s,n}}{V_{im}} \dot{m}_{at,n} \tag{D.12}$$

where $\eta_0 = V_{cyl}\, \eta$.

An extended Kalman filter was used to identify the model parameter $\eta_0 = V_{cyl}\, \eta$ and V_{im}. Additional states (unknown parameters) were expressed as follows:

$$\eta_{0,n} = \eta_{0,n} + \xi_n \tag{D.13}$$
$$V_{im,n} = V_{im,n}$$

where the Gaussian noise was defined as ξ_n which depends on a singular performance of the driving cycle. Intake manifold pressure P_{im} and the speed of the engine $N(t)$ are the independent variables and they will define the value of the parameter η_0. From equation (D.12) the expression for the parameter η_0 was obtained as follows:

$$\eta_{0,n} = \frac{R_{air}\, T_{im,n}\, T_{s,n}\, \dot{m}_{at,n} - \left(P_{im,n+1} - P_{im,n}\right) V_{im}}{P_{im,n}} \tag{D.14a}$$

or

$$\eta_{0,n} = \frac{R_{air}\, T_{im,n}\, T_{s,n}\, \dot{m}_{at,n}}{P_{im,n}} - \left(\frac{P_{im,n+1}}{P_{im,n}} - 1\right) V_{im} \tag{D.14b}$$

Using the previous expression it was proved that the autocorrelation of the volumetric efficiency noise ξ_n was periodic with a period of 8 events (8-cylinder engine), which meant the intake manifold pressure was not constant in the intake manifold. The physical (nominal) volume of the intake manifold was $V_{im} = 12\ [dm^3]$, which was used to compute the volumetric efficiency from

equation (D.14). As a initial value was used the mean value of the volumetric efficiency $mean\ (\eta_0) = 0.41$ and the covariance of the noise ξ used in the covariance matrix was $cov(\xi) = 0.0093$. Equations (D.12) and (D.13) were used for the computed Extended Kalman Filter.

The sampling period of one cycle engine (8 events per 8-cylinder engine) was used because of the periodic behaviour of the autocorrelation function. This sampling period was $T_{s,cycle} = 8 \times T_s = 120/N$. Over 8 events the throttle airflow measurements $\dot{m}_{at}$ was averaged and the pressure measurements were taken from the data set every 8 events. The variable measurements procedure covered the mass conservation law.

The nominal volumetric efficiency of the intake manifold η_0 was computed using the equation (D.14) and the measurements. With the value of η_0 did not need the value of the cylinder displacement volume V_{cyl}. The typical value for the volumetric efficiency was expressed for the following inequality: $0 < \eta_0 < 1.$ After that a look-up table was developed for the volumetric efficiency $\eta(P_{im}, N)$ using as coordinates the intake manifold pressure P_{im} and the engine speed N. The model was validated obtaining a very good approximation with the data taken from the driving cycle. During the validation, the integrated squared and absolute error performance indexes were also computed.

D.2.2. Dynamic Model based on Mass and Energy Conservation Law

The two-state model was built with a hybrid structure (gray box) due to the nonlinear structure based on physical laws (white box) and the look-up table (black box) which was used to obtain the model of the volumetric efficiency. The dynamic model based on mass and energy conservation laws has two states (equations (D.15)-(D.16)). As a consequence of the temperature change, the heat transfer equation was used in the development of the model. The variations of the intake manifold wall temperature (different to the ambient temperature) were included in the model using the heat transfer equation as follows:

$$\dot{P}_{im}(t) = P_{im}(t)\frac{k R_{air} T_a(t)}{V_{im} P_{im}(t)}\left[\dot{m}_{at}(t) - \frac{T_{im}(t)}{T_a(t)}\dot{m}_{ac}(t) + \frac{k-1}{k R_{air}}\frac{Q_{ext}}{T_a(t)}\right] \quad \text{(D.15)}$$

$$\dot{T}_{im}(t) = T_{im}(t)\frac{k R_{air} T_a(t)}{V_{im} P_{im}(t)}\left[\dot{m}_{at}(t)\left(1 - \frac{T_{im}(t)}{k T_a(t)}\right) - \frac{T_{im}(t)}{T_a(t)}\dot{m}_{ac}(t)\left(1 - \frac{1}{k}\right) + \frac{k-1}{k R_{air}}\frac{Q_{ext}}{T_a(t)}\right] \quad \text{(D.16)}$$

and $\dot{Q}_{ext} = h_1(T_{coolant} - T_{im}) + h_2(T_a - T_{im})$ (the heat transfer equation [J/s])

where $P_{im}(t)$ and $T_{im}(t)$ are the pressure [kPa] and the temperature [^{o}K] of the intake manifold. $T_a(t)$ and $T_{coolant}$ are the ambient and coolant temperatures in [^{o}K]. $\dot{m}_{at}(t)$ and $\dot{m}_{ac}(t)$ are the air flow rate [g/s] through the throttle and the intake valve (in- cylinder). R_{air} and V_{im} are the gas constant [J/(g ^{o}K)] and the intake manifold volume $[dm^3]$. h_1 and h_2 are the heat transfer coefficients from intake engine temperature and the ambient air temperature both in [J/(s ^{o}K)].

The heat transfer equation of the two-state model was modified including two heat transfer components. For simplicity, the intake manifold was expressed as the weighted average of the ambient and coolant temperatures but the real situation is that the intake manifold wall temperature was not measured and uniform. Avoiding to loss simplicity, the intake manifold wall temperature was modelled as a weighted average of the ambient and coolant temperatures. Making the heat transfer equation $\dot{Q}_{ext} = h_1(T_{coolant} - T_{im}) + h_2(T_a - T_{im})$ equals to the following equation:

$$\dot{Q}_{ext} = h_0(T_{wall} - T_{im}) \quad \text{(D.17)}$$

where

$T_{wall} = \frac{h_1 T_{coolant} + h_2 T_a}{h_0}$ and $h_0 = h_1 + h_2$

Enough degree of freedom for modelling with minimum number of unknown parameters was expressed by the wall temperature of equation (D.17). The intake manifold wall temperature would need to be directly measured throughout thermo-resistive material wrapped to the wall in order to obtain the average temperature. The speed-density equation was used to obtain the model of the port (valve) flow rate (4.9). A first-order model with lag was used in the temperature sensor. The inverse of the time constant of the sensor is defined as $\tau_{inv\ Temp}\ [s^{-1}]$.

$$\dot{T}_{im,measured} = -\tau_{inv\ Temp}\ T_{im,measured} + \tau_{inv\ Temp}\ T_{im} \quad \text{(D.18)}$$

After that, a 90^o event basis $(T_s = 15/N)$ was used to obtain the discrete model which was described by the following equation:

$$P_{im,n+1} = \left(1 - \frac{k}{V_{im}} V_{cyl}\eta_n\right) P_{im,n} + \frac{k\,R_{air}\,T_{a,n}}{V_{im}} T_{s,n}\dot{m}_{at,n} + \frac{k-1}{V_{im}} T_{s,n}\dot{Q}_{ext,n} \quad \text{(D.19)}$$

$$T_{im,n+1} = \left(1 - \frac{k}{V_{im}} V_{cyl}\eta_n\left(1 - \frac{1}{k}\right)\right) T_{im,n}$$
$$+ \left(\frac{k\,R_{air}\,T_{a,n}}{V_{im}\,P_{im,n}} T_{im,n} - \frac{R_{air}}{V_{im}\,P_{im,n}} T_{im,n}^2\right) T_{s,n}\dot{m}_{at,n} + \frac{k-1}{V_{im}\,P_{im,n}} T_{im,n} T_{s,n}\dot{Q}_{ext,n} \quad \text{(D.20)}$$

$$T_{im\ measured,n+1} = \left(1 - \tau_{inv\ Temp}\ T_{s,n}\right) T_{im\ measured,n} + \tau_{inv\ Temp}\ T_{s,n} T_{im,n} \quad \text{(D.21)}$$

with $\dot{Q}_{ext,n} = h_1\left(T_{coolant,n} - T_{im,n}\right) + h_2\left(T_{a,n} - T_{im,n}\right)$ and $V_{cyl} = \frac{V_d}{8}$

where V_{cyl} and V_d are the cylinder and engine displacements.

The parameters identified in model (D.19) are: h_1, h_2, V_d, V_{im}, and $\tau_{inv\ Temp}$.
Combining the engine displacement and the volumetric efficiency was used against the model parameter $\eta_0 = V_{cyl}\,\eta$. For identification parameters a total amount of 720 degrees of the crankshaft revolution was used as the engine cycle based sampling period.

An extended Kalman filter was used for parameters estimation. As a part of this technique (D.19) the following additional states were included in the model as follows:

$$\eta_{0,n+1} = \eta_{0,n} + \xi_n$$
$$V_{im,n+1} = V_{im,n}$$
$$h_{1,n+1} = h_{1,n}$$
$$h_{2,n+1} = h_{2,n}$$
$$\tau_{inv\ Temp,n+1} = \tau_{inv\ Temp,n} \quad \text{(D.22)}$$

where ξ_n is the Gaussian noise

The noise analysis was developed after the parameters were identified (totally different to the procedure used in the one-state model). The intake manifold volume V_{im} was fixed to the value identified with the one-state model $(11.87\ [dm^3])$.

As a conclusion, was used the engine cycle in the parameter identification as the sampling period. The simultaneous parameter identification for all the parameters was not successful. The identification results are in function of the assumed covariance. For parameter identification purpose, the values for the intake manifold volume and the temperature sensor time constant has to be known in advance. Using the one-state model, the identification of the intake manifold volume was more reliable. The intake manifold volume and the temperature sensor time constant may be known in advance. As a physical parameter, the intake manifold volume was known for a specific engine type. Also, the typical value of the manufacture for the temperature sensor time constant could be used as the temperature sensor time constant.

The validation of model (D.19) was carried out by the look-up table of the volumetric efficiency against the pressure and temperature measurements. The two-state model was compared against the one-state model by computing performance indexes of the integrated squared and absolute errors. After that, the two-state model shown to be more accurate than the one-state model because of its low value of the

performance index. The temperature sensor time constant was very slow in the one-state model and because of that, the temperature sensor was not capable to take the measurements in fast transients. For control design, the temperature has to be estimated in order to obtain better results.

D.3. Air Mass Estimation in the Cylinder

For the air mass estimation in the cylinder the following steps were applied:

- Step 1: the one-state model with cycle-sampled data was used to identify the volume of the intake manifold.
- Step 2: the two-state model with the cycle-sampled data was used to identify the heat-transfer parameters and the temperature sensor time constant (if it is not known).
- Step 3: the estimation of the volumetric efficiency with the look-up table was built (this express the volumetric efficiency in function of the intake manifold pressure and engine speed) using the parameters of steps 1 and 2.

The cylinder (or port) airflow rate is computed as follows:

$$m_{ac} = \frac{V_d}{120\, R_{air}\, T_{im}} \eta\, P_{im}\, N$$

$$\eta = f_1(P_{im}, N) \qquad \text{(D.23)}$$

The look-up table of the volumetric efficiency, the measurement of the intake manifold pressure, the engine speed and the estimation of the intake manifold temperature were used. The second equation of the two-state model (D.19) with the extended Kalman filter (EKF) could be used to compute the intake manifold temperature. Also, the EKF generated could be used to estimate the volumetric efficiency for the port flow of the airflow rate estimation in equation (D.21).

The high level of noise in the direct identification of the flow rate by using the EKF of the volumetric efficiency is a great challenge. The noise could have been removed by changing the covariances in the EKF but doing that important dynamic

information are removed of the high frequencies (transients). Nevertheless, it will produce modifications in the fuelling and exhaust of the engine model. The accurate value of the cylinder air charge is a function of the model structure and the measurement accuracy of the several states. An upper limit over the model accuracy was produced by a model mismatch between the real intake manifold and the identified model. Models without a good accuracy produce the parameter mismatch model, which was exposed by an offset in the estimated cylinder charge air.

D.4. Air-Fuel Ratio and Fuel Delivery Model

The estimated port flow rate $\dot{m}_{ac,n}$ at every event was used to compute the cylinder air charge (CAC) by means of the following equation:

$$CAC_n = \dot{m}_{ac,n} \frac{15}{N_n} \tag{D.24}$$

The amount of air fed in the cylinders over the time of event (i.e. 90^o) was provided by CAC. Three cylinders were charged simultaneously in an 8-cylinder engine. There is not relationship between one cylinder and the amount of air inducted during one engine event (even if one cylinder has most of the estimated air charge). However, it was assumed that the estimated air charge was associated with only one cylinder for a mean-value model. In other words, the mass of air fed in all the cylinders over one event was equivalent to the mass of air per cylinder for the 8 cylinders engine. Two revolutions of the crankshaft (equivalent to 720 degree cycle) were divided by the amount of cylinders that were filled with air over one cycle.

The FPW delay, the injector parameters and the fuel film dynamics were defined as the fuel delivery path. Also, the lambda path was defined as the exhaust manifold transport delay and the lambda sensor dynamics. Once, the cylinder air charge CAC is know, it was possible to identify the fuel delivery and the lambda paths. The air and fuel path represent the in-cylinder air-fuel ratio. Because of the constant changes of the operating point over the range of the driving cycle, the nonlinearity implicit in

the division (ratio) could be a cause of problems in the identification process. To avoid the previous problem the intake manifold was identified independently and the lambda measurement was used to identify only the fuel delivery parameters.

First at all, the time delays have to be computed (or known) in advance before removing them from the in-cylinder air-fuel ratio dynamics (this is an inappropriate way to tackle the delays problem) before the identification. After that, the identification of the system without delays could be simplified by data pre-processing.

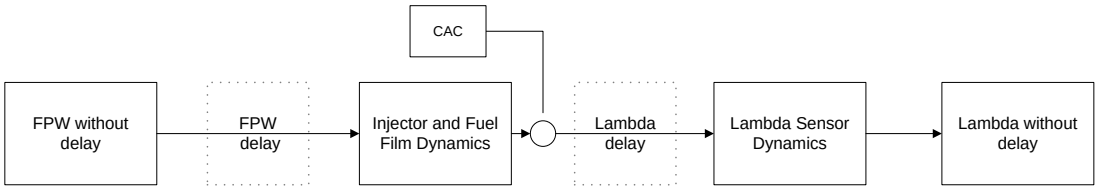

Figure D.2. Block Diagram of the Free Delay Model for Identification

The simplified model used for identification is shown in Figure D.4. The free delay FPW signal was used as pre-processed input signal and the free delay lambda signal was used as pre-processed output signal. Also, the time-varying parameter was used in the cylinder air charge (CAC).

D.4.1. Fuel Injection Time Delay

The pulse width modulation used for the fuel measuring and injection strategy produced the fuel injection delay. The two possible strategies used for the port fuel injection were:

- First method: When the valve is open then injection starts.
- Second method: Before the intake valve opening the end injection was fixed at a few degrees of the crankshaft rotation.

In an specific fuel injection strategy, the fuel injection was ended before the intake valve opens for the vehicle under study. From the engine cycle, 90^{o} event were taking, which belongs to take 720^{o} of the crankshaft rotation. The engine cycle started with the position of the 60^{o} of the crankshaft before the Top Dead Centre (TDC) is compressed. The rotation of the crankshaft was relative to the beginning of the cycle 60^{o} before TDC was defined as the k-th cycle at this position when it was assumed $C_k^0 = 0$. Figure D.3. shows the explanation of these by the distribution of the FPW delay timing.

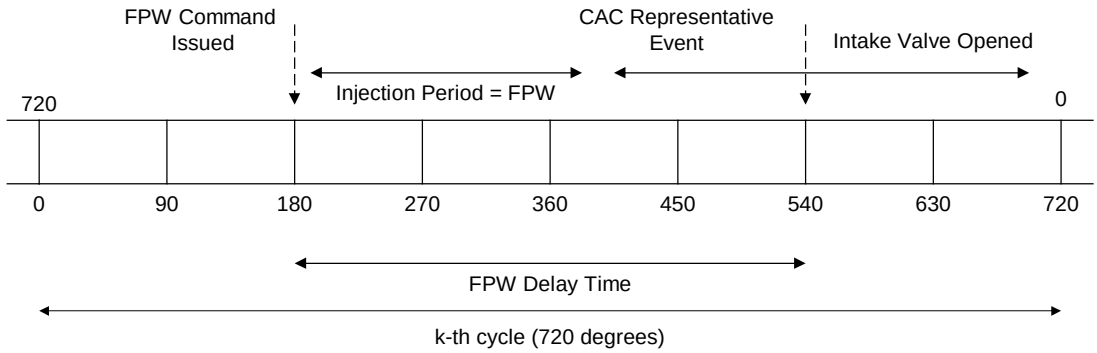

Figure D.3. Distribution of the Fuel Pulse Width Delay Timing

The valve timing for an engine with one cylinder was considered in Figure 4.30. The period of the intake valve opened defines when the valve opens at $\alpha_{open} = 403^{\circ}$ and closes at $\alpha_{close} = 697^{\circ}$. Relative to 60° before the TDC on compression, the angles are computed. The intake valve has discrete events between the opening and closing at:

$C_k^5 = 450^{\circ}$, $C_k^6 = 540^{\circ}$ (highest port flow rate assumed) and $C_k^7 = 630^{\circ}$. Before the intake valve opens the fuel injection has to finish α_c degrees. $C_k^4 = 360^{\circ}$ was the last discrete event before the valves opens.

The fuel injection angle may be computed depending on the amount of the required fuel to be injected, which defines the period for the injector opening $FPW_{i,n}$. The fuel injection angle could be defined as follows:

$$\alpha_{injection} = 6 \cdot N_n \cdot FPW_{i,n} \quad \text{(D.25)}$$

where N_n is the engine speed.

The command available for the controller CAFC could be computed using the following formula:

$$CAFC = \begin{cases} C_k^4 = 360^\circ, if\ \alpha_{open} - \alpha_c - \alpha_{injection} \geq 360^\circ \\ C_k^3 = 270^\circ, then\ \alpha_{open} - \alpha_c - \alpha_{injection} < 360^\circ \end{cases} \quad \text{(D.26)}$$

The difference $\alpha_{open} - \alpha_c$ represents the period where the fuel injection should end. The time delay was computed using the information of the engine speed N_n and the fuel pulse width $FPW_{i,n}$.

D.4.2. Transport Time Delay in the Exhaust Manifold

At each event in the cylinder a certain amount of air and fuel enters, which define the air-fuel ratio. The air and fuel were converted in a homogeneous mix which was compressed and combusted in the cylinders and finally released through the exhaust valves. The complete processes took approximately 6 engine events. The exhaust manifold and pipes produced a variable time delay. Most of the delay transport were lumped in the lambda sensor in order to avoid problems to compute the time constant of the exhaust manifold gas mixing. The lambda sensor dynamics take into account some of the mixing effects.

The intake manifold and pipes volumes have to be known in advance. The variable time delay could be computed by means of an iterative (adaptive) identification approach, taking the time delay as a proportional constant to the integrated exhaust gas flow rate into the intake manifold.

The ideal gas law was used to compute the volume gas flow with the know value of the air mass flow into the cylinder. The following assumptions were established:

- Any cylinder blow-by during compression and combustion were negligible.

- Stoichiometric reaction for the air-fuel ratio was maintained all the times.

The exhaust manifold pressure and gas temperature measurements were used to compute the volume of the gas feeding the exhaust manifold over one engine event, using the following equation:

$$V_{cyl,n} = \frac{m_{a,n}\left(1+\frac{1}{AF_{stoich}}\right)R_{EM}\,T_{EM,n}}{P_{EM,n}} \tag{D.27}$$

where R_{EM} , $m_{a,n}$ and AF_{stoich} are the ideal gas constant for the exhaust gas, the air mass trapped into the cylinder and the stoichiometric air-fuel ratio. $P_{EM,n}$ and $T_{EM,n}$ are the exhaust gas pressure and temperature.

The discrete time delay $k_{EM,n}$ at time *n* was computed as follows:

$$V_{EM} = \sum_{i=n}^{n+k_{EM,n}} V_{cyl,i} \tag{D.28}$$

where V_{EM} is the exhaust manifold volume including the pipe.

The formula (D.28) describes how in the next engine events, the exhaust gases were pushed out of the exhaust manifold by gases leaving the combustion chamber.

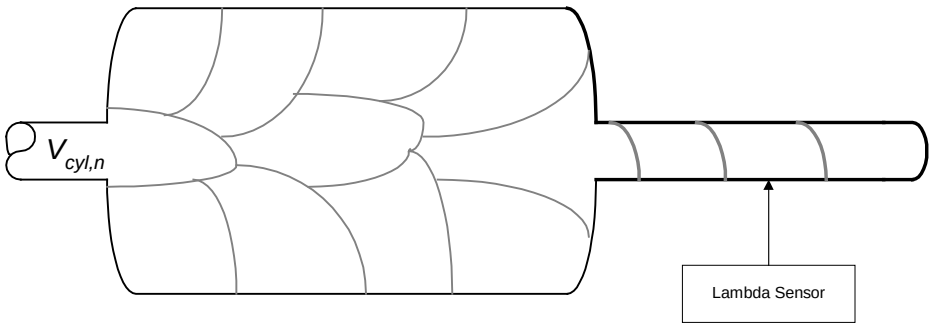

Figure D.4. Exhaust Manifold Delay Modelling

The discrete time delays $k^{-}_{EM,n} \leq k_{EM,n} \leq k^{+}_{EM,n}$ were expressed as follows:

$$k^{-}_{EM,n}: V_{EM} \geq \sum_{i=n}^{n+k^{-}_{EM,n}} V_{cyl,i} \tag{D.29}$$

$$k^{+}_{EM,n}: V_{EM} < \sum_{i=n}^{n+k^{+}_{EM,n}} V_{cyl,i} \tag{D.30}$$

and

$$k^{+}_{EM,n} = k^{-}_{EM,n} + 1 \tag{D.31}$$

From the discrete event $k^{-}_{EM,n}$ and $k^{+}_{EM,n}$ of equations (D.29) and (D.30), the real (or continuous) time delays were defined by the sampling times: $t^{-}_{n} = t_{k^{-}_{EM,n}}$ and $t^{+}_{n} = t_{k^{+}_{EM,n}}$. The exact time delay t^{0}_{n} could be computed using the following formula:

$$t^{0}_{n} \approx t^{-}_{n} + (t^{+}_{n} - t^{-}_{n}) \frac{V_{EM} - \sum_{i=n}^{n+k^{-}_{EM,n}} V_{cyl,i}}{V_{cyl,n+k^{+}_{EM,n}}} \tag{D.32}$$

The sampling period for the lambda sensor was computed by the time delay of equation (D.33). Another option was to use an approximated relationship from the samples $\lambda(t + t^{+}_{n})$ and $(t + t^{-}_{n})$, defined as follows:

$$\lambda(t + t^{0}_{n}) \approx \lambda(t + t^{-}_{n}) + [\lambda(t + t^{+}_{n}) - \lambda(t + t^{-}_{n})] \frac{t^{0}_{n} - t^{-}_{n}}{t^{+}_{n} - t^{-}_{n}} \tag{4.33}$$

In order to apply the above method on line for computing the time delay shift registers were used to store the data there. The sampling time of the lambda sensor will be used from the result of equation (4.32). The lambda sensor was sampled each event in the FTP dataset. The linear interpolation (4.33) was used to obtain the lambda value.

Simplifying the calculations, the transport time delay may be assumed equal to $k^{-}_{EM,n}$ $(or\ k^{+}_{EM,n})$. Also, to the exhaust manifold transport delay has to be added the six-event time delay due to gas entrapment in the cylinder. $k_{EM,n} + 6$ events after the related lambda measurements of the intake event were available.

The time delay is a very complicated mathematical expression. Because of that, it is recommended that it is removed from the data before the off-line identification.

D.4.3. Time Delay Identification in the Exhaust Manifold

The measurements volume V_{EM}, pressure and temperature of the exhaust manifold could be used altogether. V_{EM} could be different to the effective volume. The addition of the two volumes for ″V″ engines is a known engine parameter called physical volume of the exhaust manifold. An additional lambda measurement $wraf5$ close to the exhaust valve was used in order to compute iteratively the effective exhaust manifold volume. The lambda measurement $wraf5$ at the exhaust valve location and the shifted main lambda measurement $wraf3$ were used to compute the correlation between them.

The exhaust manifold volume and the estimated exhaust gas flow rate based on the cylinder air charge were estimated by the equations (D.32) and (D.33). After the estimation, was found exhaust manifold volume 2.9 L, where the maximum correlation was obtained. The final exhaust manifold transport delay calculation was developed with the effective exhaust manifold volume. The effective exhaust manifold volume 2.9 L is very close to the physical measured exhaust manifold volume which is 3.0 L.

D.4.4. Lambda Sensor Dynamics

The lambda sensor was used to obtain the air-fuel ratio measurement in the exhaust manifold. It was described as a first order lag model. The lambda measured was expressed as follows:

$$\lambda = \frac{1}{s\,\tau_\lambda + 1}\lambda_{EM} \tag{D.34}$$

where τ_λ and λ_{EM} are the time constant of the lambda sensor and the real lambda of the exhaust gas.

The discrete version of the model was defined as follows:

$$\lambda_{n+1} = \left(1 - \frac{T_{s\lambda,n}}{\tau_\lambda}\right)\lambda_n + \frac{T_{s\lambda,n}}{\tau_\lambda}\lambda_{EM} \tag{D.35}$$

where $T_{s\lambda,n}$ is the sampling period.

The lambda sensor model includes the exhaust manifold mixing. An approximate way to include an approximation of the exhaust manifold mixing is to increase the time constant of the lambda sensor. The effective exhaust manifold volume was used in order to compute the exhaust manifold time delay. The lambda sensor time constant was computed by removing the delay from the lambda measurements pre-processed. The correlation analysis for the measured and modelled lambda was computed after the time delay was removed from the data. The correlation was also used to check the lambda model accuracy with the assumed lambda sensor time constant. The maximum correlation occurred at $\tau_\lambda = 125\ [ms]$.

The previous methodology was used because the extended Kalman filter (EKF) did not produce a good result. The EKF converges to an not real value $(1\ [s])$. The lambda sensor time constant was increasing by the estimation algorithm which heavily filters the modelled lambda signal.

D.4.5. Fuel Injection Model

The fuel injection model was expressed as follows:

$$m_{fi,n} = k_{fi,n}\left(FPW_{fi,n} - O_{fi,n}\right) \tag{D.36}$$

where $m_{fi,n}$, $k_{fi,n}$, $FPW_{fi,n}$, and $O_{fi,n}$ are the mass of the fuel injected $[g]$, the injector gain $[g/s]$, the pulse-width command $[s]$ and the offset $[s]$.

D.4.6. Dynamic Models of the Fuel Film

The dynamic models of the fuel film could be modelled by a first-order $X-\tau$ models as follows:

$$\dot{m}_w = -\frac{1}{\tau_n} m_w + X_n \dot{m}_{fi} \tag{D.37}$$

$$\dot{m}_{fc} = -\frac{1}{\tau_n} m_w + (1 - X_n) \dot{m}_{fi} \tag{D.38}$$

where m_w, $\dot{m}_{fi}$ and $\dot{m}_{fc}$ are the mass of the wall fuel, fuel mass flow rate through the injector and the fuel mass flow rate into the cylinder. τ_n and X_n are the model parameters.

The discrete dynamic models of the fuel film obtained by Euler method were as follows:

$$m_{w,n+1} = \left(1 - \frac{T_{s,n}}{\tau_n}\right) m_{w,n} + X_n \, m_{fi,n} \tag{D.39}$$

$$m_{fc,n+1} = \frac{T_{s,n}}{\tau_n} m_{w,n} + (1 - X_n) \, m_{fi,n} \tag{D.40}$$

$$m_{fi,n} = T_{s,n} \dot{m}_{fi,n} \tag{D.41}$$

$$m_{fc,n} = T_{s,n} \dot{m}_{fc,n} \tag{D.42}$$

where $T_{s,n}$ is the sampling period at the current engine event. $m_{fi,n}$ and $m_{fc,n}$ are the mass of fuel injected and the cylinder fuel charge during one event.

The time period of injector opening is the input signal. The amount of fuel injected was controlled by the pulse-width modulation.

D.4.7. Fuel System Identification

The fuel film dynamics and fuel injector were included in the fuel system model. In the identification process three models were proposed and used with high degree of complexity and uncertainties.

D.4.7.1. Model 1

The first model used for parameter identification was describes as follows:

$$m_{w,n+1} = \left(1 - \frac{T_{s,n}}{\tau_n}\right) m_{w,n} + X_n\, m_{i,n}$$

$$\lambda_{n+1} = \left(1 - \frac{T_{s\lambda,n}}{\tau_n}\right) \lambda_n + \frac{T_{s\lambda,n}}{\tau_n} \frac{m_{ac,n}}{\frac{T_{s,n}}{\tau_n} m_{w,n} + (1 - X_n) m_{i,n}} \qquad \text{(D.43)}$$

$$m_{i,n} = k_{fi,n}\left(FPW_{fi,n} - O_{fi,n}\right)$$

$$m_{ac,n} = T_{s,n}\, \dot{m}_{ac,n}$$

where $m_{ac,n}$ is the Cylinder Air Charge (CAC) as a parameter.

The EKF was used to identify unknown parameters which were defined as additional states:

$$\Theta_{M1,n+1} = \Theta_{M1,n} \qquad \text{(D.44)}$$

where

$$\Theta_{M1,n} = \left[X_n, \frac{1}{\tau_n}, k_{fi,n}, O_{fi,n}\right]^T \qquad \text{(D.45)}$$

An average value of the current wall wetting parameters was identified by equation (D.44) taking the values of X_n and τ_n as variables and functions, which are depending of the other states (and several variables as intake manifold pressure, engine speed, and the Cylinder Air Charge). The modelling of the structure parameter was developed as time invariant. The selection of the initial values and the initial covariance P_o represented the main problem in the EKF parameter estimation. The initial values used were $m_{ac,0} = 0.005$, $\lambda_0 = 14.57$, $X_0 = 0.05$, $1/\tau_0 = 5$, $k_{fi,0} = 3.6$ and $O_{fi,0} = 5 \times 10^{-4}$.

The identification approach used the EKF was iteratively repeated at the end of the driving cycle. The covariance computed at the initial state estimated P_o (experimentally derived tuning parameter) was always scaled at 20% of the state estimate value. On the other hand, the covariance may be iteratively reduced. The validation of the model was developed by computing the performance index of the sum of the value absolute or square values of the difference between the model and the measurement lambda.

The mean values estimated were: $X = 0.122$, $1/\tau = 4.169$, $k_{fi} = 3.692$ and $O_{fi} = 4.912 \times 10^{-4}$.

D.4.7.2. Model 2

The state-dependent injector gain was included in the model 1 and expressed as a linear function of the battery voltage and intake manifold pressure. The complete model includes equation (D.43) and the following injector model expressed as follows:

$$m_{i,n} = \left[k_{1,fi,n} + k_{2,fi,n} U_{batt,n} + k_{3,fi,n} P_{im,n}\right]\left[FPW_{fi,n} - O_{fi,n}\right] \quad \text{(D.46)}$$

where $U_{batt,n}$ and $P_{im,n}$ are the battery voltage and the intake manifold pressure. $k_{1,fi,n}$, $k_{2,fi,n}$ and $k_{3,fi,n}$ are the linear coefficients.

The identification approach used was the extended Kalman filter (EKF), where the unknown parameters were included as additional states. The additional states were as follows:

$$\Theta_{M2,n+1} = \Theta_{M2,n} \tag{D.47}$$

where

$$\Theta_{M2,n} = \left[X_n, \frac{1}{\tau_n}, k_{1,fi,n}, k_{2,fi,n}, k_{3,fi,n}, O_{fi,n}\right]^T \tag{D.48}$$

The mean values identified were: $X = 0.123$, $1/\tau = 4.273$, $k_{1,fi} = -6.251$, $k_{2,fi} = 0.747$, $k_{3,fi} = -0.00687$ and $O_{fi} = 5.787 \times 10^{-4}$.

D.4.7.3. Model 3

Model 3 includes model 2 and the state-dependent X and τ parameters as linear functions of the intake manifold pressures. Again the state-dependent injector gain was expressed as a linear function of the battery voltage and the intake manifold pressure. The injector model and the fuel film dynamics were used with the model (D.43) as follows:

$$m_{i,n} = \left[k_{1,fi,n} + k_{2,fi,n}\, U_{batt,n} + k_{3,fi,n}\, P_{im,n}\right]\left[FPW_{fi,n} - O_{fi,n}\right]$$

$$\frac{1}{\tau_n} = \frac{1}{\tau_{1,n}} + \frac{1}{\tau_{2,n}} P_{im,n}$$

$$X_n = X_{1,n} + X_{2,n}\, P_{im,n}$$

$$m_{ac,n} = T_{s,n}\, \dot{m}_{ac,n} \tag{D.49}$$

where $m_{ac,n}$ is the cylinder air charge over one event.

One more time, the estimation of the unknown parameter was developed by an extended Kalman filter adding the following states:

$$\Theta_{M3,n+1} = \Theta_{M3,n} \tag{D.50}$$

where

$$\Theta_{M3,n} = \left[X_{1,n}, X_{2,n}, \frac{1}{\tau_{1,n}}, \frac{1}{\tau_{2,n}}, k_{1,fi,n}, k_{2,fi,n}, k_{3,fi,n}, O_{fi,n}\right]^T \tag{D.51}$$

After the identification, the estimated parameters were as follows:

$X_{1,n} = 0.0334$, $X_{2,n} = 0.00168$, $\frac{1}{\tau_{1,n}} = 3.511$, $\frac{1}{\tau_{2,n}} = 0.0166$, $k_{1,fi} = -6.174$, $k_{2,fi} = 0.740$, $k_{3,fi} = -0.00647$, $O_{fi} = 5.687 \times 10^{-4}$.

The performance indexes of the absolute value of the error and the square error were used for the validation of the model.

D.4.7.4. Corrected Model 3

The cylinder air charge (CAC) was assumed to be computed by the intake manifold model in the identification of the fuelling and lambda models. If there exist measurement errors or model structure mismatch due to the CAC and/or fuel models then the lambda model would be inaccurate. The corrected model 3 (includes equations (D.43), (D.49) and (D.50)) was used with the identified parameters and an application of static correction.

$$m_{w,n+1} = \left(1 - \frac{T_{s,n}}{\tau_n}\right) m_{w,n} + X_n \, m_{i,n}$$

$$\lambda_{n+1} = \left(1 - \frac{T_{s\lambda,n}}{\tau_\lambda}\right) \lambda_n + \frac{T_{s\lambda,n}}{\tau_\lambda} \frac{k_{corr,n} \, m_{ac,n}}{\frac{T_{s,n}}{\tau_n} m_{w,n} + (1 - X_n) m_{i,n}}$$

$$m_{ac,n} = T_{s,n} \, \dot{m}_{ac,n} \tag{D.52}$$

where $m_{ac,n}$ is the cylinder air charge. The parameters $\frac{1}{\tau_n}$, X_n and $m_{i,n}$ were computed by the equation (D.46).

Applying the extended Kalman filter (stochastic model with white noise ξ_n) in order to identify the parameters, the variable $k_{corr,n}$ was defined as additional state as follows:

$$k_{corr,n+1} = k_{corr,n} + \xi_n \tag{D.53}$$

A time series was generated by the stochastic estimation and after that, it was used to build a look-up table. It used exactly the same method used to build the look-up table of the throttle flow discharge and the intake manifold volumetric efficiency.

The corrected model 3 was validated using the performance indexes of the sum of the absolute and square values of the difference between the model and measurement lambda values.

D.4.8. Analysis and Conclusions for the Air-Fuel Ratio Model

Finally, a comparative analysis of two sensor measurements (one on each bank of V8 engine) for the air-fuel ratio was related to the model output. The accuracy (or improvements) of the identification process depend on the two sensor measurements used. The performance indexes of the integrated and absolute error measures were minimum for the model 3. Nevertheless, the maximum correlation with the air-fuel ratio measurement was for the model 2. The correction coefficients included in the models represented a highly improvements achieved in the models. There is an approximated performance between the models 2 and 3 due to the nature of the validation data. Most of the fuel injected enters in the cylinder in the first event when there is a warmed-up engine. In other words, the fuel injector (static) characteristics are more important than the wall-wetting dynamics. Moreover, the

improvements in the inject model is directly reflected in the accuracy of model 1, model 2 and model 3.

D.5. Net Torque Model

A brake torque measurements between the engine and the transmission was produced by the Net Torque model in order to identify itself. The combustion decreased by energy dissipation (non conservative forces as the friction, pumping and the load torque produced by the accessories attached to the crankshaft) produce the net torque or the total torque generated. The engine dynamics block diagram is shown in Figure D.5.

The data collected during the FTP driving cycle was sampled based on the event-based sampling period corresponding to every 90° crank angle. At the nth event the engine speed N_n was differentiated. At the beginning, the engine speed was represented as $\dot{\varphi} = \frac{2\pi}{60} N_n$ and after that the acceleration was computed as follows:

$$\ddot{\varphi}_n = \frac{\dot{\varphi}_n - \dot{\varphi}_{n-1}}{T_{s,n}} = \frac{\pi(N_n - N_{n-1})N_n}{450} \tag{D.54}$$

Finally, the net torque $M_{P,n}$ (after the subtracting of the friction and the accessories load) was expressed by:

$$M_{P,n} = M_{B,n} + I_E \ddot{\varphi}_n \tag{D.55}$$

where $M_{B,n}$ and I_E are the measured brake torque and the engine inertia (e.g. for Corvette $I_E = 0.35\ [kg \cdot m^2]$).

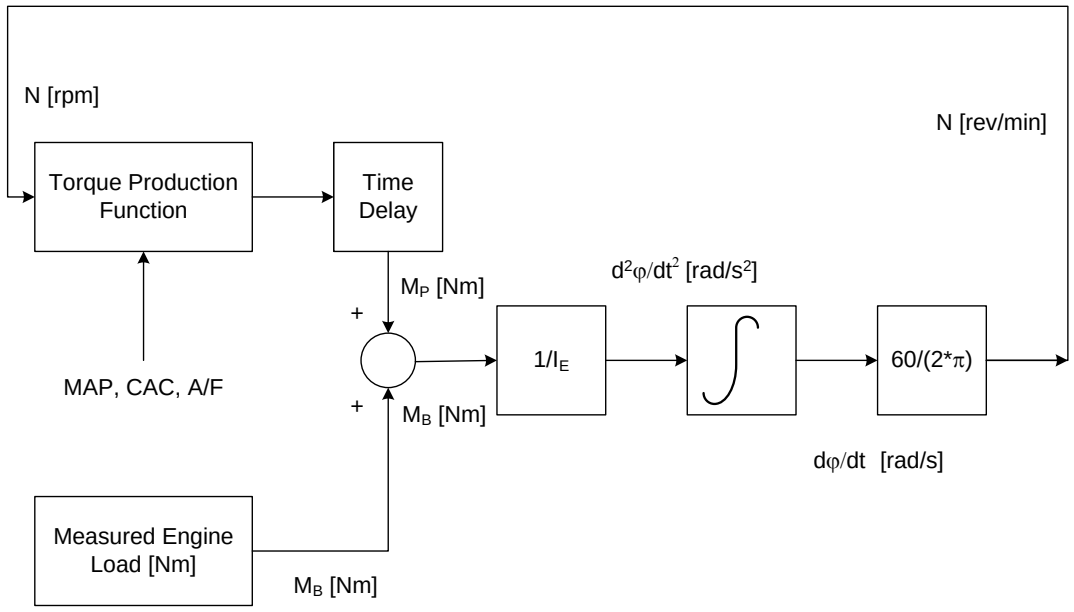

Figure D.5. General Engine Dynamics Block Diagram

The net torque was computed from equations (D.54), (D.55) and the FTP driving cycle datasets. The flywheel and accessories define the inertia which was estimated in an independent experiment (by clustering technique and least-square fitting). Nonlinear torque modelling used the same approaches than the throttle flow modelling and the intake manifold volumetric efficiency look-up table construction.

The torque model was developed as a function of MAP and Engine Speed (RPM) without taking into account the influence of the variable intake manifold temperature. Another corrected model could be developed including a correction function of the intake manifold temperature. Perhaps, a model which uses the cylinder air charge (CAC) as input is implicitly taking into account the intake manifold temperature. The net torque was expressed as a function of CAC and RPM:

$$M_{p,n} = function(CAC_{n-1}, N_{n-1}) \quad \text{(D.56)}$$

The model (D.56) also included implicitly the spark advance obtained from the existing controller of engine load and speed. Lambda was considered to be

regulated close to the unity (complete combustion in air-fuel ratio or reaction with stoichiometry balance). Lambda inaccuracies in the above level mentioned could have zero mean value considering these as a disturbance.

Figure D.6. shows the block diagram of the car engine model with multivariable feedforward controller. Finally, the complete car engine model was simulated with the more representative process variables shown from Figure D.7 to Figure D.10. The process variables simulated were the throttle position *TP (TA: Throttle Angle)*, Mass Airflow Rate *MAF*, Intake Manifold Pressure *MAP*, Fuel Pulse Width *FPW*, Brake Torque *BT* and Engine Speed *RPM* and the Normalized Air-Fuel Ratio λ (Lambda) with the Feed-Forward Control System (Dutka, 2002).

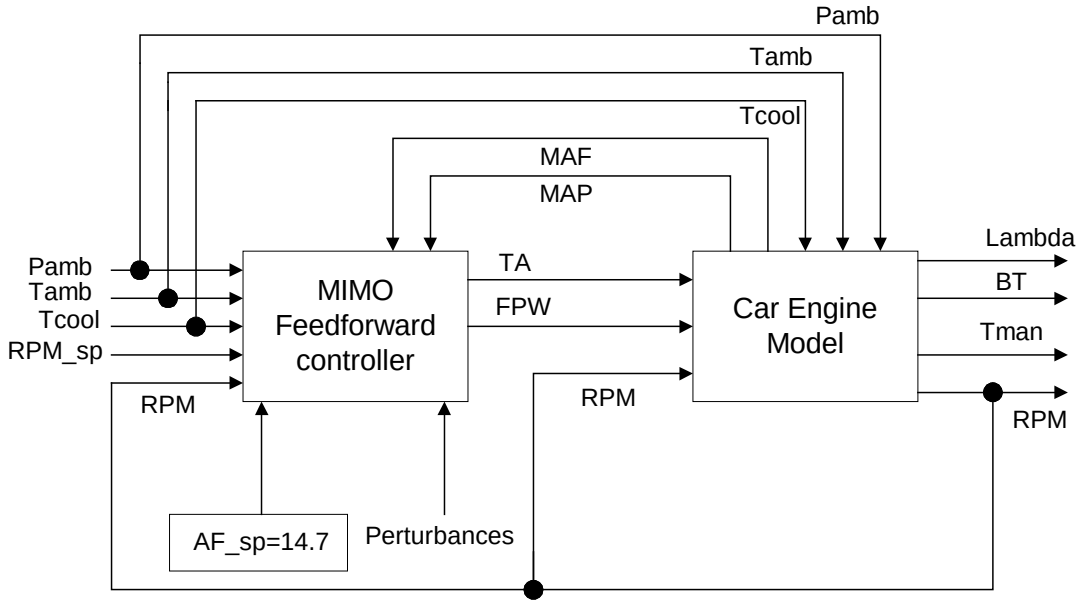

Figure D.6. Block Diagram of the Car Engine Model with Multivariable Feedforward Controller

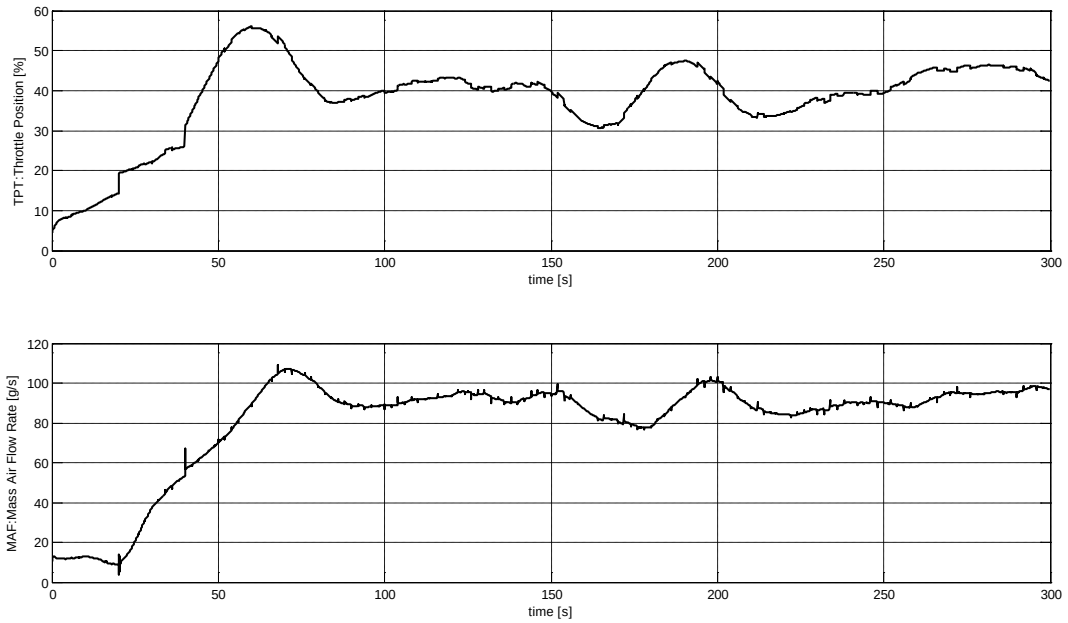

Figure D.7. Dynamic Behaviour of the Throttle Position *TP* and Mass Airflow Rate *MAF* with the Feed-Forward Control System

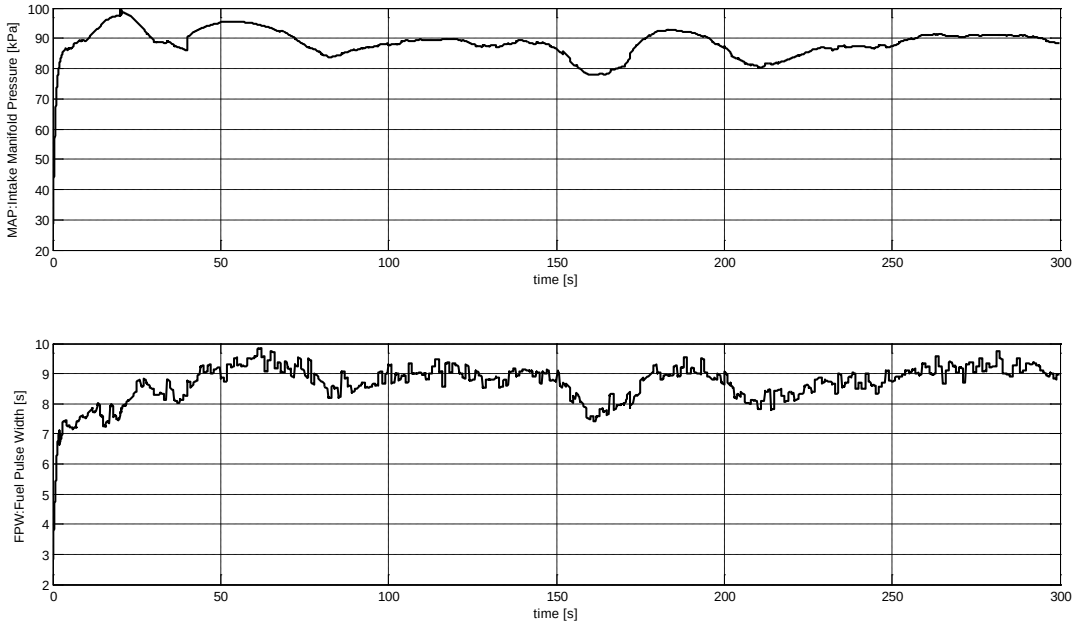

Figure D.8. Dynamic Behaviour of the Intake Manifold Pressure *MAP* and Fuel Pulse Width *FPW* with the Feed-Forward Control System

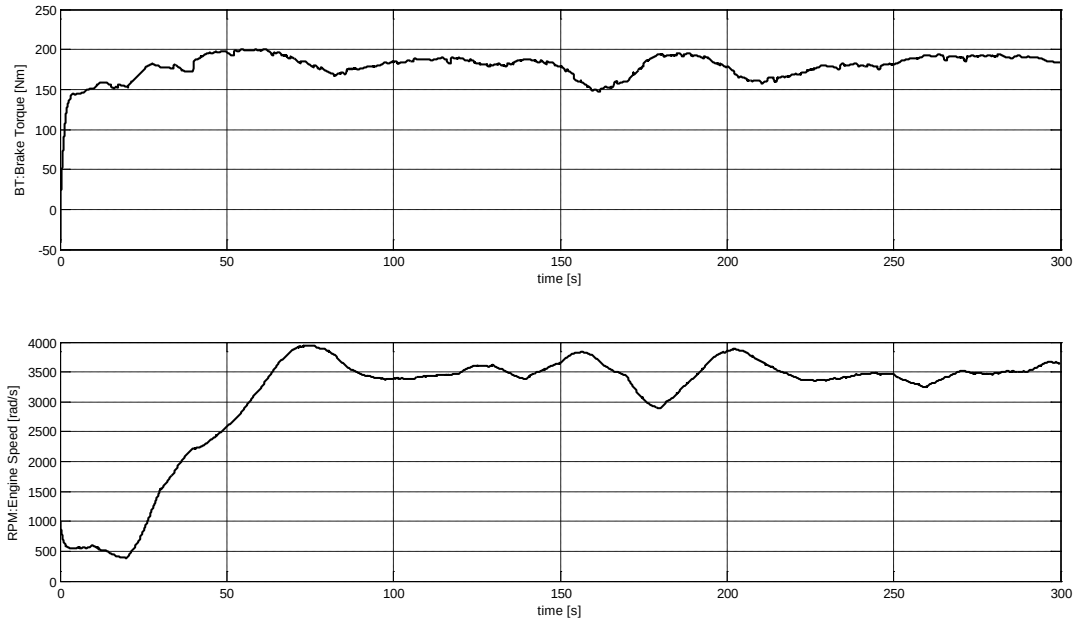

Figure D.9. Dynamic Behaviour of the Brake Torque *BT* and Engine Speed *RPM* with the Feed-Forward Control System

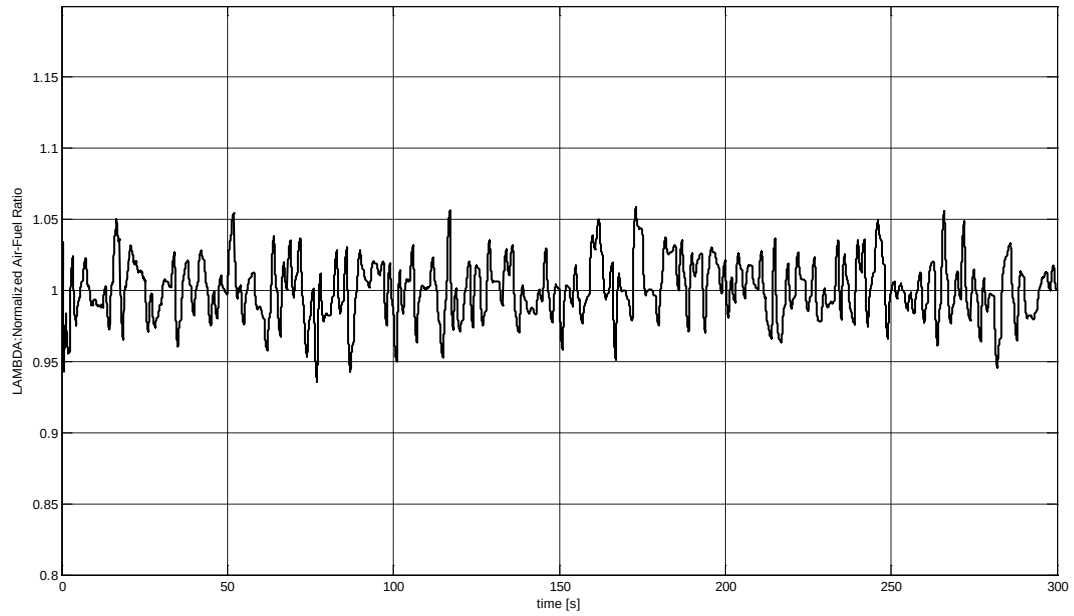

Figure D.10. Dynamic Behaviour of the Normalized Air-Fuel Ratio λ (Lambda) with the Feed-Forward Control System

The car engine model was satisfactorily controlled by the feed-forward control (FFC) system setting the normalized air-fuel ratio to its optimum value of 1 (complete combustion). A reaction of complete combustion is reached by keeping constant the

air-fuel ratio to the value of 14.7. A normalized air-fuel ratio λ was defined as follows:

$$\lambda = \frac{A/F}{A/F_{stoich}}$$

$$A/F = \frac{\text{Air mass}}{\text{Fuel mass}}$$

$$A/F_{stoich} = \beta = 14.7 \qquad \text{(D.57)}$$

where A/F_{stoich} is the air-fuel ratio in stoichiometry reaction with complete combustion.

REFERENCES

(Agarwal and Seborg, 1987) Agarwal M. and D. E. Seborg (1987), *Self-tuning controller for nonlinear systems*, Automatica, Vol. 23, No. 2, pp. 209-214.

(Agarwal, et. al., 2005) Agarwal R. P. and D. O'Regan and V. Lakshmikantham (2005), *Viability theory and fuzzy differential equations*, Fuzzy Sets and Systems, Vol. 151, pp. 563-580.

(Alayón, et. al., 2004) Alayón M. and D. Sáez and R. Veiga (2004), *Comparative analysis of neural predictive controllers and its application to a laboratory tank system*, International Joint Conference on Neural Networks, IJCNN'2004.

(Alpbaz, et. al., 1998) M. Alpbaz and H. Hapoğlu. and Ç. Güresinli (1998), *Application of Nonlinear Generalised Minimum Variance Control to a Tubular Flow Reactor*, Computers Chem. Eng., Elsevier Science Ltd., Vol. 22, pp.S839-S842.

(Anbumani, et. al., 1981) Anbumani K. and L. M. Patnaik and L. G. Sarma (1984), *Self-tuning minimum-variance control of nonlinear system of the Hammerstein model*, IEEE Trans. Autom. Control, Vol. 26, No. 4, pp. 959-961.

(Anderson and Anderson, 2008) Anderson M. and S. Anderson (2008), *Ethical Healthcare Agents*, Studies in Computational Intelligence, Springer, vol. 107, pp. 233-25, 2008.

(Angelis, 2001) Angelis G. Z. (2001), *System Analysis Modelling and Control with Polytopic Linear Model*, Doctoral Thesis, Technische Universiteit Eindhiven, ISBN 900-386-2672-X.

(Arsie, et. al., 1996) Arsie I. and R. Flora and C. Pianesse and G. Rizzo (1996), *ODEC-a computer code for the optimal design of S.I. engine control estrategies*, In T.

Morel (Ed.), SAE Special Publication (Vol. SP-1168), SAE Paper 960359, Warrendale: Sae International.

(Arsie, et. al., 2002) Arsie I. and C. Pianese and G. Rizzo and V. Cioffi (2002), *An adaptive estimator of fuel film dynamics in the intake port of a spark ignition engine*, Control Engineering Practice, Vol. 11, pp. 303-309.

(Astolfi and Marconi, 2007) Astolfi A. and L. Marconi (2007), , Analysis and Design of Nonlinear Control Systems: In Honor of Alberto Isidori, Springer, First edition, ISBN: 354074357X

(Åström, 1979) Åström K.J. (1979), *Introduction to stochastic control theory*, Academic Press, London.

(Åström, et. al., 1977) Åström, K. J. and U. Borisson and L. Ljung and B. Wittenmark (1977), *Theory and applications of self-tuning regulators*, Automatica, Vol. 13, pp. 457-476.

(Åström and Wittenmark, 1973)Åström, K. J. and B. Wittenmark (1973), *On self tuning regulation*, Automatica, Vol. 9 ,pp.185-199.

(Åström and Wittenmark, 1989)Åström, K. J. and B . Wittenmark (1995), *Adaptive Control*, Addison-Wesley Publishing Company, Lund Institute of Technology.

(Åström and Wittenmark, 1995)Åström, K. J. and B. Wittenmark (1995), *Adaptive Control*, Addison-Wesley Publishing Company, Lund Institute of Technology.

(Atherton, 1982) Atherton D. P. (1982), Nonlinear Control Systems, Springer Verlag, London.

(Babuška, 1996) Babuška, R. (1996), *Fuzzy Modeling and Identification*, Doctoral Thesis, Technische Universitie of Delft, ISBN: 90-9010153-5.

(Babuška, 1998) Babuška, R. (1998), *Fuzzy Modeling for Control*, Kluwer Academic Publisher, International Series in Intelligent Technologies.

(Babuška, et. al., 2002) Babuška, R. and J. Oosterhoff and A. Oudshoorn and P. M. Bruijn (2002), *Fuzzy self-tuning PI control of pH in fermentation*, Engineering Applications of Artificial Intelligence, Vol. 15, pp. 3-15.

(Babuška and Verbruggen, 2003) Babuška, R. and H**.** Verbruggen (2003), *Neuro-fuzzy methods for nonlinear system identification*, Annual Reviews in Control ,27, 73-78, Pergamon.

(Baptista, et. al., 2001) Baptista L. F. and J. M. Souza and J. M. G. Sá da Costa (2001), Fuzzy predictive algorithms applied to real-time force control, Control Eng. Practice, Vol. 9, pp. 411-423.

(Balakrishnan and Honavar, 2009) Balakrishnan K. and V. Honavar (2009), *Evolutionary and Neural Synthesis of Intelligent Agents*, IUI 2009, February 8-11, 2009, Sanibel Island, FL, USA, Copyright 2009 ACM 978-1-60558-246-7/07/0004...$5.00.

(Barricelli, 1954) Barricelli, Nils Aall (1954), Esempi numerici di processi di evoluzione, Methodos: 45–68.

(Barricelli, 1957) Barricelli, Nils Aall (1957). "Symbiogenetic evolution processes realized by artificial methods". Methodos: 143–182.

(Bezergianni and Georgakis, 2000) Bezergianni S. and Ch. Georgakis (2000), Controller *performance assessment based on minimum and open-loop output variance*, Control Engineering Practice, Vol. 8, pp. 791-797.

(Bhama and Singh,1993) Bhama, S. and H. Singh (1993), *Single Layer Neural Network for Linear System Identification Using Gradient Descent Technique*, IEEE Trans. on Neural Networks, Vol. 4, No. 5, pp.884-888.

(Bernieri, et. al., 1994) Bernieri A. and M. D'Apuzzo and L. Sansone and M. Savastano (1994), A neural network approach for identification and fault diagnosis on dynamic systems, IEEE Transactions on Instrumentation and Measurement, ISSN: 0018-9456, Vol. 43 Issue:6, pp. 867 – 873.

(Bishop, 1996) Bishop C. M. (1996), Neural Networks for Pattern Recognition, Oxford University Press, ISBN 0-19-853864-2.

(Bittani and Piroddi, 1997) Bittani, S. and L. Piroddi (1997), *Neural implementation of GMV control schemes based on affine input/output models*, Journal IEE Procceding of Control Theory Appl., Vol. 144, No.6, pp. 521-530.

(Borison, 1979) Borison U. (1979), Self-tuning regulators for a class of multivariable systems, Automatica, Vol. 15, pp. 209-215.

(Brandt, et. al., 2000) Brandt E. P. and Y. Wang and J. W. Grizzle (2000), *Dynamic Modeling of a Three-Way Catalyst for SI Engine Exhaust Emission Control*, IEEE Transaction on Control Systems Technology, Vol.8, No.5, pp. 767-776.

(Brdys, et. al., 2002) Brdys M. A. and J. Diaz-Marquez (2002), *Application of fuzzy model predictie control to the dissolved oxygen concentration tracking in an activated sludge process*, 15th IFAC Triennial World Congress. Barcelona, Spain.

(Brown and Harris, 1994) Brown, M. and C. Harris (1994), Neurofuzzy Adaptive Modelling and Control, New York:Prentice Hall.

(Bucley and Qu, 1991a) Bucley J.J. and Y. Qu (1991), *Solving systems of fuzzy linear equation*, Fuzzy Sets and Systems,43, pp. 33-43.

(Bucley and Qu, 1991b) Bucley J.J. and Y. Qu (1991), *Solving fuzzy equations: a new solution concept*, Fuzzy Sets and Systems, 39, pp. 291-301.

(Bucley, 1992a) Bucley J.J. (1992), *Solving fuzzy equations in economics and finance*, Fuzzy Sets and Systems,48, pp. 289-296.

(Bucley, 1992b) Bucley J.J. (1992), *Solving fuzzy equations, Fuzzy Sets and Systems*, Vol. 50, pp. 1-14.

(Bucley, 1992c) Bucley J.J. (1992a), *Solving fuzzy equations in economics and finance*, Fuzzy Sets and Systems, Vol. 48, pp. 289-296.

(Bucley, 1995) Bucley J.J. (1995), *Joint solution to fuzzy linear programming*, Fuzzy Sets and Systems, 72, pp. 215-220.

(Bucley and Feuring, 1999a) Bucley J.J. and T. Feuring (1999), *Comments on frequency/time domain methods for solutions of N-order fuzzy differential equations by Yue, Guangyuan and Sufang*, Fuzzy Sets and Systems, 105, pp. 185-185.

(Bucley and Feuring, 1999b) Bucley J.J. and T. Feuring (1999), *Introduction to fuzzy partial differential equations*, Fuzzy Sets and Systems, 195, pp. 241-248.

(Bucley and Feuring, 2000) Bucley J.J. and T. Feuring (2000), *Fuzzy differential equations*, Fuzzy Sets and Systems, Vol. 110. pp. 43-54.

(Bucley and Feuring, 2001) Bucley J.J. and T. Feuring (2001), *Fuzzy initial value problem for N-th order linear differential equations*, Fuzzy Sets and Systems, Vol. 110, pp. 247-255.

(Çağlayan, et. al., 1997) Çağlayan N. and S. Karacan and H. Hapoğlu and M. Alpbaz (1997), *Application of Optimal Adaptive Control Based on Generalized Minimum Variance to a Packed Distillation Column*, Computers Chem. Eng., Elsevier Science Ltd., Vol. 21, pp.S607-S612.

(Camacho, 1993) Camacho E. F. (1993), *Constrained generalized predictive control*, IEEE Trans. Automatic Control, Vol. 38, pp.327-332.

(Camacho and Bordons, 2004) Camacho E. F. and C. Bordons (2004), *Model Predictive Control*, Advanced Textbooks in Control & Signal Processing, Second Edition, Grimble M. J. and M. J. Johnson Editors, ISBN 1852336943, Springer.

(Cembrano, et. al., 2004) Cembrano G. and J. Quevedo and M. Salamero and V. Puig and J. Figueras and J. Marti (2004), *Optimal control of urban drainage systems – A case of study*, Control Engineering Practice, Vol. 12, No. 1, pp. 1-9.

(Chambers, 2000) Chambers L. (2000), The Practical Handbook of Genetic Algorithms: Applications, Second Edition, Chapman & Hall/CRC, ISBN: 1584882409.

(Chatchanayuenyong and Parnichkun, 2006) Chatchanayuenyong T and M. Parnichkun (2006), *Neural network based-time optimal sliding mode control for an autonomous underwater robot*, Mechatronics 16 , pp. 471–478.

(Choi and Hedrick, 1998) Choi S. B. and J. K. Hedrick (1998), *An Observer-Based Controller Design Method for Improving Air/Fuel Characteristics of Spark Ingnition Engines*, IEEE Transactions on Control System Technology, Vol. 10, pp. 325-333.

(Cirstea, et. al., 2002) Cirstea M. and A. Dinu and M. McCormick and J. G. Khor (2002), Neural and Fuzzy Logic Control of Drives and Power Systems, Newnes, ISBN: 0750655585.

(Clark and Hastings-James, 1971) Clark D.W. and R. Hastings-James (1971), *Design of digital controllers for randomly disturbed systems*, Proc. IEE, Vol. 118, No. 10, pp.1502-1506.

(Clark and Gawthrop, 1975) Clark D. W., and Gawthrop, P. J. (1975), *Self-tuning controllers,* Proc. IEE, Vol. 122, N^{o} 9, pp 929-934.

(Clarke and Gawthrop, 1979) Clark D. W., and Gawthrop, P. J. (1975), *Self-tuning controllers,* Proc. IEE, Vol. 126, N^{o} 6, pp 633-640.

(Clarke, et. al., 1987) Clarke D.W. and C. Mohtadi and P.S. Tuffs (1987), Generalized predictive control-part 1 and 2, Automatica, Vol. 23, Issue 2, pp.137-160.

(Conatser, et. al., 2004) Conatser R. and J. Wagner and S. Ganta and I. Walker (2004), *Diagnosis of automotive electronic throttle control system*, Control Engineering Practice, Vol. 12, pp. 23-30.

(Clarke, et. at., 1987a) Clarke D. W. and C. Mohtadi and P.S. Tuffs (1987), *Generalized Predictive Control-Part I, The Basic Algorithm*, Automatica, Vol. 23, pp. 137-148.

(Clarke, et. at., 1987b) Clarke D. W. and C. Mohtadi and P.S. Tuffs (1987), *Generalized Predictive Control-Part II, Extension and Interpretations Algorithms*, Automatica, Vol. 23, pp. 149-160.

(Clarke and Mohtadi, 1989) Clarke D. W. and C. Mohtadi (1987), *Properties of generalized predictive control*, Automatica, Vol. 25, No. 6, pp. 859-875.

(Clarke and Scattolini, 1991) Clarke D. W. and R. Scattolini (1987), *Constrained receding-horizon predictive control*, IEE Proceedings Part D, Vol. 138, No. 4, pp. 347-354.

(Clarke, 1996) Clarke D. W. (1996), *Adaptive Predictive Control*, A. Rev. Control, Vol. 20, pp.83-94.

(Copp, 2002) Copp J. (Ed.) (2002), COST Action 624 – *The COST Simulation Benchmark Description and Simulation Manual*, European Commision - European cooperation in the field of scientific and technical research, COST Action 624/682.

(Correa et. al., 2002) Correa J. and M. Ponce, J. Arau, J. M. Alonso, “Dimming in Metal-Halide and HPS Lamps operating al HF: Effects and Modeling”, Industry Applications Conference, IAS’2002, pp. 1467 –1474.

(Cuesta, et. al., 1999) Cuesta F. and F. Gordillo and J. Aracil and A. Ollero (1999), *Stability Analysis of Nonlinear Multivariable Takagi-Sugeno Fuzzy Control Systems*, IEEE Transactions on Fuzzy Systems, Vol. 7, No. 5, October, pp. 508-520.

(Dayan and Abbott, 2001) Dayan P. and L. F. Abbott (2001), Theoretical Neuroscience Computational and Mathematical Modeling of Neural Systems ,The MIT Press, ISBN-10:0-262-04199-5, ISBN-13: 978-0-262-04199-7.

(DeCarlo, et. al., 1988) DeCarlo R. A. and S. Zack and G. P. Mattews (1988), Variable Structure Control of Nonlinear Multivariable Systems: A Tutorial, proceedings of the IEEE, vol. 76 No. 3, March, pp. 212-232.

(Denaï, et. al., 2009) Denaï M., M. Mahfouf and J.J. Ross (2009), *A Hybrid Hierarchical Decision Support System for Cardiac Surgical Intensive Care Patients. Part I- Physiological Modeling and Decision Support Design*, Artificial Intelligence in Medicine Journal, 45(1), 35-51.

(Deng, 1995) Deng E. (1995), Negative incremental impedance of fluorescent lamp, Ph.D. Thesis, California Institute of Technology, Pasadena.

(Deng and Cuk, 1997) Deng E. and S. Cuk (1997), Negative incremental impedance and stability of fluorescent lamp, Applied Power Electronic Conference, APEC'97, pp. 1050-1056.

(Desborough and Harris, 1992) Desborough L. and T. Harris (1992), *Performance assessment measure for univariate feedback control*, Can. J. Chem. Eng., Vol. 70, pp. 1186-1197.

(Diamond, 2002) Diamond P. (2002), *Brief note on the variation of constants formula for fuzzy differential equation*, Fuzzy Sets and Systems, Vol. 129, pp. 65-71.

(Di Palma and Magni, 2004) Di Palma F. and L. Magni (2004), A multi-model structure for model predictive control, Annual Review in Control, Vol. 28, pp. 47-52.

(Dochain and Bastin, 1984) Dochain D. and G. Bastin (1984), *Adaptive identification and control algorithms for nonlinear bacterial growth systems*, Automatica, Vol. 20, pp. 612-634.

(Dorffner, 1996) Dorffner, G. 1996, Neural Networks for Time Series Processing. Neural Network World, 4/96, 447-468.

(Dougherty and Cooper, 2003a) Dougherty D. and D. Cooper (2003), *A practical multiple model adaptive strategy for single-loop MPC*, Control Eng. Practice, Vol. 11, pp. 141-159.

(Dougherty and Cooper, 2003b) Dougherty D. and D. Cooper (2003), *A practical multiple model adaptive strategy for multivariable model predictive control*, Control Eng. Practice, Vol. 11, pp. 649-664.

(Driankov, et. al, 1996) Driankov D. and H. Hellendoorn and M. Reinfrank (1996), *An Introduction to Fuzzy Control*, Springer, Second Edition.

(Dutka, 2005) Dutka A. S. (2005), *Non-linear Identification, Estimation and Control of Automotive Powertrains*, Doctoral Thesis, Industrial Control Center, University of Strathclyde, Scotland, UK.

(Erdogmus, et. al., 2002) Erdogmus D. and A. U. Genç and J. C. Principe (2002), *A Neural Network Perspective to Extended Luenberger Observers*, Institute of Measurement and Control, vol. 35, pp. 10-16, (Special Feature on Recent Advances in Neural Networks, Part 2).

(Ertnuç, et. al., 2003) Ertnuç S. and B. Akay and N. Bursali and H. Hapoğlu and M. Alpbaz (2003), *Generalized Minimum Variance Control of Growth Medium Temperature of Baker's Yeast Production*, Trans. IChemE, Vol. 81, Part C., pp. 327-335

(Evans-Pughe, 2006) Evans-Pughe C. (2006), *LERNING TO DRIVE: Car manufacturers are exploiting the self-learning powers of neural networks in the battle to meet ever-tightening emission requirements*, IEE Proc. Engineering and Technology, pp. 42-45.

(Fantuzzi and Rovatti, 1996) Fantuzzi C. and R. Rovatti (1996), *On the approximation capabilities of the homogeneous Takagi-Sugeno fuzzy systems by Lyapunov Method*, Proccedings Fifths IEEE International Conference on Fuzzy Systems, New Orleans, USA, pp. 1067-1072.

(Farley and Clark, 1954) Farley, B and W.A. Clark (1954). "Simulation of Self-Organizing Systems by Digital Computer". IRE Transactions on Information Theory 4: 76–84.

(Ferrari and Stengel, 2002) Ferrari S. and R. F. Stengel (2002), *Clasical /Neural Synthesis of Nonlinear Control Systems*, Journal of Guidance, Control, and Dynamics, Vol. 25, No. 3, pp. 442-449.

(Fischer, et. al., 1998) Fischer M. and O. Nelles and R. Isermann (1998), *Adaptive predictive control of a heat exchanger based on a fuzzy model*, Control Eng. Practice, Vol. 6, pp. 259-269.

(Findeisen, et. al., 2007) Findeisen R. and F. Allgower, and L. T. Biegler (2007), *Assessment and Future Directions of Nonlinear Model Predictive Control*, Lecture Notes in Control & Information Sciences, ISBN 3540726985, Springer-Verlag Berlin and Heidelberg GmbH & Co. K.

(Floreano and Mattiussi, 2008) Floreano D. and C. Mattiussi (2008), Bio-Inspired Artificial Intelligence: Theories, Methods, and Technologies, The MIT Press, ISBN: 0262062712.

(Flynn, et. al., 1997) Flynn D. and S. McLoone and G. W. Irwin and M. D. Brown and E. Swidenbank and B. W. Hogg (1997), *Neural Control of Turbogenerator Systems*, Automatica, Vol. 33, No. 11, pp. 1961-1973.

(Frank, et. al., 2001) Frank R. J. and N. Davey and S. P. Hunt (2001),Time Series Prediction and Neural Networks, Journal of Intelligent and Robotic Systems, Volume 31 Issue 1-3, Kluwer Academic Publishers Hingham, MA, USA.

(Fraser, 1957) Fraser, Alex (1957), Simulation of genetic systems by automatic digital computers. I. Introduction, Aust. J. Biol. Sci. 10: 484–491.

(Fraser and Burnell, 1970) Fraser A. and D. Burnell (1970), Computer Models in Genetics, New York: McGraw-Hill. ISBN 0070219044.

(Friedman, 1991) Friedman, J.H. (1991). Multivariate adaptive regression splines. The Annals of Statistics 19(1), 1–141.

(Galavec, 2001) Galavec M. (2001), *Solvability and unique solvability of max-min fuzzy equations*, Fuzzy Sets and Systems, Vol. 124, pp. 385-393.

(Garcia, et. al., 1989) Garcia C. E. and D. M. Prett and M. Morari (1989), *Model predictive control: theory and practice-a survey*, Automatica, Vol. 25, Issue 3, pp.335-348.

(Gasparyan, 2008) Gasparyan O. N. (2008), Linear and Nonlinear Multivariable Feedback Control: A Classical Approach, John Wiley & Sons, Ltd. ISBN: 978-0-470-06104-6.

(Gawthrop, et. al., 1996) Gawthrop P. J. and R. W. Jones and D. G. Sbarbaro(1996), *Emulator-based Control and Internal Model Control: Complementary Approaches to Robust Control Design*, Automatica, Vol. 32, pp. 1223-1227.

(Ge and Zhang, 2003) Ge S.S. and J. Zhang (2003), *Neural-network control of nonaffine nonlinear system with zero dynamics by state and output feedback*, IEEE Transactions on Neural Networks, ISSN: 1045-9227, Vol. 14 Issue: 4, pp. 900 – 918.

(Gessing and Błachuta, 1996) Gessing R. and M. Błachuta (1996), *SET POINT AND IDENTIFIABILITY IN THE CLOSED LOOP WITH A MINIMUM-VARIANCE CONTROLLER*, Control Eng. Practice, Vol. 4, No. 5, pp.665-670.

(Gen, et. al., 2008) Gen M. and R. Cheng and L. Lin (2008), Network Models and Optimization: Multiobjective Genetic Algorithm Approach, Springer, ISBN: 1848001800.

(Gomez-Ortega and Camacho, 1996) Gomez Ortega J. and E. F. Camacho (1996), *Mobile Robot Navigation In A Partially Structured Static Enviroment, Using Neural Predictive Control*, Control Eng. Practice, Vol. 14, No. 12, pp. 1669-1679.

(Gomm, et. al., 1997) Gomm J. B. and J. T. Evans and D. Williams (1997), *Development and Performance of a Neural-Network Predictive Controller*, Control Eng. Practice, Vol. 5, No. 1, pp. 49-59.

(Goodwin, et. al., 1980) Goodwin G. C. and K. S. Sin and K. K. Saluja (1980), *Stochastic adaptive control and prediction – the general delay-coloured noise case*, IEEE Trans. Automat. Control, Vol. 25, pp. 946-950.

(Goodwin, et. al., 1981) Goodwin G. C. and P. J. Ramadge and P.E. Caines (1981), *Discrete-time stochastic adaptive control*, SIAM J. Control, Vol. 19, pp. 826-853.

(Goodwin and Sin, 1984) Goodwin G. C. and K. S. Sin (1984), *Adaptive Filtering Prediction and Control*, Prentice Hall, Englewood Cliffs.

(Goowin, et. al., 2000) Goodwin G. C. and S. Graebe and O. Rojas (2000), *Control System Design*, Prentice-Hall, Upper Saddle River, N.J.

(Goodwin, et. al., 2001) Goodwin G. C. and O. Rojas and H. Takata (2001), *NONLINEAR CONTROL VIA GENERALIZED FEEDBACK LINEARIZATION USING NEURAL NETWORKS*, Asian Journal of Control, Vol. 3, No.2, pp. 79-88.

(Gorzalczany and Gluszek, 2000) Gorzalczany M. B. and A. Gluszek (2000), *Neuro-fuzzy systems for the rule-based modeling of dynamic processes*, ESIT 2000, 14-15 September 2000, Aachen, Germany, pp. 416-422.

(Grassmann and Anlauf, 1999) Grassmann C. and J. K. Anlauf (1999), Fast digital simulation of spiking neural networks and neuromorphic integration with spikelab, International Journal of Neural Systems, Vol9, No. 5 473–478.

(Grimble, 1981) Grimble M. J. (1981), *A control weighted minimum-variance controller for non-minimum phase systems*, International Journal of Control, Vol. 33, No. 4, pp. 751-762.

(Grimble, 1982) Grimble M. J. (1982), *Weighted minimum variance self-tuning control*, International Journal of Control, Vol. 36, No. 4, pp. 831-842.

(Grimble, 1984) Grimble M. J. (1984), *LQG multivariable controllers: minimum variance interpretation for use in self-tuning systems*, International Journal of Control, Vol. 40, No. 4, pp. 831-842.

(Grimble, 1988) Grimble M. J. (1988), *Generalized minimum variance control law revisited*, Optimal Control Applications and Methods, Vol. 9, pp.63-77.

(Grimble, 1993) Grimble M. J. (1993), H_∞ *Multivariable control law synthesis*, IEE Proceedings, Control Theory and Applications, Vol. 140, No. 5, pp. 353-363.

(Grimble, 1994) Grimble, M.J. (1994), *Robust Industrial Control, Optimal Design Approach for Polynomial Systems*, Prentice Hall Int., Series in Systems and Control Engineering , Prentice Hall, Hemel Hempstead, UK.

(Grimble, 2002) Grimble M. J. (2002), *Controller performance benchmarking and tuning using generalised minimum variance control*, Automatica, Vol. 38, pp. 2111-2119.

(Grimble, 2003) Grimble, M.J. (2003), *Generalized Minimum Variance Control of Nonlinear Multivariable Systems*, Internal report ICC-210, Industrial Control Centre, Univ. of Strathclyde.

(Grimble, 2004) Grimble M. J. (2004), *Integral minimum variance control and benchmarking*, Journal of Process Control, Vol. 14, pp. 177-191.

(Grimble and Ordys, 2001) Grimble M. J. and A. W. Ordys (2001), *Predictive Control for Industrial Applications*, Annual Reviews in Control, Vol. 25, pp. 13-24.

(Grizzle, et. al., 1994) Grizzle J. W. and J. Cook and W. Milam (1994), Improved cylinder air charge estimation for transient air fuel ratio control, Proc. of the American Control Conference, Baltimore, USA, pp. 1568-1573.

(Groot and Van Vliet, 1986) Groot J. J. and J. A. J. M. Van Vliet (1986), The high-pressure sodium lamp, Editorial Macmillan Education.

(Gulko and Ben-Yaakov, 1993) Gulko M. and S. Ben-Yaakov, Current Sourcing Push-Pull Parallel-Resonance Inverter (CS-PPRI): Theory and application as a Fluorescent lamp Driver, IEEE APEC'93, pp. 411-417.

(Guo and Chen, 1991) Guo L. and H. F. Chen (1991), *The astron-wittenmark self-tuning regulator revisited and els-based adaptive trackers*, IEEE Trans. Autom. Control, Vol. 36, pp. 802-812.

(Haefke, C. and C. Helmenstein, 1996) Haefke, C. and C. Helmenstein (1996), Neural *Networks in the Capital Markets: An Application to Index Forecasting*, Computational Economics 9, pp. 37–50.

(Hafner, et. al., 2000) Hafner M. and M. Schüller and O. Nelles and R. Isermann (2000), *Fast neural networks for diesel engine control design*, Control Engineering Practice, Vol. 8, pp. 1211-1221.

(Hageman, et. al., 2003) Hageman J.J. , M. S. Smith, and S. Stachowiak (2003), Integration of Online Parameter Identification and Neural Network for In-Flight

Adaptive Control, NASA Dryden Flight Research Center Edwards, California, NASA/TM-2003-212028.

(Harris, 1989) Harris T. J. (1989), *Assessment of closed loop performance*, Can. J. Chem. Eng., Vol. 67, pp. 856-861.

(Harris, et. al., 1996) Harris T. J. and F. Boudreau and J. F. Macgregor (1996), *Performance Assessment of Multivariable Feedback Controllers*, Automatica, Vol. 32, No. 11., pp. 1505-1518.

(Harris and MacGregor, 1987) Harris and MacGregor (1987), Design of multivariable linear quadratic controllers using transfer function, AIChE J., Vol. 33, pp. 1481-1495.

(Hastings-James, 1970) Hastings-James R. (1970), *A linear stochastic controller for regulation of systems with pure delay*, University of Cambribge, Department of Engineering, Research Report No. CN/70/3.

(Hang, et. al., 1991) Hang C. C. and K.W. Lim and W. K. Ho (1991), Generalized minimum-variance stochastic self-tuning controller with pole restriction, IEE Proc, Vol. 138, Issue 1, pp. 25-32.

(He and Jagannathan, 2005) He P. and S. Jagannathan (2005), *Neuro-controller for reducing cyclic variation in lean combustion spark ignition engines*, Automatica, Vol. 41, pp. 1133-1142.

(Hebb, 1949) Hebb, Donald (1949). The Organization of Behavior. New York: Wiley.

(Hellerdoorn and Driankov, 1997) Hellerdoorn, H. and D. Driankov (1997), *Fuzzy Model Identification*, Springer-Verlag.

(Hernández, et. al., 2001) Hernández C. and N. Vázquez and E. Rodríguez and R. Osorio and J. Arau (2001), Voltage regulator with unity power factor and high efficiency, Power Electronics Specialists Conference, PESC'01, Vol. 3,pp. 1653-1658.

(Herrick, 1980) Herrick P. R. (1980), Mathematical Models for High-Intensity Discharge Lamps, IEEE Trans. on industrial Applications, Vol. IA-16, No. 5, September/October, pp. 648-654.

(Hiemstra, 1996) Hiemstra, Y.(1996), *Linear Regression versus Backpropagation Networks to Predict Quarterly Stock market Excess Returns*, Computational Economics 9, pp. 67–76.

(Hirota and Sugeno, 1995) Hirota K. and M. Sugeno (1995), *Industrial Applications of Fuzzy Technology in the World*.

(Holland, 1975) Holland J. H.(1975), Adaptation in Natural and Artificial Systems: An Introductory Analysis with Applications to Biology, Control, and Artificial Intelligence, Ann Arbor, MI: University of Michigan Press, 1975.

(Horch and Isaksson, 1999) Horch A. and A. J. Isaksson (1999), A modified index for control performance assessment, J. Process Control, Vol. 9, Issue 6, pp. 1-17.

(Horch and Isaksson, 2001) Horch A. and A. J. Isaksson (2001), Assessment of the sampling rate in control systems, Control Engineering Practice, Vol. 9, pp. 533-544.

(Horowitz and Li, 1996) Horowitz R. and R. Li (1996), *Adaptive track-following servos for disk file actuators*, IEEE Trans. Magn., Vol. 32, Issue 3, pp. 1779-1786.

(Horowitz, et. al., 1998) Horowitz R. and B. Li and J. W. McCormick (1998), *Wiener-filter-based Minimum Variance Self-tuning Regulation*, Automatica, Vol. 34, No. 5, pp. 531-545.

(Hsu, et. al., 1995) Hsu K.-L. and H.V. Gupta and S. Sorooshian (1995), Artificial Neural Network Modeling of the Rainfall-Runoff Process, WATER RESOURCES RESEARCH, VOL. 31, NO. 10, PP. 2517-2530, doi:10.1029/95WR01955.

(Hu and Hwang, 2001) Hu Y. H. and J.-N. Hwang (2001), *Handbook of Neural Network Signal Processing*, Electrical Engineering & Applied Signal Processing Series, Edited by Yu Hen Hu and Jenq-Neng Hwang, CRC Press; 1 edition, (September 21, 2001), ISBN-10: 0849323592, ISBN-13: 978-0849323591.

(Huang, et. al., 1997a) Huang B. and S. L. Shah and E. K. Kwok (1997), *Good, Bad or Optimal? Performance Assessment of Multivariable Processes*, Automatica, Vol. 33, No. 6, pp. 1175-1183.

(Huang, et. al., 1997b) Huang B. and S. L. Shah and H. Fujii (1997), *The unitary interactor matrix and its estimation using closed-loop data*, J. Proc. Control, Vol. 7, No. 3, pp. 195-207.

(Huang and Shah, 1997) Huang B. and S. L. Shah (1997), *The Role of the Unitary Interactor Matrix in the Explicit Solution of the Singular LQ Output Feedback Control Problem*, Automatica, Vol. 33, No. 11, pp. 2071-2075.

(Huang, 1999) Huang B. (1999), *Performance assessment of processes with abrupt changes of disturbances*, Canadian Journal of Chemical Engineering, Vol. 77, Issue 5, pp. 1044-1054.

(Huang, et. al., 2000a) Huang B. and R. Kadali and X. Zhao and E. C. Tamayo and Ahmed Hanafi (2000), *An investigation into the poor performance of a model predictive control system on an industrial CGO coker*, Control Eng. Practice, Vol. 8, pp. 619-631.

(Huang, et. al., 2000b) Huang Y. L. and H. H. Lou and J. P. Gong and T. F. Edgar (2000), Fuzzy model predictive control, IEEE Trans. on Fuzzy Systems, Vol. 8, No. 6, pp. 665-678.

(Huang, 2002) Huang B. (2002), *Minimum variance control and performance assessment of time-variant processes*, Journal Process Control, Vol. 12, pp. 707-719.

(Hung, et. al., 1993) Hung J. Y. and W. Gao and J. C. Hung (1993), Variable Structure Control: A Survey, IEEE Transactions on Industrial Electronics, Vol. 40, No. 1, Feb., pp. 2-18.

(Ibarrola, et. al, 2002) Ibarrola J. J. and J. M. Sandoval and M. García-Sanz and M. Pinzotas (2002), *Predictive control of a high temperature-short time pasteurisation problem*, Control Eng. Practice, Vol. 10, pp. 713-725.

(Isermann, et. al., 2002) Isermann R. and R. Schwarz and S. Stölzl (2002), *FAULT-TOLERANT Drive-by-Wire Systems*, IEEE Control Systems Magazine , Vol. 10, No. 5, 0272-1708/02, pp. 64-81.

(Isidori, 1986) Isidori A. (1986), Nonlinear Control Systems: An Introduction, Springer, 1986, ISBN: 3540155953.

(Isidori, 1995) Isidori A. (1995), Nonlinear Control Systems, Springer Verlag, London.

(Isidori, 1999) Isidori A. (1999), Nonlinear Control Systems II, Springer, ISBN: 1852331887.

(Jalal, et. al., 1998) Jalal A. M. and A. M. Farboud and A. A. Ghandadly (1998), *Adaptive enhancement of synchronous generator stabilizer performance by including the external utility system dynamics*, Electric Power Systems Research, Vol. 46, pp. 111-117.

(Jang, 1992a) Jang J.-S. R (1992), *Neuro-Fuzzy Modeling: Architectures, Analyses and Applications*, PhD Thesis, University of California, Berkeley, July.

(Jang, 1992b) Jang J.-S. R. (1992), *Self-Learning Fuzzy Controller Based on Temporal Back Propagation*, IEEE Transactions on Neural Networks, Vol. 3, Issue 5, September, pp.714-723.

(Jang and Sun, 1993) Jang J.-S. R. and C.-T. Sun (1993), *Functional equivalence between radial basis function networks and fuzzy inference systems*, IEEE Transactions on Neural Networks, Vol. 4, Issue 1, pp.156-159.

(Jang and Sun, 1995) Jang J.-S. R. and C.-T. Sun (1995), *Neuro-Fuzzy Modeling and Control*, Proceedings of the IEEE, Vol. 83, No. 3, pp.378-406.

(Jang, et. al., 1997) Jang J.-S. R. and C.-T. Sun and E. Mizutani (1997), *Neuro-Fuzzy and Soft Computing- A Computational Approach to Learning and Machine Intelligence*, ISBN 0-13-261066-3**,** Pearson Education editorial.

(Joh, et. al., 1998) Joh J. and Y.-H. Chen and R. Langari (1998), *On the Stability Issues of Linear Takagi-Sugeno Fuzzy Models*, IEEE Transaction on Fuzzy Systems, Vol. 6, No. 3, pp. 402- 410.

(Johansen, et. al., 2000) Johansen T. A. and Shorten R. and Murray-Smith R. (2000), *On the Interpretation and Identification of Dynamic Takagi-Sugeno Fuzzy Models*, IEEE Transaction on Fuzzy Systems, Vol. 8, No. 3, pp. 297-313.

(Kaewkongka, et. al., 2001) Kaewkongka T., Y H Joe Au, R Rakowski and B E Jones (2001), *Continuous wavelet transform and neural network for condition monitoring of rotodynamic machinery*, IEEE Instrumentation and Measurement Technology Conference Budapest, Hungary, May 21-23.

(Kalman, 1958) Kalman R.E. (1958), Design of a self-optimizing control system, Trans. ASME, Vol. 80, pp. 468-478.

(Kalman, 1960a) Kalman R. E. (1960), *Contribution to theory of optimal control*, Bulletin de la Societe Mathematique de Mexicana, Vol. 5, pp. 102-119.

(Kalman, 1960b) Kalman R. E. (1960), *A new approach to linear filtering and prediction problems*, Transaction of ASME, Journal of Basic Engineering, Vol. 87, pp. 35-45.

(Karagöz, et. al., 2000) Karagöz A. R. and H. Hapoğlu and M. Alpbaz (2000), *Generalized minimum variance control of optimal temperature profiles in a polystyrene polymerization reactor*, Chemical Engineering and Processing, Vol. 39, pp. 253-262.

(Kawamoto, et. al., 1992) Kawamoto S. and K. Tada and A. Ishigame and T. Taniguchi (1992), *An approach to stability analysis of second order fuzzy system*, Ist Proc. IEEE Int. Conf. Fuzzy System, San Diego, CA, March, pp. 1427-1434.

(Khomfoi and Tolbert 2007) Khomfoi S. and L. M. Tolbert (2007), *Fault Detection and Reconfiguration Technique for Cascaded H-bridge 11-level Inverter Drives Operating under Faulty Condition*, PEDS 2007, 1-4244-0645-5/07/$20.00©2007 IEEE, pp. 1035-1042.

(Kilmer, et. al., 1999) Kilmer R. A., A. E. Smith and L. J. Shuman (1999), Computing confidence intervals for stochastic simulation using neural network metamodels, Computers & Industrial Engineering, Vol. 36, Issue 2, Pages 391-407.

(Kim, 2004) Kim E. (2004), *A New Computational Approach to Stability Analysis and Synthesis of Linguistic Fuzzy Control System*, IEEE Transaction on Fuzzy Systems, Vol. 12, No. 3, June, pp. 379-388.

(Kim, et. al., 2007) Kim M.-C., S.-K. Park and G.-P. Kwak (2007), *Design of robust optimal controller using neural network*, International Conference on Control, Automation and Systems, 2007. ICCAS '07, ISBN: 978-89-950038-6-2, pp. 532 – 535.

(Ko and Edgar, 2001) Ko B.-S. and T. F. Edgar (2001), *Performance assessment of multivariable feedback control systems*, Automatica, Vol. 37, pp. 899-905.

(Koivo, 1980) Koivo H. N. (1980), A multivariable self-tuning controller, Automatica, Vol. 16, pp. 351-366.

(Kolmanovsky and Stefanopoulou, 2001) Kolmanovsky I. and A. G. Stefanopoulou (2001), *Optimal Control Techniques for Assessing Feasibility and Defining Subsystem*

Level Requirements: An Automotive Case Study, IEEE Transactions on Control, Systems Technology, Vol. 9, No. 3, pp. 524-534.

(Kolmanovsky, et. al, 2002) Kolmanovsky I.V. and M. Druzhinina and J. Sun (2002), *Speed-Gradient Approach to Torque and Air-to-Fuel Ratio Control in DISC Engines*, IEEE Transaction on Control, Systems Technology, Vol. 3, No. 5, pp. 671-678.

(Kouvaritakis, et. al., 1992) Kouvaritakis B. and J. A. Rossiter an A.O.T. Chang (1992), *Stable generalised predictive control: An algorithm with guaranteed stability*, IEE Proceedings Part D, Vol. 139, No. 4, pp. 349-362.

(Kovačić and Bogdan, 2006) Kovačić Z. and S. Bogdan (2006), Fuzzy Controller Design: Theory and Applications, A Series of Reference Books and Textbooks, CRC Press, Taylor & Francis Group, LLC, ISBN 0-8493-3747-X.

(Kozub and Garcia, 1993) Kozub D. J. and C. E. Garcia (1993), Monitoring and diagnosis of automated controllers in the chemical process industries, In: AIChE Annual Metting, St. Louis, MO, 9 November.

(Krauss, et. al., 1994) Krauss P. and K. Dass and H. Rake (1994), *Model based predictive controller with Kalman filtering for state estimation*, Advances in model-based predictive control, Oxford University Press, pp. 69-83.

(KRI, 2006) KRI (2006), KENT Ridge Instruments, http://www.kri.com.sg/dsim.html#start and http://www.kri.com.sg/dps101.pdf

(Kung and Womack, 1984) Kung M. and B. F. Womack (1984), *Discrete time adaptive control of linear systems with preload nonlinearity*, Automatica, Vol.20, No.4, pp. 477-479.

(Lai and Wei, 1986) Lai T. L. and C. Z. Wei (1986), Extended least squares and their applications to adaptive control and prediction in linear systems, IEEE trans. Autom. Control, Vol. 31, pp. 898-906.

(Laskowski and Donoghue, 1981) Laskowski E. L. and J.F. Donoghue (1981), A model of a Mercury Arc Lamp's Terminal V-I behavior, IEEE Trans. on industry Applications, Vol. IA-17, No. 4, July/August, pp. 419-426.

(Lee, 1990a) Lee Chuen Chien (1990), *Fuzzy Logic in Control Systems: Fuzzy Logic Controller-Part I*, IEEE TRANSACTIONS ON SYSTEMS, MAN, AND CYBERNETICS, Vol. 20, No. 2, March/April.

(Lee, 1990b) Lee Chuen Chien (1990), *Fuzzy Logic in Control Systems: Fuzzy Logic Controller-Part II*, IEEE TRANSACTIONS ON SYSTEMS, MAN, AND CYBERNETICS, Vol. 20, No. 2, March/April.

(Lee, 2006) Lee R. S.T. (2006), *Fuzzy-Neuro Approach to Agent Applications*, ISBN 978-3-540-21203-4, Springer.

(Leland, 1995) Leland R.P. (1995), *Fuzzy differential systems and Malliavin calculus*, Fuzzy Sets and Systems, Vol. 70, pp. 59-73.

(Leontaritis and Billings, 1985a) Leontaritis I. J. and S. A. Billings (1985), *Input-output parametric models for nonlinear systems – part I: deterministic nonlinear system*, Int. J. Control, Vol. 41, No. 2, pp. 303-328.

(Leontaritis and Billings, 1985b) Leontaritis I. J. and S. A. Billings (1985), *Input-output parametric models for nonlinear systems – part II: stochastic non-linear systems*, Int. J. Control, Vol. 41, No. 2, pp. 329-344.

(Li and Evans, 1997) Li Z. and R. J. Evans (1997), *Minimum-variance Control of Linear Time-varying Systems*, Automatica, Vol. 33, No. 8, pp. 1531-1537.

(Liand, et. al., 1998) Liang T. J. and K. H. Su and W. H. Fu (1998), High Frequency Electrical Circuit Model of Metal-Halide Lamp, IEEE PESC'98, pp. 1163-1167.

(Lin and Lee, 1996) Lin C.-T. and C.-C. Lee (1996), *Neural Fuzzy Systems. A Neuro-Fuzzy Synergism to Intelligent Systems*, Prentice-Hall, Englewood Cliffs, NJ.

(Liu, et. al., 1998) Liu T. and K. J. Tseng and D.M. Vilathgamuwa (1998), A PSpice Model for the Electrical Characteristics of Fluorescent Lamps, IEEE PESC'98, pp. 1749-1754.

(Liu and Stefanopoulou, 2002) Liu S. and A. G. Stefanopoulou (2002), *Effects of Control Structure on Performance for an Automotive Powertrain With a Continuously Variable Transmission*, IEEE Transactions on Control Systems Technology , Vol. 10, No. 5, pp. 701-708.

(Liu, 2001) Liu G. P. (2001), *Nonlinear Identification and Control: A Neural Network Approach*, Advances in Industrial Control, ISBN 1852333421, Springer.

(Lu, et. al., 2001) Q. Lu and Y. Sun and S. Mei (2001), Nonlinear Control Systems and Power System Dynamics,Springer, 2001, ISBN: 079237312X.

(Lynch and Dumont, 1996) Lynch C. B. and G. A. Dumont (1996), Control loop performance monitoring, IEEE Trans. Control Sys. Tech., Vol. 4, Issue 2, pp. 185-192.

(Maciejowski, 2002) Maciejowski J. M. (2002), *Predictive Control with Constraints*, ISBN 0 201 39823 0 PPR., Prentice Hall.

(Mahfouf, et. al., 2003) Mahfouf M. and A. J. Asbury and D. A. Linkens (2003), *Unconstrained and constrained generalised predictive control of depth of anaesthesia during surgery*, Control Eng. Practice, Vol. 11, pp. 1501-1515.

(Mader and Horn, 1992) Mader U. and P. Horn (1992), A dynamic model for the electrical characteristics of fluorescent lamps, Industry Applications Society Annual Meeting, 1992., Conference Record of the 1992 IEEE, 4-9 Oct 1992, pp. 1928 -1934.

(Maiers and Sherif, 1985) Maiers J. and Y.S. Sherif, "Applications of Fuzzy Set Theory", IEEE TRANSACTIONS ON SYSTEMS, MAN, AND CYBERNETICS, Vol. SMC-15, No. 1, January/February.

(Maiellaro, et. al., 2004) Maiellaro P. A. , R. Cozzolongo and P. Marino (2004), *Artificial Neural Networks for the Prediction of Response to Interferon Plus Ribavirin Treatment in Patients with Chronic Hepatitis C*, Current Pharmaceutical Design, 2004,10, 2101-2109.

(Malmgren, et. al., 2000) Malmgren, H., M. Borga and L. Niklasson (2000), *Artificial Neural Networks in Medicine and Biology*, Proceedings of the ANNIMAB-1 Conference, Göteborg, Sweden, 13-16 May 2000, Perspectives in Neural Computing, Malmgren, H.; Borga, M.; Niklasson, L. (Eds.), 1st Edition., 2000, XII, ISBN 978-1-85233-289-1.

(Mamdani and Assilian, 1974) Mamdani, E.H. and S. Assilian (1974). Application of fuzzy algorithms for control of simple dynamic plant, Proc. IEE vol. 121, pp.1585-1588.

(Mamdani and Assilian, 1975) Mamdani E. H. and S. Assilian (1975), *An experiment in linguistic synthesis with a fuzzy logic controller*, Int. J, Man Mach. Studies, vol. 7, no. 1, pp.1-13, 1975.

(Martin, et. al., 1986) Martin G. D. and J. W. Caldwell and T. E. Ayral (1986), Predictive control applications for the petroleum refining industry, In: Petroleum Refining Conference, Japan Petroleum Institute ,Tokyo, Japan.

(Marsili-Libelli and Giunti, 2002) Marsili-Libelli S. and L. Giunti (2002), *Fuzzy predictive control for nitrogen removal in biological wastewater treatment*, Water Science and Technology, Vol. 45, No.4-5, pp. 37-44.

(Mastorakis, 2004) Mastorakis N. (2004), *Modeling Dynamical Systems via the Takagi-Sugeno-Fuzzy Model*, In preparation.

(Matlab, 1999) The MATH WORKS Inc. (1999) *Fuzzy logic Toolbox*, For Use with MATLAB.

(Mattavelli, et. al., 1993) Mattavelli P. and L. Rossetto and G. Spiazzi (1993), General Purpose Sliding Mode Controller For DC/DC Converter Applications, IEEE Power Electronics Specialists Conference - PESC'93, pp. 609-615.

(McCullock and Pitts, 1943) McCullock W. and W. Pitts (1943). "A Logical Calculus of Ideas Immanent in Nervous Activity". Bulletin of Mathematical Biophysics 5: 115–133. doi:10.1007/BF02478259

(Mesquita Brandão, et. at., 2010) Mesquita Brandão R. F., J. A. Beleza Carvalho and F. P. Maciel Barbosa (2010), *Neural Networks for Condition Monitoring of Wind Turbines,* Modern Electric Power Systems 2010, Wroclaw, Poland.

(Mogens, et. al., 2000) Mogens, H., G. Willi, M. Takashi, and M. Van Loosdrecht (2000). *Activated sludge models ASM1, ASM2, ASM2d and ASM3,*. London: IWA publishing. ISBN 1-900222-24-8.

(Mohtadi, et. al., 1987) Mohtadi C. and S. L. Shah and D. W. Clarke (1987), *Multivariable adaptive control without a prior knowledge of the delay matrix*, System and Control Letters, Vol. 9, pp. 295-306.

(Mollov, 2002) Mollov S. (2002), *Fuzzy Control of Multiple-Input Multiple-Output Processes*, Doctoral Thesis, Technische Universitie of Delft, ISBN: 90-9016413-8.

(Mollov, et. al., 2002) Mollov S. and T. van den Boom and F. Cuesta and A. Ollero and R. Babuška (2002), *Robust stability constraints for fuzzy model predictive control*, IEEE Trans. on Fuzzy Systems, Vol. 10, No. 1, pp. 50-64.

(Mollov, et. al., 2004) Mollov S. an R. Babuška and J. Abonyi and H. B. Verbruggen (2004), *Effective Optimization for fuzzy model predictive control*, IEEE Trans. on Fuzzy Systems, Vol. 12, No. 5, pp. 661-675.

(Mosca and Zhang, 1992) Mosca E. and J. Zhang (1992), Stable redesign of predictive control, Automatica, Vol.20, No. 6, pp. 1229-1233.

(Mourot, et. al., 1999) Moutot G. and K. Gasso and J. Ragot (1999), *Modeling of ozone concentrations using a Takagi-Sugeno model*, Control Engineering Practice, Vol. 7, pp. 707-715.

(Miaosen, et. al., 2002a) Miaosen S. and Q. Zhaoming and F. Z. Peng**,** Control strategy of a novel two-stage acoustic resonance free electronic ballast for HID lamps**,** Power Electronics Specialists Conference, PESC'02, pp. 209 –212.

(Miaosen, et. al., 2002b) Miaosen S. and Q. Zhaoming and F. Z. Peng, A novel two-stage acoustic resonance free electronic ballast for HID lamps**,** Industry Applications Conference, IAS'02, pp. 1869 –1874.

(Miaosen, et. al., 2003) Miaosen S. and Q. Zhaoming and F. Z. Peng, Design of two-stage low-frequency square-wave electronic ballast for HID lamps**,** IEEE Transactions on Industry Applications, pp. 424-430.

(Mudi and Nikhil, 1999) Mudi R. K. and R. P. Nikhil, A Robust Self-Tuning Scheme for PI- and PD-Type Fuzzy Controllers, IEEE TRANSACTIONS ON FUZZY SYSTEMS, Vol. 7, No.1, February.

(Nauck and Kruse, 1997) Nauck D. and R. Kruse (1997), *Neuro-Fuzzy for Function Approximation*, 4th International Workshop Fuzzy-Neuro Systems.

(Nauck, 1997) Nauck D. (1997), *NEURO-FUZZY SYSTEMS: REVIEW AND PROSPECTS, Proc. Fifth European Congress on Intelligent Techniques and Soft Computing*, EUFIT'97, September 8-11, pp. 1044-1053.

(Nauck, et al., 1997) Nauck D. and F. Klawonn and R. Kruse (1997), *Foundations of Neuro-Fuzzy Systems*, Wiley, Chichester.

(Negoita and Hintea, 2009) Negoita M. G. and S. Hintea (2009), Bio-Inspired Technologies for the Hardware of Adaptive Systems: Real-World Implementations and Applications, Springer, ISBN: 3540769943.

(Nyberg and Nielsen, 1997) Nyberg M. and L. Nielsen (1997), *Model Based Diagnosis for Air Intake System of SI-Engine*, Transactions of Commercial Vehicles, SAE paper 9702009

(Nyberg, 1999) Nyberg M. (1999), *Automatic design of diagnosis system with application to an automotive engine*, Control Engineering Practice, Vol. 7, pp. 993-1005.

(O'Brien, et. al., 2005) O'Brien M. and S.E. Pinto Castillo and R. Katebi (2005), Model Based Predictive Control for Wastewater Application, 16th IFAC World Congress in Prague, ISBN-13:978-0-08-045108-4, ISBN-10: 0-08-045108-X, Czech Republic.

(Odom and Sharda, 1990) Odom M. D. and R. Sharda (1990), A neural network model for bankruptcy prediction, 1990 IJCNN International Joint Conference on Neural Networks,17-21 Jun 1990, Vol. 2, pp. 163 – 168.

(Omatu, et. al., 1995) Omatu, S. and M. Khalid and R. Yusof (1995), *Neuro-Control and Its Applications*, Advances in Industrial Control, Springer.

(Onnen, et. al., 1997) Onnen C. and R. Babuška and U. Kaymak and J. M. Souza and H. B. Verbruggen and R. Isermann (1997), *Genetic Algorithms for Optimization in Predictive Control*, Control Eng. Practice, Vol. 5, No. 10, pp. 271-278.

(Orosco and Vazquez, 2000) Orosco R. and N. Vazquez (2000), Discrete sliding mode control for DC/DC converters, Power Electronics International Congress, pp.231 – 236.

(Osorio, et. al., 2004a) Osorio R. and M. Ponce and M. A. Oliver (2004), Simplified Thermal-Electric Dynamic Model for HID lamps, Power Electronics Specialists Conference, PESC'04.

(Osorio, et. al., 2004b) Osorio R. and M. Ponce and M. A. Oliver (2004), ANALYSIS AND DESIGN OF A DIMMING CONTROL USING SLIDING MODE CONTROL

STRATEGY FOR ELECTRONIC BALLAST FREE OF ACOUSTIC RESONANCES, IEEE Applied Power Electronic Conference, APEC-04.

(Osorio, et. al., 2004c) Osorio R. and M. Ponce and M. A. Oliver (2004)R. Osorio, M. Ponce, M. A. Oliver, Control por Modos Deslizantes en Corriente Aplicado a un Balastro Electrónico Libre de Resonancias Acústicas, Congreso Latinoamericano de Control Automático, CLCA'04.

(Osorio, et. al., 2005a) Osorio R. and M. A. Oliver and M. Ponce and S. E. Pinto, M. Juárez and R. Katebi and M. J. Grimble (2005), Analysis and Design of Discrete-Sliding-Mode Control for a Square-Waveform-Ballast, 44th IEEE Conference on Decision and Control and European Control Conference, CDC-ECC 2005.

(Osorio, et. al., 2005b) Osorio R. and M. A. Oliver and M. Ponce and S. E. Pinto and R. Katebi, Simplified-Stability Analysis of Square-waveform Ballast Using a Non Linear Lamp Model, Congreso Nacional de Control Automático, CNCA'05.

(Osorio, et. al., 2005c) Osorio R. and M. A. Oliver and M. Ponce and S. E. Pinto, V. H. Olivares, M. J. Grimble, R. Katebi, Linear-Thermal Model for HID lamps, Congreso Nacional de Control Automático, CNCA'05.

(Osorio, et. al., 2006a) Osorio R. and M. A. Oliver and M. Ponce and S. E. Pinto and R. Katebi and M. J. Grimble (2006)**,** Thermal Dynamic Model for HID Lamps with the Outer-Bulb Effetcs**,** Congreso de Electrónica, Robótica y Mecánica Automotriz, CERMA'06.

(Osorio, et. al., 2006b) Osorio R. and M. A. Oliver and M. Ponce and S. E. Pinto and R. Katebi and M. J. Grimble (2005), Dimming Control Using Adaptive-Fuzzy-Sliding Surface for Square-Waveform Ballast, Congreso Nacional de Control Automático, CNCA'05.

(Pande, et. al., 2008) Pande A., A. K. Thakur and S. Roy (2008), *Complex-Valued Neural Network in Signal Processing: A Study on the Effectiveness of Complex Valued*

Generalized Mean Neuron Model, World Academy of Science, Engineering and Technology 37 2008.

(Papaschinopoulos and Papadopoulos, 2002) Papaschinopoulos G. and Papadopoulos B. K. (2002), *On the fuzzy difference equation* $x_{n+1} = A + x_n / x_{n-m}$, Fuzzy Set and Systems, Elsevier, Vol. 129, pp.73-81.

(Park and Han, 2000) Park J. Y. and H. K. Han (2000), *Fuzzy differential equations*, Fuzzy Sets and Systems, Vol. 110, pp.69-77.

(Park, et. al., 2000) Park J. Y. and H. K. Han and K.-H. Son (2000), *Fuzzy differential equations with nonlocal condition*, Fuzzy Sets and Systems, Vol. 115, pp.365-369.

(Passino, 2004) Passino K. M.(2004), Biomimicry for Optimization, Control, and Automation, Springer, ISBN 1852338040.

(Pefefferl and Färber, 1998) Pefefferl J. and G. Färber (1998), *Applying load adaptive real-time algorithms to a vehicle control system*, Control Engineering Practice, Pergamon-IFAC, Vol. 6, pp. 541-546.

(Peterka, 1972) Peterka V. (1972), On steady state minimum variance control strategy, Kybernetika, Vol. 8, Issue 3, 219-232.

(Pinto and Madrigal, 2001) Pinto Castillo S. E. and G. Madrigal Espinosa (2001), Adaptive Fuzzy Control System for the Load Regulation of the Fossil Power Plant, 3rd International Conference on Control, Virtual Instrumentation and Digital Systems, CICINDI, CIC-IPN, ISBN 970-18-8887-0,México, August, pp. 46-54.

(Pinto, 2001) Pinto Castillo S. E. (2001), *Control System with Adaptive Fuzzy Decoupling for the Regulation of Load of a Fossil Power Plant*, Thesis of Master in Science in Electronic Engineering, CENIDET, Cuernavaca - Morelos, Mexico.

(Pinto, et. al., 2004a) Pinto Castillo S.E. and M.J. Grimble and R. Katebi (2004), *Neuro-Fuzzy Generalized Minimum Variance for Nonlinear Systems*, 2nd IFAC Symposium on System, Structure and Control, Mexico

(Pinto, et. al., 2004b) Pinto Castillo S.E. and M.J. Grimble and R. Katebi (2004), *Neuro-Fuzzy Generalized Minimum Variance for Nonlinear Systems*, Internal Report (Extended Version), Industrial Control Center.

(Pinto, et. al., 2004a) Pinto Castillo S.E. and M.J. Grimble and R. Katebi (2004), *Neuro-Fuzzy Generalized Minimum Variance for Nonlinear Systems*, 2nd IFAC Symposium on System, Structure and Control, Mexico.

(Pinto, et. al., 2004b) Pinto Castillo S.E. and M.J. Grimble and R. Katebi (2004), *Neuro-Fuzzy Generalized Minimum Variance for Nonlinear Systems*, Internal Report ICC-REP 214, Industrial Control Centre, University of Strathclyde, UK.

(Pinto, et. al., 2005) Pinto Castillo S.E. and M.J. Grimble and R. Katebi (2005), *Self-Tuning Neuro-Fuzzy Generalized Minimum Variance Controller*, 16th IFAC World Congress in Prague, ISBN-13:978-0-08-045108-4, ISBN-10: 0-08-045108-X, Czech Republic.

(Pinto, 2006) Pinto Castillo S. E. (2006), Lecturing Notes of the Course: Artificial Neural Networks imparted to British Aerospace Systems, Hosted by SEIC, Leicester, 8 – 10 November**,** University of Strathclyde - Industrial Control Centre, November, Glasgow-Scotland - UK.

(Pinto, et. al., 2009) Pinto Castillo, S. E. and M. J. Grimble and R. Katebi (2009), *Fuzzy Differential Equation founded in Neuro-Fuzzy Systems with Takagi-Sugeno-Kang Models*, IEE Proceedings Fuzzy Set and Systems, (In preparation).

(Pinto, et. al., 2009b) Pinto-Castillo S. E. and M. J. Grimble and R. Katebi (2009), Affording the Challenges in the Fault Tolerant Control Systems in Industrial Processes with Artificial Intelligence – A Bio-Inspired Approach, Computer and Chemical Engineering, Elsevier, (In preparation).

(Pischinger, et. al., 2004) Pischinger S. and C. Schernus and G. Lütkemeyer and H. J. Theuerkauf and T. Winsel and M. Ayeb (2004), *Investigation of Predictive Models for Application on Engine Cold-Start Behavior*, SAE World Congress 2004, SAE paper 2004-01-0994.

(Ponce, et. all, 2001) Ponce M. and A. Lopez and J. Correa and J. Arau and J. M. Alonso (2001), Electronic ballast for HID lamps with high frequency square waveform to avoid acoustic resonances, Applied Power Electronics Conference and Exposition, APEC'2001, Vol. 2, pp. 658 -663.

(Porfirio, et. al., 2003) Porfirio C. R. and E. Almeida Neto and D. Odloak (2003), *Multi-model predictive control of an industrial C3/C4 splitter*, Control Eng. Practice, Vol. 11, pp. 765-779.

(Powers and Nicastri, 2000) Powers W. F. and P. R. Nicastri (2000), *Automotive vehicle control challenges in the 21st century*, Control Engineering Practice, Elsevier Science Ltd., Vol. 8, pp. 605-618.

(Psichogios and Ungar, 1992) Psichogios D.C. and L. H. Ungar (1992), *A hybrid neural network-first principles approach to process modeling*, AIChE Journal, Volume 38, Issue 10, p.p. 1499–1511, DOI: 10.1002/aic.690381003.

(Puri and Ralescu, 1983) Puri M. L. and D. A. Ralescu (1983), *Differential of fuzzy functions*, Journal Math. Anal. Appl., Vol. 91, pp. 552-558.

(Qin and Badgwell, 2003) Qin S. Joe and T. A. Badgwell, (2003), *A survey of industrial model predictive control technology*, Control Eng. Practice, Vol. 11, pp. 733-764.

(Razi and Athappilly, 2005) Razi M. A. and K. Athappilly (2005), *A comparative predictive analysis of neural networks (NNs), nonlinear regression and classification and regression tree (CART) models*, Expert Systems with Applications 29 , pp. 65–74.

(Rauch, 1994) Rauch, H.E. (1994), *Intelligent fault diagnosis and control reconfiguration*, Vol. 14 Issue:3, ISSN: 1066-033X, pp. 6 – 12.

(Rawlings and Muske, 1993) Rawlings J. B. and K. R. Muske (1993), *The stability of constrained receding horizon control*, IEEE Transactions on Automatic Control, Vol. 38, No. 10, pp. 1512-1516.

(Rawlings, 2000) Rawlings J. B. (2000), *Tutorial overview of model predictive control*, IEEE Control System Magazine, Vol. 20, pp. 38-52.

(Ren and Kumar, 1991) Ren W. and P. R. Kumar (1991), *Stochastic adaptive system theory: recent advances and a reappraisal*, In Foundation of Adaptive Control, P.V. Kokotovic, pp. 269-307, Springer, Berlin.

(Reese, 2001) Reese M.G. (2001), *Application of a time-delay neural network to promoter annotation in the Drosophila melanogaster genome*, Comput Chem 26(1), 51-6.

Reese M. G. (2000), *Computational prediction of gene structure and regulation in the genome of Drosophila melanogaster*, PhD Thesis (PDF), UC Berkeley/University of Hohenheim.

(Reznik, 1997) Reznik L. (1997), Fuzzy Controllers, Newnes.

(Ribas, et. al., 2003) Ribas J. and J. M. Alonso and A. J. Calleja and E. Lopez and J. Cardesin and J. Garcia and M. Rico (2003), Arc stabilization in low-frequency square-wave electronic ballast for metal halide lamps, Applied Power Electronics Conference and Exposition, APEC '03, pp. 1179 -1184.

(Richalet, 1993) Richalet J. (1993), *Industrial application of model based predictive control*, Automatica, Vol. 29, pp. 1251-1274.

(Ripley, 1996) Ripley B. D. (1996), *Pattern Recognition and Neural Networks*, Cambridge University Press, ISBN 0 521 46086 7.

(Rochester, et. al., 1956) Rochester, N.; J.H. Holland, L.H. Habit, and W.L. Duda (1956), *Tests on a cell assembly theory of the action of the brain, using a large digital computer*, IRE Transactions on Information Theory 2: 80–93.

Rosenblatt, F. (1958). "The Perceptron: A Probalistic Model For Information Storage And Organization In The Brain". Psychological Review 65: 386–408.

(Ross, et. al., 2009) Ross J.J., M. A. Denaï, M. Mahfouf (2009), *A Hybrid Hierarchical Decision Support System for Cardiac Surgical Intensive Care Patients. Part II- Clinical Implementation and Evaluation*, Artificial Intelligence in Medicine Journal, 45(1), 53-62.

(Rovatti, 1996) Rovatti R. (1996), *Takagi-sugeno model as approximator in Sobolev norms the SISO case*, Proceedings Fifth IEEE International Conference on Fuzzy Systems, New Orleans, USA, pp. 1060-1066.

(Rudin, 1976) Rudin W. (1976), *Principles of Mathematical Analysis*, McGraw-Hill, Inc., New York.

(Russell, et. al., 2000) Russell and H. H. C. Bakker and R. I. Chaplin (2000), *Modular neural network modelling for long-range prediction of an evaporator*, Control Eng. Practice, Vol. 8, pp. 49-59.

(Sáez and Cipriano, 2001) Sáez D. and A. Cipriano (2001), *Design of supervisory predictive controller based on fuzzy models*, Proceedings of the 10th IEEE International Conference on Fuzzy Systems, FUZZ-IEEE'2001, Melbourne, Australia, December 2-5.

(Sáez and Keremer, 2003) Sáez D. and E. Kemerer (2003), *Fuzzy predictive control strategies and its application to a laboratory tank*, Proceedings of European Control Conference, ECC' 2003,University of Cambridge, UK, September 1-4, pp. 37-42.

(Sakawa, 2005) Sakawa M. (2005), Genetic Algorithms and Fuzzy Multiobjective Optimization, Springer, ISBN 0792374525.

(Sales and Billings, 1990) Sales K. R. and S. A. Billings (1990), *Self-tuning control of nonlinear ARMAX models*, Int. J. Control, Vol. 51, No. 4, pp. 753-769.

(Sarpturk, et. al., 1987) Sarpturk S. and Y. Istefanopulos and O. Kaynak (1987), *On the stability of discrete-time sliding mode control systems*, IEEE Transactions on Automatic Control, vol. 32, Oct 1987, pp. 930 – 932.

(Sato, 2003) Sato, Y. (2003), *Robust Fuzzy Neural Network Based Control in a Mechatronic Servo System*, Journal of the Japan Society of Mechanical Engineers，69C-687: 2929–2936.

(Saxena and Saad 2005) Saxena A. and A. Saad (2005), *Evolving an Artificial Neural Network Classifier for Condition Monitoring of Rotating Mechanical Systems*, Journal of Applied Soft Computing Elsevier Publishers, ISSN:1568-4946.

(Sbarbaro, et. al., 2004) Sbarbaro D. and R. Murria-Smith and A. Valdes (2004), Multivariable Generalized Minimum Variance Control Based on Artificial Neural Networks and Gaussian Process Models, International Symposium Neural Networks, F. Yin and J. Wang and C. Quo Editors, Springer-Verlag, LNCS 3174, pp.52-58.

(Schaft, 2000) Schaft A. V. D. (2000), L_2-Gain and Passivity Techniques in Nonlinear Control, ISBN: 1-85233-073-2, Springer-Verlag London Berlin Heidelberg.

(Scokaert, 1997) Scokaert P. O. M. (1997), *Infinite horizon generalised predictive control*, International Journal of Control, Vol. 66, No. 1, pp. 161-175.

(Seborg, 1986) Seborg D.E. and S. L. Shah and T. F. Edgar (1986), *Adaptive control strategies for process control: a survey*, AIChE J., Vol. 32, pp.881-913.

(Shen, et. al., 2003) Shen M. and Z. Qian and F. Z. Peng (2003), Design of a two-stage low-frequency square-wave electronic ballast for HID lamps, IEEE Transactions on Industry Applications, pp. 424-430.

(Shen, et. al., 2002a) Shen M. and Z. Qian and F. Z. Peng (2002), Control strategy of a novel two-stage acoustic resonance free electronic ballast for HID lamps, Power Electronics Specialists Conference, PESC'02, pp. 209 –212.

(Shen, et. al., 2002b) Shen M. and Z. Qian and F. Z. Peng (2002), A novel two-stage acoustic resonance free electronic ballast for HID lamps, Industry Applications Conference, IAS'02, pp. 1869 –1874.

(Shvartsas and Ben-Yaakov, 1999) Shvartsas M. and S. Ben-Yaakov (1999), A SPICE compatible model of high intensity discharge lamps, IEEE Power Electronics Specialists Conference, PESC-99, 1037-1042, Charleston.

(Sira-Ramirez, et. al., 1995) Sira-Ramirez H. and R. A. Perez-Moreno and R. Ortega and G. Esteban (1995), Passivity-Based Controllers for the Stabilization of DC-to-DC Power Converter, IEEE Conference on decision and Control, pp. 3471 –3476.

(Skogestad and Postlethwaite, 1996) Skogestad S. and I. Postlethwaite (1996), MULTIVARIABLE FEEDBACK CONTROL - Analysis and Design, Editorial John Wiley & Sons, ISBN 0-471-94277-4.

(Soeterboek, 1992) Soeterboek R. (1992), Predictive Control: A Unified Approach, Prentice Hall, New York-USA.

(Song, et. al., 2000) Song S., Guo L. and Feng C. (2000), *Global existence of solutions to fuzzy differential equations*, Fuzzy Sets and Systems, Vol. 115, pp. 371-376

(Song and Wu, 2000) Song Sh. and C. Wu (2000), *Existence and uniqueness of solutions to Cauchy problem of fuzzy differential equation*, Fuzzy Sets and Systems, Vol. 110, pp. 55-67.

(Souza, et. al., 1997) Souza J. M. and R. Babuška and H. B. Verbruggen (1997), *Fuzzy predictive control applied to an air-conditioning system*, Control Eng. Practice, Vol. 5, N0. 10, pp. 1395-1406.

(Spooner, et. al., 2002) Spooner J. T. and M. Maggiore, R. Ordoñez and K. M. Passino (2002), *Stable Adaptive Control and Estimation for Nonlinear Systems: Neural and Fuzzy Approximator Techniques*, John Wiley & Sons, Inc., ISBN:0-471-41546-4 (Hradback); 0-471-22113-9.

(Stanfelj, et. al., 1993) Stanfelj N. and T. E. Marlin and J. F. MacGregor (1993), *Monitoring and diagnosing process control performance: the single-loop case*, Ind. Eng. Chem. Res., Vol. 32, pp. 301-314.

(Stephanopoulos, 1984) Stephanopoulos G. (1984), *Chemical Proccess Control: An Introduction to Theory And Practice*, Prentice Hall-Englewood.

(Stefanopoulou, et. al., 2000) Stefanopoulou A. G. and I. Kolmanovsky and J. S. Freydenberg (2000), *Control of Variable Geometry Turbocharged Diesel Engines for Reduced Emissions*, IEEE Transactions on Control, Systems Technology, Vol. 8, No. 4, pp. 733-745.

(Stotsky, et. al., 1997) Stotsky A. and J. K. Hedrick and P. P. Yip (1997), The use of sliding modes to simplify the backstepping control method, of the American Control Conference, Albuquerque, pp. 1703-1708.

(Stotsky and Forgo, 2004) Stotsky A. and A. Forgo (2004), *Recursive spline interpolation method for real time engine control applications*, Control Engineering Practice, Vol. 12, pp. 409-416.

(Stotsky and Kolmanovsky, 2002) Stotsky A. and I. Kolmanovsky (2002), *Application of input estimation techniques to charge estimation and control in automotive engines*, Control Engineering Practice, Vol. 10, pp. 1371-1383.

(Su, 1997) Su M.-Ch. (1997), *Fuzzy Model Identification*, Hellerdoorn, H. and D. Driankov Editors, Springer-Verlag.

(Suah, et. al., 2003) Suah F. B. M., M. Ahmad, M. N. Taib (2003), *Applications of artificial neural network on signal processing of optical fibre pH sensor based on bromophenol blue doped with sol–gel film*, ELSEVIER, Sensors and Actuators B 90 , pp. 182–188.

(Sugeno and Kang, 1988) Sugeno M. and G.T. Kang (1988), *Structure identification of fuzzy model*, Fuzzy Sets and Systems, Vol. 28, pp. 15-55.

(Sugeno and Yasukawa, 1993) Sugeno M. and T. Yasukawa (1993), *A Fuzzy-Logic-Based Approach to Qualitative Modeling*, IEEE Transaction on Fuzzy Systems, Vol. 1, No.1, February, pp. 7-31.

(Sun and Hesterman, 1996) Sun N. y B. Hesterman (1996), PSpice High Frequency Dynamic Fluorescent Lamp Model, APEC'96, pp. 641-647.

(Svoronos, et. al., 1981) Svoronos S. and G. Stephanopoulos and R. Aris (1981), *On bilinear estimation and control*, Int. J. Control, Vol. 34, pp. 651-684.

(Takagi and Sugeno, 1985) Takagi T. and M. Sugeno (1985), *Fuzzy identification of systems and its application to modeling and control*, IEEE Trans. System, Man and Cybernetics, Vol. SMC-15, No.1, pp. 116-132.

(Tanaka and Sugeno, 1992) Tanaka K. and M. Sugeno (1992), *Stability analysis and design of fuzzy control systems*, Fuzzy Sets and Systems, Vol. 45, Issue 2, pp.135-156.

(Tanaka, 1995) Tanaka K. (1995), *Stability and stabilizability of fuzzy-neural-linear control system*, IEEE Trans. Fuzzy Systems, Vol. 3, November,pp. 438-447

(Tanaka, et. al., 1996) Tanaka K. and T. Ikeda and H. O. Wang (1996), *Robust Stabilization of a Class of Uncertain Nonlinear Systems via Fuzzy Control Quadratic*

Stabilizability, H^{∞} Control Theory, and Linear Matrix Inequalities, IEEE Transactions on Fuzzy Systems, Vol. 4, No. 1, February, pp. 1-13.

(Tanaka and Wang, 2001) Tanaka K. and H. O. Wang (2001), *Fuzzy Control Systems Design and Analysis: A Linear Matrix Inequalities Approach*, John Wiley & Sons, Inc., ISBNs: 0-471-32324-1.

(Tanaka, et. al., 2003) Tanaka K. and T. Ikeda and H. O. Wang (2003), *A Multiple Lyapunov Function Approach to Stabilization of Fuzzy Control System*, IEEE Transactions on Fuzzy Systems, Vol. 4, No. 1, August, pp. 1-13.

(Thapa, 2001) Thapa B. K. (2001), *Neural network enhanced self tuning adaptive control application for non-linear control of dynamic systems*, PhD thesis, Aston University.

(Thornhill, et. all., 1999) Thornhill N. F. and M. Oettinger and P. Fedenzuk (1999), *Refinery-wide control loop performance assessment*, J. Process Control, Vol. 9, Issue 2, pp. 109-124.

(Tseng and Cheng, 1998) Tseng T.-C. and W. K. Cheng (1998), *An Adaptive Air/Fuel Ratio Controller for SI Engine Throttle Transients*, SAE Paper 1999-01-0552, Sae International.

(Tsukamoto, 1979) Tsukamoto, Y. (1979). An approach to fuzzy reasoning method, In Madan M. Gupta, Rammohan K. Ragade and R. Yager edts. Advances in fuzzy set theory and applications, North-Holland, Amsterdam, pp. 137-149.

(Utkin, 1974) Utkin V. I. (1974), Sliding Modes and Their Application in Variable Structure Systems, MIR Publishers, Moscow.

(Utkin, 1977) Utkin, V. (1977), Variable structure systems with sliding modes, Transactions on Automatic Control, pp. 212 –222.

(Vaes, et. al., 2002) Vaes D. and W. Souverijns and J. De Cuyper and J. Swevers and P. Sas (2001), *Decoupling feedback control for improved multivariable vibration test rig tracking*, Proceeding of ISMA2002, Vol. II, pp. 525-534.

(Van Overschee and De Moor, 1996) Van Overschee P. and B. De Moor (1996), *Subspace Identification for Linear System: Theory – Implementation-Applications*, Kluwer Academic Publishers.

(Vázquez, et. al., 2000) Vázquez N. and C. Hernández and R. Cano and J. Antonio and E. Rodríguez and J. Arau (2000), An efficient single-switch voltage regulator, Power Electronics Specialists Conference, PESC'00, Vol. 2, pp. 811-816.

(Veaux, et. al., 1998) Veaux R. D. D., J. Schumi, J. Schweinsberg and L. H. Ungar (1998), *Prediction Intervals for Neural Networks via Nonlinear Regression*, *Technometrics*, JSTOR, Vol. 40, No. 4.

(Vemuri and Polycarpou, 1997) Vemuri A.T.and M.M. Polycarpou (1997),Neural-network-based robust fault diagnosis in robotic systems, IEEE Transactions on Neural Networks, ISSN: 1045-9227, Volume: 8 Issue:6 , pp. 1410 – 1420.

(Verdult, 2002) Verdult, V. (2002), *Nonlinear System Identification- A State-Space Approach*, Twente University Press, Netherlands.

(Vorobiev and Seikkala, 2002) Vorobiev D. and S. Seikkala (2002), *Towards the theory of fuzzy differential equations*, Fuzzy Sets and Systems, Vol. 125, pp.231-237.

(Wang and Mendel, 1992) Wang L.-X. and J.M. Mendel (1992), *Fuzzy basis functions, universal approximations, and orthogonal least-squares learning*, IEEE Trans. Neural Networks, Vol. 3, pp. 807-814.

(Wang, 1997) Li-Xin Wang (1997), *A Course in Fuzzy Systems and Control*, ISBN 0-13-540882-2, Prentice Hall PTR.

(Wang and Kuo, 1998) Wang L. and S.-C. Kuo (1998), Modeling High Frequency Fluorescent Lamp Using EMTP, IEEE PESC'98, pp. 1744-1748.

(Wang, et. al., 1995) Wang H. O. and K. Tanaka and M. Griffin (1995), *Parallel distributed compensation of nonlinear systems by Takagi-Sugeno fuzzy model*, Proceedings FUZZ-IEEE/IFES'95, Yokohama, Japan, pp. 531-538.

(Wang and Wei, 2000) Wang L.-X.. and C. Wei (1995), *Approximation Accuracy of Some Neuro-Fuzzy Appproaches*, IEEE Transactions on Fuzzy Systems, Vol. 8, No. 4, pp. 470-478.

(Wang and Lee, 2002) Wang J.-S. and C.S.G. Lee (2002), *Self-Adaptive Neuro-Fuzzy Inference Systems for Classification Applications*, IEEE Transactions on Fuzzy Systems, Vol. 10, No. 6, December, pp. 790-802.

(Wagner, et. al., 1998) Wagner R. M. and J. A. Drallmeier and C. S. Daw (1998), *Origins of cyclic dispersion patterns in spark ignition engines*, Proceedings of the 1998 spring technical meeting of the central states section of the combustion institute, Lexington, Kentucky, USA, May 31-June 2, pp.213-218.

(Wellstead and Zarrop, 1991) Wellstead P. E. and M. B. Zarrop (1991), *Self-tuning Systems – Control and Signal Processing*, John Wiley & Sons.

(Weeks and Moskwa, 1995a) Weeks R.W. and J. J. Moskwa (1995), *Transient Air Flow Rate Estimation in a Natural Gas Engine Using a Nonlinear Observer*, SAE paper 940759.

(Weeks and Moskwa, 1995b) Weeks R. W. and J. J. Moskwa (1995), *Automotive Engine Modeling of Real-Time Control Using MATLAB/SIMULINK*, SAE International, SAE paper 950417, pp. 1-15.

(Wellstead, 1979) Wellstead P.E. (1979), "Introducing to Physical System Modeling", Academic Press.

(Winsel, et. al., 2004) Winsel T. and M. Ayeb and H. J. Theuerkauf and S. Pischinger and C. Schernus and G. Lütkemeyer (2004), *Hil-Calibration of SI Engine Cold Start*

and Warm-Up Using Neural Real-Time Model, SAE World Congress 2004, SAE paper 2004-01-1362.

(Won, et. al., 1998) Won M. and S. B. Choi and J. K. Hedrick (1998), *Air-to-Fuel Ratio Control of Spark Ignition Engines Using Gaussian Network Sliding Control*, IEEE Transaction on Control Systems Technology, Vol. 6, No. 5, September.

(Wu, et. al., 1997) Wu T.-F. and J.-C. Hung and T.-H. Yu (1997), A PSpice Circuit Model for Low-Pressure Gaseous Discharge Lamps Operating at High Frecuency. IEEE Transactions on Industrial Electronics, Vol. 44, No. 3, June, pp. 428-431.

(Wu, 1999) Wu, W. (1999), *Stable Inverse Control for Nonminimum Phase Nonlinear Processes*, J. Process Control, Vol. 9, No. 2, pp. 171-183.

(Xia and Chai, 1995) Xia L. and T. Chai (1995), *Assessment on robustness properties of a class of nonlinear systems with fuzzy logic controllers*, Proc. Int. Joint Conf. CFSA/IFIS/SOFT Fuzzy Theory Applications, Taipei, Taiwan, December, pp. 271-276.

(Xu, et. al, 2008) Xu B., D. Yang and X. Wang (2008), Neural network based fault diagnosis and reconfiguration method for multilevel inverter, CCDC 2008. Chinese Control and Decision Conference, ISBN: 978-1-4244-1733-9, pp. 564 – 568.

(Xue and Fu, 2002) Xue X. and Y. Fu (2002), *Carathéodory solutions of fuzzy differential equations*, Fuzzy Sets and Systems, Vol. 125, pp. 239-243.

(Yan, et. al., 2003) Yan W. and Hui S.Y.R. and H. Chung (2003), Nonlinear high-intensity discharge lamp model including a dynamic electrode voltage drop**,** IEE Proceeding of Science, Measurement and, July, pp.161–167.

(Yang and Chundi, 1999) Yang S. and M. Chundi (1999), *Robust and optimal control for robotic manipulator based on linear-parameter-neural-networks*, Proceedings of the 38th IEEE Conference on Decision and Control, USA, ISBN: 0-7803-5250-5, Vol.3, pp. 2174 – 2179.

(Ying, 1998) Ying H. (1998), *General SISO Takagi-Sugeno Systems with Linear Rule Consequent Are Universal Approximators*, IEEE Transactions on Fuzzy Systems, Vol. 6, No. 4, November, pp. 582-587.

(Ying, et. al., 1999) Ying H. and Y. Ding and S. Li and S. Shao (1999), *Comparison of Necessary Conditions for Typical Takagi-Sugeno and Mamdani Fuzzy Systems as Universal Approximators*, IEEE Transactions on Systems, Man and Cybernetics-Part A: Systems and Human, Vol. 29, No. 5, September, pp. 508-514.

(Yiyoung-Sun, 1993) Yiyoung-Sun, P.E. (1993), PSpice Modeling of Electronically Ballasted Compact Fluorescent Lamp Systems. IEEE IAS'93, pp. 2311-2316.

(Yu and Fei, 2005) Yu Z. and Q. Fei (2005), *A method of constructing Lyapunov functions of continuous TSK fuzzy model*, IMA Journal of Mathematical Control and Information, Vol. 22, pp. 251-256.

(Yu and Gomm, 2003) Yu D. L. and J. B. Gomm (2003), *Implementation of neural network predictive control to a multivariable chemical reactor*, Control Eng. Practice, Vol. 11, pp. 1315-1323.

(Zadeh, 1965) Zadeh L. A. (1965), *Fuzzy Sets*, Information and Control, vol. 8, pp. 338-353.

(Zayed, et. al., 2004) Zayed A. S. and A. Hussain and L.S. Smith (2004), *A multivariable generalised minimum-variance stochastic self-tuning controller with pole-zero placement*, Int. J. of Control and Intelligent Systems, Vol. 32, pp. 35-44.

(Zanin, et. al., 2002) Zanin A. C. and M. Tvrzká de Gouvêa and D. Odloak (2002), Integrating real-time optimization into the model predictive controller of the FCC system, Control Eng. Practice, Vol. 10, pp. 819-831.

(Zbigniew, 1998) Zbigniew M. (1998),Genetic Algorithms + Data Structures = Evolution Programs, Springer; 3rd edition, ISBN: 3540606769.

(Zelinka, et. al., 1999) Zelinka P. and B. Rohal-Ilkiv and A. G. Kuznetsov (1999), *Experimental verification of stabilising predictive control*, Control Eng. Practice, Vol. 7, pp. 601-610.

(Zhang and Lang, 1988) Zhang J. and S. Lang (1988), *Indirect adaptive suboptimal control for linear dynamic system having polynomial nonlinearities*, IEEE Trans. Autom. Control, Vol. 33, No. 4, pp. 389-392.

(Zhang and Lang, 1988) Zhang J. and S. Lang (1989), *Explicit self-tuning control for a class of nonlinear systems*, Automatica, Vol. 25, No. 4, pp. 593-596.

(Zhan and Kovacevic, 1998) Zhan Y. M. and R. Kovacevic (1998), *Neurofuzzy model-based predictive control of weld fusion zone geometry*, IEEE Trans. on Fuzzy Systems, Vol. 6, No. 3, pp. 389-401.

(Zhang, et. al., 2000) Zhang T., S. S. Ge and C. C. Hang (2000), *Adaptive neural network control for strict-feedback nonlinear systems using backstepping design*, Automatica 36 (2000), pp. 1835-1846.

(Zhao, 1995) Zhao J. (1995), *Fuzzy logic in modeling and control*, PhD Dissertation, CESAME, Louvain la Neuve, Belgium.

(Zhao, et. al., 2001) Zhao H. and J. Guiver and R. Neelakantan and L. T. Biegler (2001), *A nonlinear industrial model predictive controller using integrated PLS and neural net state-space model*, Control Eng. Practice, Vol. 9, pp. 125-133.

(Zhu, et. al., 1999) Zhu,Q. M. and Z. Ma and K. Warwick (1999), *Neural Network enhanced generalised minimum variance self-tuning controller for nonlinear discrete-time systems*, Journal IEE Proceeding of Control Theory Appl., Vol. 146, No.4, pp. 319-326.

(Žilková, et. al., 2006) Žilková J., J. Timko and P. Girovský (2006), Nonlinear System Control Using Neural Networks, Acta Polytechnica Hungarica, Vol. 3, No. 4, pp. 85-94.